Characterising the role of inflammatory lipids in regulating systemic inflammation in arthritis

A thesis submitted to Cardiff University in accordance with the requirements for the degree of Doctor of Philosophy in the School of Medicine

By

Daniela Filipa de Oliveira Costa

September 2022

This project has received funding from the European Union's Horizon 2020 research and innovation programme under the Marie Skłodowska-Curie grant agreement No 812890.

Acknowledgements

Firstly, I would like to thank my supervisor Professor Valerie O'Donnell for giving me a chance to do this PhD, and for the help and guidance throughout. I am looking forward to the next project together.

I would also like to thank everyone in the Lipidomic lab that made this thesis possible. To Vikki, who helped me with the LC/MS/MS. To Majd, for a lot of my protocols and advice, and of course, for your phlebotomy skills. To Professor Peter Collins and Dr Vince Jenkins for all the help understanding a bit of coagulation. To Beth Morgan, for all the help with the mice, the phlebotomies, and for enduring my late rant sessions. To Ali, for all the trips and company thought most of my PhD. To Anastasia and Beth McGill, which shared an office with me and made my life so much better. To Brendon, who always has patience and a piece of friendly advice for me.

A special thank you to everyone in the Arthritis Lab. To Robert Jenkins, Ana Cardus Figueras, James Burston and Stuart Hughes for all the help me with all my mice models. To Gareth Jones and Aisling Morrin for being my eyes scoring the mice joints. And a special thank you to Professor Simon Jones, for allowing me to do all this animal work.

I must thank Marie Skłodowska-Curie Actions, not only for providing the funds for this project but for allowing me to learn so much during this PhD, alongside all the other 11 ESRs. A big thank you to them for all their support. A big thank you to Martin Giera, Marieke Bax, and Suzanne Plas-Duivesteijn for making ArthritisHeal an amazing project to work on. A thank you to all the other PIs for their feedback throughout all the WP meetings.

A big thank you to all the volunteers who gave me blood despite the troubling time. This thesis wouldn't have been possible without your help.

Aos meus pais, ao meu irmão e a Carla, por acreditarem, mais cedo ou mais tarde, eu conseguiria uma bolsa de doutoramento, e encorajarem a procurar lá fora, sem me pressionarem a seguir o caminho de farmácia comunitária. Ao Dio, por todas as chamadas e vídeos, não teria sobrevivido ao lockdown sem ti. A Diane pelo porto de abrigo em Londres. Pelo Maria e as suas longas histórias. A minha minion Catarina, que me acompanha no percurso difícil de tentar ser cientista, vais conseguir também vais ver! E claro, ao CPM e a Elsa Rodrigues, que me abriu caminho para conseguir chegar aqui. A Nídia, a Maia, a Botão e a Guida pela conversa de grupo parvas, e pelas visitas. Por fim, thank you to Stuart, for being here.

Summary

Rheumatoid arthritis (RA) is linked to an elevated risk of thrombotic events, however, the mechanisms behind this are so far unknown. The activity of coagulation factors requires a pro-coagulant membrane provided by aminophospholipids, including phosphatidylserine (PS). Alongside this, enzymatically oxidised phospholipids (eoxPLs), including hydroxyeicosatetraenoic acid–phospholipids (HETE-PLs) enhance coagulation by supporting PS-dependent binding and activity of coagulation factors. EoxPL levels are elevated in human thrombotic disorders, namely abdominal aortic aneurysm, and anti-phospholipid syndrome.

To determine whether eoxPLs are elevated in arthritis-associated coagulopathies, antigen-induced arthritis (AIA) was generated in *WT*, *Il27ra*$^{-/-}$, *Il6ra*$^{-/-}$ and *Il6*$^{-/-}$ mice, which develop histological phenotypes similar to humans. *WT* and *Il27ra*$^{-/-}$ AIA mice showed elevated eoxPLs, primarily 12-HETE-PEs in whole blood cells, which included red blood cells, white blood cells and platelets. In addition, higher thrombin-antithrombin complexes (TAT) levels were observed in these mice. However, neither *Il6ra*$^{-/-}$ nor *Il6*$^{-/-}$ mice exhibited increased levels of TATs or eoxPLs during AIA development. These results suggest that IL6 plays a role in increased coagulation, which may be linked with eoxPL levels in whole blood cells. Furthermore, in *Alox15*$^{-/-}$ mice, levels of whole blood cell 12-HETE-PEs were similar to WT, indicative of platelet 12-LOX activity, therefore suggesting platelets as the primary source of these lipids in whole blood. Human RA was also studied, however, no significant difference in eoxPLs and aminophospholipid exposure was seen in platelets and white blood cells (WBCs). Nevertheless, thrombocytosis was observed in these patients, which may increase circulating eoxPLs and aminophospholipid levels. Furthermore, EV-containing plasma from RA patients displayed higher levels of eoxPLs and externalized aminophospholipids, as well as supporting more thrombin generation than EVs from healthy controls. Last, an increased plasma IgG immunological response was observed against oxPLs in these patients, especially towards 12-HETE-PE. Overall, these results indicate that eoxPLs are elevated in arthritis and may play a role in the increased coagulation observed in RA, and platelets (or platelet-derived EVs), are important players in the elevated systemic coagulation of this disease.

Abbreviations

AA	Arachidonic acid
ACD	Acid Citrate Dextrose
ACN	Acetonitrile
ACPA	Anti-citrullinated protein antibody
AIA	Antigen-induced arthritis
AminoPL	Aminophospholipid
APS	Antiphospholipid syndrome
CE	Collision energy
CIA	Collagen-induced arthritis
COX	Cicloxygenase
CRP	C-reactive protein
CXP	Cell exit potential
DHA	Docosahexaenoic acid
DP	Declustering potential
DMPC	1,2-dimyristoyl-sn-glycero-3-phosphocholine
DMPE	1,2-dimyristoyl-sn-glycero-3-phosphoethanolamine
DMPS	1,2-dimyristoyl-sn-glycero-3-phosphoserine
DMSO	Dimethyl sulfoxide
DPBS	Dulbecco's phosphate-buffered saline
EDTA	Ethylenediaminetetraacetic acid
EoxPLs	Enzymatically oxidised phospholipids
EP	Entrance potential
EV	Extracellular vesicles
FLAP	5-LOX-activating protein
G6P1	Glucose-6-phosphate isomerase
GPX4	Glutathione peroxidase 4
HC	Healthy control
HDL	High density lipoprotein
HDOHE	Hydroxydocosahexaenoic acid
HETE	Hydroxyeicosatetraenoic acid
HpETE	Hydroperoxytetraenoic acid
HPLC	High performance liquid chromatography
HODE	Hydroxyoctadecadienoic acid
IS	Internal standard
KO	Knockout
LA	Linoleic acid
LC	Liquid chromatography

LC/MS/MS	Liquid chromatography coupled to tandem mass spectrometry
LDL	Low density lipoprotein
LOX	Lipoxygenase
LT	Leukotriene
m/z	Mass/charge ratio
MRM	Multiple reaction monitoring
MS	Mass spectrometry
MP	Microparticle
NB	EZ-link NHS-biotin
NET	Neutrophil extracellular traps
NSAID	Non-steroidal anti-inflammatory drugs
OA	Osteoarthritis
OxPLs	Oxidised phospholipids
PAR	Proteases activate receptor
PC	Phosphatidylcholine
PE	Phosphatidylethanolamine
PG	Prostaglandin
PLA_2	Phospholipase A2
PMP	Platelet-derived microparticle
PL	Phospholipid
PRP	Platelets rich plasma
PPP	Platelets poor plasma
PS	Phosphatidylserine
PUFA	Polyunsaturated fatty acids
RBC	Red blood cells
RA	Rheumatoid arthritis
RF	Rheumatoid arthritis factor
SAPE	1-stearoyl-2-arachidonoyl-sn-glycero-3-phosphoethanolamine
SAPS	1-stearoyl-2-arachidonoyl-sn-glycero-3-phosphoserine
SOPS	1-stearoyl-2-oleoyl-sn-glycero-3-phospho-L-serine
SpAPE	1-(1Z-octadecenyl)-2-arachidonoyl-sn-glycero-3-phosphoethanolamine
ROS	Reactive oxygen species
SNB	EZ-Link Sulfo-NHS-Biotin
SPM	Specialized pro-resolving mediator
TAT	Thrombin Antithrombin Complex
TF	Tissue Factor
TFPI	Tissue factor pathway inhibitor
Tg	Transgenic
TX	Thromboxane
TAFI	Thrombin activable fibrinolysis inhibitor
tPA	tissue type plasminogen activator

VTE	Venous thromboembolism
vWF	von Willebrand Factor
uPA	urokinase type plasminogen activator
WBC	White blood cell

Table of Content

List of Figures

Chapter 1: General Introduction

Chapter 2: Materials and Methods

Chapter 3: Elevated circulating oxidised phospholipids as possible players in the increased coagulation observed in Inflammatory arthritis in WT and *IL27ra*$^{-/-}$ mice

Chapter 4: *Alox15* deletion is not associated with altered coagulation in AIA

Chapter 5: *Alox15*-deficient mice show elevated inflammation and swelling during AIA development

Chapter 6: Total oxPLs in rheumatoid arthritis patients' blood cells are elevated, resulting in immunological consequences and increase thrombin generation

List of Equations

List of Tables

General Introduction

Chapter 1

1. Introduction

1.1. Lipids

Lipids play core functions in cell signalling, being involved in a multitude of cellular processes owing to their large range of structural and physiochemical properties[1]. Lipidomics, as the large-scale profiling and quantification of lipid molecules, applies techniques of analytical chemistry and bioinformatics to comprehend the physiological importance of lipids, as well as their mechanistic pathways. The analytic toolbox for lipid analysis was expanded significantly in recent years. The increasing number of chromatographic techniques and mass analysers with improved selectivity and sensibility has led to the development of one of the major lipidomic setups: the LC/MS/MS lipidomics[1,2]. By analysing the formation of specific lipids in signalling pathways in auto-immune diseases, lipidomics might shed some light on auto-immune-associated coagulopathies[3].

1.1.1. Phospholipids

The lipidome consists of all lipids present within the cell. These lipids can be subdivided into eight groups, one of which is glycerophospholipids, also known as phospholipids (PL). In eukaryotic cells, phosphatidylcholine (PC) and phosphatidylethanolamine (PE) are the most abundant PL present in the plasma membrane [4]. Conventionally, in resting healthy cells, the outer leaflet of the phospholipid membrane is mainly composed of sphingomyelin and PC, considered neutrally charged phospholipids, while aminophospholipids, more commonly PS and PE, are found in the membranes' inner leaflet [5,6].

Phospholipids are the structural blocks of cellular membranes, as well as important substrates for the generation of bioactive molecules such as eicosanoids and lysophospholipids, playing numerous functional roles. They are amphipathic molecules, combining a polar head group, a glycerol backbone, and two hydrophobic acyl chains in the *Sn-1* and *Sn-2* positions (Figure 1.1). This distinctive organization, with opposing polar and non-polar moieties, forces PLs to self-assemble into organized membranes which enclose as vesicles[7,8]. The *Sn-1* position can be occupied by fatty acyls linked by either acyl, alkyl ether or plasmalogen bonds[9]. Plasmalogen phospholipids are composed of a vinyl-ether at the *Sn-1* position and an acyl bond at the *Sn-2* position. Representing about 20 % of human phospholipids, plasmalogens are implicated in oxidative damage protection attributable to the vulnerability of the vinyl ether bond to reactive oxygen species[10].

The *Sn-2* position of phospholipids is primarily occupied by polyunsaturated fatty acids (PUFAs). Arachidonic acid (AA) is considered the most common PUFA in mammalian cells. In fact, in platelets, mononuclear cells and neutrophils, AA composes up to 25% of total PUFAs[11]. Other common PUFAs, are linoleic acid (LA), linolenic acid, docosahexaenoic acid (DHA) and eicosapentaenoic acid (EPA). In addition, PUFAs are considered important lipid mediators. For instance, AA is a second messenger signalling molecule, acting as an inflammatory mediator by inducing vasodilatation[12]. In addition, PUFAs are susceptible to oxidation, which combined with their ability to integrate into PLs, generates a remarkable diversity of molecules with important metabolic functions[7,8]. Phospholipases A2 (PLA_2), as lipolytic enzymes, catalyse the hydrolysis of the ester bond at the sn2-position of membrane phospholipids. Mediators such as cytokines, ADP and calcium, activate PLA_2, releasing AA, and other PUFAs from the plasma membrane, and therefore, also generating lysophospholipids[7,13].

The phospholipid composition is an important contributor to the biophysical properties of a cell membrane. PLs can be generated *de novo* through the Kennedy pathway, a three-step enzymatic process that metabolises choline or ethanolamine into phosphocholine or phosphoethanolamine, respectively, followed by the rate-limiting step of the pathway, the transfer on to a diacylglyceride, resulting in phosphatidylcholine (PC) or phosphatidylethanolamine (PE), respectively[14]. The cell membrane composition is dictated by the diversity of fatty acyl chain composition of PLs, which is controlled by a remodelling process, referred to as Lands'cycle. PLA_2 first hydrolysis phospholipids at the *sn-2* position, generating lysophospholipid and free PUFA. Through a series of deacylations and reacylations, different PUFA are incorporated at the *sn-2* position of phospholipids. Lysophospholipid acyltransferases (LPLATs), as phospholipid remodelling enzymes, which perform acylation reactions, incorporate a second PUFA to the *sn-2* position, forming a new PL species [15,16]."

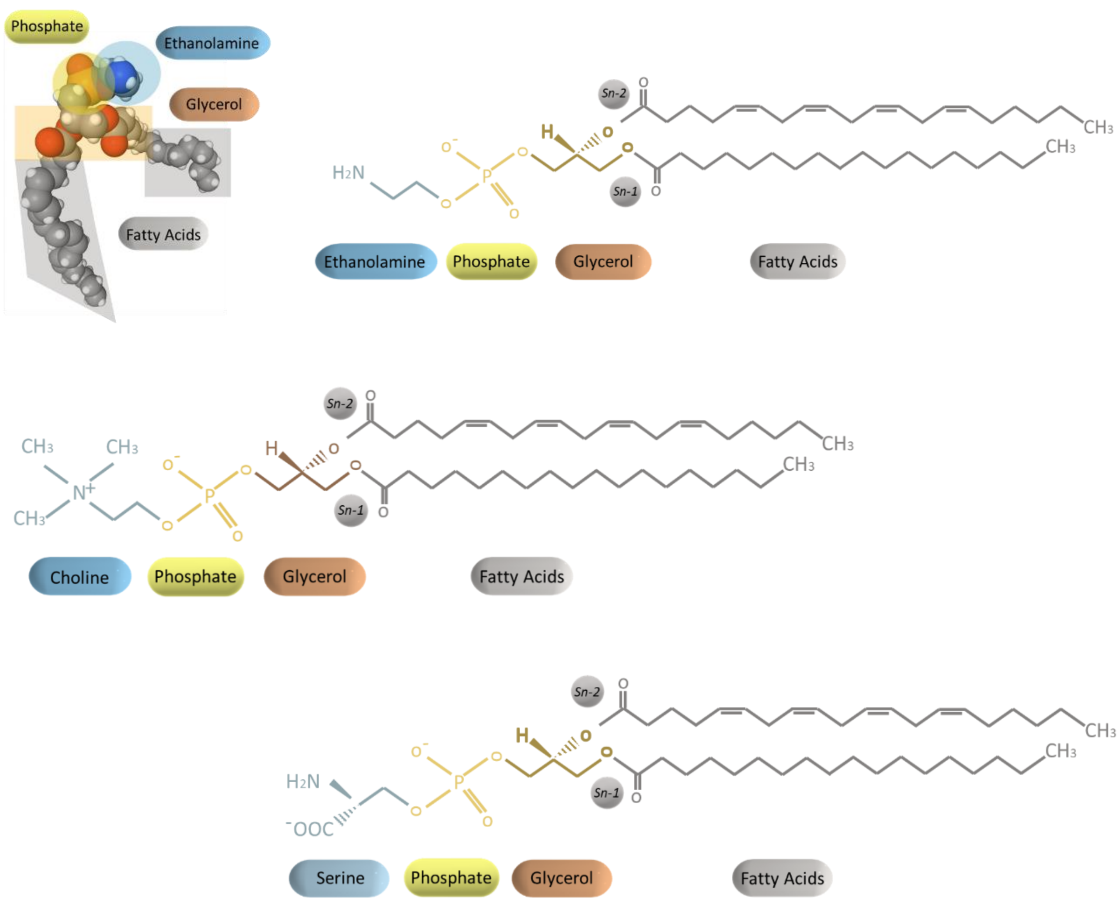

Figure 1.1: Phospholipid structure

The 3D structure, adapted from PubChem, exhibits the general structure of a PE with the hydrophilic portion featuring an ethanolamine group[350]. The 2D structures, designed using PowerPoint, illustrates diacyl glycerophospholipids, from top to bottom, 1-stearoyl-2-arachidonoyl-sn-glycero-3-phosphoethanolamine (PE 18:0/20:4), 1-octadecanoyl-2-(5Z,8Z,11Z,14Z-eicosatetraenoyl)-sn-glycero-3-phosphocholine (PC 18:0/20:4), and 1-stearoyl-2-eicsoatetraenoyl-sn-glycero-3-phosphoserine (PS 18:0/20:4), where the fatty acids of the hydrophobic portion are comprised of stearic acid in the *sn-1* position and arachidonic acid in the *sn-2* position.

1.1.2. Oxylipin pathways

Free intracellular PUFAs serve as a substrate for cyclooxygenase (COX), lipoxygenase (LOX) and, to a smaller extent, cytochrome P450 (CYP) enzymes.[7,13] These enzymes insert oxygen at different positions in PUFAs, generating biologically active lipid mediators known as oxylipins, which include eicosanoids, an important sub-family of 20-carbon lipids which the PUFA substrate is arachidonic acid (AA) (Figure 1.2)[17].

In resting cells, oxylipin production is negligible. However, upon activation, oxylipin production is induced. The lipids generated are specific to the enzymatic profile and PUFAs substrates of the different cell types, therefore, limiting the variety of products.

However, the convergence of a large variety of cells at inflammatory sites allows the synthesis of additional molecules, following a cell-cell transfer of intermediate metabolites; a process known as transcellular biosynthesis[3,18]. This dynamic synthesis, dependent on time, condition, and cell type establish oxylipins as important lipid mediators involved in the immune system, with both anti- and pro-inflammatory functions[19].

Oxylipins are important inflammatory molecules, that have dual functions as pro- and anti-inflammatory mediators. Oxylipin production is thought to be involved in the development of rheumatic diseases. Nonetheless, even potent anti-inflammatory drugs, such as steroids and non-steroidal anti-inflammatory drugs (NSAIDs), are unable to halt oxylipin production, resulting in a subclinical inflammation characteristic of RA[3].

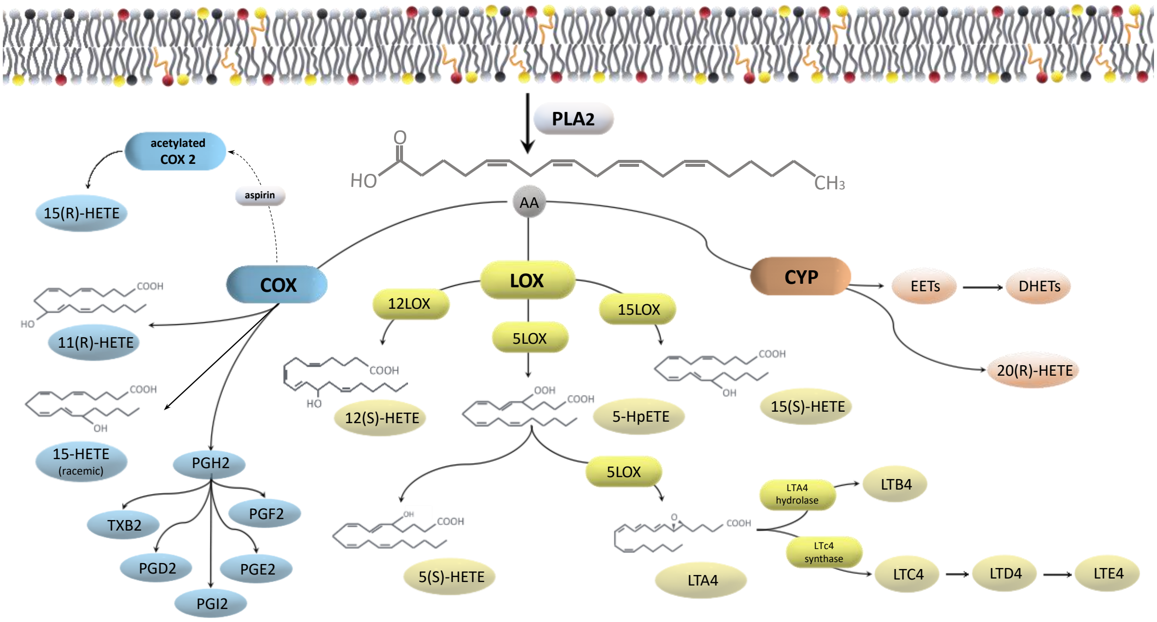

Figure 1.2: Oxylipin pathway

Activated phospholipase A2 (PLA_2) releases arachidonic acid (AA), and other PUFAs from the plasma membrane. Once free, intracellular arachidonic acid (AA) serves as a substrate for cyclooxygenase (COX), lipoxygenase (LOX) and cytochrome P450 (CYP) enzymes, generating a diversity of bioactive lipid mediators. Hydroxyeicosatetraenoic acids (HETEs) are bioactive isomers which can be produced by both COX, LOX and CYP, however the carbon which is oxygenated is specific to each enzyme. While, 11(R)-HETE is generated by COXs, 12(S)-HETE and 5(S)-HETE are specific to LOXs. Plus, each enzyme appears to be responsible for different stereoisomers. Molecular oxidation by LOX leads to the generation of S-configuration HETEs, while COX and CYP generate HETEs R-enantiomers. The main exception is 15-HETE, where both COX and LOX are responsible for its generation, however, the stereoisomeric difference remains. While 15-LOX generates 15(S)-HETE, COX can generate small amounts of a racemic mixture of 15-HETEs. In addition, upon aspirin acetylation, COX-2 exclusively generates 15(R)-HETE. These enzymatically generated HETEs can either remain free or be re-esterified into the membrane through the Lands' cycle. Figure designed using PowerPoint.

1.1.2.1. Oxylipins

Oxylipins comprise a wild range of oxygenated lipids, from mono-oxygenated, dihydroxy- and trihydroxy-PUFAs, to epoxy-, oxo-FAs and endoperoxides products. As potent modulators of immune responses, these have distinct biological activities and can even act as antagonists, despite deriving from the same precursor. Oxylipins carry out important pro-inflammatory actions such as chemotaxis[20], vasodilatation[21], stimulation of vascular endothelial growth factor production[22], as well as anti-inflammatory functions[23], coupled with a role in blood pressure regulation[24]. The structural specificity of these lipids leads to specific biological activities, therefore, oxylipin profiling is considered an important tool for the characterization of inflammatory status[25].

The most well-known oxylipins include mono-oxygenated products such as prostaglandins (PGs), leukotrienes (LTs), hydroxyeicosatetraenoic acids (HETEs) and hydroxyoctadecadienoic acids (HODEs). While PGs are COX products, LTs are products of LOX-catalysis. Both PGs and LTs exhibit pro-inflammatory properties and are involved in various inflammatory and auto-immune diseases, including rheumatoid arthritis (RA)[23,26].

Oxylipins can also exert beneficial effects. As a result of transcellular biosynthesis, specific oxylipin enantiomers derived from eicosapentaenoic acid (EPA) and docosahexaenoic acid (DHA) are hypothesised to exert roles in inflammation resolution, and as results have been termed specialized pro-resolving mediators (SPMs)[27].

It is proposed that DHA substrates originate SPMs, such as D-resolvins, maresins and protectins, through crossover oxidation between COX and LOX [28]. These oxylipins are currently being analysed for their potential pharmacological proprieties, however, the concentrations used in most studies far exceed the low levels found in biological samples, and some recent studies of these SPMs use ELISA methods, instead of lipidomic tools for their detection [29]. It has been shown that oxylipin ELISAs can suffer from significant cross-reactivity issues, where structurally similar molecules are recognized [30].

Therefore, LC/MS/MS is considered the only method of analysis with enough sensitivity and selectivity to analyse SPMs or even oxylipins in general [31]."

Regardless, pro-resolution mediators are not limited to SPMs, and they are attracting scientific interest. Instead of having anti-inflammatory activity, pro-resolution mediators are suggested to lead to the restoration of tissue homeostasis[32]. This restoration can occur through the clearance of immune cells from inflamed tissue, either through apoptosis and subsequent efferocytosis or through the re-entering of immune cells into systemic circulation[33].

It is essential to further study oxylipins, such as HETEs, HODEs and other LOX products, and evaluate their potential role as therapeutic targets or biomarkers for inflammatory and auto-immune diseases.

1.1.3. Lipoxygenase

LOX enzymes are expressed in numerous cell types, including immune cells and epithelial cells, and they are responsible for diverse functions ranging from immunity to barrier formation[34]. In mammals, the most common substrates for LOX enzymes are AA, followed by linoleic acid (LA) and linolenic acid, while also metabolizing EPA and DHA. The availability of these PUFAs is dependent on the actions of fatty acid desaturases and elongases, in the case of AA, and on dietary consumption, for essential PUFAs, such as linoleic acid and linolenic acid.

Following Ca^{2+} mobilisation, cytosolic PLA_2 is translocated to the plasma membrane, hydrolysing AA from PL pools, which becomes available to be catalysed by LOXs.[35,36] LOX enzymes are responsible for the generation of a large array of lipid mediators, including LTs, HETEs and HODEs (Figure 1.2)[34].

LOXs are non-heme iron enzymes with a common core consisting of a single polypeptide chain that is folded into two domains, a large α-helical catalytic domain and the N-terminal β-barrel domain, also known as the PLAT domain. The catalytical domain houses the non-heme iron, while the PLAT domain consists of eight anti-parallel β-stands, containing calcium binding sites, which are involved in membrane binding[37,38].

LOXs recognize 1,4-pentadiene motifs within PUFAs and introduce molecular oxygen, producing regio- and stereoselective hydroperoxides with different functional roles. AA, the main mammalian LOX substrate, contains four cis-double bonds that form three pentadiene moieties. The non-heme iron initiates oxidation by abstracting the molecular hydrogen at one end or another of the pentadiene, ensuring regioselectivity. Molecular oxygen is then introduced on the opposite face, in an antarafacial relationship, which results in either an *R* or *S* configuration (stereospecificity). This catalysis generates a specific hydroperoxyeicosatetraenoic acid (HpETE) enantiomer product. All HpETEs are then reduced into a less chemically reactive PL hydroxide product, HETE, catalysed by glutathione reductase 4 (GPX4) (Figure 1.3.A)[5,39,40].

5-LOX, in a catalytic complex with 5-LOX-activating protein (FLAP), oxygenates AA to 5-HpETE. This unstable product can be rapidly converted into LTA4, a precursor for other LTs, through leukotriene A4 synthetase activity of 5-LOX[41,42].

In addition to AA, LOX enzymes are equally able to monooxygenase LA, generating HODEs. In macrophages, LA is oxidised, at position 13, by 15-LOX, and then reduced by glutathione-dependent peroxidases, generating 13-HODE, the stable hydroxy-form. LA can also be non-enzymatically oxidised, either at position 9 or 13, generating 9-HODE and 13-HODE, respectively[43]. Elevated HODEs are associated with diseases such as atherosclerosis[44], multiple sclerosis[45] and non-alcoholic steatohepatitis[46]. In addition, pro-apoptotic effects have been attributed to HODEs, especially associated with monocytic cells[47,48].

Termed arachidonic acid lipoxygenase (*ALOX*), humans express six LOX genes (*ALOX5*, *ALOX12, ALOX12B*, *ALOX15*, *ALOX15B* and *ALOXE3*). Most are constitutively expressed, with the exception of *ALOX15,* which is induced in macrophages by inflammatory cytokines, such as IL-4 and IL-13, however, ALOX15B expression can also be increased by cytokines, hypoxia and lipopolysaccharide [42,49]. Mice, on the other hand, express seven *Alox* genes: *Alox5*, *Alox15*, *Alox15b* (also known as *Alox8*), *Alox12*, *Alox12b*, *Aloxe3*, *Aloxe12*, all orthologs of human functional genes, except the *Alox12e* gene, which, despite being present in the human genome, it is corrupted and functionless [39,42].

Expression of the different LOX isoforms is tissue specific. In fact, LOX enzymes can be termed accordingly to the cell of origin, namely platelet-type 12-LOX (ALOX12 in humans, Alox12 in mice), leukocyte-type 12-LOX (ALOX15 and ALOX15B in humans, Alox15 in mice) and epidermis-type (ALOX15B[50], ALOX12B and *ALOXE3* in humans, Alox12B, Alox15B or Alox8, *Aloxe3 and Aloxe12* in mice)[51]. Nevertheless, this classification can be misleading, considering that ALOX15B was found to be constitutively expressed in macrophages [52].

Mammalian LOXs can catalyse a total of four different reactions: 5*S*, 12*R*, 12*S*, or 15*S* oxygenations, therefore, LOXs are also named according to the oxygen insertion position in the AA substrate. Furthermore, LOX enzymes generate one specific product enantiomer, commonly an *S*-configuration in the case of platelets and leukocyte-type LOXs. In contrast, non-enzymatic lipid oxidation produces a racemic mixture, which is a mix comprised of 50% of *R*- and 50% of *S*-hydroperoxides. Despite *ALOX*-isoform classification being according to their reaction specificity, some LOX enzymes can exhibit a dual reaction specificity. Therefore, LOX isoforms are also classified according to their genetic sequence. For example, the murine *Alox15* gene, as an orthologue leukocyte-type 12-LOX, can also be termed 12/15-LOX, as it produces primarily 12(*S*)-HETE, as well as small amounts of 15(*S*)-HETE, in a 3:1 ratio [53–55].

In contrast, human *ALOX15*, termed 15-LOX1, converts AA to 15(*S*)- HETE along with generating small amounts of 12(*S*)-HETE, in a 9:1 ratio, while ALOX15B exhibits a singular positional specificity, generating almost exclusively 15(S)-HETE [53–55].

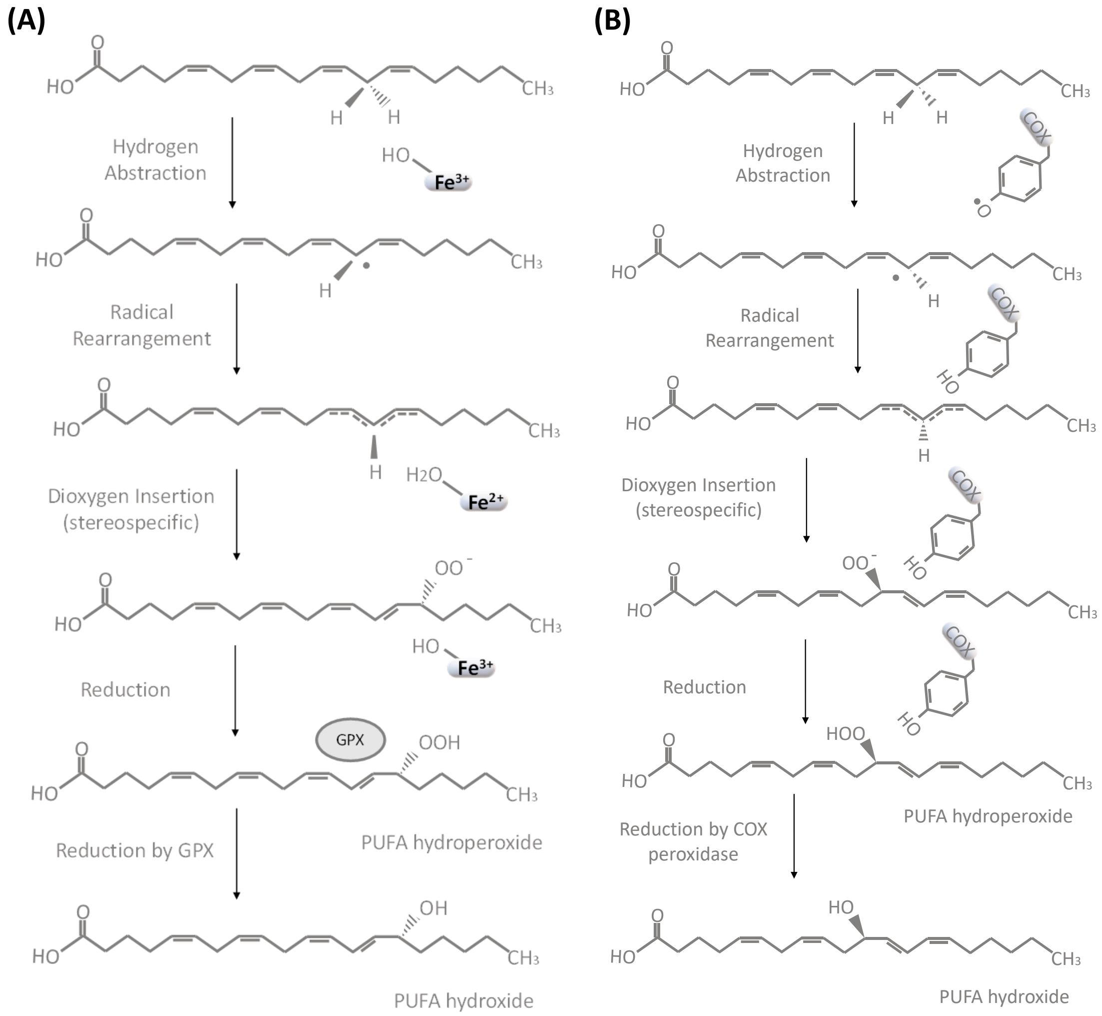

Figure 1.3: Lipoxygenase and cyclooxygenase catalysis
(Panel A) LOX catalysis is a redox reaction, where the non-heme ferric iron (Fe^{3+}) initiates the rate limiting step of the catalytic reaction through stereospecific hydrogen abstraction. A lipid alky radical is generated, through the iron reduction into its ferrous state (Fe^{2+}). The generated radical rapidly rearranges into a more stable configuration, followed by the insertion of dioxygen, producing a lipid peroxyl radical. The formed radical is then reduced by ferrous iron (Fe^{2+}) and protonated to generate a lipid hydroperoxide. The peroxidation reaction occurs between a pair of cis double bound, leading to a radical rearrangement, prior the introduction of molecular dioxygen on the opposite face. This antarafacial relationship is characteristic to all LOX catalysis, resulting in stereospecificity. The generated superoxide is protonated, generating (S)-hydroperoxide enantiomer as the end-product of LOX oxidation. The PUFA hydroperoxide can then be further reduced by glutathione peroxidase enzyme (GPX) to form an (S)-hydroxide, known as hydroxyeicosatetraenoic acid (HETEs). (Panel B) COX reaction starts with the activation of the enzyme, which originates a tyrosyl radical. this radical abstract the (S)-hydrogen from the carbon at position 13. After radical rearrangement, an oxygen can be introduced either at carbon-11 or 15. After protonation, either 11(R)-HETE or 15(R)-HETE is generate and the tyrosyl radical is recovered. Contrary to LOX catalyse, COX is also able to generate small amounts of 15(S). Figure based on O'Donnell et al. 2019 and designed using PowerPoint [5].

1.1.4. Cyclooxygenase

Cyclooxygenases, contrary to LOX, are heme-containing enzymes, with both di-oxygenase and peroxidase activities (Figure 1.3.B). There are two COX isoforms, which differ in their expression pattern. While COX-1 is expressed in most tissues, COX-2 is inducible by inflammatory cytokines and immune mediators, such as TNF-α, interferon γ and LPS. COX is responsible for the generation of PGs, important eicosanoids, with both functions in inflammation and homeostasis, including the control platelet activation[56]. COXs convert AA into PGG_2, which is then reduced to PGH_2, a precursor for other PGs, namely PGD_2, PGE_2, $PGF_{2\alpha}$, PGI_2, as well as thromboxane (TX) A_2, which is rapidly converted into TXB_2, generated by tissue-specific CYP isoforms[42,57].

Both COX-1 and COX-2, are also able to catalyse LOX-type reactions, generating limited amounts of 11(*R*)-HETE and 15(*R*)-HETE, as well as small quantities of 15(*S*)-HETE as a by-product of PG biosynthesis[58]. Interestingly, acetylsalicylic acid, commercially known as aspirin, induces the production of HETEs by COXs. Aspirin is a widely used COX-inhibitor, irreversibly inhibiting COX-1 while acetylating COX-2. Acetylated COX-2 can generate 15(*R*)-HETE and 11(*R*)-HETE, ultimately functioning as a LOX enzyme[59,60].

1.1.5 Cytochrome P450

AA is metabolised CYP to form less common HETEs isomers including 16-, 17-, 18-,19-, and 20-HETEs. In contrast with LOX, and similar to COX, CYP-generated HETEs are generally *R*-enantiomers[61,62].

1.1.6 Oxidized phospholipids

HETEs generated by LOX, COX and CYP can be incorporated into cellular membrane lysophospholipids, though the Lands'cycle, regardless of the enzyme responsible, forming enzymatically oxidized phospholipids (oxPLs) [59,60]. These enzymatically oxPLs (eoxPLs) display distinct physiological actions compared to free HETEs[39].

Generation of eoxPLs by blood cells occurs in a similar timescale to the free eicosanoid, with both generated acutely upon stimulation by inflammatory agonists [63–65]. This suggests that the hydrolysis, oxidation and re-acylation process is fast and highly regulated. As previously described in Section 1.1.1 of this Chapter, the Lands' cycle can form PLs by catalysing the incorporation of PUFAs into lysoPLs through LPATs enzymes. A total of 5 LPATs enzymes have been found to be expressed in human cells, and this provides specific degrees of specificity for both PUFAs and lysoPLs acceptors that goes beyond the abundance of substrate [64,66]. However, how exactly LPATs enzyme selectivity works is still unknown[64]. While oxylipins have established G-protein-coupled receptors[67], eoxPLs studies have so far only shown their impact as modulators of membrane biophysics [68] or through Peroxisome proliferator- activated receptor gamma (PPARγ) activation [69].

To further add complexity to this membrane-bound PLs can be directly oxidised by 15-LOX, unlike 5- and 12-LOX, and COXs, which can only oxygenate free FA substrates. The majority of eoxPLs are generated indirectly, after oxidation of the free fatty acid, followed by insertion of the resulting oxylipin into a membrane lysophospholipid using the enzymes of the Lands' remodelling cycle. For instance, in the case of platelets, the formation of 12(S)-HETE-PLs is exclusively generated through this type of indirect oxidation. However, 15-LOX isoforms are unique in their ability to oxidize membrane-bound PLs directly without requiring PLA_2 hydrolysis and re-esterification. However, *in vitro,* the rate of direct PL oxidation was significantly lower when compared to the free substrate[5].

EoxPLs generation is cell-specific. In fact, as previous described in Section 1.1.3 of this Chapter, LOX enzymes can be termed based on their cell expression, in addition to their characteristic oxygen insertion position. Several cells of the innate immune system express cell-specific LOX isoforms: 12-LOX in platelets (also termed platelet 12-LOX), 5-LOX in neutrophils, and 15-LOX in monocytes/eosinophils. These LOX enzymes generate 12-HETE-PLs, 5-HETE-PLs and 15-HETE-PLs, respectively. Furthermore, just like free oxylipins, these eoxPLs will be enantiomers specific, with the *S*-configuration almost exclusively derived from LOX oxidation, while the *R*-configuration is indicative of COX or CYP oxidation.

Last, OxPLs can also be originated non-enzymatically as a result of free radical reactions, linked to oxidative stress states during inflammation [5]. PUFAs are primary targets for reactive oxygen species (ROS) and reactive nitrogen species (RNS)[12]. Oxidative stress has long been identified as an important etiologic factor in the pathogenesis of chronic inflammatory diseases, hence, oxPLs, along with the lipid peroxidation process, have assumed a prominent role in inflammatory states. Thus, oxidation of PLs, either enzymatic or non-enzymatically, can lead to a generation of diverse structures due to the complexity of lipid substrates. Non-enzymatically generated oxPLs show a huge range of biological activities, which have been previously associated with pathological states [9].

1.1.7 Physiological functions of LOX products

LOX products are classified as immunomodulators, confirmed by their dysregulation in autoimmune diseases, such as systemic lupus erythematosus and RA[70,71]. Consequently, modulation of LOX oxidation has been considered a potential therapeutic target. However, available pharmacological inhibitors lack specificity, being either antioxidants or lipid analogues. Only one LOX-inhibitor is approved for clinical use: Zileuton, which is indicated for the treatment of asthma as a 5-LOX inhibitor, and prevents both the formation of LTs, as well as 5-HETEs[72].

Phagocytosis has profound consequences on innate and adaptive immune responses in the context of tissue inflammation [73,74]. 12/15-LOX in resident macrophages plays a crucial factor in the clearance of apoptotic cells, including lymphocytes and neutrophils. However, contrary to resident macrophages, the engulfment of apoptotic cells by inflammatory monocytes is blocked by 12/15-LOX activity [75]. In fact, it is through the exposure of eoxPLs, especially HETE-PEs, on the outer leaflet of resident macrophages that the uptake of apoptotic cells by inflammatory monocytes is actively blocked. Since inflammatory monocytes are able to present apoptotic cell-derived antigens to T-cells, blocking their phagocytosis, while allowing clearance by resident macrophages, is key for the maintenance of self-tolerance (Figure 1.4). This is confirmed by the break of self-tolerance seen in 12/15-LOX deficient animals, which develop spontaneous autoimmune-like diseases, including RA[5,75,76]. Based on this observation, eoxPLs can be considered pro-resolving mediators, playing a key role in the initiation of the resolution phase of inflammation[8]. However, uncontrollable generation of non-enzymatic oxPLs through oxidative stress could arise from different insults, particularly oxidative stress, and is often associated with excess cell death[77].

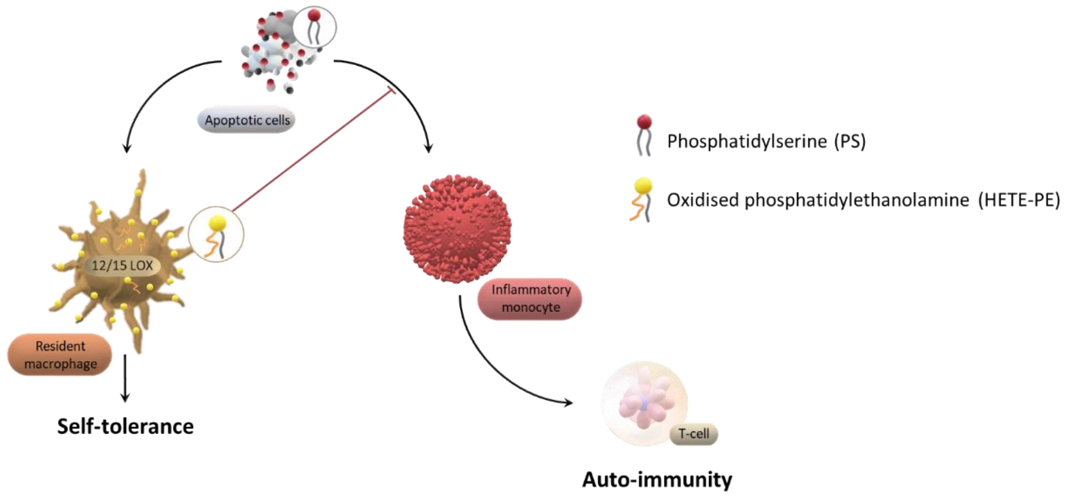

Figure 1.4: Oxidised phospholipids play a role in the maintenance of self-tolerance
Apoptotic cells expose PS, signalling macrophages for engulfment. This uptake is confined to resident macrophages expressing 12/15-LOX, inhibiting the uptake of apoptotic cells by inflammatory monocytes. Therefore, the subsequent antigen presentation of apoptotic cell-derived antigens by inflammatory monocytes is blocked, preventing the development of autoimmune like diseases. Figure adapted from O'Donnell et al. 2019 using PowerPoint [5].

Furthermore, free HETEs, along with other oxylipins can also be anti-inflammatory, For example, several 15-LOX-derived lipids, along with some COX metabolites, are known ligands for peroxisome proliferator-activated receptor-γ (PPARγ), a nuclear receptor with an important role in reducing the expression of proinflammatory mediators[78]. 15-deoxy-$\Delta^{12,14}$-prostaglandin J217, 15-HETE, 13-HODE and 9-HODE, along with other HODEs, have been described as PPARγ ligands[79–81], giving these lipids anti-inflammatory, anticatabolic and antifibrotic properties[78]. PPARγ activators inhibit nuclear factor kB (NF-kB)[82] while upregulation of antioxidant enzymes such as hemoxygenase[83]. Furthermore, PPARγ agonists potentiate the anti-inflammatory M2 macrophage phenotype[84]. Importantly, macrophages lacking 12/15-LOX are unable to activate PPARγ in response to IL-4[85].

In arthritis, PPARγ activation has been shown to inhibit inflammatory pathways and cartilage destruction[86]. Furthermore, active RA showed lower levels of PPARγ expression in monocytes, which ultimately displayed an inverse correlation between PPARγ and disease severity in these patients [87,88].

Despite these physiological functions, the effect of *Alox12* and *Alox15* gene products and their lipid products in human and mouse RA is poorly studied. So far only two papers have been published, with contradicting results[76,89]. In this thesis, the consequences of *Alox15* deletion will be studied during the development of arthritis in a murine model. In addition, these lipids will be analysed in human RA to further understand their impact on this disease.

1.2 Haemostasis & Coagulation

There is growing interest in the study of coagulation-driven inflammation and immunity as a result of an escalating incidence of *multimorbidity* conditions. The coexistence of multiple chronic illnesses is an increasing challenge for public health due to their subsequent high death rates[90]. An example of *multimorbidity* is the high incidence of thromboembolic events in auto-immune diseases, such as RA[91]. As an auto-immune disease initiated by local inflammation, RA is responsible for the systemic activation of the coagulation pathway that results in thrombosis, but so far the mechanisms involved are unclear[92]. Thus, the study of lipid mediators that link haemostasis and auto-immunity, either through direct signalling, or provision of a pro-coagulant membrane, as described below, is crucial for the development of effective therapies to reduce thrombotic risk in RA.

1.2.1 Coagulation pathway

Haemostasis is the complex mechanism that halts haemorrhage, allowing the continuous circulation of blood when challenged by vessel rupture. Upon vascular damage, a haemostatic response is triggered through vasoconstriction, platelet aggregation and coagulation. Coagulation is the most important response to the loss of integrity of blood vessels. This requires a sustained balance between anticoagulant response, which when disproportionate might lead to haemorrhage, and procoagulant responses, resulting in thrombosis[93,94].

The concept of coagulation has progressed from a cascade of independent and parallel pathways to an overlapping and complex process which requires cell participation, reflected in the form of platelet activation and tissue factor-bearing cells[95].

Coagulation factors are enzymes, generally, serine proteases, that circulate through the bloodstream in inactive, zymogen forms. Once activated, these serine proteases cleave and activate the next coagulation factor in the sequence. The activated forms of the coagulation factors are commonly denominated by their factor number followed by a lowercase “a”. This process eventually results in the activation of prothrombin to thrombin, which ultimately cleaves fibrinogen into fibrin, forming a thrombus[96].

The classic coagulation model is divided into two distinct pathways, extrinsic and intrinsic, which culminate in a final common pathway. The extrinsic pathway is triggered by the post-injury exposure of tissue factor (TF) from subendothelial cells, while the intrinsic pathway is an *ex vivo* pathway triggered by contact activation. Despite its importance *in vitro* assays, the intrinsic pathway contact activation appears to have no significant contribution *in vivo*, substantiated by the lack of bleeding disorders in patients with factor XII deficiency[97]. Factor Xa, generated from both pathways, along with its co-factor Va, culminate in the common pathway, cleaving prothrombin (factor II) to thrombin (factor IIa). Thrombin cleaves fibrinogen (factor I) into fibrin (factor Ia), as well as other coagulation factors which will be fed into the intrinsic pathway. Fibrin polymerises to generate a clot, which is stabilised by cross-linkage with factor XIIIa[96].

The classic model of coagulation has since been replaced by the cell-based model (Figure 1.5). This takes into account the importance of cells, and their respective surfaces, in the coagulation process. Traditionally, haemostasis has been divided into primary haemostasis, where a platelet plug is formed, and secondary haemostasis, responsible for the insoluble fibrin mesh clot structure. In the cell-based model, primary and secondary haemostasis take place concomitantly and are dependent on each other, being simultaneously restrained by the fibrinolytic pathway[95,98].

Platelets are a key player in the formation of the initial haemostatic plug. The platelet's phospholipid membrane provides a surface where activated coagulation factors assemble, generating thrombin. Upon vascular injury, platelets adhere to the exposed collagen in the subendothelial matrix through von Willebrand Factor (vWF), which cross-links the platelets' GPIb-IX-V receptor to collagen. This is particularly important in arteries and capillaries, where high shear exposes vWF binding sites, allowing interaction with platelets, and binding them to the collagen present in the vessel wall. It is through this attachment to the vessel tissue that platelets undergo activation. This induces morphological changes, including increased surface area and secretion of important coagulation factors, like factor V and vWF, as well as pro-coagulant and pro-inflammatory molecules such as ADP, serotonin, calcium and inorganic polyphosphate[99,100]. In addition, TXA_2 is synthesized *de novo* by activated platelets. The release of these autacoids promotes the recruitment of other immune cells and further activation of platelets. This results in an activation feedback loop, leading to platelet aggregation and the formation of a platelet plug, which temporarily seals the vessel injury. Aside from stimulating platelet recruitment, activated coagulation factors also trigger fibrin formation, which stabilizes the platelet plug and generates a blood clot[95,101].

Tissue factor (TF) is constitutively expressed in subendothelial cells such as fibroblasts and smooth muscle cells. In addition, it can be expressed in monocytes and microparticles (MPs) derived from monocytes in response to a variety of stimuli, such as inflammation. These TF-bearing cells support the extrinsic tenase complex constituted of TF, factor VIIa and calcium. The extrinsic tenase complex converts factor X to factor Xa and factor IX to factor IXa. The small amount of factor Xa generates a small amount of thrombin, which then activates co-factor V to co-factor Va and factor X to factor Xa. In addition, thrombin cleaves factor XI to factor XIa, which further activates platelets. This process is called initiation since only trace amounts of thrombin are generated.

This small amount of generated thrombin is rapidly suppressed by tissue factor pathway inhibitor (TFPI) that binds to factor Xa to form the TFPI/FXa complex, which then inhibits the extrinsic tenase complex. The initiation step is insufficient to generate a blood clot, therefore, in order to induce a burst of thrombin generation, a positive feedback loop is put in place involving factor IXa and its co-factor FVIIIa. This process is known as amplification and leads to the formation of the intrinsic tenase complex on the surface of activated platelets. The large quantities of factor Xa lead to the accumulation of prothrombinase complexes, resulting in the continuous generation of thrombin during the propagation phase. In this model, thrombin generation is a key element in the connection between primary and secondary haemostasis [95,98,101–104].

Lastly, thrombin activates factor XIII to factor XIIIa, enabling the formation of insoluble fibrin through covalent cross-linkage of soluble fibrin, which ultimately forms a blood clot. This build-up of aggregated platelets and fibrin deposits covers the injured vessel and eventually halts thrombin generation by inhibiting access of factor VII to TF. Excess thrombin can be directly inactivated by antithrombin, forming thrombin-antithrombin (TAT) complexes, or indirectly by binding to thrombomodulin, thus limiting the mass of the thrombus to a size proportional to the extent of the injury[95,98,101–104].

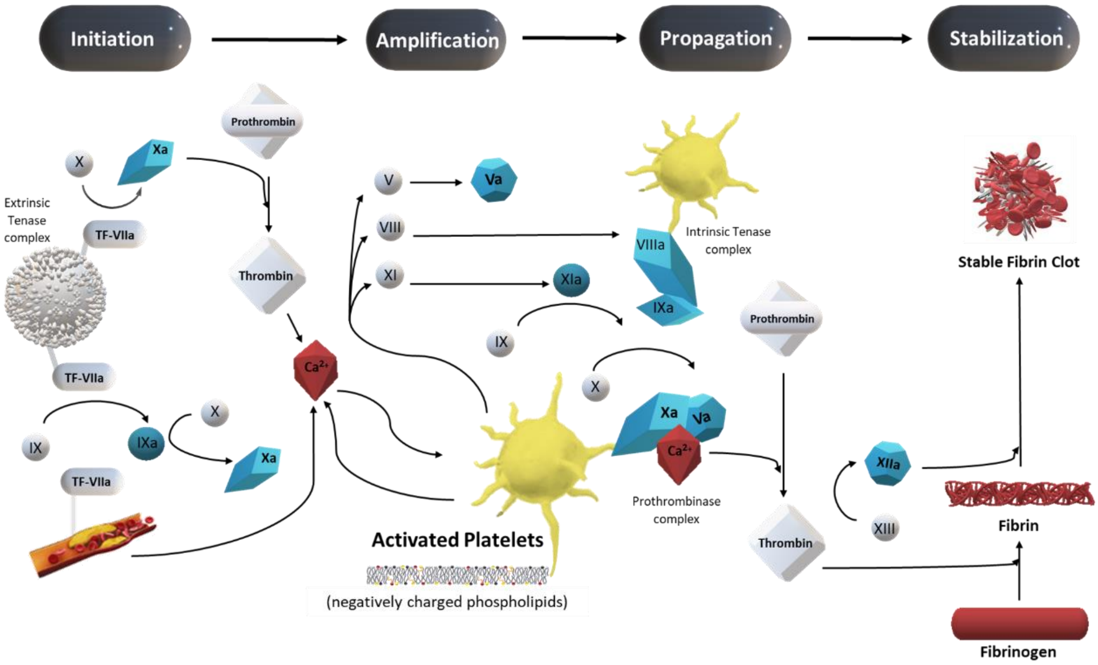

Figure 1.5: Cell-based Haemostasis Model
Secondary haemostasis provides stability to the platelet plug, originating the fibrin clot. This coagulation cascade is divided in four steps: Initiation, amplification, propagation, and stabilization. Activated platelets are a vital element in the coagulation cascade. It is in the phospholipid layer of the activated cells that the prothrombinase complex assembles, generating large quantities of thrombin, which ultimately form the insoluble fibrin strains that constitute a blood clot. Figure based on Pérez-Gómez et al. 2007 and designed by PowerPoint [102].

1.2.2 Fibrinolysis and coagulation inhibitors

Coagulation requires a balance between thrombus formation and its dissolution. Thrombogenesis must be limited to a critical threshold, proportional to injury extent, in order to prevent vessel blockage. Once the clot is large enough to prevent haemorrhage, its growth must be halted and subsequently retracted, simultaneously with the wound healing process[105]. Therefore, the inhibitory pathway adds another layer of complexity to the coagulation system.

An important coagulation regulator is the protease inhibitor antithrombin. Antithrombin acts by inhibiting factor Xa and thrombin, forming thrombin-antithrombin (TAT) complexes. This complex is clinically used as a thrombin generation marker. Together with heparin present on the endothelial layer, antithrombin inhibits factors IXa and XIa at the site of injury [104].

The fibrinolytic system, however, represents the focal antithrombotic mechanism. Fibrinolysis is the system that gradually dissolves blood clots during the healing process, reinstating vessel patency. This dissolution is an enzymatic process that occurs in parallel with the coagulation cascade. The fibrin clot is degraded by plasmin, generating fibrin fragments, such as X, Y, D and E fragments, as degradation products. These have anticoagulant properties since they obstruct fibrin polymerization and platelet activation. The D-Dimer fragment, contrary to other fibrin fragments, is a specific breakdown product of cross-linked fibrin, and consequently, a frequently used clinical marker of thrombosis. A failure to limit thrombin generation can lead to exacerbated fibrin production, resulting in widespread thrombosis[101,104,106,107]. Despite the increased risk of thrombosis in RA[91], the impact on the fibrinolysis process is not well understood, therefore, it will be investigated in this thesis.

1.2.3 Thrombosis

Thrombosis is considered *haemostasis in the wrong place*, resulting in compromised blood flow that ultimately leads to tissue damage[108]. Thrombotic diseases including myocardial infarction, ischemic stroke, or deep vein thrombosis, represent major healthcare issues and are leading causes of death worldwide[109]. When coagulation control feedback fails, a procoagulant vicious cycle is generated, leading to uncontrolled thrombus growth, which results in partial or total vessel occlusion[110]. Thrombosis can occur in either venous or arterial vessels and can have distinct pathogenic phenotypes. The architecture of the clot is dependent on blood flow, turbulence and shear, along with platelet concentration. These are typically different between arterial and venous blood circulation, resulting in structurally different clots[111]. Arterial thrombosis, also known as atherothrombosis, is the development of a thrombus triggered by the rupture of atherosclerotic plaques, or atheromas. The exposure of damaged endothelium and leak of highly thrombogenic content of the atheroma to high-shear blood circulation leads to the formation of large platelet aggregates, which recruit a high number of leukocytes, forming a white clot. By contrast, venous thrombi are mainly composed of erythrocytes trapped in a fibrin laminar structure, forming a red clot. The generation of venous clots is not correlated with endothelial damage but rather associated with activation of the coagulation pathway due to a pro-inflammatory response [112,113].

A new concept in thrombosis has arisen due to the importance of the immune system in the formation of the clot. Immunothrombosis consists of the activation of coagulation assisted by the innate immune system, particularly monocytes, neutrophils and dendritic cells in response to sepsis-driven inflammation. It is through the activated innate immune response that coagulation is initiated and propagated via platelet activation, leading to thrombosis. The action of inflammatory cytokines further reinforces the involvement of the immune system [114,115]. Immunothrombosis serves different purposes in the immune system. First, it enables the confinement of pathogens by trapping them in the fibrin mesh and by impairing pathogen circulation through the formation of microthrombi in microvessels surrounding the damaged/inflamed tissue.

A small amount of microthrombi is enough to preclude the extravasation of the pathogens, centring the immune response in one place. Lastly, fibrin and fibrinogen promote the recruitment of immune cells to the inflamed site, triggering an immune response. This results in an overlap of haemostasis and immunity roles among immune cells[112,115]. Therefore, immunothrombosis can be viewed as a component of the innate immune system in its own right, outlining a clear connection between coagulation, inflammation and immunity that remains to be fully understood.

Recent studies have linked the abnormal function of the innate immune system to the development of thrombotic events, including deep vein thrombosis[116,117] and arterial thrombosis[118,119]. The accumulation of cellular and molecular mediators following sepsis is often associated with the continuous induction of immunothrombosis[112,120]. Therefore, thrombosis may be caused by exacerbated activation of the immune system, either directly by cellular mediators or indirectly by proinflammatory cytokines, and not necessarily due to direct coagulation dysfunction. Despite auto-immune diseases being responsible for immune cell activation, along with the generation of pro-inflammatory mediators, there is still a lack of studies concerning immunothrombosis in this disease[112,114]. Therefore, understanding the role of immune cells in coagulation, along with cytokines, is essential to prevent the increase in thrombotic events in autoimmune diseases, such as RA.

1.2.4 The role of phospholipid membranes in driving coagulation

The plasma membrane constitutes a key player in haemostasis, providing a negatively charged lipid surface for the assembly of the intrinsic tenase complex (IXa/VIIIa) and the prothrombinase complex (Xa/Va). Plasma membranes consist of microdomains with a diverse lipid composition. An asymmetry of lipids across the membrane occurs not only horizontally, through the formation of lipid rafts, rich in cholesterol and glycosphingolipids, but also vertically, through a distinctive composition between the inner and outer membrane leaflet. As previously described in Section 1.1.1 of this Chapter, in resting cells, the outer leaflet is mainly composed of sphingomyelin and PC, all neutrally charged phospholipids, while aminophospholipids, more commonly PS and PE, are sequestered in the membrane inner leaflet (Figure 1.6)[5,6]. This asymmetry is maintained through the action of ATP-dependent translocators, namely flippases, which shuttle aminophospholipids inwards to the cytoplasmic leaflet, and floppases, which shuttle in the opposite direction. This membrane asymmetry is maintained until cell lysis, damage, or activation. Upon cell activation, aminophospholipid translocases are inhibited, while calcium-dependent scramblase is activated. This allows PS and PE to shuffle to the outer leaflet, resulting in a loss of membrane asymmetry[121,122]. These aminoPLs are responsible for the negatively-charged membrane, essential for coagulation. The negatively charged GLA domain in coagulation factors, abundant in γ-carboxyglutamate, associates with the negatively charged aminophospholipids on the activated membrane cell in a calcium-dependent interaction[68].

Despite PE being considerably more abundant, by itself it has no significant clotting activity. In fact, PS is the key phospholipid required for the assembly of coagulation factors. Nevertheless, PE is required to establish binding sites for blood clotting proteins[123]. It is hypothesised that PE cooperates with PS to create membrane-binding sites, by sustaining more phosphate-specific interactions, which frees PS to engage with clotting proteins[123,124] The extended phosphate-specific interactions by PE are believed to be related to its less bulky phospholipid headgroup, which provides increased flexibility. Based on this hypothesis, several glycerophospholipids can be equally effective in synergizing with PS, such as *myo*-inositol (PI) or glycerol (PG), as well as other negatively charged phospholipids. The role of PI and PG in coagulation has been already observed *in vitro*, however, due to their minor presence in the phospholipid membrane, their effect *in vivo* is been generally dismissed[123,125].

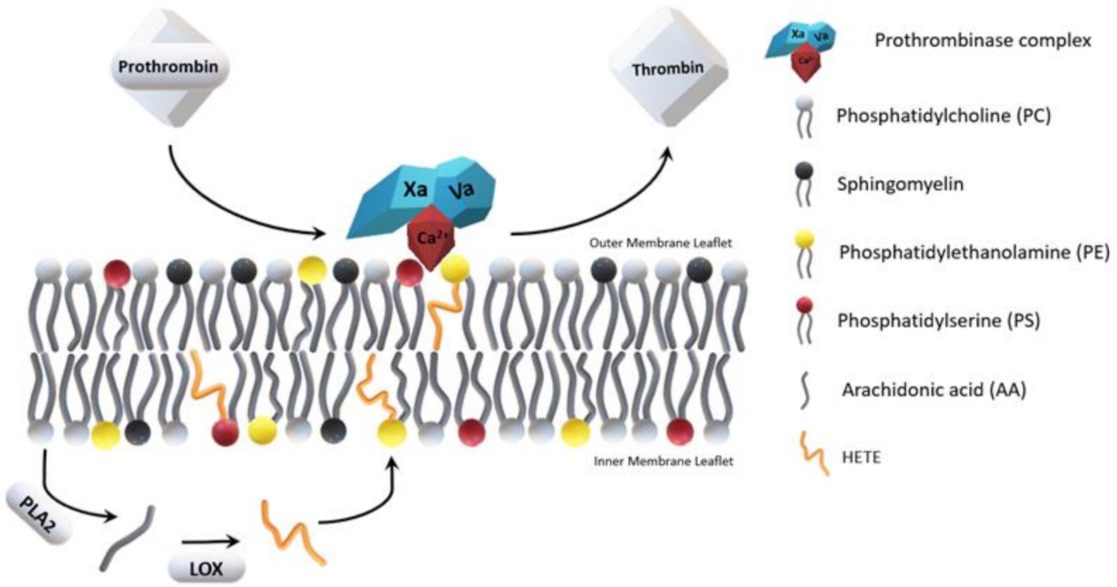

Figure 1.6: Phospholipid membrane driving coagulation

The asymmetric phospholipid membrane is comprised of neutral phospholipids, such as phosphatidylcholine (PC) and sphingomyelin, and aminophospholipids (negatively charged phospholipids), such as phosphatidylserine (PS) and phosphatidylethanolamine (PE). PS is the key phospholipid supporting coagulation; however, PE is essential to boost coagulation. Oxidised phospholipids also increase coagulation due to their electronegative charge. Phospholipase A2 (PLA_2) releases arachidonic acid (AA) from the cell membrane. Once free, AA can be oxidized by lipoxygenase (LOX), generating hydroxyeicosatetraenoic acid (HETE), which can be re-esterified into oxidised phospholipids (HETE-PLs) and reintroduced into the phospholipid membrane. Figure adapted from O'Donnell et al. 2019 using PowerPoint [5].

Another class of phospholipids has been shown to participate in coagulation. As previously described, oxPLs can be generated enzymatically by particular circulating immune cells through the action of cell-specific human LOX, namely 12-LOX in platelets, 5-LOX in neutrophils, and 15-LOX in monocytes/eosinophils, that generate 12-HETE-PLs, 5-HETE-PLs and 15-HETE-PLs, respectively [5,68]. These PLs are also implicated in normal haemostasis[125].

Based on molecular dynamics simulation studies, the hydroxyl group of the HETE moiety in the HETE-PLs appears to be positioned near the outer surface of the membrane, where could potentially interact with calcium ions. In the upward-facing position, the hydroxyl group could potentially establish hydrogen bound with neighbouring lipid phosphate, and even some carboxylic acid groups, thus facilitating the formation of negatively charged spaces. Alternatively, by pushing headgroups apart, the hydroxyl group could enable greater accessibility to the phosphate group, offering an anchor for positively charged calcium ions. The binding of calcium to the membrane surface through HETE-PLs could further increase the accessibility of coagulation factors to the negatively charged PS headgroup. This was so far only seen *in vitro* assays, where these lipids enhanced binding and activation of coagulation factors (Figure 1.7)[5,68,125].

The importance of eoxPLs in coagulation has been supported by demonstrations of a bleeding phenotype in *Alox15*$^{-/-}$ and *Alox12*$^{-/-}$ mice. Local administration of HETE-PEs halted bleeding in these mice, which displayed a decrease in tail bleeding time[125]. HETE-PLs were also able to prevent a haemorrhaging phenotype in mice with haemophilia A, a disease characterized by a deficiency in the VIII coagulation factor. This was further corroborated by the correction of thrombin generation in FVIII-deficient human plasma [68]. In addition, a tail injection of HETE-PLs resulted in increased TAT complexes in wild-type mice[125]. Furthermore, non-enzymatically generated oxPLs have also been observed to up-regulate TF in endothelial cells *in vitro*, a response which was not mirrored by native phospholipids[126].

The characterisation of blood cell levels of aminophospholipids and oxPLs from patients with RA and healthy controls might reveal how the development of coagulopathies occurs in this disease. Therefore, it is vital to study these lipids to determine their potential as therapeutic targets to prevent thrombotic disorders in these patients.

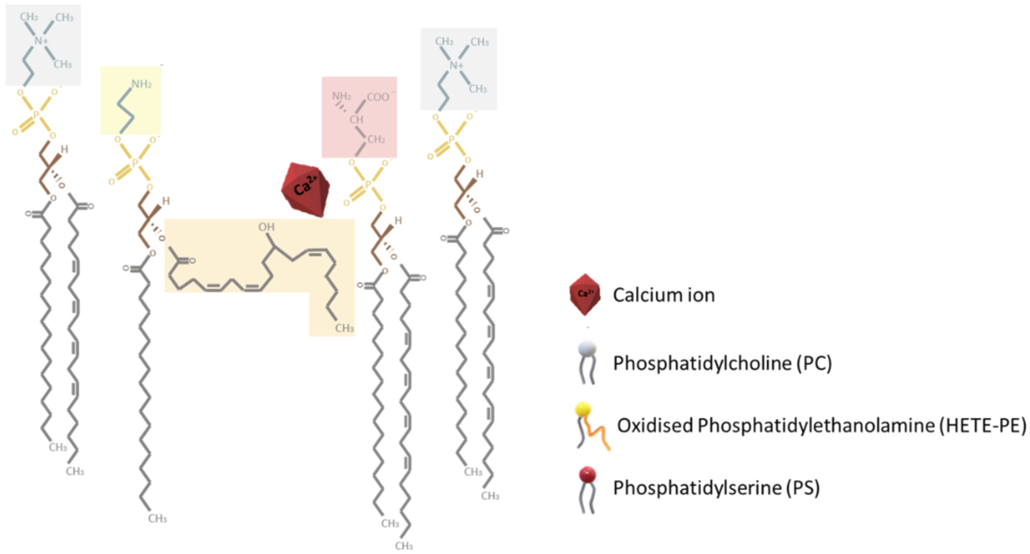

Figure 1.7: HETE-PL hydroxyl group mechanism to promote coagulation.
The hydroxyl group of HETE-PLs is proposed to establish hydrogen bounds with phosphate groups, generating a negatively charged space, which might act as anchor for the calcium ion. The oxPLs would push the phosphate group away, offering greater accessibility to coagulation factors, and therefore promoting coagulation. Figure based on Lauder at al. 2017 and design by PowerPoint [125].

1.3 Rheumatoid Arthritis

Rheumatoid arthritis (RA) is an auto-immune disease characterized by chronic inflammation affecting synovial joints in a symmetric pattern, which ultimately results in cartilage and bone degradation. Joint inflammation leads to the formation of abnormal granulation tissue, known as pannus, and to hyperplasia of the synovial membrane, developing a condition known as synovitis, causing pain and impaired mobility[127].

RA displays an overall incidence between 0.5% to 1% worldwide [128], with a clear prevalence in females over males, starting with a 4:1 female-to-male ratio in the younger population, to 2:1 after the age of 60. RA development is associated with genetic and environmental risk factors that include smoking, obesity and hormonal factors (menopause) [129].

Increased reactivity of immune cells is central to an auto-immune disease such as RA. The abnormal immune response causes cell recruitment to the joints, producing cytokines, which instigate an inflammatory reaction and generation of damaging oxidants[130]. In addition, in RA, B-cells produce self-reactive antibodies[131], which along with cytokines, induce an influx of immune cells, coupled with increased angiogenesis, establishing a link between immunity and inflammation. The presence of autoantibodies is not essential for a RA diagnosis; however, it is associated with more severe symptoms and increased mortality [132]. The two most common autoantibodies in RA are against citrullinated proteins (ACPA) and rheumatoid factor (RF). Interestingly, ACPAs can be detected in circulation long before diagnosis, establishing the pre-RA phase [132]. Overtime, and with disease development, the concentration of these auto-antibodies increases, until effective therapy is achieved, resulting in a decrease in both ACPA and RF levels [132].

RA is highly heterogeneous, as reflected by the different rates of disease progression and structural damage, as well as inconsistent response to therapy [133,134]. Different synovial pathotypes have been described by *Lewis et al.*, namely myeloid- or macrophage-rich, lymphoid-rich and fibroblastic-rich pauci-immune pathotypes, through the analysis of synovial tissue transcriptome of early/naïve RA patients. These pathotypes are suggested to be a spectrum of synovium immune cell infiltration, with the fibroblastic-rich (pauci-immune) at the lower end lacking in immune-inflammatory infiltrates. In the middle of the spectrum is the diffuse-myeloid group with a rich infiltrate composed of macrophages/ monocytes. The spectrum is then finished with the lympho-myeloid group, with a diverse immune cell infiltrate that includes natural killer cells and plasmacytoid dendritic cells, in addition to displaying aggregates of B and T lymphocytes, which ultimately form ectopic lymphoid structures. This stratification is further evidenced by the correlation observed between disease severity and the increase in immune cell infiltration of the synovial tissue of these patients [134].

Whole blood transcriptome of RA patients was also analysed by *Lewis et al.*; however, there were significantly fewer differently expressed transcripts compared to synovium tissue, resulting in less differentiation between pathotypes, with only the delineation of fibroblastic-rich (pauci-immune) and diffuse-myeloid groups. Nevertheless, this poses the question of whether differences can be observed in either protein or lipid content of these cells between the distinct pathotypes [134].

1.3.1 Rheumatoid Arthritis and Thrombosis

A classic example of pathophysiological *multimorbidity* is displayed in RA[92] since several extra-articular manifestations are seen, including pulmonary involvement or vasculitis, and systemic comorbidities [128]. One example, with direct relevance to my thesis, is the increased risk factor for cardiovascular disease in RA patients, associated with both arterial and venous thromboembolic events [91]. Not only RA but autoimmune diseases in general, such as chronic inflammatory illnesses, often display a hypercoagulation state [135]. Their characteristic elevated immune response forms a vicious pro-inflammatory loop, leading to thrombosis and cardiovascular complications. In the case of RA the incidence of thrombosis, both arterial and venous, is increased from 30 % to 50 % when compared to a healthy population or even to osteoarthritis patients [91,135].

The increase in thrombotic incidences in RA patients has also been described when compared to osteoarthritis patients population [91,135]. Osteoarthritis (OA) is often considered a non-auto-immune disease, which causes joint degeneration, affecting primarily the articular cartilage [136]. Compared to RA, OA presents considerably lower inflammation levels and reduced immune cell involvement, and therefore, is often used as a comparator [137]. In clinical studies, synovial fluid collection from living healthy controls is extremely difficult due to low volume in healthy synovium (≈ 1 ml) and the invasive nature of the procedure [138]. Therefore, OA synovial fluid has often been used as a non-immunological arthritis control for RA synovial fluid, further establishing OA as a disease comparator in numerous RA studies, and vice-versa [139,140].

The thrombotic phenotype observed in RA is not restricted to the systemic circulation. A hypercoagulation state in the synovial cavity has been frequently observed during arthritic flares. This leads to the formation of *rice bodies*, an agglomerate of entrapped cells within a fibrin mesh, which is often associated with severe pain[141]. Molecular markers such as TAT complexes and D-dimers levels are also significantly increased, along with TF activity in the joint. Synovial TAT levels correlate with the augmented levels of TF activity, suggesting that this local hypercoagulation state is TF-mediated. In addition, increased D-dimer levels correlate with CRP and TAT levels, implying that fibrinolysis is associated with inflammation. TF expressing cells from the arthritic synovial tissue might overspill to the intravascular circulation, activating systemic coagulation and inflammation[142–144].

Previous studies confirm an active coagulation process in RA, both extra and intravascular[91,145] However, the molecular mechanisms responsible for thrombosis in these patients are not fully understood. A series of factors are assumed to contribute to this thrombotic phenotype, namely hypercoagulability (dyslipidaemia and fibrin deposition), endothelial dysfunction (increased expression of adhesion molecules), inflammation (acute-phase reactants) or direct induction of a prothrombotic state (decrease antithrombin III, protein S and C). Nevertheless, the role of the pro-thrombotic membrane of immune cells, including platelets, has not been analysed in RA yet.

Plasma from RA patients displays high levels of thrombin activation, reflected by elevated TAT complexes [142,146]. Besides the formation of clots, coagulation can also be influenced by abnormal fibrinolysis. The proteolysis process of fibrin generates degradation products called D-dimers, widely used as a biomarker for venous coagulopathies. Due to their unique fibrin cross-linkage, D-dimers cannot be further degraded, therefore they constitute a useful marker for fibrinolysis. D-dimers were previously shown to be increased in human RA, both in synovial fluid and in plasma[142,147,148]. However, their formation in arthritis *in vivo* models has not been reported. Furthermore, other thrombin fragments, such as Bβ12-42 and fibrinogen have also been described as increased in human RA. Therefore, in this thesis, plasma from arthritic mice will be analysed for both coagulation and fibrinolysis, by quantifying TAT complexes and D-dimers.

In RA, TF activity positively correlates with plasma CRP levels, synovial fluid volume and leukocyte count, further suggesting that thrombin activation is TF-mediated[142,147,148]. Furthermore, plasmin is frequently observed in RA patients' plasma, indicative of increased fibrinolytic activity[149]. RA platelets also display an altered activation and reactivity state, specifically a small, but consistent, increase in mean platelet count, along with an increased platelet volume[150–152].

However, prothrombin and thrombin times are found normal in the plasma of RA patients[148]. Normal prothrombin time reveals there are no defects in the extrinsic and common coagulation pathways, and therefore, it indicates that in human RA, the increased coagulation described is not due to a dysfunction in coagulation factors [153,154]. Furthermore, TF activity doesn't appear significantly altered despite the observed positive correlation with CRP levels in the plasma of these patients [142]. The heightened levels of coagulation markers might be due to an increased intravascular activation or an overspill of the inflamed joints[142].

Virchow's triad postulates that thrombosis is a combined result of vessel wall condition, blood flow and blood composition alterations[155]. And in fact, endothelium dysfunction plays a pivotal role in thrombosis in RA. During inflammation, endothelial cells become activated, forming a prothrombotic surface[156]. Endothelial cells are responsible for the increased expression of adhesion molecules, proinflammatory and prothrombotic factors. Endothelial dysfunction, despite being more associated with atherogenesis, is equally important in the venous thrombosis process. Upon inflammation, endothelial cells may become dysfunctional, producing high levels of pro-inflammatory cytokines, namely IL-1, IL-6 and TNF-α, which deregulated the vessel tonus and permeability[157,158]. The increase in coagulation factors is accompanied by impaired fibrinolysis. As a response to inflammatory cytokines, such as TNF-α and IL-1, an unbalance between profibrinolytic and antifibrinolytic factors develops, resulting in an ineffective fibrinolytic response. The build-up of fibrin meshwork serves as a matrix to which inflammatory cells adhere, resulting in a sustained inflammation state, which often triggers thrombosis[157,158]. This overall dysregulation may result in systemic vasculitis, an inflammatory condition targeting blood vessels that derives from endothelial cell activation and is often associated with RA[159]. The increased circulatory levels of immune cells and cytokines derived from endothelial activation suggest a complex systemic mechanism beyond the spill of these molecules from the synovial cavity. Therefore, it is important to study these immune cells in circulation, and analyse their procoagulant membrane in RA.

In summary, despite the elevated thrombotic risk and evidence for dysregulated coagulation parameters, how the procoagulant membrane is involved is still unknown. Considering the role of oxPLs in coagulation, and the lack of studies regarding their impact their pro-thrombotic impact in arthritis, especially in murine models, this thesis will focus on the analysis of these lipids in membranes of immune cells from both murine arthritis and human RA.

1.3.1.1 Arterial thromboembolism in Rheumatoid Arthritis

RA is associated with a characteristic systemic inflammation phenotype along with an increased incidence of arterial thromboembolism [91]. This is mainly due to the rupture of an atherosclerotic plaque [160]. In fact, RA patients display a 3 times higher prevalence of carotid atherosclerotic plaque compared to healthy controls [161].

Curiously, RA is associated with a phenomenon known as the *Lipid Paradox,* where lower levels of total cholesterol (TC), low-density lipoprotein cholesterol (LDLc) and high-density lipoprotein cholesterol (HDLc) are observed. These lipid levels correlate negatively with the increasing risk of cardiovascular events in RA. The decrease of these lipids is proposed to modulate immune functions and possibly alter signalling pathways that instigate endothelial dysfunction and upregulation of atherogenic T cells, both mechanisms responsible for atherosclerosis [162,163]. Indeed, an increased prevalence of atherosclerosis is found in RA patients [164]. Furthermore, RA patients' atherosclerotic plaques are morphologically different to those in the non-RA atherosclerotic population. Specifically, RA-related plaques display greater instability and are more prone to rupture [165]. Once the rupture occurs, highly thrombogenic content is exposed to blood flow, while, concomitantly, occluding partially or completely the vessel, which results in an acute thrombosis event [166].

1.3.1.2 Venous thromboembolism in Rheumatoid Arthritis

RA has only been recently recognized as a risk factor for venous thromboembolism (VTE)[167]. As a coagulopathy, VTE includes deep vein thrombosis and pulmonary embolism, both of which have a higher incidence in RA[168]. In fact, the incidence of VTE is known to be correlated with disease activity, more specifically to the high inflammatory response characteristic of RA flares[169]. The underlying mechanisms for the increased incidence of VTE in RA patients are supported by Virchow's triad [157]. As an inflammatory process, rheumatic diseases modulate endothelial activation, stasis of blood flow and blood cell disorders, leading to the observed hypercoagulation state. Plus, the increased levels of procoagulant and fibrinolysis factors observed in RA appear to be directly involved in the pathophysiological mechanism of VTE observed in these patients [157].

Acute-phase reactants, such as CRP, fibrinogen and von Willebrand factor (vWF), are responsible for the increase in plasma viscosity present during inflammatory RA[157,170]. Increased blood viscosity due to acute-phase proteins is a known characteristic of inflammation, as measured by erythrocyte sedimentation rate and plasma viscosity. Plus, RA patients frequently display pathologic megakaryocytopoiesis and thrombocytopoiesis, further boosting viscosity[171]. Subsequently, this increased viscosity leads to blood flow disturbances. A turbulent blood flow, coupled with sedentary behaviour common during rheumatic flares, leads to a high-risk factor of VTE in inflammatory RA[157,170].

1.3.2 Rheumatoid Arthritis therapy and thrombosis

RA therapies consist in achieving remission, coupled with control of acute inflammation symptoms. Glucocorticoids and nonsteroidal anti-inflammatory drugs (NSAIDs) are prescribed for the treatment of inflammatory symptoms, specifically pain management. Interestingly, NSAIDs are COX inhibitors, therefore, prevent the synthesis of thromboxane A_2, a potent platelet activator and aggregator, which ultimately results in an increased bleeding time. In fact, aspirin is a commonly used antiplatelet drug due to its irreversible blockage of COX, through covalent acetylation of the active site of this enzyme. With other NSAIDs, such as ibuprofen and naproxen, the inhibition is reversible [160,172]. Despite the common intake of NSAIDs, including aspirin, by RA patients, thrombosis is still highly increased in these patients. Platelets have a lifespan between 7 to 10 days[173], therefore, healthy volunteers were asked not to intake NSAIDs 14 days before blood collection, and excluded accordingly so as to not alter coagulation markers and lipid oxidation.

In order to achieve remission, RA therapy includes disease-modifying anti-rheumatic drugs (DMARDs), which can be divided into two groups: biological and synthetic, which are then further classified into conventional synthetic and targeted synthetic DMARDs[174].

Monotherapy of conventional DMARDs, such as methotrexate, sulfasalazine, leflunomide and hydroxychloroquine, is the first-line treatment of RA. In fact, methotrexate is considered an anchor in RA therapy. However, upon increased disease activity, a combination with biological DMARDs is introduced. The biological therapies include inhibitors of TNF-α, such as infliximab and adalimumab, interleukin-6 (IL-6) antagonists, such as tocilizumab, chimeric anti-CD20 monoclonal antibody, rituximab and T-cell co-stimulation blocker, abatacept. These biological therapies decrease the hyperactivate state of the immune system, alleviating inflammation. In addition to the biological, new DMARDs are being introduced in combination with conventional. These therapeutic agents, such as baricitinib and tofacitinib, target the Janus-activated kinase

(JAK) transduction pathway, suppressing the production of inflammatory mediators[128,175].

The impact of DMARDs on thrombosis became a concern when both the European Medicines Agency and the U.S. Food and Drug Administration issued a warning about the use of Tofacitinib in high doses. This JAK inhibitor, at a dose of 10 mg twice a day, was associated with an increased risk of blood clots.[176,177] Large observational studies are required to properly analyse the effect of JAK inhibitors in thrombosis and differentiate these results from the impact of comorbidities attributed to RA. In the case of other DMARDs, there are conflicting results regarding thrombosis incidence. While an increased risk of hospitalization for VTE was found in RA patients initiating biological therapy[178], other populational studies found no significant difference in VTE incidence between biological and conventional DMARDs [179], while other studies described reduced coagulation with Tocilizumab, a biological DMARDs in comparison with methotrexate, a conventional DMARD [180]. Nevertheless, these studies vary massively, with Kim et al. analysing a total of 29,481 RA patients and observing an increase in VTE hospitalizations for RA patients initiating different bDMARDs compared to methotrexate and other conventional DMARDs in the United States of America[178], versus Davies et al. study which analysed 15,554 British RA patients displaying no significant differences between anti-TNF therapy (a common bDMARDs) and conventional DMARDs, which were not specified [179]. Lastly, the reduced coagulation with Tocilizumab compared to methotrexate was observed in a small population of RA patients from the Netherlands by Dijkshoorn et al. [180] Therefore, the contradicting results might be the result of the distinct populations and patient numbers investigated in these studies, along with the variety of drugs within the DMARDs and bDMARDs analysed.

Overall, the impact of different medications on auto-immune associated coagulopathies further complicates the understanding of thrombosis in these patients.

1.4 LOX and COX in Rheumatoid Arthritis

In this thesis, I will not only analyse LOX-generated lipid mediators in arthritis, but I will also use *Alox15* knockout mice to further understand the impact of lipids generated by 12/15-LOX in inflammation and coagulation upon arthritis induction.

Previous studies have shown a distinct expression profile of *ALOX* and *COX* gene expression in the synovial tissue of RA patients[181]. For example, fibroblast-like synoviocytes express high levels of COX-1, COX-2[182] and 15-LOX [89] during active states of RA. Plus, 5-LOX expression was significantly increased in the lining and sublining macrophages from RA patients' synovial tissue when compared to osteoarthritis tissue[183]. RA synovial fluid and serum also displayed high levels of LTB_4, a downstream product of 5-LOX and a pro-inflammatory mediator with powerful chemotactic capacity[184]. Consistent with increased 5-LOX expression in RA, LTB_4 levels were elevated in synovial fluid of RA compared to osteoarthritis, with its levels correlating with disease activity[185]. In addition, high amounts of 5S-12S diHETE, an isomer of LTB_4 and a transcellular biosynthesis product, were also increased in the synovial fluid of RA patients[186]. This increase in 5-LOX products indicates a possible role of 5-LOX-derived oxylipins in RA pathogenesis[187]. This hypothesis is further supported by the protection from RA development in mice lacking 5-LOX[183].

Increased expression of 15-LOX has been described in both RA and OA patients in resident macrophages, fibroblasts and endothelial cells of arthritic synovium tissue[183], as well as in articular chondrocytes in OA joints[188]. The expression of 15-LOX in RA synovium was significantly higher than in OA synovium. Curiously, intraarticular administration of corticosteroids in RA patients leads to the decreased expression of 5-LOX, while leaving the expression of 15-LOX unchanged[183]. However, despite high 15-LOX expression, 15-HETE products were not detected in the synovial fluid of these patients [183].

A similar increase in *Alox15* expression was also found in mouse synovial tissue after arthritis induction by serum-transfer[189] and in joints of rats upon destabilization of the medial meniscus, a common OA model[190]. Krönke *et al.* showed that when *Alox15*-deficient mice were induced to overexpress TNF-α, they exhibited increased destruction of hind paws, accompanied by enlarged inflammatory infiltrates when compared to WT TNF- α Tg mice[189]. Additionally, these mice display enhanced gene expression of IL-6 and IL-1β, leading to pronounced systemic inflammatory response[189]. This indicated a detrimental effect of *Alox15* deletion in arthritic mice.

Separately, *Krönke et al*. studied *Alox15*-deficient mice subjected to a K/BxN serum-induced arthritis model[189]. This is induced by the transfer of serum from arthritic K/BxN tg mice to naïve and causes an inflammatory response through systemic self-reactivity. Therefore, this model is exclusively mediated by antibodies. Here, antibodies against the ubiquitously expressed enzyme glucose-6-phosphate isomerase (G6PI) lead to the formation of immune complexes, which activate different innate immune cells such as neutrophils, macrophages, and even mast cells[191]. Upon arthritis induction in *Alox15*$^{-/-}$ mice through K/BxN serum transfer, an exacerbated arthritis phenotype was observed. An aggravated bone erosion with pronounced joint swelling and an increase in IL-6 and IL-1β expression reflected a more severe and accelerated inflammatory arthritis upon *Alox15* deletion[189].

In contrast to the above studies, arthritis in the adjuvant inducted model was inhibited in *Alox15*$^{-/-}$ mice when measured by paw swelling and cartilage destruction[89]. However, a significant limitation of this model is the capacity to effectively cure arthritis through the use of COX inhibitors, which is not mirrored in human disease [192]. With both COX and LOX being major players in oxylipins production, a cure of adjuvant-induced arthritis observed by *Wu et al.* through the deletion of *Alox15* was not surprising.

Notably, no *in vivo* arthritis model is perfectly aligned with human disease. Although, two distinct murine arthritis models demonstrated that 12/15-LOX were protective against inflammatory arthritis. Nevertheless, these conflicting results indicate that each model has a distinct pathological mechanism of RA, and each model shows different results upon LOX modulation.

1.4.1 Antigen -induce arthritis murine model

There is no universal pathological murine model of RA, nevertheless, the different arthritis phenotypes can be studied separately in order to draw parallels with the human disease. To do this, I will study different arthritis phenotypes generated using the antigen-induced arthritis (AIA) murine model and analyse their lipid profile, as well as coagulation and inflammatory markers. This model will allow me to characterize procoagulant lipids, namely eoxPLs, in murine arthritis, as well as determine their potential impact on inflammation and coagulation by using different disease phenotypes.

AIA is one of the most commonly used experimental murine models for the study of inflammatory arthritis [193]. This model is induced through systemic immunization against methylated BSA (mBSA) emulsified with an immune response enhancer, complete Freund's adjuvant (CFA) coupled with *Bordetella pertussis* toxin. After pre-immunization, arthritis is induced in both knees through intra-articular injection of mBSA which, as a cationic antigen, is retained in the negatively charged cartilage of the joint. An Arthus reaction is induced, where an immune complex-mediated reaction occurs, triggered by the deposition of antigen-antibody complexes. This generates a humoral and cell-mediated immune response, dependent on $CD4^+$ T lymphocytes and neutrophils[194,195]. In addition, AIA induction results in local vasculitis, accompanied by oedema and pain, therefore, sharing a lot of symptoms with human RA [196]. A localized inflammatory arthritis is therefore induced in the injected joints. This model has been previously described as depicting two different disease phases, early arthritis (Day 3), featuring an acute inflammatory response, and established arthritis (Day 10), exhibiting chronic-like characteristics.

Early disease (Day 3) is characterised by severe synovitis, resulting in the recruitment of innate leukocytes, such as neutrophils and inflammatory macrophages, which marks the acute response. Established disease (Day 10), represents the chronic-like phase of AIA, characterised by a high T-cell response, as well as B-cell infiltration. Higher levels of Th1 cytokines, namely interleukin 17 (IL-17), interferon-γ (IFN γ), and TNF-α, are found expressed within the joints. Plus, as a consequence of synovitis developed during the acute response of AIA, bone and cartilage erosion is often observed during the chronic-like phase of AIA, when the disease is established [193,197–199]. However, as with every *in vivo* model, AIA has limitations. This model is mono-arthritic, with arthritis confined to the injected joint. This indicates that the AIA model does not breach immune tolerance to result in the systemic polyarticular disease that is RA [193].

As previously discussed in this thesis, RA is a highly heterogeneous disease, with a broad spectrum of synovium pathotypes described in patients[133,134]. It is, therefore, important to study multiple animal model pathotypes that align broadly with the different human forms of RA when trying to delineate underlying mechanisms of inflammatory arthritis, including the role of coagulation. The AIA model can be induced in various strains of mice, including genetically modified, for instance in mice which are lacking IL-6 family proteins (e.g. IL-27 or IL-6), resulting in a disease with similar synovial pathology to that observed in RA patients, namely myeloid- or macrophage-rich, lymphoid-rich and fibroblastic-rich pauci-immune pathotype.

When AIA is induced in wild-type (WT) mice, a myeloid-rich arthritis pathotype, with more diffuse immune infiltration, driven mainly by macrophages develops as previously described. On the other hand, IL-6*,* as a hallmark of chronic inflammation and an acute phase protein, when deleted provides protection from chronic inflammation. *IL6* knockout (KO) mice upon AIA development exhibit a mild arthritis pathotype, characterized by a reduced thickness of synovial lining and preservation of articular cartilage compared to AIA development in WT mice, which, in contrast, often displays cartilage erosion [200,201]. In the case of *IL6ra* KO mice, a fibroblastic-rich pathotype with reduced immune infiltration (pauci-immune) is also described [202]. The role of IL-6 in RA is further evidenced by the clinical benefits of blocking IL-6 in RA with the use of Tocilizumab [203].

Despite being from the same IL-6 family proteins, IL-27 has several opposite effects of IL-6 and is often considered an anti-inflammatory cytokine. In fact, the balance between IL-6 and IL-27 plays a role in the management of synovitis, as well as in cartilage and bone erosion [204]. In fact, upon IL-27 deletion, mice characteristically develop an amplified T cell-mediated disease [205]. Therefore, when AIA was performed in *IL27ra* deficient mice, a hyper-inflammatory pathotype, characterized by a lymphoid-rich phenotype developed. This pathotype featured ectopic lymphoid-like structures and a more severe form of synovitis, along with an elevated adaptive immune response reflected by increased T cell numbers and antibody response [206]. Considering that these structures are present in around 40% of human RA patients, and their presence correlates with disease severity, making the study of the AIA model developed in *IL27ra$^{-/-}$* mice *is* essential in order to draw conclusions with human RA [207,208].

1.5 Hypothesis and Aims

This literature review presented above demonstrates the association of LOX products, limited. In fact, no study to date analysed oxPLs in RA, despite being an auto-immune disease with a high risk of thrombosis. The hypothesis of the thesis is that a procoagulant surface in immune cells contributes to the increased coagulation observed in RA.

In order to test this hypothesis, I will:

- Characterise coagulation and inflammatory markers in plasma from *WT*, *IL27ra$^{-/-}$*, *IL6ra$^{-/-}$* and *IL6$^{-/-}$* mice during AIA development (Chapter 3).
- Characterize eoxPLs generation in whole blood cells of *WT*, *IL27ra$^{-/-}$*, *IL6ra$^{-/-}$* and *IL6$^{-/-}$* mice during AIA development (Chapter 3).
- Characterise coagulation and inflammatory markers in plasma from *Alox15$^{-/-}$* mice during AIA development, as well as oxPL composition in whole blood cells (Chapter 4).
- Characterise the phenotype of *Alox15$^{-/-}$* mice during AIA development and analyse oxPL generation in joint tissue (Chapter 5).
- Determine the capacity of the platelet, WBC and EV membrane surfaces to support coagulation in RA patients compared to healthy controls (Chapter 6).
- Characterize the oxPL composition of the membrane surface of platelets, WBCs and EVs in RA patients compared to healthy controls (Chapter 7).
- Characterize the aminoPL composition and exposure of the membrane surface of platelets, WBCs and EV in RA patients compared to healthy controls (Chapter 8).

Materials and Methods

Chapter 2

2.1 Materials

2.1.1 Chemicals

The following chemical powders for buffers were purchased from Sigma Aldrich (Missouri, USA): Sodium chloride (NaCl), Sodium Bicarbonate ($NaHCO_3$), Potassium Chloride (KCl), Sodium Phosphate dibasic (Na_2HPO_4), Magnesium Chloride anhydrous ($MgCl_2·6H_2O$), HEPES, Glucose, Trisodium Chloride ($Na_3Citrate.2H_2O$), Citric Acid (Citric acid.H_2O), Sodium dihydrogen orthophosphate dehydrate ($NaH_2PO_4·2HO$), Trisodium Citrate, Tris(hydroxymethyl)aminomethane, Hydrochloric acid (HCl), Calcium chloride ($CaCl_2$), EDTA, Diethylenetriaminepentaacetate (DTPA), Acetaminophen, Butylated hydroxytoluene (BHT), Tin(II) chloride ($SnCl_2$), bovine thrombin, calcium ionophore (A23187), L-lysine, sodium hydroxide (NaOH), Trimethylamine, Ammonium acetate ($NH_4CH_3CO_2$), Pentamethylchromanol. *Bordetella Pertussis* toxin, Complete Freund's adjuvant (CFA), Bovine serum albumin (BSA) and methylated BSA (mBSA) were also purchase from Sigma Aldrich (Missouri, USA).

HPLC grade solvents were purchased from ThermoFisher Scientific (Hemel Hempstead, Hertfordshire UK) as follows: HPLC grade water (H2O), glacial acetic acid, propan-2-ol (IPA), hexane, chloroform, methanol (MeOH) and acetonitrile (ACN). Dulbecco's phosphate-buffered saline (DPBS), EZ-Link™ NHS-biotin and EZ-Link™ Sulfo-NHS-biotin were also from ThermoFisher Scientific.

2.1.2 Coagulation factors and chromogenic substrates

Coagulation factors, specifically Factor II (Human Prothrombin), Factor Xa and Factor IIa (Human Alpha Thrombin), as well as chromogenic substrate Pefachrome TH 8198 (S-2238) were obtained from Enzyme Research Laboratories (Swansea, UK), while Factor Va was obtained from Haematologic/Cambridge Bioscience (Cambridge, UK). HetasSep™ was purchased from StemCell Technologies, Canada.

Coagulation factors were reconstituted in H_2O as follows: Factor II - 20 µM, Human Factor Va - 1 µm, Human Factor Xa - 10 µM, and Factor IIa - 10 µM. The chromogenic substrate S-2238 was reconstituted at 2.8 mM [209–211].

2.1.3 Lipids

1-Stearoyl-2-arachidonoyl-phosphatidylethanolamine (SAPE) and -phosphatidylserine (SAPS), 1,2-dimyristoyl-sn-glycero-3-phosphocholine (DMPC), 1,2-dimyristoyl-sn-glycero-3-phosphoethanolamine (DMPE), 1,2-dimyristoyl-sn-glycero-3-phospho-L-serine (DMPS), 1,2-dioleoyl-sn-glycero-3-phospho-L-serine (DOPS), 1-stearoyl-2-oleoyl-sn-glycero-3-phospho-L-serine (SOPS), 1-(1Z-stearoyl)-2-arachidonoyl-sn-glycero-3-phosphoethanolamine (SpAPE) and SPLASH® LIPIDOMIX® Mass Spec Standard, were obtained from Avanti Polar Lipids (Alabaster, Alabama, USA).

Deuterated eicosanoid standards were purchased from Cayman Chemical (Michigan, USA) as follows: 13(S)-HODE-*d4*, 5(S)-HETE-*d8*, 12(S)-HETE-*d8*, 15(S)-HETE-*d8*, 20-HETE-*d6*, Leukotriene B4-*d4*, Resolvin D1-*d5*, Prostaglandin E2-*d4*, Prostaglandin D2-*d4*, Prostaglandin F2α-*d4*, Thromboxane B2-*d4*, 11-dehydro Thromboxane B2-*d4*, 11(12)-EET (EpETrE) -*d11*, as well as 11-dehydro Thromboxane B2.

2.1.4 Buffers

2.1.4.1 Acid Citrate Dextrose (ACD)

25g of Trisodium citrate, 13.7 g citric acid and 20 g glucose were dissolved in 900 ml of H_2O. The pH was adjusted to 5.4 and the solution was made up to 1 L with H_2O to give a final concentration of 85 mM trisodium citrate, 65 mM citric acid and 100mM glucose. The solution was syringe filtered through a 0.22 µm filter, aliquoted, and stored at -20°C [125,212].

2.1.4.2 Tyrode's buffer

7.84 g NaCl, 1.02 g $NaHCO_3$, 0.22 g KCl, 0.09 g di-sodium hydrogen orthophosphate, 0.3 g magnesium chloride hexahydrate, 2.38 g HEPES and 0.9 g glucose were dissolved in 900 ml H_2O. The pH was adjusted to 7.4 and the solution was made up to 1 L with H_2O to give a final concentration of 134 mM NaCl, 12 mM $NaHCO_3$, 2.9mM KCl, 0.34 mM di-sodium hydrogen orthophosphate, 1 mM magnesium chloride hexahydrate, 10mM HEPES and 5 mM glucose. The solution was vacuum filtered through a 0.22 µm filter, aliquoted, and stored at -20 °C [125,212].

2.1.4.3 Stock bovine thrombin (20 U/ml)

Lyophilized bovine thrombin powder (100 U) was reconstituted in 5 ml sterile DPBS to give a stock of 20 U/ml. The solution was aliquoted and stored at -80 °C [125,212].

2.1.4.4 Krebs buffer

5.8 g NaCl, 11.37 g HEPES, 0.37 g KCl, 0.16 g sodium dihydrogen orthophosphate dihydrate and 0.36 g glucose were dissolved in 900 ml H_2O. The pH was adjusted to 7.4 and the solution was made up to 1 L with H_2O to give a final concentration of 100 mM NaCl, 48 mM HEPES, 5 mM KCl, 1 mM sodium dihydrogen orthophosphate dihydrate and 2 mM glucose. The solution was vacuum filtered through a 0.22 µm filter, aliquoted, and stored at -20 °C [125].

2.1.4.5 DPBS/0.4 % trisodiumcitrate (w/v)

4 g trisodium citrate was dissolved in 900 ml Dulbecco's phosphate-buffered saline (DPBS). The pH was adjusted to 7.4 and the solution was made up to 1 L with DPBS. It was then vacuum filtered through a 0.22 µm filter, aliquoted, and stored at -20 °C [125].

2.1.4.6 2 % Citrate (w/v)

20 g trisodium citrate was dissolved in 900 ml H_2O. The pH was adjusted to 7.4 and the solution was made up to 1 L with H_2O. It was then vacuum filtered through a 0.22 µm filter, aliquoted, and stored at -20 °C [125].

2.1.4.7 RBC lysis buffer (0.2% hypotonic saline)

2 g NaCl was dissolved in 1 L H_2O. The solution was vacuum filtered through a 0.22 µm filter, aliquoted, and stored at -20 °C [125,212].

2.1.4.8 Stock A23187 (2 mM)

5 mg of A23187 powder was reconstituted in 4.8 ml DMSO to give a stock of 2 mM. The solution was aliquoted and stored at -80 °C [209–211].

2.1.4.9 Tris-buffered saline (TBS)

24 g Tris and 88 g NaCl were dissolved in 900 ml H_2O. The pH was adjusted to 7.4 and the solution was to 1 L with H_2O. This created a 10x TBS stock to be diluted 1:10 (v/v) with H_2O immediately prior to use to give a final TBS composition of 20mM Tris and 150 mM NaCl. The stock was vacuum filtered through a 0.22 µm filter, aliquoted, and stored at -20 °C [209–211].

2.1.4.10 Stock 5 % BSA (w/v)

5 g of BSA was dissolved in 100 ml TBS. The solution was filter sterilised through a 0.22 µm filter and stored at -20 °C [209–211].

2.1.4.11 TBS/BSA Prothrombinase buffer

100 µl of stock 5 % BSA was added to 1 ml of 10x TBS and the volume was made up to 10 ml with H_2O. The final composition, therefore, was 0.05 % BSA (w/v) in TBS. The solution was vacuum filtered through a 0.22 µm filter and stored at 4 °C for a maximum of 2 weeks [209–211].

2.1.4.12 Pentamethylchromanol (10 mM)

220 mg of pentamethylchromanol was dissolved in 100 ml chloroform. The solution was prepared immediately before use [213].

2.1.4.13 $CaCl_2$ (1 M)

7.35 g $CaCl_2$ was dissolved in 50 ml H_2O. The solution was filter sterilised with a 0.22 µm filter, aliquoted and stored at -20 °C [209–211].

2.1.4.14 EDTA (35 mM)

1.02 g EDTA was dissolved in 100 ml H_2O. The solution was filter sterilised with a 0.22 µm filter, aliquoted and stored at -20 °C [209–211].

2.1.4.15 DTPA stock solution (10 mM)

DTPA stock solution (10 mM) was prepared by dissolving 3.93 mg of DTPA in 1 ml H_2O, followed by the addition of 30 µl NaOH (1 M) in order to accelerate dissolution at 37 °C [212,213].

2.1.4.16 Acetaminophen stock (7.5 mM)

Acetaminophen stock solution (7.5 mM) was prepared by dissolving 1.13 mg in 1 ml H_2O [212].

2.1.4.17 BHT Stock (10 mM)

BHT 10 mM stock was prepared by dissolving 2.20 mg in 1 ml of MeOH [212,213].

2.1.4.18 $SnCl_2$ (7.5 mM)

$SnCl_2$ 100 mM stock was prepared by dissolving 18.9 mg into 1 ml of H_2O. All $SnCl_2$ solutions were prepared fresh on the day of lipid extraction [212,213].

2.1.4.19 Antioxidant buffer

This buffer was prepared as a stock solution consisting of 25 ml of cold DPBS (4 °C) containing DTPA (100 µM), BHT (100 µM) and acetaminophen (7.5 µM). This was prepared fresh on the day of lipid extraction and placed on ice [212].

2.1.4.20 Sodium Citrate 3.8 %

3.8 g of sodium citrate was dissolved in 100 ml of H_2O. The solution was stored at room temperature [212,213].

2.1.4.21 mBSA solution

10 mg of mBSA was dissolved in 1 ml of H_2O in a sterile flask, generating a 10 mg/ml solution for intra-articular injection [193].

2.1.4.22 mBSA/ Complete Freund's Adjuvant emulsion

10 mg of mBSA was dissolved in 5 ml of H_2O in a sterile flask, generating a 2 mg/ml solution. 5 ml of Complete Freund's Adjuvant (CFA) was removed using a 10 mL syringe with a 21 G needle. The needle was then changed to an 18 G blunt fill needle, before injecting the CFA into the prepared mBSA solution. Using a glass syringe with an

18 G blunt fill needle, a white emulsion was obtained by repeatedly uptaking and flushing the mBSA/CFA mixture. When droplets of the mixture remained intact when placed onto a petri dish containing water, was the emulsion considered stable and kept on ice until ready to use [193].

2.1.4.23 Bordetella Pertussis toxin

Pertussis toxin, at a stock solution of 0.2 mg/ml was diluted 125 times in DPBS, generating a 160 ng/100 µl concentration for intraperitoneal injection [193].

2.2 Methods

2.2.1 Mouse strains

All animal experiments were implemented in accordance with Home Office–approved project licenses (PE8BCF782 and PC1FFFEE3). The ethical approval of these licenses covers all aspects of the study, including breeding and maintaining genetically altered animals, and all the animal models conducted.

Inbred IL-27 receptor-deficient (*IL27ra*$^{-/-}$) were originally sourced from The Jackson Laboratory (line B6N.129P2-Il27ratm1Mak/J). Briefly, these mice were generated using a target vector, which replaced a coding exon for a portion of the extracellular fibronectin type III domain of the *IL27ra* and positively selected through a neomycin resistance cassette[214].

Inbred IL-6 receptor-deficient (*IL6ra*$^{-/-}$) mice were generated at GlaxoSmithKline (Stevenage, UK) through a replacement vector designed to disrupt key structural regions for IL-6 recognition, namely exons 4,5 and 6[215].

IL-6 cytokine-deficient (*IL6*$^{-/-}$) mice were sourced from Charles River (Bristol, UK), and generated using a target vector, which disrupted the first coding exon and positively selected through a neomycin resistance cassette.[216]

Alox15 knockout (*Alox15*$^{-/-}$) mice were sourced from Charles River (Bristol, UK), generated through a targeting vector, which interrupts exon 3 and positively selected through a neomycin resistance cassette [217].

All transgenic colonies were from a C57BL/6 background and were bred under specific pathogen-free conditions at Cardiff University (Cardiff, Wales). *Alox15*$^{-/-}$ mice were bred under PC0174E40 license (Lipid regulation of cardiovascular disease), while the remaining genetically altered animals were bred under PE8BCF782 (How does inflammation shape the course of disease in arthritis?).

Inbred WT C57BL/6J mice were purchased from Charles River UK and acclimatized at Cardiff University for at least one week before any experiments.

Experimental mice were housed in either filter top cages or scantainers, in the case of *IL6*$^{-/-}$ and *IL6ra*$^{-/-}$, with 12-h light/dark cycles and controlled temperature (20 – 22°C). Mice were fed a standard chow diet with unrestricted water access and sacrificed via CO_2 inhalation (cardiac puncture/exsanguination as confirmation of death).

2.2.2 Genotyping

Ear clippings were used for genotyping mouse strains. DNA extraction was performed through Monarch® Genomic DNA Purification Kit (New England Biolabs® inc., USA), as per the manufacturer's instructions. Ear clippings, while still frozen, were cut into smaller pieces to provide a higher DNA extraction yield. Each macerated ear clipping was transferred into a 1.5 ml reaction tube, where 200 µl of Tissue Lysis Buffer and 3 µl of Proteinase K were added. Samples were incubated at 56 °C in a dry bath, with occasional vortex, until tissue dissolution. Subsequently, 3 µl of RNAse A was added to each sample and incubated at 56 °C for a further 5 minutes.

For the DNA isolation, 400 µl of DNA binding buffer mix provided by the Monarch® Genomic DNA Purification Kit Kit (New England Biolabs® inc., USA) was added to each sample and then, vortexed. The resultant lysate was transferred to genomic DNA purification columns attached to collection tubes. Samples were then centrifuged (accuSpin Micro 17R, Fisher Scientific) at 1000 g for 3 minutes, immediately followed by centrifugation at the maximum rotation of 17000 g for 1 minute, at room temperature. The flow-through from each purification column was discarded, and the purification columns were then transferred to new collection tubes. The columns were washed by adding 500 µl of gDNA wash buffer. The columns were then inverted several times, before centrifugation at 17000 g for 1 minute. The flow-through from the latter step was discarded and the wash step was repeated once more. Purification columns were then transferred to 1.5 ml reaction tubes, and 100 µl of preheated (60°C) gDNA elution buffer was added, followed by a 1-minute incubation at room temperature. Finally, samples were centrifugated at 17000 g for 1 minute to elute the isolated DNA.

The isolated DNA samples were then amplified through PCR. A PCR cocktail mix was designed using GoTaq® PCR Core Systems (Promega) (Table 2.1). The primers (Thermo Fisher Scientific) employed were for the genotyping of the *Alox15*$^{-/-}$ mice colony and are described in Table 2.2. Subsequently, the PCR mix was run on a PCR thermal cycler (Thermo Fisher) using the program presented in Table 2.3.

The amplified DNA was then separated through agarose gel electrophoresis. Agarose gel at 1.5% was prepared by adding 100 ml of TBE [89 mM tris; 89 mM boric acid; 2 mM EDTA (pH 8.05)] to 1.5 g of agarose (Thermo Fisher Scientific, UK). The mixture was heated for 30-sec intervals and swirled until the agarose was completely dissolved. While this mixture was still in its liquid form, 10 µL SYBR™ Safe DNA Gel Stain (Invitrogen™, UK) was added. The agarose mixture was then poured into the gel mould, followed by carefully placing the comb to create the wells, and then allowed to cool down until solidifying.

The gel was placed into the running tray, along with Tris/Borate/EDTA buffer (TBE) as running buffer and DNA ladder (Invitrogen™, UK) and samples were loaded into the wells of the gel, consisting of 18 µL of the amplified sample with 2 µL of TriTrack DNA Loading Dye (Thermo Fisher Scientific). Bio-Rad PowerPac™ 300 Power supply was employed at 100 V at constant voltage for 30 minutes or until adequate ladder separation. The gel was documented through G:BOX Chemi XX6 and XX9 and DNA fragments were imaged using GeneSys software (Syngene, UK).

Table 2.1: Cocktail PCR mix.

Cocktail PCR mix	
$MgCl_2$	3.94 µL
Primers (x 3)	0.2 µL
PCR Nucleotide Mix (dNTP)	1 µL
GoTaq® DNA Polymerase	0.5 µL
DNAse free water	33.96 µL - Volume of sample
Colorless GoTaq® Flexi Buffer	10 µL
Sample for genotyping	Between 5-9 µL
	Final volume: 50 µL

Table 2.2: Primer's composition.

Primers	
Alox 15	GGGAGGATTGGGAAGACAAT
Alox 15 common	GGCTGCCTGAAGAGGTACAG
Alox 15 Wild type	CCATAGACGAGACCAGCACA

Table 2.3: PCR program stages.

Stage 1			Stage 2			Stage 3	
Initial denature	95°C	3 min	**Denature**	95°C	30 sec	72°C	10 min
Denature	95°C	30 sec	**Annealing**	65°C	60 sec	4°C	Forever
Annealing	65°C	60 sec	**Extension**	72°C	60 sec		
Extension	72°C	60 sec					

2.2.3 AIA mouse model

Induction of experimental arthritis was implemented in accordance with the Home Office–approved project license (PE8BCF782). In all animal models performed, the 3 R's (Replace, Reduce, Refine) were taken into consideration. The mice in this animal model were shared between three different groups, studying different components of inflammatory arthritis, therefore complying with the 3 R's. To reduce confounding factors and facilitate the induction of this model, only male mice were analysed in this study. This is a limitation of this study considering that the majority of RA patients are from the female gender [129].

Power calculations were performed using data from a previous study on TAT complex values after the development of murine abdominal aorta aneurysm [212], using an online sample size calculator[218]. It was determined that each study group should be composed of at least 8 mice. This number was then reduced to 4 in the case of both *IL6ra*$^{-/-}$ and *IL6*$^{-/-}$ mice, since a significant difference was achieved before reaching the calculated n value of 8.

Experimental mice were divided into four study groups: (i) naïve control, (ii) immunized or primed controls, (iii) early arthritis disease (Day 3) and (iv) established arthritis disease (Day 10).

All experiments using transgenic mice were done simultaneously with WT mice, as to try to compensate for possible variations due to the arthritis induction between experiments. A total of 8 separate AIA model experiments were performed, namely: (i) naïve control (n = 8) and primed controls mice (n = 8); (ii) naïve control (n = 3), primed controls mice (n=8), WT (n = 8) and *IL27ra*$^{-/-}$ mice (n = 8) until day 3 of AIA development; (iii) naïve control (n = 3), WT (n = 8) and *IL27ra*$^{-/-}$ mice (n = 8) until day 10 of AIA development; (iv) naïve control (n = 3), WT (n = 6) and *IL6ra*$^{-/-}$ mice (n = 6) until day 3 of AIA development; (v) naïve control (n = 3), WT (n = 6) and *IL6ra*$^{-/-}$ mice (n = 6) until day 10 of AIA development; (vi) naïve control (n = 3), WT (n = 4) and *IL6*$^{-/-}$ mice (n = 4) until day 3 of AIA development; (vii) naïve control (n = 3), WT (n = 4) and *IL6*$^{-/-}$ mice (n = 4) until day 10 of AIA development. (viii) naïve control (n = 3), WT (n = 8) and *ALox15*$^{-/-}$ mice (n = 8) until day 3 of AIA development; (ix) WT (n = 8) and *ALox15*$^{-/-}$ mice (n = 8) until day

10 of AIA development. Experiments (i) to (vii) were pooled and analysed in Chapters 3 and 4, while experiments (viii) and (ix) were pooled alongside experiment (i) and WT results from experiments (iii) to (vii) and discussed and analysed in Chapter 5 and 6. Unfortunately, not all mice that completed successfully the AIA model were able to be analysed due to failed cardiac puncture.

Mice, aged between 9 - 11 weeks of age, were injected with 100 µL of mBSA/CFA emulsion subcutaneously (s.c.) using a 1 ml syringe and 25-gauge needle. The emulsion was prepared by adding mBSA (2 mg/ml) and CFA examples in equal parts and forcefully mixed using a glass syringe and an 18-gauge needle until a stable emulsion was generated. Simultaneously, 100 µL of *Bordetella Pertussis* toxin (1.6 ng/µl) was administered intraperitoneally (i.p.) using a 1 mL syringe with a blue 25-gauge needle (day -21). After 7 days (day -14), the mice were immunized for a second time with 100 µL of mBSA/CFA (s.c.) in the opposite flank. From this point, mice either underwent arthritis induction or were harvested as primed (or immunized) controls. The unimmunized, naïve mice were culled on the same day as the primed controls (Day 0). Arthritis was induced 14 days after the second immunization. For this, mice were injected with 10 µL of mBSA solution (10 mg/ml), intraarticularly (i.a.) using an insulin syringe with a 29-gauge, to induce inflammatory arthritis, which result in an increase infiltration of immune cells, with a peak of the acute inflammatory response at day 3 – Early arthritis. Arthritis progression was monitored by measuring knee joint swelling with a POCO 2T micrometer (Kroeplin) on days 0, 1, 2, 3, 7 and 10, and used as a measurement of inflammation. After day 3, swelling decreases until it reaches chronic-like inflammation around day 7, where an intensified adaptive immunity response is present, as observed by an increase in T and B-cells into the joint [193].

Three days after the i.a. injection, mice were culled for the early disease time point, where the peak of swelling was observed. The established disease time point was defined as 10 days post i.a. injection, where the diameter of the joint was observed at baseline levels (Figure 2.1) [193].

Animals were observed daily for the first 3 days following each injection, followed by observation every other day. Minor inflammatory reactions from the administration of CFA were observed in some mice. These animals were observed daily and monitored for signs of distress. Food pellets were placed in the cage to minimise the stress of feeding. Any mice showing signs of pain received a subcutaneous injection of Buprenorphine (0.05 mg/kg dose) [219] and were removed from the experiments described in this thesis. This situation only occurred with one *IL6ra*$^{-/-}$ mouse, before the i.a. injection, and it was excluded from the study. Any animal not responding to pain relief, exhibiting signs of distress for 3 consecutive days or showing a showing ≥ 20% weight loss would be humanely culled. In addition, any mice presenting an increase of joint swelling superior to 2 times the baseline on 3 consecutive days would also be humanely killed. These signs and conditions were not observed in any mice during all AIA experiments.

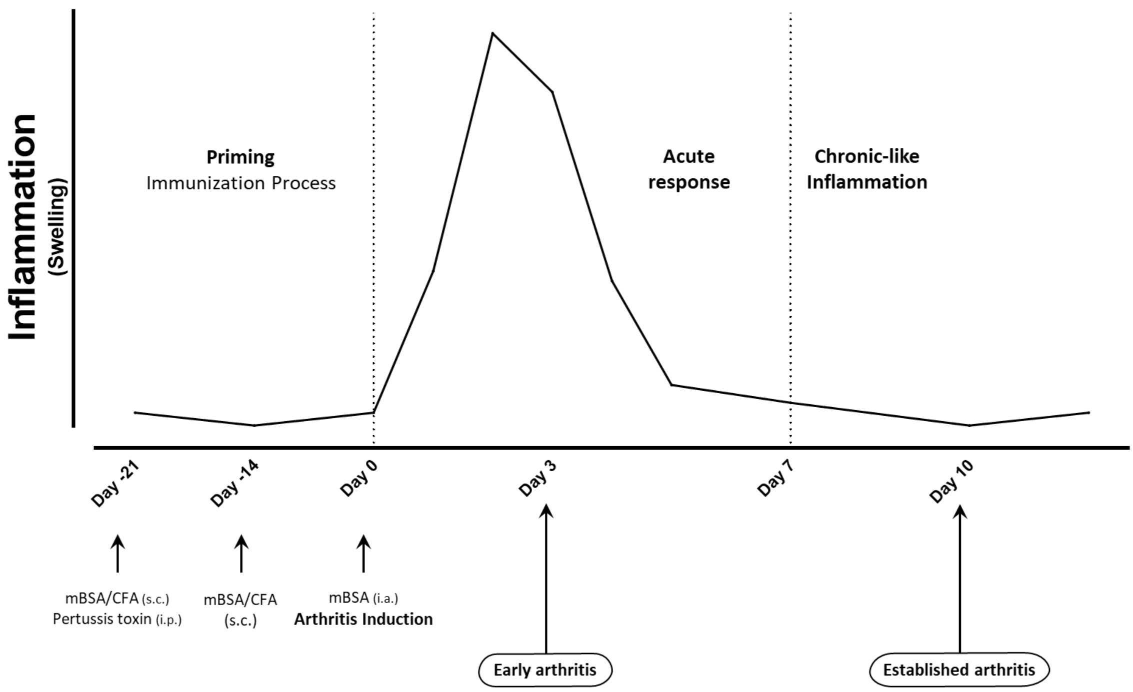

Figure 2.1: Antigen-induced arthritis model
Schematic representation of the inflammatory response of AIA model, including endpoints used. Arrows indicate the time and respective routes of administration for the induction of AIA model, along with the timepoints used for tissue collection on different disease stages. The model is initiated by a priming phase, where an antigen-specific response against mBSA is generated. On day -21, the mice are challenged with a mBSA/CFA subcutaneously (s.c) and Pertussis toxin intraperitoneally (i.p.) administration, followed by a booster injection of mBSA/CFA (s.c.) 7 days later (day -14). The acute inflammation is then generated by an intra-articular (i.a.) injection of mBSA on day 0, resulting in an increase infiltration of immune cells. Joint swelling is measured on day 0, 1, 2, 3, 7 and 10, and used as a reflection of inflammation. After 7 days of the arthritis induction, the swelling of the AIA model is minor, and a chronic-like phase is achieved. Scheme designed using PowerPoint and Excel using readout for AIA development in WT mice.

2.2.4 Mouse Blood Collection

Mouse blood collection and processing were performed as previously described [212]. Mice were sacrificed through schedule 1, via CO_2 inhalation. From each mouse, whole blood was collected via cardiac puncture, using a 1 ml syringe with a blue 23-gauge needle, preloaded with 100 µl of an anticoagulant mixture consisting of sodium citrate 3.8% (9:1, v/v) and 0.1 mg/ml corn trypsin inhibitor (Haematologic Technologies Inc., USA). The harvested blood was distributed equally into Eppendorf tubes. With a total volume of 200 µl in each, the Eppendorf tubes were centrifuged at 3000 g for 5 minutes at room temperature, with plasma and whole blood cells isolated and immediately snap-frozen in liquid nitrogen. Plasma was stored at -80 °C until further analysis.

2.2.5 Mouse-washed platelet isolation

Mouse blood was performed as previously described [125,212], starting with the blood collection by cardiac puncture (as above) into a syringe containing 150 µl of Acid Citrate Dextrose (ACD) [2.5 % (w/v) trisodium citrate, 1.5 % (w/v) citric acid, and 100 mM Glucose]. The syringe with anticoagulant and the collected blood was gently inverted before being transferred into an Eppendorf containing 150 µl 3.8 % w/v sodium citrate, and 300 µl of modified Tyrode's buffer was then added (145 mM NaCl, 12 mM $NaHCO_3$, 2.95 mM KCl, 1 mM $MgCl_2$, 10 mM HEPES, 5 mM Glucose). The blood was spun at 200 g for 5 minutes, at room temperature. The top layer consisting of platelet-rich plasma (PRP) was transferred to an Eppendorf containing 400 µl of Tyrode's buffer, and gently mixed before being spun for 2 minutes at 200 g. More PRP was isolated and transferred to a fresh Eppendorf and 400 µl of Tyrode's buffer was added. A third spin was performed at 500 g for 5 minutes. The plasma was removed, and the platelets were resuspended in Tyrode's buffer at 2 x 10^8 cells/ml [212].

2.2.6 Mouse whole blood cells lipid extraction

Mouse whole blood cells lipid extraction was performed using the same protocol as previously described for lipid extraction of murine blood clots [212]. Immediately before lipid extraction, each mouse whole blood cell pellet generated in Section 2.2.4 was resuspended in 1 ml antioxidant buffer [ice-cold DPBS, 100 µM diethylenetriaminepentaacetic acid, 100 µM butylated hydroxytoluene, 7.5 µM acetaminophen, pH 7.4]. The reduction of hydroperoxides was achieved by the addition of 10 µl of $SnCl_2$ (100 mM), and incubation for 10 minutes on ice.

Internal standards (IS), 10 ng PE 15:0/18:1-*d7* [SPLASH® LIPIDOMIX® Mass Spec Standard], along with eicosanoids ISs [13(S)-HODE-*d4*, 5(S)-HETE-*d8*, 12(S)-HETE-*d8*, 15(S)-HETE-*d8*, 20-HETE-*d6*, Leukotriene B4-*d4*, Resolvin D1-*d5*, Prostaglandin E2-*d4*, Prostaglandin D2-*d4*, Prostaglandin F2α-*d4*, Thromboxane B2-*d4*, 11-dehydro Thromboxane B2-*d4*, 11(12)-EET (EpETrE) -*d11*] were added before lipid extraction. For whole blood lipidomics, SPLASH® LIPIDOMIX® Mass Spec Standard was used as the IS mix for oxPLs, since it contained deuterated PE and PC, which are not present in whole blood. For oxylipin analysis, the IS used were deuterated lipids of the same class as the analysed lipids, which are also not present in the sample.

Samples were transferred to 10 ml glass vials with a screw-top (Chromacol 10-SV, Thermo Scientific) containing 2.5 ml of ice-cold methanol. Lipids were extracted by adding 1.25 ml of chloroform to each sample followed by incubation on ice for 30 minutes. Then, 1.25 ml of chloroform and 1.25 ml of water were added, and the mixture vortexed. The samples were then centrifuged (Megafuge 40R, Thermo Scientific) at 400 g for 5 minutes at 4 °C to obtain a biphasic solution. Lipids were then recovered from the bottom chloroform layer using a glass Pasteur pipette. To obtain a higher extraction yield, an additional 2.5 ml of chloroform was then added, followed by another round of vortexing and centrifugation at 400 g for 5 minutes at 4 °C. The bottom chloroform layer was recovered and pooled with the previously collected layer. The chloroform extracts were dried using a Rapidvap N2/48 evaporation system (Labconco Corporation), re-suspended in 150 µl of methanol, and transferred to HPLC vials with fixed glass inserts and stored at − 80 °C in an N_2 atmosphere prior to analysis by LC/MS/MS as described in Section 2.2.28, 2.2.30 and 2.2.31.

2.2.7 Mouse Synovial tissue isolation

Synovial tissue was dissected from the joint cavity. For this, the articular capsule from animals was opened and the synovial membrane, together with the infrapatellar fat pad, was excised from the joint capsule and patellar ligament after detachment from the tibia[220]. After synovial isolation, the tissue was weighed, snap-frozen and stored at − 80 °C until lipid extraction.

2.2.8 Mouse synovial tissue processing and lipid extraction

Mouse synovial tissue processing and lipid extraction was adapted from the protocol described in *Allen-Redpath et al.* 2019 for murine abdominal aorta aneurysm tissue [212]. Firstly, mouse synovial tissue was resuspended in 0.5 ml antioxidant buffer [ice-cold DPBS, 100 µM diethylenetriaminepentaacetic acid, 100 µM butylated hydroxytoluene, 7.5 µM acetaminophen, pH 7.4].

Internal standards (IS), 10 ng of PE(15:0/18:1(d7)) [SPLASH® LIPIDOMIX® Mass Spec Standard], along with the eicosanoid IS mix [23 ng 13(S)-HODE-d4, 25 ng 5(S)-HETE-d8, 25 ng 12(S)-HETE-d8, 25 ng 15(S)-HETE-d8, 25 ng 20-HETE-d6, 26 ng Leukotriene B4-d4, 29 ng Resolvin D1-d5, 25 ng Prostaglandin E2-d4, 27 ng Prostaglandin D2-d4, 27 ng Prostaglandin F2α-d4, 28 ng Thromboxane B2-d4, 28 ng of 11-dehydro Thromboxane B2-d4, 25 ng of 11(12)-EET (EpETrE) -d11] was added to each sample before tissue homogenisation. Synovial tissue samples were homogenised in a Bead Rupture Elite®, with the following settings: 2 cycles at 5 m/s for 20 seconds with a dwell time of 10 seconds. Tissue samples were then transferred to fresh glass vials and the remaining tissue was washed out with a further 0.5 ml antioxidant buffer and combined with the previous tissue samples. The reduction of hydroperoxides was achieved by the addition of 10 µl of $SnCl_2$ (100 mM), and incubation for 10 minutes on ice.

Lipids were extracted from the processed mouse synovial tissue initially using a double extraction method. For this, the lipids were first extracted using an isopropanol/hexane method, by adding 2.5 ml of hexane/isopropanol/acetic acid (30:20:2, v/v/v) extraction solution to each sample. After vortexing, 2.5 ml of hexane was added, followed by another vortexing step. The separation of phases was achieved by centrifugation at 400 g for 5 minutes at 4 °C. Lipids were then recovered from the upper layer and transferred to new extraction vials. Another 2.5 ml of hexane was then added to the original extraction vial, followed by another round of vortexing and centrifugation. The upper phase was once again recovered and combined with the previously recovered layer. The remaining bottom layer was then extracted through the Bligh and Dyer method by adding 2.5 ml of methanol and 1.25 ml of chloroform. Samples were then vortexed before adding 1.25 ml of chloroform and 1.25 ml of water. After vortexing and centrifugation at 400 g for 5 minutes at 4°C, the bottom layer was recovered and combined with the previously isolated hexane layers. The combined chloroform and hexane extraction recoveries were dried using a Rapidvap N2/48 evaporation system (Labconco Corporation), re-suspended in 150 µl of methanol, and transferred to HPLC vials, capped in an N_2 atmosphere, and stored at -80 °C, before further processing.

Due to the complex nature of these tissue samples, it was suspected that these lipid extracts had contaminating particles (bone or cartilage) that scratched the injector in the LC/MS/MS. Therefore, in order to prevent more damage to the injector needle and HPLC column, these samples were further extracted, as to remove these possible contaminating particles. The lipid extracts were split into 2, with 75 µl further extracted for oxPLs analysis by hexane/isopropanol extraction, while the other 75 µl of extract were processed through solid-phase extraction for oxylipin analysis, as described below.

For the hexane/isopropanol extraction, the 75 µl of lipid were diluted in 925 µl of water, prior to its addition to the extraction solution. To each sample, 2.5 ml of hexane/isopropanol/acetic acid (30:20:2, v/v/v) extraction solution was added. Following vortexing, 2.5ml of hexane was added. The separation of phases was achieved by centrifugation at 400 g for 5 minutes at 4°C. Lipids were then recovered from the upper layer, dried, re-suspended in 75 µl of methanol and then transferred to HPLC vials with fixed glass inserts, capped in an N_2 atmosphere and stored at -80 °C prior to analysis by LC/MS/MS.

Solid-phase extraction (SPE) method uses cartridges containing silica beads with C18 bound for the extraction of lipids, removing phospholipids and neutral lipids. The samples were prepared by adding 75 µl of lipid extract into Eppendorf's containing 1.9 ml of 15% MeOH/85% water (v.v) acidified with 45 µl of glacial acetic acid, and vortexed. For each lipid extract, an SPE cartilage (Sep-Pak C18 Cartridge, Waters) was set up on the positive pressure manifold (Pressure⁺ 48, Biotage®), with an outgoing pressure set to approximately 20 psi. The cartridges were conditioned by running 6 ml of Methanol, twice, using a quick flow of about 2 ml/min. Next, a total of 6 ml of 0.25% glacial acetic acid in water (v/v) (pH 3), was eluted at 1 ml/min. Once the acidified water reaches the meniscus of the column, the run was stopped, and the samples were loaded into each column. The samples were slowly forced into the column through positive pressure. Once the level reached the meniscus, 5 ml of 0.25% Glacial acetic acid in water (v/v) was run twice slowly through the column. Following, 3 ml of hexane was run twice before allowing the column to dry for about 30 minutes. Oxylipins were eluted by adding 8 ml of methyl formate under gravity into glass extraction tubes. The samples were dried using a Rapidvap N2/48 evaporation system (Labconco Corporation), at room temperature, with no shaking, starting with a vacuum set to 700 mbar and decreasing gradually by 50 mbar every 15 minutes, as to ensure no spillage occurs. Samples were resuspended in 75 µl methanol and then transferred to HPLC vials with fixed glass inserts, capped in an N_2 atmosphere and stored at -80 °C prior to analysis by LC/MS/MS as described in Section 2.2.28 and 2.2.31.

2.2.9 Mouse knee joint histology

Mouse knee joint histology was performed as previously described [193,221]. Whole knee joints were recovered by cutting through the femur and tibia. Following the removal of skin, knees were placed into histology cassettes and fixed in 10 % formalin for three days. This was followed by a decalcification process, where the cassettes were incubated in a decalcification buffer (10 % formic acid in water), which was changed every three days until no calcium was detected. The endpoint calcium assay was performed using the method of Rosen[222]. For this, the recovered acidic decalcification solution was neutralized using an accumet™ basic pH meter (Denver Instrument) by adding 5 M NaOH solution, until reaching pH 7. This was followed by the addition of 5 ml of saturated ammonium oxalate [$(NH_4)_2C_2O_4$]. After vortexing, the solution was incubated for 30 minutes, and the formation of a white precipitate was indicative of the presence of Ca^{2+}. When no Ca^{2+} precipitate was observed in the decalcification buffer after two assays in a row, the process was considered complete. The tissue was then processed using the HistoCore PEARL before being embedded into paraffin blocks through Arcadia H instruments (Leica Biosystems). Parasagittal serial sections of 6 µm were obtained via a Leica RM2235 rotary microtome. Slides were baked at 60 °C overnight to ensure adherence to the glass.

2.2.10 Histological staining of mice knee joints

Knee parasagittal sections were prepared for histological staining through a de-waxing protocol as previously described [193,221]. Sections were submerged in three xylene baths, before rehydration in a decreasing concentration of ethanol (100 %, 90 % and 70 %), and a final wash in distilled water. Subsequently, sections were submerged in Weigert's iron haematoxylin solution (VWR International, Ltd) for 7 minutes. Excess stain was removed by running tap water before transferring into Fast Green [0.01 % (w/v)] for 5 minutes. Next, sections were dipped for 10 seconds in acetic acid [1 % (v/v)], and finally incubated for 5 minutes in safranin O [0.2% (w/v)] before dehydration. Finally, sections were dehydrated through sequential incubation in 70%, 90% and 100% absolute ethanol and cleared by three changes of xylene. Coverslips were mounted using DPX mountant for histology (Sigma-Aldrich®) and dried overnight. Sections were accessed as described in Section 2.2.11, using a Leica DM 2000 microscope and Leica Application Suite v4.9 software.

2.2.11 Histological assessment of mice joint pathology

Inflammation and cartilage erosion and overall joint damage were evaluated through histological staining as previously described [193,221], outlined in Table 2.4.

Histology was scored by at least two independent analysts blinded to the experimental design, namely Gareth Jones, PhD and David Hill, PhD from Bristol University, and Aisling Morin, PhD from Cardiff University. The scoring assessed synovial exudate, synovial inflammation and hyperplasia and cartilage and bone erosion. Haematoxylin staining indicates cellular infiltration, while safranin-O indicates cartilage erosion (Figure 2.2). The combined score is presented as an arthritis index of disease activity. Statistical analysis was performed as described in Section 2.2.36.

Table 2.4: **Scoring criteria for histological evaluation of joint pathology**

Synovial Infiltrate	
0	Normal
1	Focal inflammatory infiltrates, adiposity hardly affected
2	Focal inflammatory infiltrates equal adiposity
3	Random inflammatory infiltrates dominating cellular histology
4	Substantial inflammatory infiltrates with severe loss of adiposity
5	Ablation of adiposity due to inflammatory infiltrates
Synovial Exudate	
0	Normal
1	Evidence of inflammatory cells in space
2	Moderate numbers of inflammatory cells in space, with evidence of fibrin deposits
3	Substantial number of inflammatory cells with large fibrin deposits
Synovial Hyperplasia and Pannus Formation	
0	Normal (between one and three layers)
1	Over three-layer thick synovial lining and evidence of thickening and/ or invasion of joint space
2	Over three-layer thick synovial lining 'creeping' over cartilage surfaces and/or finger-like processes into joint space
3	Over three-layer thick synovial lining showing substantial covering of cartilage surfaces with evident cartilage loss
Cartilage and Bone Erosion	
0	Normal
1	Detectable loss of cartilage detected by Safranin O staining
2	Detectable erosion of underlying bone by pannus activity
3	Pannus has destroyed a significant part of the bone

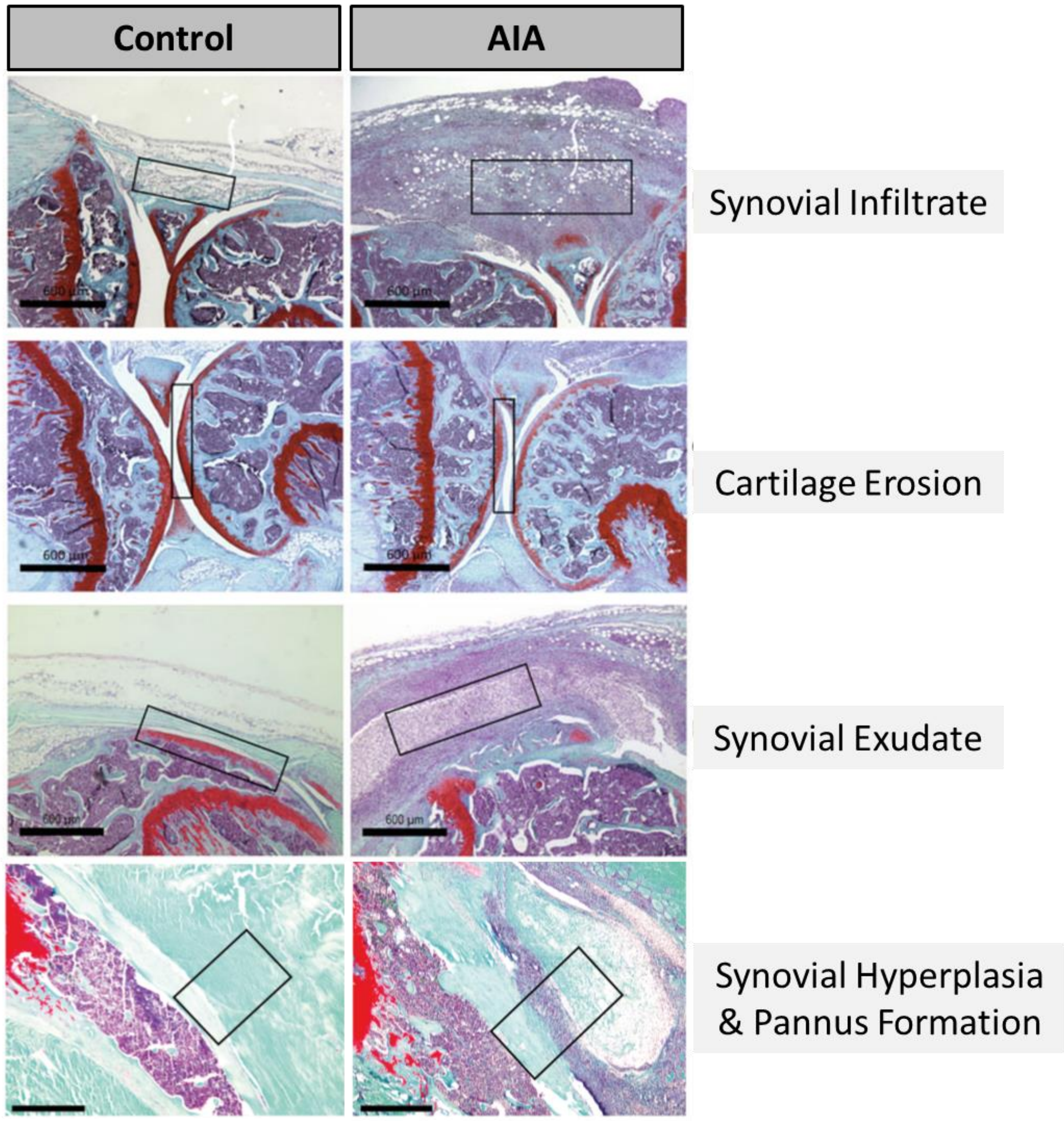

Figure 2.2: Examples of Histological evaluation of joint pathology
Haematoxylin, fast green, and safranin O staining of knee joints at day 10. From top to bottom, boxes focusing areas of synovial infiltrate, cartilage erosion, synovial exudate and synovial hyperplasia and pannus formation. Scale bars: 600 µm. Figure adapted from *Jones et al. 2018* [193,351].

2.2.12 TAT complexes

Plasma thrombin/antithrombin (TAT) complexes were quantified using a murine TAT ELISA Kit, as per the manufacturer's instructions (ab137994, Abcam, UK). Here, plasma samples were diluted at 1:100 before an 2h incubation with a TAT complex-specific antibody. TAT complexes standards were also incubated, with a concentration ranging from 1.95 to 500 pg/ml. After three manual washes with the provided wash buffer, 50 µl of TAT complex-specific biotinylated detection antibody was added to each well and incubated for another 2 h. Followed by another wash, 50 µl of Streptavidin-Peroxidase conjugate was added to each well and incubated for an hour. The plate was once again washed before adding 50 µl of Chromogen Substrate, which was left to react for 20 minutes before adding the Stop Solution. Absorbance was immediately read on a microplate reader (CLARIOstar Plus, BMG Labtech) at 450 nm and values were corrected for background by subtracting readings at 570 nm. All samples and standards were analysed in triplicate. Sample concentrations were calculated by interpolating the blank control subtracted absorbance values against the standard curve, following multiplication by the dilution factor. Statistical analysis was performed as described in Section 2.2.36.

2.2.13 D-Dimers

D-Dimers were analysed using a Mouse D-Dimer, D2D ELISA Kit as per the manufacturer's instructions (CSB-E13584m, Cusabio). Plasma samples were diluted at 1:500 prior to the addition of 100 µl in each well containing immobilized D-Dimer antibody. Standards were also incubated with a concentration ranging from 31.25 to 2000 pg/ml. Samples and standards were incubated for 2h at 37°C, followed by the removal of liquid and the addition of 100 µl of biotin-conjugated antibody specific for D-dimers. The plate was then incubated for an hour at 37°C. Each well was washed manually 3 times with wash buffer, before the addition of 100 µl of avidin-conjugated horseradish peroxidase. After incubation for an hour at 37°C, another washing step was performed.

Subsequently, 90 µl of TMB substrate was added and incubated for 15 minutes protected from light. After incubation with substrate solution, colour develops proportionally with D-Dimer concentration. Colour development is stopped using a stop solution and optical density was read immediately on a microplate reader (CLARIOstar Plus, BMG Labtech) at 450 nm with the background of 570 nm subtracted. All samples and standards were analysed in triplicate. Sample concentrations were calculated by interpolating the blank control subtracted absorbance values against the standard curve, following multiplication by the dilution factor. Statistical analysis was performed as described in Section 2.2.36.

2.2.14 mBSA-specific antibody response

Antigenic response against mBSA was determined through mBSA-specific IgG presence in murine plasma, as previously described [206]. mBSA (5 µg/mL DPBS) was coated on half-area flat bottom 96-well plates and incubated overnight. The plate was washed three times with 0.05% (v/v) Tween 20 in DPBS. Each coated well was then blocked with 5% (w/v) milk in DPBS, with 0.05 % (v/v) Tween 20 for 1 hour, followed by another washing step. Mouse plasma was serially diluted – 1/100; 1/1000; 1/10000; 1/100000 – in 5 % (w/v) milk in DPBS and added to the plate and incubated for 2h. Following another washing step, 0.5 µg/ml of horseradish peroxidase-conjugated goat anti-mouse IgG (ab6789, Abcam, UK) was added to each well and incubated for another 2 hours. The plate was developed through the addition of 90 µl of chromogenic peroxidase substrate 3,3',5,5'-tetramethylbenzidine blue (TMB Development Solution). Colour development was stopped by adding 40 µl of stop solution, followed by the absorbance being immediately read at 450 nm on a microplate reader (CLARIOstar Plus, BMG Labtech). Data expressed as optical density values at 450 nm (OD_{450}). Statistical analysis was performed as described in Section 2.2.36.

2.2.15 C-reactive protein (CRP) levels

CRP in plasma was determined using a Mouse CRP ELISA Kit as per the manufacturer's instructions (ab157712, Abcam, UK). Plasmas were diluted 1:200 before the addition of 100 µl in each well covered with anti-CRP antibodies. Standards were also incubated at concentrations ranging from 0.78 to 25 ng/ml. After a 10 minutes incubation, a manual wash with the provided wash buffer was performed 3 times, followed by the addition of 100 µl of anti-CRP antibodies conjugated with horseradish peroxidase. The plate was then incubated for 10 minutes protected from light. After another washing step, 100 µl of chromogen substrate solution was added to each well and incubated for 5 minutes. Stop solution was then added and absorbance was read immediately at 450 nm on a microplate reader (CLARIOstar Plus, BMG Labtech). All samples and standards were analysed in triplicate. Sample concentrations were calculated by interpolating the blank control subtracted absorbance values against the standard curve, following multiplication by the dilution factor. Statistical analysis was performed as described in Section 2.2.36.

2.2.16 Serum amyloid A1 (SAA) levels

SAA in plasma was determined using a Mouse SAA ELISA Kit as per the manufacturer's instructions (ab215090, Abcam, UK). Plasma samples were diluted 1:1000 before adding 50 µl to each well. Standards were also added in each well, with concentrations ranging from 0.22 to 2.5 ng/ml. This was followed by the addition of 50 µl of antibody cocktail. After a 1-hour incubation, a manual washing step using the provided wash buffer was performed 3 times. Subsequently, 100 µl of TMB Development Solution was added to each well and incubated for 10 minutes whilst protected from light. A stop solution was added before reading absorbance at 450 nm on a microplate reader (CLARIOstar Plus, BMG Labtech). All samples and standards were analysed in duplicate. Sample concentrations were calculated by interpolating the blank control subtracted absorbance values against the standard curve, following multiplication by the dilution factor. Statistical analysis was performed as described in Section 2.2.36.

2.2.17 Prothrombin time

Prothrombin time was measured in plasma using a coagulation analyser (Amelung KC 10) as previously described [212]. Plasma (40 µl) was added to plastic cuvettes with a magnetic bead and incubated at 37 °C for 5 minutes. The cuvette was rotating, while the bead was aligned with a detector, restraining it in a locked position. Next, 100 µl RecombiPlasTin 2G reagent (Werfen) was added. This is a liposomal preparation with recombinant tissue factor relipidated in a phospholipid blend, with calcium chloride [$CaCl_2$], which promotes coagulation. The forming clot entangles the magnetic bead, rupturing the electromagnetic coupling, resulting in the rotation of the bead within the cuvette. The time between the addition of RecombiPlasTin 2G reagent and the termination of the electromagnetic coupling represents the designated prothrombin time, which is measured in seconds. Statistical analysis was performed as described in Section 2.2.36.

2.2.18 Human experimental study design

All experiments followed the principles of the Declaration of Helsinki and were performed with informed consent and with full ethical approval.

Experiments were performed under the project titled *Cardiff Regional Experimental Arthritis Treatment and Evaluation Centre* approved by the Ethics Committee for Wales (Reference No 12/WA/0045). RA patients receiving biological therapies and conventional DMARDs were recruited for venous blood sampling. Patients had no history of venous and/or arterial thrombosis at the time of venipuncture. Details concerning the clinical characteristics of recruited volunteers in this Cardiff clinical cohort can be found in chapter 5. Blood samples were collected from patients during a routine clinic appointment, as described in sections 2.2.22, 2.2.23 and 2.2.24 of this chapter.

Power calculations were performed using data from a previous study on antiphospholipid syndrome[125], where through an online sample size calculator[218], it was determined that each study group should be composed of at least 25 participants in order to achieve statistical significance. The recruitment took place between February 2020 to April 2022, recruiting a total of 25 age and gender-matched healthy volunteers for cell isolation and lipid characterization.

For the analysis of autoantibodies against lipids to identify markers of disease and immune responses against lipids, experiments were performed under the project titled *Study of the lipidomic profile of blood clots from healthy volunteers* approved by the School of Medicine Ethics Review Committee for the study of autoantibodies against lipids relevant in coagulation (REC/SREC reference No 16/02, study 10). Serum samples of RA and osteoarthritis patients were obtained from Leiden University Medical Center collaborators, more precisely through the Early Arthritis Cohort (EAC) biobank. This Leiden clinical cohort study was compared with serum samples generated from blood obtained from 10 healthy volunteers from Cardiff, UK. Details concerning the clinical characteristics of both these cohorts can be found in Chapters 7 and 8.

2.2.19 Healthy volunteers' recruitment

Healthy controls from both studies were recruited with informed consent from the general population (Figure 12.3, Figure 12.4, Figure 12.5, Figure 12.6). Exclusions included a history of arterial or venous thrombosis, recurrent foetal loss, cardiac disease, or any other chronic inflammatory diseases such as diabetes and high cholesterol or any other diseases that may conflict with the study. Healthy control individuals were instructed to not take aspirin, non-steroidal anti-inflammatory drugs, or any other medications in the 14 days before blood donation.

2.2.20 Human Serum isolation

Serum for the *Study of the lipidomic profile of blood clots from healthy volunteers* was obtained employing the same protocol used by the Leiden University Medical Centre Biobank in the *Early Arthritis Cohort.* Using a 21-gauge butterfly needle and a BD vacutainer® (clot activator tube, Thermo-Fisher Scientific, UK) blood was collected from healthy volunteers. Each BD vacutainer® was used to draw blood to a final volume of 10 ml. The vacutainer® tube was then inverted five to ten times, followed by a 30-minutes incubation at room temperature to allow blood to clot. The vacutainer® tube was then centrifuged at 2,340 g for 10 minutes at room temperature. The serum was then isolated and stored immediately at -80 °C until analysis, as described in section 2.2.21.

2.2.21 Determination of autoantibodies against HETE-PLs positional isomers

HETE-PL autoantibody titres were determined by a chemiluminescent ELISA assay as previously described.[125] Here, oxidised phospholipids, namely HETE-PCs and HETE-PE isomers: 5-HETE-PLs, 12-HETE-PLs, 15-HETE-PLs and 8-HETE-PLs, synthesised and isolated as described in Section 2.2.26, along with non-oxidised phospholipids: 1-Stearoyl-2-arachidonoyl-phosphatidylethanolamine (SAPE) and -phosphatidylserine (SAPS), were diluted to 20 µg/µl, and 25 µl was added to each well of a PolySorp® surface plate (ThermoFisher Scientific). The lipids were then dried under an N_2 stream, before each well was blocked using 0.5 % (w/v) fish-gelatine in 0.27 mM EDTA/DPBS (55 µl) and incubated for an hour. In each well, 50 µl serum samples, diluted (1:12) in DPBS-0.27 mM EDTA volumes, were incubated for 1 hour and 30 minutes at room temperature. Wells were manually washed 3 times with DPBS/EDTA solution, before adding 25 µl anti-human IgG alkaline phosphatase-conjugated secondary antibody (Sigma Aldrich) diluted 1:20,000 in blocking solution. After another washing step, 25 µl of LumiPhos 530 (Lumigen, Inc), diluted 1:3 in H_2O, was added to each well. Following incubation for 1 hour and 30 minutes, luminescence was read on a microplate reader (CLARIOstar Plus) and data were expressed as relative light units per 100 ms (RLU/100 ms) values. Statistical analysis was performed as described in Section 2.2.36.

2.2.22 Washed platelet isolation from human blood

Human blood from *Cardiff Regional Experimental Arthritis Treatment and Evaluation Centre* project was collected as previously described [125], using a 21-gauge butterfly needle and two 20 ml venepuncture syringes. Each syringe contained 3.6 ml of ACD [2.5% (w/v) trisodium citrate, 1.5% (w/v) citric acid, and 100 mM Glucose], and blood was slowly drawn until a final volume of 18 ml was obtained. The blood was centrifuged at 400 g for 10 minutes without brake at 22°C. The platelet-rich plasma (PRP) was carefully isolated and recentrifuged at 1400 g without brake for 8 minutes at 22 °C. The platelet-poor plasma (PPP) supernatant was carefully isolated and transferred into Eppendorf tubes for extracellular vesicle (EV) isolation, as described in section 2.2.23.

The platelet pellet was re-suspended with 10 ml of ACD: Tyrode's buffer [145 mM NaCl, 12 mM $NaHCO_3$, 2.95 mM KCl, 1 mM $MgCl_2$, 10 mM HEPES and 5 mM glucose] (1:9 v/v), before centrifuging at 1400 g, without brake, for 8 minutes at 22 °C. Platelets were then isolated and resuspended in 1 ml of Tyrode's buffer. Platelets were counted with a haemocytometer and resuspended at a concentration of 2 x 10^8 cells per ml in Tyrode's buffer. A total of 3 x 10^8 platelets were used as unstimulated controls, while another 3 x 10^8 platelets were stimulated with 0.2 U/ml thrombin and 1 mM $CaCl_2$ for 30 minutes at 37 °C.

Platelets, both in the basal state (unstimulated) and thrombin stimulated, were immediately used for lipid extraction, as described in sections 2.2.27 and 2.2.33. Washed resting platelets were also employed for coagulation studies, namely prothrombinase assay, as outlined in section 2.2.25.

2.2.23 Extracellular vesicle-enriched plasma from human blood

Extracellular vesicles (EV) enriched plasma was obtained as described in *Protty et al. 2021* [223]. PPP, isolated in section 2.2.22, was centrifuged at 300 g for 30 minutes at room temperature. The top layer was discarded and 750 µl of Tyrode's buffer was added to the bottom layer. To generate a washed EV fraction, additional centrifugation at 300 g for 30 minutes was performed. The bottom 5 % fraction was considered an EV's-rich fraction and subsequently, lipids were extracted as outlined in 2.2.28 and 2.2.23, as well as studied through the prothrombinase assay detailed in 2.2.28.

2.2.24 White blood cell isolation from human blood

Human white blood cells were isolated as previously described [125]. Human blood collection was performed using a 21-gauge butterfly needle and a 60-ml syringe. The syringe, containing 4 ml Hetasep™ (Stem Cell Technologies, France) and 4 ml 2 % Citrate, was used to draw 20 ml of blood. After inversion, to ensure the mixing of the anticoagulants with the blood, the syringe was left in an upright position for gravity separation of the blood components. After one hour, the top layer was isolated and centrifuged at 400 g, without brake, for 10 minutes at 4 °C. The pellet was resuspended in ice-cold DPBS/0.4 % citrate before centrifuging again at 400 g for 6 minutes at 4 °C. Red blood cells (RBCs) were lysed through the addition of 5 ml of 0.2 % hypotonic NaCl. After a one-minute incubation, 50 ml of ice-cold DPBS/0.4 % Citrate was added as a washing step. The WBCs were centrifuged at 400 g for 6 minutes at 4°C and second lysis was performed. After pelleting the WBCs, they were resuspended in 1 ml of Krebs buffer [0.1 M NaCl, 5 mM KCl, 47.7 mM HEPES, 1 mM $NaH_2PO_4{\cdot}2H_2O$, 2 mM glucose, pH 7.4] and counted with a haemocytometer. Cells were then resuspended at a concentration of 4 x 10^6 WBCs per ml. A total of 6 x 10^6 WBCs were used in a resting state (unstimulated controls), and 6 x 10^6 WBCs were stimulated with 10 µM Calcium Ionophore A23187 and 1 mM $CaCl_2$ for 30 minutes at 37 °C. Lipids were then extracted as outlined in 2.2.28 and 2.2.23.

2.2.25 Prothrombinase assay

Thrombin generation was determined using an adapted chromogenic assay from previously described prothrombinase assays[209,210]. This was based on the activity of coagulation factors that constitute the prothrombinase complex, enabling the cleavage of prothrombin (Factor II) to thrombin (Factor IIa) (Figure 2.3).

Isolated blood components, namely platelets (4 x 10^6 cells), WBCs (8 x 10^4 cells) or EVs (non-normalised – the equivalent of 6 ml of plasma) were tested. To each well, 20 µl cells/EVs were added, along with 20 µl of coagulation factors, then mixed to initiate the coagulation pathway [1 uM Factor II, 50 nM Factor Xa, 5 mM $CaCl_2$ (Enzyme Laboratories, UK), 15 nM Factor Va (Haematologic, Cambridge Bioscience)]. After 5 minutes, the reaction was quenched with 7 mM EDTA. For the standard curve, a serial dilution of Factor IIa, ranging from 3.125–400 nM, was used. Chromogenic substrate (S2238, 2.8 mM, Enzyme Research), was added to each well. Thrombin cleaves S-2238, freeing p-nitroaniline dye, which is read in a plate reader using absorbance at 405 nm for 15 minutes on a microplate reader (CLARIOstar Plus). The area under the curve of the kinetic reaction was used for quantification purposes. Statistical analysis was performed as described in Section 2.2.36.

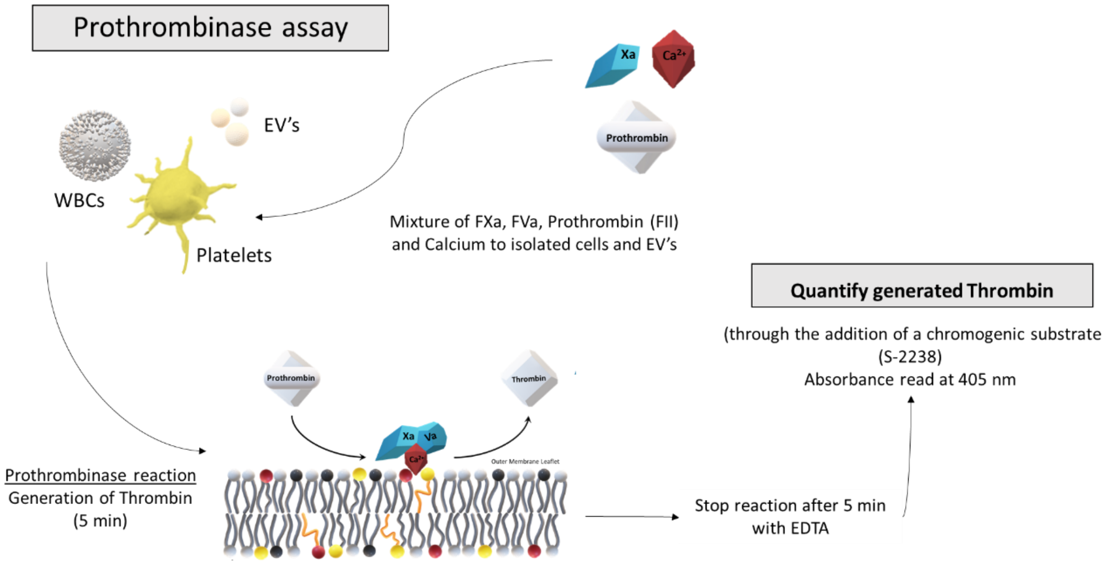

Figure 2.3: Prothrombinase assay

Platelets, white blood cells (WBC's), and extracellular vesicles (EV's) were pipetted into a 96-well half-area plate, as to provide a phospholipid membrane. Coagulation mix containing calcium, FII, FXa, FVa was added to each well, generating thrombin. The reaction was allowed to proceed for 5 minutes, before being quenched with EDTA. The amount of thrombin (FIIa) made was quantified using a chromogenic substrate S-2238 and a plate reader in absorbance mode (405nm) against a standard curve of human thrombin. Figure designed using PowerPoint.

2.2.26 HETE-PL standards

HETE-PLs were generated as mixed isomers, being used both as a racemic mixture and as individual positional isomers once isolated and purified, as previously described by Morgan et al.[213]. Specifically, 5 mg of 1-Stearoyl-2-arachidonoyl-phosphatidylethanolamine (SAPE) or -phosphatidylserine (SAPS), was resuspended in 1.5 ml methanol, in the presence of 64 µl of 10 mM pentamethylchromanol, which, as a reducing agent, will convert lipid peroxyl radicals to lipid hydroperoxides and stabilise them. The mixture was then dried under an N_2 stream and air oxidized through incubation at 37 °C for 24 hours. Subsequently, this lipid mixture was resuspended in 200 µl of methanol, and the lipid hydroperoxides were reduced to hydroxides by the addition of 10 µl of 100 mM $SnCl_2$, generating an isomeric mixture of PC 18:0a/HETE or PE 18:0a/HETE. Lipids were extracted by adding 3.3 ml of extraction solvent [MeOH: $CHCl_3$: H_2O (8:20:5, v/v/v)] to the lipids, followed by vortexing and centrifugation at 1475 g for 5 minutes. Lipids were recovered from the bottom chloroform layer using a glass Pasteur pipette. The recovered layer was then dried under N_2 and resuspended in 200 µl of methanol prior to the purification protocol.

HETE-PLs were purified as a mixed isomer mixture, free from the unoxidized substrate or other products using reversed-phase liquid chromatography on an HPLC instrument (1260 Infinity, Agilent Technologies). The column used was a Supelco Discovery C_{18} (25 cm x 4.6 mm x 5 µm). A gradient elution method with a flow rate of 1 ml/min was used: 50 % - 100 % mobile phase B (A: H_2O, 5 mM $NH_4CH_3CO_2$, B: MeOH, 5 mM $NH_4CH_3CO_2$) for 15 minutes, then held at 100 % of B for 20 minutes. The elute was monitored at 205 nm for unoxidized lipid substrate and 235 nm for oxidized lipids (HETE-PLs). The HETE-PLs are typically eluted between 24–26 minutes with six closely eluting chromatographic peaks, each peak representing a positional isomer. Fractions were collected that contain all 6 positional isomers in a single sample and stored at -80 °C prior to further analysis.

For the isolation of individual positional isomers, a reversed-phase liquid chromatography HPLC method was performed using two Supelco Discovery C18 columns (25 cm x 21.2 mm x 5 µm) connected in series, with a gradient of 100 % mobile phase B (A: 100 % MeOH, B: 95 % MeOH, 5% H_20) for 200 minutes, followed by 100 %

mobile phase A for 100 minutes with a total flow rate of 10 ml/min. The elution was monitored at 205 nm for unoxidized lipid substrate and 235 nm for oxidized lipids (HETE-PLs). The HETE-PLs eluted at approximately 100 minutes, in the following order: 15-, 11-, 12-, 8-, 9- and 5-HETE-PL, with sufficient separation to enable the collection of individual isomers separately. The eluted HETE-PLs were collected in 30 ml glass vials with screw phenolic caps (Fisherbrand®, Fischer Scientific), dried under N_2 and resuspended in 200 µl of methanol. Generation of HETE-PLs isomers was confirmed on a 4000 Q-Trap® (Sciex, Cheshire, United Kingdom), through direct injection of diluted standards at 10 µl/min with a 1 ml Hamilton® Gas-tight glass syringe (4.61 mm diameter) with a needle. Purity was confirmed through a Q1 ion scan, while an enhanced product ion (EPI) scan was used to monitor the precursor ion to product ion transitions (Table 2.5) for each isomer for either PC or PE was monitored, with a dwell time of 100 ms, using the following ion source parameters:

Temperature: 500 °C, Curtain gas (CUR): 20 psi, Source Gas 1 (GS1): 40 psi, Source Gas 2 (GS2): 30 psi, Ion spray voltage: -4500 V, entrance potential (EP): − 10V

Once isolation and purity of the oxPLs was confirmed, HETE-PLs were quantified by spectrophotometry using absorbance at 235 nm, using $\varepsilon_{1mm,1cm}$ = 28 absorbance units (au). Once quantified, HETE-PLs were stored at − 80 °C under N_2 until further use as standards in Section 2.2.28. or used to analyse autoantibodies against HETE-PLs in Section 2.2.21.

Table 2.5: Multiple reaction monitoring (MRM) transitions for oxPL standards precursor ion to product ion transitions for EPI
[Declustering potential (DP), collision potential (CE), Collision cell exit potential (CXP)]

Standard	Molecular mass (g/mol)	MRM transition	Q1	Q3	DP (V)	CE (V)	CXP (V)
PC(18:0a_5-HETE)	825.6	810.7 → 115.1	810.7	115.1	-140	-45	-7
PC(18:0a_12-HETE)	825.6	810.7 → 179.1	810.7	179.1	-140	-45	-7
PC(18:0a_15-HETE)	825.6	810.7 → 219.1	810.7	219.1	-140	-45	-7
PC(18:0a_11-HETE)	825.6	810.7 → 167.1	810.7	167.1	-140	-45	-7
PC(18:0a_8-HETE)	825.6	810.7 → 155.1	810.7	155.1	-140	-45	-7
PC(18:0a_9-HETE)	825.6	810.7 → 151.1	810.7	151.1	-140	-45	-7
PE(18:0a_5-HETE)	783.6	782.6 → 115.1	782.6	115.1	-140	-45	-7
PE(18:0a_12-HETE)	783.6	782.6 → 179.1	782.6	179.1	-140	-45	-7
PE(18:0a_15-HETE)	783.6	782.6 → 219.1	782.6	219.1	-140	-45	-7
PE(18:0a_11-HETE)	783.6	782.6 → 167.1	782.6	167.1	-140	-45	-7
PE(18:0a_8-HETE)	783.6	782.6 → 155.1	782.6	155.1	-140	-45	-7
PE(18:0a_9-HETE)	783.6	782.6 → 151.1	782.6	151.1	-140	-45	-7

2.2.27 Lipid extraction of washed cells

Washed cells isolated in sections 2.2.21 and 2.2.23 were diluted into 1 ml of sample volume, and lipids were extracted as previously described [125,212]. Platelet samples contained a total of 2 x 10^8 cells in the 1 ml of sample, whereas white blood cell samples contained 4 x 10^6 cells. The EV samples obtained in section 2.2.22 were diluted 1:6 (v/v) with Tyrode's buffer, in a total volume of 1.5 ml. Of this, 1 ml was used for EV oxPLs lipid extraction.

To each of these samples (resting/activated platelets, resting/activated WBC or plasma EV), 2.5 ml of a solvent mix was added containing hexane: IPA:1 M acetic acid (30:20:2 v/v), along with 10 ng of DMPE [PE(14:0/14:0)] and DMPC [PC(14:0/14:0)] as internal standard. The mixture was then vortexed and incubated at 4 °C for 30 minutes. Then, 2.5 ml of hexane was added to each extraction tube, followed by vortexing and centrifuging at 4 °C for 5 minutes at 1475 g. The top layer was recovered using glass Pasteur pipettes and transferred to clean extraction vials and placed at 4 °C. This extraction step was repeated by adding 2.5 ml of hexane, vortexing and centrifuging again at 4 °C for 5 minutes at 1475 g. The top layer was recovered and added to the previously isolated top phase. The recovered top layers were combined and then dried using a Rapidvap N2/48 evaporation system (Labconco Corporation), They were resuspended in 200 µl methanol, and stored at − 80 °C under N_2 prior to analysis by LC/MS/MS, as described in section 2.2.28 below.

2.2.28 LC/MS/MS analysis of oxPLs

Lipid extracts were separated using reverse-phase HPLC on a Luna C_{18} column (150 mm x 2 mm x 3µm) (Phenomenex, Torrance, CA). A gradient elution method of 50 – 100 % B over 10 minutes followed by 30 minutes at 100 % B (A, methanol:acetonitrile:water, 1 mM $NH_4CH_3CO_2$, 60:20:20; B, methanol, 1 mM $NH_4CH_3CO_2$) was applied with a total flow rate of 200 µl/min.

Products were analysed in multiple reaction monitoring (MRM) mode, on a 6500 Q-Trap (Sciex, Cheshire, United Kingdom) using the following ion source parameters:

Temperature: 500 °C, Curtain gas (CUR): 35 psi, Source Gas 1 (GS1): 40 psi, Source Gas 2 (GS2): 30 psi, Ion spray voltage: -4500 V, entrance potential (EP): − 10V

Transitions were monitored from precursor mass (Q1 *m/z*) to product ion mass (Q3 *m/z*) in negative ion mode, with a dwell time of 75 msec (Table 2.6).

The area under the curve for the precursor ion to product ion transition was integrated using Multiquant 3.0.2. (AB Sciex, Canada) and normalized to the corresponding IS. For mouse samples, both whole blood pellets and synovial tissue lipidomics, SPLASH® LIPIDOMIX® Mass Spec Standard was used as an IS mixture, containing 10 ng of PE(15:0/18:1(*d7*)) and 284 ng of PC(15:0/18:1(*d7*)) added per sample as outlined in section 2.2.6 and 2.2.8. In the case of human-washed cells, IS mixture used consisted of 10 ng of DMPE and 10 ng of DMPC, as described in section 2.2.27. For quantification, a mixed isomer HETE-PLs standard curve was generated and a known isomer ratio was used for the determination of each lipid isomer concentration[213]. Statistical analysis was performed as described in Section 2.2.36.

Table 2.6: MRM transition for oxPL precursor ion to product ion transitions
Declustering potential (DP), collision potential (CE), Collision cell exit potential (CXP)

Analyte		Molecular mass (g/mol)	MRM transition	Q1	Q3	DP (V)	CE (V)	CXP (V)
PE(16:0p_5-HETE)		739.6	738.6 → 115.1	738.6	115.1	-50	-38	-11
PE(16:0p_12-HETE)		739.6	738.6 → 179.1	738.6	179.1	-50	-38	-11
PE(16:0p_15-HETE)		739.6	738.6 → 219.1	738.6	219.1	-50	-38	-11
PE(16:0p_11-HETE)		739.6	738.6 →167.1	738.6	167.1	-50	-38	-11
PE(16:0p_8-HETE)		739.6	738.6 → 155.1	738.6	155.1	-50	-38	-11
PE(16:0p_HETE)		739.6	738.6 → 319.2	738.6	319.2	-50	-38	-11
PE(18:1p_5-HETE)		765.6	764.6 → 115.1	764.6	115.1	-50	-38	-11
PE(18:1p_12-HETE)		765.6	764.6 → 179.1	764.6	179.1	-50	-38	-11
PE(18:1p_15-HETE)		765.6	764.6 → 219.1	764.6	219.1	-50	-38	-11
PE(18:1p_11-HETE)		765.6	764.6 → 167.1	764.6	167.1	-50	-38	-11
PE(18:1p_8-HETE)		765.6	764.6 → 155.1	764.6	155.1	-50	-38	-11
PE(18:1p_HETE)		765.6	764.6 → 319.2	764.6	319.2	-50	-38	-11
PE(18:0p_5-HETE)		765.6	766.67 → 115.1	766.6	115.1	-50	-38	-11
PE(18:0p_12-HETE)		767.6	766.6 → 179.1	766.6	179.1	-50	-38	-11
PE(18:0p_15-HETE)		767.6	766.6 → 219.1	766.6	219.1	-50	-38	-11
PE(18:0p_11-HETE)		767.6	766.6 → 167.1	766.6	167.1	-50	-38	-11
PE(18:0p_8-HETE)		767.6	766.6 → 155.1	766.6	155.1	-50	-38	-11
PE(18:0p_HETE)		767.6	766.6 → 319.2	766.6	319.2	-50	-38	-11
PE(18:0a_5-HETE) or PC(16:0a_5-HETE)		783.6 or 797.6	782.6 → 115.1	782.6	115.1	-50	-38	-11
PE(18:0a_12-HETE) or PC(16:0a_12-HETE)		783.6 or 797.6	782.6 → 179.1	782.6	179.1	-50	-38	-11
PE(18:0a_15-HETE) or PC(16:0a_15-HETE)		783.6 or 797.6	782.6 → 219.1	782.6	219.1	-50	-38	-11
PE(18:0a_11-HETE) or PC(16:0a_11-HETE)		783.6 or 797.6	782.6 → 167.1	782.6	167.1	-50	-38	-11
PE(18:0a_8-HETE) or PC(16:0a_8-HETE)		783.6 or 797.6	782.6 → 155.1	782.6	155.1	-50	-38	-11
PE(18:0a_HETE) or PC(16:0a_HETE)		783.6 or 797.6	782.6 → 319.2	782.6	319.2	-50	-38	-11
PC(18:0a_5-HETE)		825.6	810.7 → 115.1	810.7	115.1	-50	-38	-11
PC(18:0a_12-HETE)		825.6	810.7 → 179.1	810.7	179.1	-50	-38	-11
PC(18:0a_15-HETE)		825.6	810.7 → 219.1	810.7	219.1	-50	-38	-11
PC(18:0a_11-HETE)		825.6	810.7 → 167.1	810.7	167.1	-50	-38	-11
PC(18:0a_8-HETE)		825.6	810.7 → 155.1	810.7	155.1	-50	-38	-11
PC(18:0a_HETE)		825.6	810.7 → 319.2	810.7	319.2	-50	-38	-11
IS	**PE(15:0_18:1(d7))** (SPLASH® LIPIDOMIX® Mass Spec Standard)	711.013	709.6 → 288.3	709.6	288.3	-50	-38	-11
IS	**PC(15:0_18:1(d7))** (SPLASH® LIPIDOMIX® Mass Spec Standard)	753.093	811.6 → 288.2	811.6	288.2	-50	-38	-11

2.2.29 Alkaline hydrolysis of lipid extracts for chiral HETE analysis

Lipid extracts were dried under a stream of N_2 and resuspended in 1.5 ml IPA. The resuspended lipids were vortexed, followed by the addition of 1.5 ml 1 M NaOH. The lipids were then incubated for 30 minutes at 60 °C in a dry bath incubator. Afterwards, the extracts were acidified to pH 3.0 using 150 µl of 1 M HCl before re-extraction, as follows: To each sample in a glass extraction tube, 3 ml hexane was added. The samples were then vortexed and centrifuged at 4 °C for 5 minutes at 1475 g. The top organic layer was recovered, and another 3 ml hexane was added to the remaining bottom layer followed by vortexed and centrifugation at 4 °C for 5 minutes at 1475 g. The top layer was recovered and combined with the previously isolated organic layer. The IS used is 12(S)-HETE-(d8), which is already present in the lipid extracts, as described in section 2.2.6. The combined hexane layers were dried using a Rapidvap N2/48 evaporation system (Labconco Corporation). Lipids were resuspended in 150 µl of methanol, and stored at − 80 °C in an N_2 atmosphere until analysis by LC/MS/MS, as described in Section 2.2.30.

2.2.30 LC/MS/MS analysis of chiral HETEs

Lipid extracts were run before and after alkaline hydrolysis, and the enantiomeric concentration of oxPLs was determined through the subtraction of total HETEs (after hydrolysis) and free HETEs (before hydrolysis). Separation was achieved using reversed-phase HPLC on a ChiralPak AD-RH column (150 mm × 4.6 mm x 5 µm; Daicel Corporation) with an isocratic gradient of methanol:water:glacial acetic acid 95:5:0.1 (v/v) with flow rate 300 µl/min for 25 minutes at 40 °C.

Products were analysed in MRM mode, on a 4000 Q-Trap (Sciex, Cheshire, United Kingdom). Transitions were monitored from precursor mass (Q1 *m/z* italics for all these) to product ion mass (Q3 m/z) in negative ion mode (Table 2.7), with a dwell time of 125 msec, and the following ion source parameters:

Temperature: 500 °C, Curtain gas (CUR): 20 psi, Source Gas 1 (GS1): 40 psi, Source Gas 2 (GS2): 30 psi, Ion spray voltage: -4500 V, entrance potential (EP): − 10V

The area under the curve for the precursor ion to product ion transition was integrated using Multiquant 3.0.2. (AB Sciex, Canada) and normalized to the corresponding IS. For quantification, specific isomeric standards were used to generate a standard curve, and lipids were quantified as described in Section 2.2.35. Statistical analysis was performed as described in Section 2.2.36 of this thesis.

Table 2.7: MRM transition for free HETEs precursor ion to product ion transitions
Declustering potential (DP), collision potential (CE), Collision cell exit potential (CXP)

	Analyte	Molecular mass (g/mol)	MRM transition	Q1	Q3	DP (V)	CE (V)	CXP (V)
	5-HETE	320.47	319.2 → 115.1	319.2	115.1	-70	-22	-7
	12-HETE	320.47	319.2 → 179.1	319.2	179.1	-75	-22	-9
	15-HETE	320.47	319.2 → 219.1	319.2	219.1	-70	-20	-13
	11-HETE	320.47	319.2 → 167.1	319.2	167.1	-75	-24	-1
	8-HETE	320.47	319.2 → 155.1	319.2	155.1	-70	-22	-9
IS	**12-HETE-d8**	328.5	327.3 → 184	327.3	184	-80	-22	-11

2.2.31 LC/MS/MS analysis of oxylipins

Lipid extracts obtained in sections 2.2.6 and 2.2.8 were analysed by LC/MS/MS. Lipids were separated using reverse phase HPLC on an Agilent Eclipse Plus C_{18} column (150 mm x 2.1 mm x 1.8 µm) (Phenomenex, Torrance, CA) t 45 °C, with a flow rate of 500 µl/min. A gradient elution method was used where mobile phase B is held at 30 % for 1 minute, then increased to 100 % B from 1 - 17.5 minutes (A: 94.9 % water, 5 % solvent B, 0.1 % glacial acetic acid; B: 84 % acetonitrile, 15.9 % methanol, 0.1 % glacial acetic acid), 100 % B is held from 17.5 -21 minutes, followed by a decrease to 30 % of B from 21 - 22.5 minutes, which is held until the end of the run at 22.5 minutes. Lipids were analysed using a scheduled MRM method on a 6500 Q-Trap (Sciex, Cheshire, United Kingdom). A time window is set for the detection of each analyte according to the expected retention time, and transitions are monitored from precursor mass (Q1 *m/z*) to product ion mass (Q3 *m/z*) in negative ion mode, under the following ion source parameters: (Table 2.8).

Temperature: 475 °C, Curtain gas (CUR): 35 psi, Source Gas 1 (GS1): 60 psi, Source Gas 2 (GS2): 60 psi, Ion spray voltage: -4500 V, entrance potential (EP): −10V.

The area under the curve for the precursor ion to product ion transition was integrated using Multiquant 3.0.2. (AB Sciex, Canada) and normalized to the corresponding IS. For quantification, specific isomeric standards were used to generate a standard curve. An equation for calculation was obtained using $1/x^2$ weighted linear regression. Statistical analysis was performed as described in Section 2.2.36.

Table 2.8: MRM transition for oxylipins precursor ion to product ion transitions
Declustering potential (DP), collision potential (CE), Collision cell exit potential (CXP)

Analyte	Molecular mass (g/mol)	MRM transition	Q1	Q3	Retention time (min)	DP (V)	CE (V)	CXP (V)
5-HETE	320.5	319.2 → 115.1	319.2	115.1	14.4	-55	-19	-7
8-HETE	320.5	319.2 → 155.1	319.2	155.1	14.1	-65	-18	-8
9-HETE	320.5	319.2 → 167.1	319.2	167.1	14.27	-50	-20	-9
11-HETE	320.5	319.2 →167.1	319.2	167.1	13.91	-60	-19	-9
12-HETE	320.5	319.2 → 179.1	319.2	179.1	14.11	-65	-18	-12
15-HETE	320.5	319.2 → 219.1	319.2	219.1	13.65	-55	-18	-14
20-HETE	320.5	319.2 → 275.1	319.2	275.1	12.64	-85	-21	-11
5-HEPE	318.4	317.2 → 115.1	317.2	115.1	13.17	-60	-20	-10
8-HEPE	318.4	317.2→ 155.1	317.2	155.1	12.8	-65	-19	-8
9-HEPE	318.4	317.2→ 167.1	317.2	167.1	12.99	-50	-18	-12
11-HEPE	318.4	317.2→ 167.1	317.2	167.1	12.69	-50	-20	-13
12-HEPE	318.4	317.2→ 179.1	317.2	179.1	12.91	-65	-18	-8
15-HEPE	318.4	317.2→ 219.1	317.2	219.1	12.63	-65	-16	-10
18-HEPE	318.4	317.2→ 259.1	317.2	259.1	12.25	-50	-15	-11
4-HDOHE	344.5	343.2 → 101.1	343.2	101.1	14.66	-50	-17	-9
7-HDOHE	344.5	343.2 → 141.1	343.2	141.1	14.2	-50	-21	-9
8-HDOHE	344.5	343.2 → 189.1	343.2	189.1	14.31	-50	-19	-9
10-HDOHE	344.5	343.2 → 153.1	343.2	153.1	13.99	-55	-21	-5
11-HDOHE	344.5	343.2 → 121.1	343.2	121.1	14.14	-60	-18	-10
13-HDOHE	344.5	343.2 → 193.1	343.2	193.1	13.87	-55	-19	-9
14-HDOHE	344.5	343.2 → 205.1	343.2	205.1	13.99	-45	-17	-9
16-HDOHE	344.5	343.2 → 233.1	343.2	233.1	13.73	-55	-17	-10
17-HDOHE	344.5	343.2 → 201.1	343.2	201.1	13.79	-70	-15	-10
20-HDOHE	344.5	343.2 → 241.1	343.2	241.1	13.47	-55	-17	-11
9-HODE	296.4	295.2 → 171.1	295.2	171.1	13.34	-85	-23	-9
13-HODE	296.4	295.2 → 195.1	295.2	195.1	13.28	-85	-23	-7
9-HOTrE	294.4	293.2 → 171.1	293.2	171.1	12	-60	-20	-8
13-HOTrE	294.4	293.2 → 195.1	293.2	195.1	12.2	-70	-22	-12
5-HETrE	322.5	321.2 → 115.1	321.2	115.1	15.49	-70	-19	-9
15-HETrE	322.5	321.2 → 221.1	321.2	221.1	14.29	-70	-21	-11
9-OxoODE	294.4	293.2 → 185.1	293.2	185.1	14	-85	-23	-13
13-OxoODE	294.4	293.2 → 195.1	293.2	195.1	13.72	-85	-25	-12
5-OxoETE	318.4	317.2 → 273.1	317.2	273.1	15.06	-65	-20	-11
12-OxoETE	318.4	317.2 → 153.1	317.2	153.1	14.36	-75	-20	-10
15-OxoETE	318.4	317.2 → 113.1	317.2	113.1	14	-60	-22	-8
9,10-DiHOME	313.5	313.2 → 201.1	313.2	201.1	10.9	-80	-29	-8
12,13-DiHOME	313.5	313.2 → 183.1	313.2	183.1	10.62	-80	-28	-12
5,6-DiHETrE	338.5	337.2 → 145.1	337.2	145.1	12.64	-75	-24	-10
8,9-DiHETrE	338.5	337.2 → 127.1	337.2	127.1	12.14	-70	-25	-8
11,12-DiHETrE	338.5	337.2 → 167.1	337.2	167.1	11.79	-65	-26	-8
14,15-DiHETrE	338.5	337.2 → 207.1	337.2	207.1	11.45	-65	-25	-10
5,6-DiHETE	336.5	335.2 → 115.1	335.2	115.1	11.2	-60	-23	-8
5,15-DiHETE	336.5	335.2 → 115.1	335.2	115.1	9.92	-60	-21	-9
8,15-DiHETE	336.5	335.2 → 235.1	335.2	235.1	9.63	-65	-22	-4
14,15-DiHETE	336.5	335.2 → 207.1	335.2	207.1	10.35	-65	-23	-10
17,18-DiHETE	336.5	335.2 → 247.1	335.2	247.1	9.97	-65	-24	-8
RvE1	350.5	349.2 → 195.1	349.2	195.1	3.21	-65	-22	-10
RvD1	376.5	375.2 → 215.1	375.2	215.1	7.47	-55	-23	-9
RvD2	376.5	375.2 → 141.1	375.2	141.1	6.8	-65	-21	-11
RvD3	376.5	375.2 → 147.1	375.2	147.1	6.49	-65	-24	-12
RvD5	360.5	359.2 → 199.1	359.2	199.1	10.09	-65	-22	-17
LTB3	338.5	337.2 → 195.1	337.2	195.1	11.5	-65	-22	-8
LTB4	336.5	335.2 → 195.1	335.2	195.1	10.22	-70	-23	-11
20-carboxy LTB4	366.4	365.2 → 347.2	365.2	347.2	3.24	-80	-25	-8
20-hydroxy LTB4	352.5	351.2 → 195.1	351.2	195.1	3.55	-80	-25	-8
6-trans LTB4	336.5	335.2 → 195.1	335.2	195.1	9.89	-65	-23	-9
LXA4	352.5	351.2 → 115.1	351.2	115.1	7.32	-55	-19	-10
Mar 1	360.5	359.2 → 250.1	359.2	250.1	10.1	-60	-23	-11
7,17-diHDPA	362.5	361.2 → 263.1	361.2	263.1	10.38	-65	-20	-4

Continuation of **Table 2.9: MRM transition for oxylipins precursor ion to product ion transitions**

Analyte	Molecular mass (g/mol)	MRM transition	Q1	Q3	Retention time (min)	DP (V)	CE (V)	CXP (V)
9(10)-EpOME	296.4	295.2 → 171.1	295.2	171.1	14.86	-80	-21	-10
12(13)-EpOME	296.4	295.2 → 195.1	295.2	195.1	14.74	-80	-19	-8
5(6)-EET	320.5	319.2 → 191.1	319.2	191.1	15.37	-60	-16	-7
8(9)-EET	320.5	319.2 → 167.1	319.2	167.1	15.15	-60	-15	-7
11(12)-EET	320.5	319.2 → 167.1	319.2	167.1	15.15	-60	-18	-8
14(15)-EET	320.5	319.2 → 219.1	319.2	219.1	14.84	-65	-18	-6
8(9)-EpETE	318.4	317.2 → 127.1	317.2	127.1	14.2	-70	-18	-8
11(12)-EpETE	318.4	317.2 → 167.1	317.2	167.1	14.12	-70	-15	-11
14(15)-EpETE	318.4	317.2 → 207.1	317.2	207.1	14.04	-70	-18	-6
17(18)-EpETE	318.4	317.2 → 215.1	317.2	215.1	13.7	-75	-16	-10
7(8)-EpDPA	344.5	343.2 → 113.1	343.2	113.1	15.2	-60	-16	-7
10(11)-EpDPA	344.5	343.2 → 153.1	343.2	153.1	15.08	-65	-15	-7
13(14)-EpDPA	344.5	343.2 → 193.1	343.2	193.1	15.02	-70	-15	-7
16(17)-EpDPA	344.5	343.2 → 233.1	343.2	233.1	14.97	-55	-16	-9
19(20)-EpDPA	344.5	343.2 → 241.1	343.2	241.1	14.71	-70	-18	-11
PGD1	354.5	353.2 → 317.2	353.2	317.2	6.65	-55	-16	-8
PGD2	352.5	351.2 → 271.1	351.2	271.1	6.61	-50	-22	-8
PGD3	350.4	349.2 → 269.1	349.2	269.1	5.26	-50	-17	-11
PGE1	368.5	353.2 → 317.1	353.2	317.2	6.53	-60	-18	-10
PGE2	352.5	351.2 → 271.1	351.2	271.1	6.2	-60	-19	-12
PGE3	350.4	349.2 → 269.1	349.2	269.1	4.86	-60	-17	-10
PGB2	334.4	333.2 → 175.1	333.2	175.1	8.82	-60	-24	-10
13,14-dihydro-15-keto PGE2	352.5	351.2 → 235.1	351.2	235.1	7.33	-55	-19	-13
13,14-dihydro-15-keto PGD2	352.5	351.2 → 207.1	351.2	207.1	8.16	-50	-25	-13
13,14-dihydro-15-keto PF2α	354.5	353.2 → 113.1	353.2	113.1	7.43	-55	-23	-11
11β-PGE2	352.5	351.2 → 271.1	351.2	271.1	6.38	-55	-23	-7
6-keto PGE1	368.5	367.2 → 143.1	367.2	143.1	3.22	-55	-23	-9
8-iso PGE2	352.5	351.2 → 271.1	351.2	271.1	5.94	-55	-21	-10
15-deoxy-Δ12,14-PGJ2	316.4	315.2 → 271.1	315.2	271.1	12.44	-65	-18	-8
8-iso-15-keto PGF2α	352.5	351.2 → 289.1	351.2	289.1	5.37	-50	-23	-12
PGF2α	354.5	353.2 → 309.1	353.2	309.2	5.89	-85	-24	-9
6-keto PGF1α	370.5	369.2 → 163.1	369.2	163.1	3.3	-75	-26	-10
Thromboxane B2	370.5	369.2 → 169.1	369.2	169.1	4.83	-60	-22	-12
IS 11-dehydro Thromboxane B2	368.5	367.2 → 305.1	367.2	305.2	6.24	-60	-20	-10
IS 13(S)-HODE-d4	300.5	327.2 → 226.1	327.2	226.1	13.22	-60	-25	-7
IS 5(S)-HETE-d8	328.5	325.2 → 281.1	325.2	281.1	14.32	-55	-19	-8
IS 12(S)-HETE-d8	328.5	339.2 → 197.1	339.2	197.1	14.02	-60	-20	-12
IS 15(S)-HETE-d8	328.5	380.2 → 141.1	380.2	141.1	13.55	-65	-22	-11
IS 20-HETE-d6	326.5	355.2 → 275.1	355.2	275.1	12.6	-70	-21	-8
IS Leukotriene B4-d4	340.5	355.2 → 275.1	355.2	275.1	10.17	-65	-21	-9
IS Resolvin D1-d5	360.5	357.2 → 313.2	357.2	313.2	7.41	-75	-18	-11
IS Prostaglandin E2-d4	356.5	373.2 → 173.1	373.2	173.1	6.16	-60	-23	-12
IS Prostaglandin D2-d4	352.5	371.2 → 309.2	371.2	309.2	6.58	-55	-23	-10
IS Prostaglandin F2α-d4	358.5	331.2 → 167.1	331.2	167.1	5.86	-80	-24	-9
IS Thromboxane B2-d4	374.5	319.2 → 115.1	319.2	115.1	4.79	-55	-22	-10
IS 11-dehydro Thromboxane B2-d4	372.5	319.2 → 155.1	319.2	155.1	6.21	-55	-21	-11
IS 11(12)-EET (EpETrE) -d11	320.5	319.2 → 167.1	319.2	167.1	15.09	-65	-18	-11

2.2.32 Biotinylated standards

Biotinylated phospholipid standards (DMPE-B, DMPS-B, SOPS-B, SAPS-B, SAPE-B, SpAPE-B, DOPS-B) were generated as previously published by Thomas et al.[224].

This was undertaken as follows: lipid (1 mg) was dried under N_2 followed by reconstitution in 330 µl of chloroform:methanol (2:1 v/v). To each lipid, 6 mg of EZ-Link™ NHS-Biotin (ThermoFisher, UK) was added to provide a final concentration of 52 mM. To the reconstituted lipid, 3.3 µl of triethylamine (Sigma-Aldrich) was added as a proton acceptor and incubated at room temperature for 30 minutes to allow biotinylation of primary amines on PS/PE head groups to occur. The solution was then centrifuged at 500 g for 5 minutes at 20 °C to sediment the excess NHS-Biotin. The solvent was transferred to a clean glass vial and the remaining NHS-biotin sediment was washed with 330 µl of chloroform: methanol (2:1 v/v), vortexed and re-spin at 500 g for 5 minutes. The solvent was merged with the previously isolated solvent. The biotinylated lipids were dried under N_2 and resuspended in 500 µl of methanol before HPLC purification.

Biotinylated standards were purified using HPLC on a Supelco Discovery C_{18} column with a 15-minute gradient elution profile of 50 % mobile phase B to 100 % mobile phase B (A: 5 mM $NH_4CH_3CO_2$ in water, B: 5 mM $NH_4CH_3CO_2$ in methanol), then held at 100 % mobile phase B for 20 minutes. The biotinylated lipids were monitored at 205 nm and eluted from the column at approximately 20 minutes. The biotinylated lipids were collected, dried using a Rapidvap N2/48 evaporation system (Labconco Corporation), and resuspended in 200 µl of methanol.

The lipids were then quantified by transferring them into fresh pre-weighed HPLC vials, dried under N_2 and accurately weighed to determine the purified mass. All biotinylated lipids were then resuspended at 100 ng/µl stocks in methanol, transferred to HPLC vials with fixed glass inserts, capped in an N_2 atmosphere and then stored at -80 °C prior to further use. Immediately before lipid extraction described in section 2.2.33, the stock solution of IS, namely biotinylated DMPS/DMPE, was diluted in methanol to a final concentration of 1 ng/µl of each IS.

2.2.33 Externalization of PE or PS on the surface of human platelets, white blood cells and EVs

Aminophospholipids externalization was analysed as previously described by as previously published by Thomas et al.[224]. Washed cells isolated in sections 2.2.22 and 2.2.24 were used at a concentration of 2 x 10^8 cells/ml, in the case of platelets, and 4 x 10^6 cells/ml in the case of WBC. The EV samples were diluted 1:6 (v/v) with Tyrode's buffer, in a total volume of 1.5 ml. Of each sample, a volume of 0.2 ml was used for this assay.

For externalised (outer membrane leaflet) aminophospholipids, 0.2 ml of washed cells, in both resting and activated states, along with EVs were incubated with 86 µl of 11 mM EZ-Link™ Sulfo-NHS-biotin for 10 minutes at room temperature. The reaction was quenched by the addition of 250 mM L-Lysine (72 µl) followed by a 10-minute incubation, which removed the unreacted biotin reagent. Finally, 42µl of DPBS was added to bring the total volume to 400 µl.

For labelling of total aminophospholipids, 0.2 ml of washed cells in both resting and activated states, along with 0.2 ml of EVs, were incubated with 20 µl of 20 mM EZ-Link™ NHS-biotin (Thermo-Fisher Scientific, UK), dissolved in dimethyl sulfoxide (Sigma-Aldrich, UK), for 10 minutes at room temperature. The final volume was made up to 0.4 ml by adding 180 µl DPBS.

Next, to each sample, 10 µl of IS mix (biotinylated DMPS/DMPE), prepared as described above in section 2.2.22, was added. Phospholipids were extracted using the Bligh and Dyer method [225]. Each sample was added to 1.5 ml of a solvent mixture composed of chloroform:methanol (1:2 v/v) and vortexed. Afterwards, 0.5 ml of $CHCl_3$ was added and vortexed. Last, 0.5 ml of HPLC-grade water was added before vortexing again and centrifuging at room temperature for 5 minutes at 500 g. The lower phase was recovered using a glass Pasteur pipette. The chloroform phase was dried using a Rapidvap N2/48 evaporation system (Labconco Corporation), re-suspended in 100 µl of methanol, and transferred to HPLC vials with fixed glass inserts, capped in an N_2 atmosphere and then stored at -80 °C prior to analysis by LC/MS/MS as described in Section 2.2.34 of this Chapter.

2.2.34 LC/MS/MS analysis of biotinylated samples

Externalization of aminophospholipids was measured following biotinylation as described above in section 2.2.33 [224]. Lipid extracts were separated using reversed-phase chromatography with an Ascentis C_{18} column (150 mm x 2.1 mm x 5 µm) (Sigma Aldrich). An isocratic elution method was used with methanol (and 0.2% (w/v) ammonium acetate), at a flow rate of 400 µl/min for 25 minutes at 22 °C. Lipids were analysed in MRM mode, on a 4000 Q-Trap (Sciex, Cheshire, United Kingdom) and biotinylated MRM transitions were monitored in negative ion mode, with a dwell time of 200 msec, under the following conditions shown in Table 2.10.

Table 2.10: MRM transition for biotinylated aminophospholipids precursor ion to product ion transitions. Declustering potential (DP), collision potential (CE), Collision cell exit potential (CXP)

Biotinylated Analyte		Biotinylated Molecular mass (g/mol)	MRM transition	Q1	Q3	DP (V)	CE (V)	CXP (V)
SpAPE-B (PE 18:0p_20:4)		977	976→303	976	303	−160	−60	−5
SAPE-B (PE 18:0a_20:4)		993	992→303	992	303	−170	−58	−5
PpAPE-B (PE 16:0p_20:4)		949	948→303	948	303	−160	−60	−5
SOPE-B (18:0a_18:1-PE)		971	970→281	970	281	−170	−58	−5
OpAPE-B (PE 18:1p_20:4)		975	974→303	974	303	−160	−60	−5
SOPS-B (PS 18:0a_18:1)		1,015	1,014→701	1015	701	−140	−44	−23
DOPS-B (PS 18:1a_18:1-PS)		1,013	1,012→699	1012	699	−150	−46	−23
SAPS-B (PS 18:0a_20:4)		1,037	1,036→723	1036	723	−145	−42	−23
IS	**DMPS-B**	905	904→591	905	591	−150	−42	−17
IS	**DMPE-B**	861	860→227	860	227	−135	−60	−13

The area under the curve for the precursor ion to product ion transition was integrated using Multiquant 3.0.2. (AB Sciex, Canada) and normalized to the relevant biotinylated IS, DMPE-B for PE lipids and DMPS-B FOR PS. For quantification, biotinylated standards, previously synthesized, were used to generate a standard curve. An equation for calculation was obtained using linear regression, and both the total and externalized concentrations of aminophospholipids were calculated as described in Section 2.2.35. Statistical analysis was performed as described in Section 2.2.36.

2.2.35 Quantification of lipids

Standard curves were generated by serial dilution of lipids, as previously depicted in sections 2.2.32 and section 2.2.26, which describe the generation of biotinylated and HETE-PLs standards, respectively. Each standard mixture contained a fixed amount of IS per vial (10 pg/µl) The range of dilutions prepared had the following amounts: 10 ng, 5 ng, 1 ng, 500 pg, 100 pg, 50 pg, 10 pg, 5 pg, 1 pg of lipid standard. These lipids were analysed using the same LC-MS/MS method as the respective samples. For each standard amount, the ratio of the integrated lipid area to the integrated IS area was calculated. A graph was generated, plotting the ratio of lipid amount (ng) against the IS amount (ng) and the slope was determined. The amount of lipid present within the samples was calculated through the following equation:

Equation 1: Lipid Quantification Calculation

$$Lipid\ (ng) = \frac{Lipid\ (integrated\ area)\ \times IS\ (ng)}{IS\ (integrated\ area)\ \times slope}$$

2.2.36 Heatmaps and statistical analysis

Statistical analysis was performed using Graphpad Prism (version 9). The normal distribution of all the data presented in this thesis was determined through the Shapiro-Wilk test. Where the data were normally distributed, and only two populations were being tested, the Student's t-test was used, while in the Mann-Whitney test was used as the non-parametric alternative.

On the other hand, with one independent variable and a normal distribution of data, a one-way ANOVA test and Tukey's multiple comparison test were performed. When two independent variables were present, and data was normally distributed two-way ANOVA was employed. The Kruskal–Wallis test was applied to examine nonparametric distributed variables. The statistical differences between conditions were calculated using Dunn's multiple comparisons test.

Unless otherwise stated, data were displayed as box and whiskers plots with the median line inside the box, and box edges indicative of the interquartile range, with the mean value represented as "+". Whiskers represent minimum and maximum values, and the respective scatter plots display individual values. Statistical significance is denoted as follows: *P < 0.05; **P < 0.01; ***P < 0.001, ****P < 0.0001.

Heatmaps were generated using the pheatmap package in R written by Raivo Kolde, PhD [226]. Heatmaps were designed by applying a log10 to the averaged lipid amounts (ng), normalized to cell count, volume (ml) or wet tissue weight (mg) for each lipid, allowing row-wise and column-wise comparison. Lipid hierarchical clustering (complete linkage method) to group similar lipids was also performed using the pheatmap package. Lipids levels were represented by a colour gradient ranging from blue (very low levels or absent) to red (highest levels).

Elevated circulating oxidised phospholipids as possible players in the increased coagulation observed in Inflammatory arthritis in WT and *IL27ra*$^{-/-}$ mice

---

Chapter 3

3.1 Introduction

RA is a highly heterogeneous disease in humans, displaying a variety of both histological pathotypes and clinical outcomes, including different responses to therapies[133,134]. Based on gene expression signatures in synovial tissue of RA patients, synovitis pathotypes are considered to be on a continuous spectrum, where four main molecular and cellular phenotypes can be classified, specifically: lymphoid, myeloid, fibroid (or pauci-immune) and low inflammation[133,134]. These different pathotypes display characteristic pathological mechanisms and distinct clinical responses to biological drugs[133,134]. However, delimitation of these synovial pathotypes through whole blood transcriptomics resulted in only the differentiation between fibroblastic-rich (pauci-immune) and diffuse-myeloid groups [134]. However, whether there are systemic differences between the synovial pathotypes that go beyond the transcriptome were not studied.

As described in Chapter 1, RA patients typically exhibit systemic effects associated with chronic inflammation. An example is RA being considered a risk factor for cardiovascular disease[91]. This is reflected in the elevated incidence of thrombosis, both arterial and venous, observed in RA patients when compared to the healthy population[91,135]. Considering the elevated incidence of thrombosis in these patients, it is imperative to study more that the synovial pathology. Furthermore, considering the heterogeneity that RA patients display, it is important to study multiple animal models phenotypes that align broadly with the different human forms of RA when trying to delineate underlying systemic mechanisms of inflammatory arthritis. This includes analysing systemic inflammation, alongside coagulation markers and lipid metabolites.

As previously described in Section 1.4.1, the antigen-induced arthritis (AIA) model can be induced in various genetically modified mice, resulting in arthritic phenotypes similar to those described in human RA. Specifically, when AIA is induced in wild-type (WT) mice, a myeloid-rich arthritis phenotype, with diffuse immune infiltration, driven mainly by macrophages develops.[193] However, when induced in *IL27ra*$^{-/-}$ mice, a lymphoid-rich phenotype and ectopic lymphoid-like structures develop, along with an elevated adaptive immune response.[206] Considering the opposite biological function between IL-27 an IL-6 in the co-ordination of adaptive immune responses, upon IL-6 deletion, a diminished immune response is observed [204]. In fact, in the case of *IL6ra*$^{-/-}$ and *IL6*$^{-/-}$ mice, a fibroblast-rich phenotype with reduced immune infiltration (pauci-immune) is observed [200,202,221]. Therefore, by studying these different phenotypes, it will be possible to understand if altered coagulation is present in the AIA model and if it varies between pathotypes or if is it a result of acute inflammation.

Despite the higher incidence of thrombosis in RA, the molecular mechanisms are not fully understood. Therefore, the characterization of both coagulation and fibrinolysis in RA is crucial for understanding RA-driven coagulopathies. Several coagulation markers have already been described as being altered in human RA[145], however, in mouse models, few studies have measured these parameters. As a marker of thrombin generation, the thrombin-antithrombin (TAT) complexes are formed when antithrombin inhibits thrombin. A large number of studies have shown TATs to be increased in plasma from RA patients[142,148]. However, only one murine was studied so far, showing a significant increase in the collagen-induced arthritis model[227]. Thus, in this chapter, coagulation markers, along with fibrinolysis, will be studied in a murine arthritis model. In addition, systemic levels of inflammation markers, namely serum amyloid A (SAA) and C-reactive protein (CRP), will also be determined.

Phospholipid membranes, despite being essential for coagulation, have not yet been analysed in circulatory blood cells of arthritis, either human or murine for the present of pro-coagulant oxPLs, despite the increased thrombosis displayed by RA patients and the respective role of these lipids in coagulation. As previously described, in Chapter 1, Section 1.2.4, oxPLs, which can be generated enzymatically (eoxPLs) by circulating immune cells, have been shown to participate in coagulation. Interestingly, as explained in Chapter 1, Section 1.1.3, eoxPLs are generally considered cell-specific, especially when solely analysing circulatory whole blood cells. In humans, *ALOX12* is primarily expressed in platelets, and encodes an enzyme called 12-LOX. As explained in Chapter 1, Section 1.1.3, this enzyme oxidates PUFAs, such as AA, by specifically introducing a dioxygen group at position 12, generating a lipid hydroperoxide, which is then reduced to form 12-HETE (Figure 1.3). The timescale for the generation of these free HETEs is similar to one for the eoxPLs, being both generated acutely in inflammation [63–65]. This indicates that the incorporation of these lipids into the phospholipid membrane is extremely fast. Hence, the Lands' cycle, as previously described in Section 1.1.1 of this thesis, is able to rapidly incorporate this oxidized fatty acid into lysoPLs through LPATs enzymes, and therefore, specifically generating 12(S)-HETE-PLs [228]. In the case of neutrophils, this generates 5-HETE-PLs through the action of 5-LOX encoded by *ALOX5* while 15-HETE-PLs can be generated by 15-LOX (from *ALOX15*) present in monocytes and eosinophils [55]. Enzymatic oxidation of free AA by LOX isoforms leads to a very specific enantiomeric composition of primarily *S* isomers, as well as a distinct isomeric composition of HETE-PEs. Besides LOX, COX is also able to generate eoxPLs, namely 11- and 15-HETE-PLs. In the case of COX oxidation, more specifically 11-HETE-PLs, the *R* enantiomer is predominant, while 15-HETE-PLs are generated as a racemic mixture [229,230]. Distinct from enzymatic generation, oxPLs can be generated non-enzymatically by reactive oxygen species (ROS) attack on lipids during inflammation. This generates a large number of positional isomers with relatively similar levels, including 8-HETE-PLs, which can be used as a marker of non-enzymatic oxidation. Furthermore, non-enzymatic oxidation originates racemic mixtures (50:50 *S/R* ratio) of HETE-PLs [5]. Therefore, by analysing the specific isomers and enantiomers generated, the origin of oxPLs can be defined, and consequently, a role for particular immune cells involved in their generation can be proposed. Despite the increased thrombosis displayed by RA patients [91], and the role of oxPLs in coagulation, these phospholipids have never been analysed in arthritis, neither in human nor in mouse models. Therefore, in this chapter, oxPLs will be analysed, differentiating positional isomers and enantiomers, to understand if these lipids may help drive the coagulation during AIA development.

Furthermore, Increased activation of PLA_2 is observed in chronic inflammatory processes characteristic of auto-immune diseases, such as RA[19]. In fact, this is observed in both the synovium fluid and serum of RA patients, with PLA_2 levels correlating with disease activity[231]. PLA_2 increases the release of PUFAs from phospholipid membranes. Cytokines, namely TNF-a and IL-1, generated in RA were seen to stimulate PLA_2 activity and directly lead to its increased[232]. The importance of these lipids, which include PGs and LTs, has been established in both human RA and experimental murine arthritis and their levels correlate with disease severity [233,234]. Therefore, I will also analyse the oxylipin profile during the development of the AIA model.

3.1.1 Aims

Mouse models are most generally used to study localised joint disease. Inflammation is analysed mainly in challenged joints, and apart from the measurement of plasma mBSA-antibody during disease progression, systemic changes, including relating coagulation have generally not been studied. Here, this AIA murine model will allow us to measure coagulation markers at different time points and in distinct arthritic pathotypes. In addition, oxidised lipids will be analysed and characterised for each strain of arthritic mice studied, on both day 3 and day 10. The overall aims of this chapter are:

- Characterise coagulation markers in *WT*, *IL27ra*$^{-/-}$, *IL6ra*$^{-/-}$ and *IL6*$^{-/-}$ mice during AIA development, namely TAT complexes, D-dimers and prothrombin time.
- Characterise inflammatory markers in *WT*, *IL27ra*$^{-/-}$, *IL6ra*$^{-/-}$ and *IL6*$^{-/-}$ mice during AIA development, namely SAA and CRP.
- Whole blood cells from mice during AIA development will be analysed for oxPLs and oxylipins using LC/MS/MS analysis.
- The enzymatic origin of oxPLs species will be evaluated through chiral analysis.
- The association of these lipids with increased coagulation and inflammation will be tested.

3.2 Results

3.2.1 Immunization of mice to induce AIA does not itself impact coagulation.

The first question, prior the analyse of the multiple pathotypes of AIA, was if the immunization protocol of this model might induce inflammation and increase coagulation. Therefore, prior to the induction of arthritis on day 0, immunization against mBSA was induced and studied for coagulation and inflammation markers.

First, mice were injected subcutaneously (s.c.) with mBSA, emulsified with complete Freund's adjuvant (CFA), combined with an intraperitoneal (i.p.) injection of *Bordetella pertussis* toxin[235]. 7 days later, immunization is then boosted through another s.c. injection of mBSA/CFA emulsion. This initial immunization causes an immune response but does not lead on its own to AIA and, thus it has the potential to impact coagulation. To exclude this possibility, I analysed plasma samples for selected coagulation and inflammatory markers on day 0 of AIA, prior to the i.a. injection of mBSA to induce disease, namely TAT complexes, as a coagulation marker, of D-Dimers as a marker for fibrinolysis, and C-reactive protein (CRP), as a marker of inflammation, were analysed.

TAT complexes, D-dimers and CRP, were measured in WT mouse plasma by ELISA, as described in Sections 2.2.12, 2.2.13 and 2.2.15, respectively. At day 0, after both s.c. injections of mBSA and without any intra-articular injection to induce arthritis, levels of these markers were all found to be unaffected (Figure 3.1). These data indicate that the immunization process does not directly result in increased coagulation or elevation of CRP.

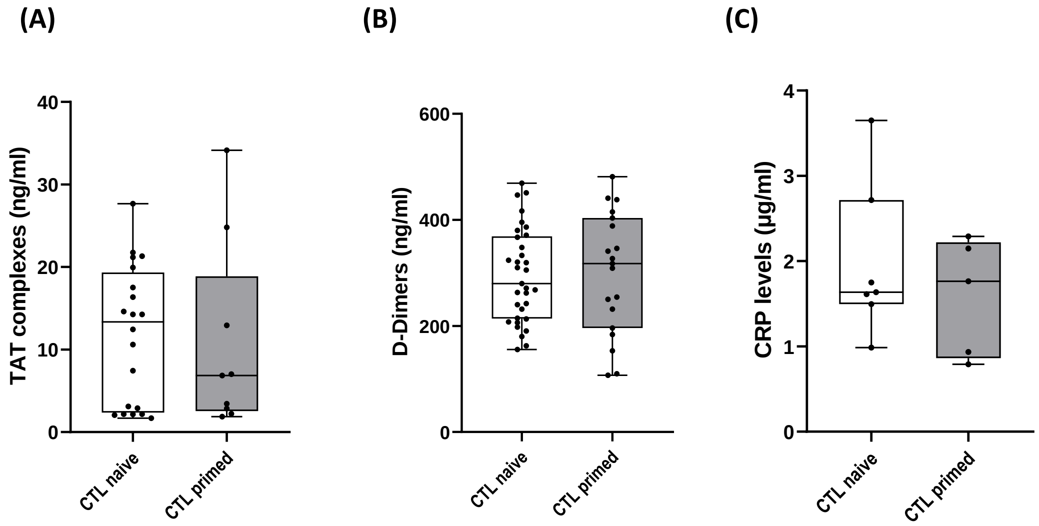

Figure 3.1: Immunization of wild type mice does not impact coagulation or induce systemic inflammation.

Plasma of CTL naïve mice was analysed for TAT complexes (ng/ml) (n = 19) (Panel A), D-dimers (ng/ml) (n = 33) (Panel B) and CRP (µg/ml) (n = 7) (Panel C) and compared to AIA immunized (CTL primed) mice [(A) n = 9; (B) n = 19; (C) n = 5], as described in Methods (Chapter 2). Data are represented as box and whisker plots. TAT complexes ($p = 0.9275$) were analysed using the Mann-Whitney test, while D-dimers ($p = 0.8655$) and CRP ($p = 0.4341$) levels were analysed using Student's t-test.

3.2.2 Immunization of mice to induce AIA does not itself impact oxPL generation.

OxPLs generation pattern in whole blood cells was relatively similar before and after immunization (Figure 4.1). Furthermore, this experiment showed that, basally, whole blood cell pellets from these mice contain higher levels of 12-HETE-PLs when compared to other HETE-PLs positional isomers, with stearic acid (18:0) constituting the most abundant fatty acid at the *Sn1*-position. The two-way ANOVA test indicated no significant difference between CTL naïve and mice after the immunization process (row factor $p = 0.1526$), while, as expected showed a significant difference between the different lipids (column factor $p < 0.0001$). Nevertheless, Tukey's multiple comparison test exhibited a significant increase of both 18:0a_12-HETE-PC and 18:0a_5-HETE-PC. Therefore, to exclude any impact of immunization, only oxPLs generated in PE will be analysed in the AIA model study, excluding HETE-PCs from the study.

These results suggest not only that the immunization process does not directly result in a difference in HETE-PE generation, but also the overall pattern of oxPL generation is not equal suggesting an enzymatic contribution.

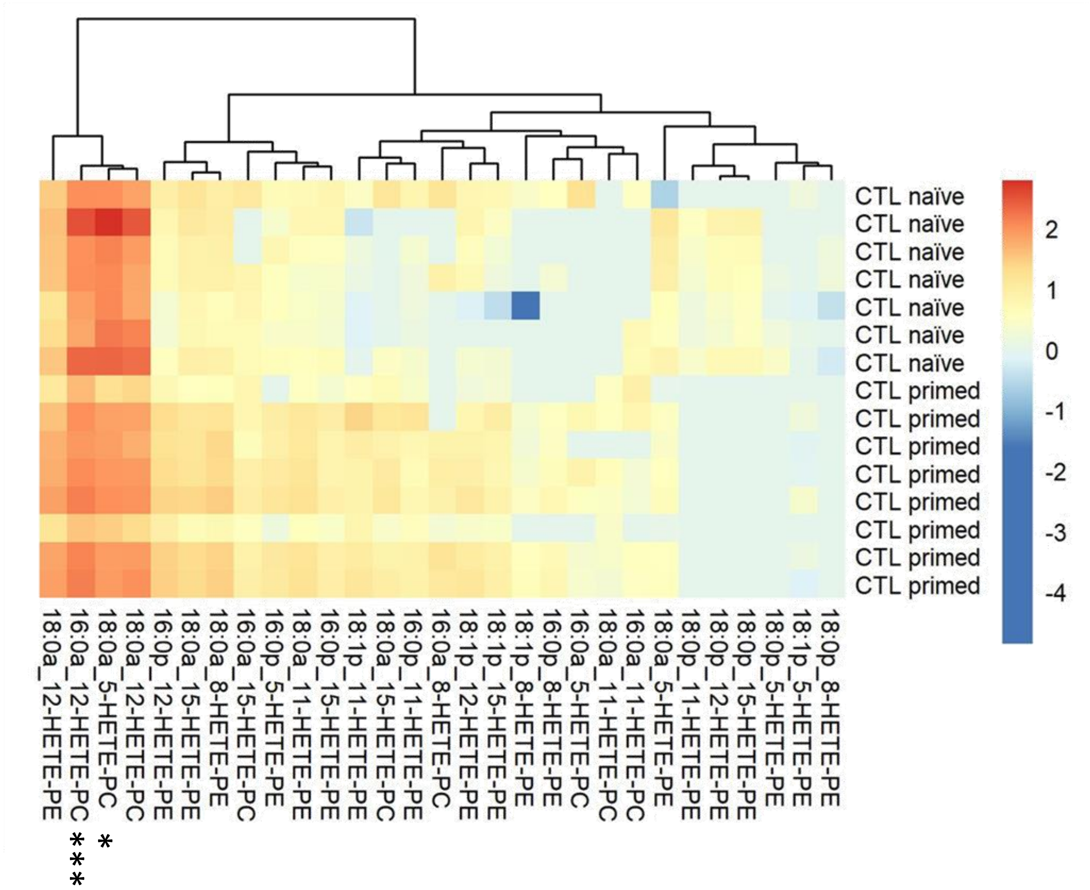

Figure 3.2: I**mmunization of wild type mice does not impact HETE-PE generation.**
Oxylipidomics of whole blood cell pellets from control naïve and immunized mouse blood was performed (n = 8) using LC/MS/MS as outlined in Methods. Heatmap shows log10 of mean quantified values of the analyte concentration (ng/ml). Data was analysed using two-way ANOVA, where no significant difference was found between the two controls (p = 0.1526). Tukey's multiple comparisons test was also used (*p>0.05, ***p>0.001)

3.2.3 AIA model was induced successfully in WT, *IL27ra*$^{-/-}$, *IL6ra*$^{-/-}$, *IL6*$^{-/-}$ mice, despite the high joint swelling variability

The AIA model was developed in WT, *IL27ra*$^{-/-}$, *IL6ra*$^{-/-}$, and *IL6*$^{-/-}$ mice. The joint swelling was measured as described in Section 2.2.3, through a POCO 2T micrometer (Kroeplin) on days 0, 1, 2, 3, 7 and 10. Joint swelling (%) was calculated in each individual mouse, and the average, along with the standard deviation (SD) is represented in Figure 3.3. On day 0, the variability of the joint diameter is also represented. All analysed pathotypes displayed a peak in joint swelling (%) on day 2, despite the relatively high dispersion of data. Considering the two-independent factors, the different time points and the different strains studied, two-way ANOVA statistical analysis was used, where a significant difference between the time points was observed (row factor $p < 0.0001$). A small but significant difference was also observed between the different pathotypes (column factor $p = 0.0179$), driven mainly by the day 10 timepoint. In summary, the arthritis induction was considered successful in these mice due to the peak joint swelling observed throughout the different analysed strains, despite the variability displayed. Therefore, these mice were considered to display the different pathotypes previously described in Section 3.1, and further analysed and discussed accordingly.

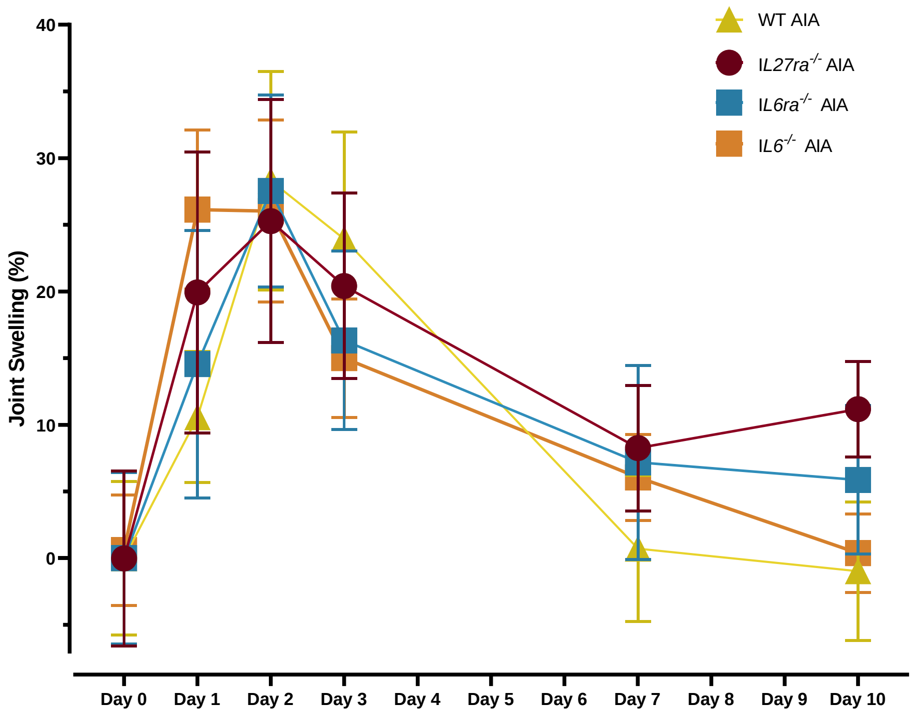

Figure 3.3: Joint swelling confirms the success of the AIA model
Mice joints diameter of WT (n = 16), *IL27ra*$^{-/-}$ (n = 9), *IL6ra*$^{-/-}$ (n = 4) and *IL6*$^{-/-}$ (n = 4) was measured on day 0, before intra-articular injection, and on day 1, day 2, day 3, day 7 and day 10 after mBSA intra-articular injection. The swelling percentage was calculated in all analysed AIA models. A peak in swelling is observed between day 2 and day 3, confirming the success of the arthritis induction in all performed AIA models. Data was analysed through Two-way ANOVA, which presented a significant difference between timepoints in all analysed pathotypes ($p < 0.0001$), between pathotypes ($p = 0.0179$), as well as a significant interaction between them ($p = <0.0001$).

3.2.4 Systemic coagulation is elevated in WT and *IL27ra* $^{-/-}$ mice on day 10 of AIA development.

With arthritis induced proven successful throughout the different strains, along with the exclusion of the immunization process as systemic instigator, coagulation was studied in the different pathotypes. Therefore, AIA was induced in *WT*, *IL27ra* $^{-/-}$, *IL6ra* $^{-/-}$, and *IL6* $^{-/-}$ mice with WT naïve mice used as controls (CTL naïve) as described in Chapter 2, section 2.2.3. Coagulation markers (TATs, D-dimers and PT) were tested during AIA development, on both day 3 and day 10 in myeloid-rich (WT developing AIA), lymphoid-rich arthritis (*IL27ra* $^{-/-}$developing AIA), fibroid (or pauci-immune) and low inflammation arthritis (*IL6ra* $^{-/-}$ and *IL6* $^{-/-}$ developing AIA) [133,134] were investigated.

Firstly, TAT complexes were analysed in the different pathotypes, as well as in both acute disease (day 3) and established disease (day 10) and compared to CTL naïve mice (Figure 3.4). Contrary to the statistical analysis of the previous section, the different samples are independent of each other. Blood collection, as described in Section 2.2.4, was a terminal procedure, the day 3 and day 10 mice were independent samples. Furthermore, the data failed the Shapiro-Wilk test, indicating the non-normal distribution of data. Furthermore, since there is no true non-parametric test for the two-way ANOVA, the Kruskal-Wallis test was used, and a significant difference was observed ($p = 0.0008$). Besides, the use of two-way ANOVA in this study is limited considering the lack of CTLs for each of the transgenic mice analysed.

Dunn's multiple comparisons test in each timepoint displayed no significant differences on day 3 in either WT, *IL27ra* $^{-/-}$, *IL6ra* $^{-/-}$ or *IL6* $^{-/-}$ mice compared to CTL naïve. However, on day 10 of AIA, *WT* mice displayed a significant rise in TAT complexes compared to CTL naïve. Similarly, *IL27ra* $^{-/-}$ mice exhibited an increase compared to CTL naïve, however, this did not reach statistical significance. Nevertheless, a significant difference was observed between *IL27ra* $^{-/-}$ and *IL6* $^{-/-}$ mice on day 10 of AIA development. In contrast, both *IL6ra* $^{-/-}$ and *IL6* $^{-/-}$ mice did not exhibit any significant increase in TAT levels throughout AIA development when compared to CTL naïve. Moreover, *IL6* $^{-/-}$ mice also displayed a significant decrease when compared to WT mice on day 10. This further indicates that *IL6* $^{-/-}$ mice maintain the same basal levels of TAT complexes on day 10 of AIA development, while WT mice significantly increase. These results suggest a potential role of IL-6 in the activation of coagulation in arthritis.

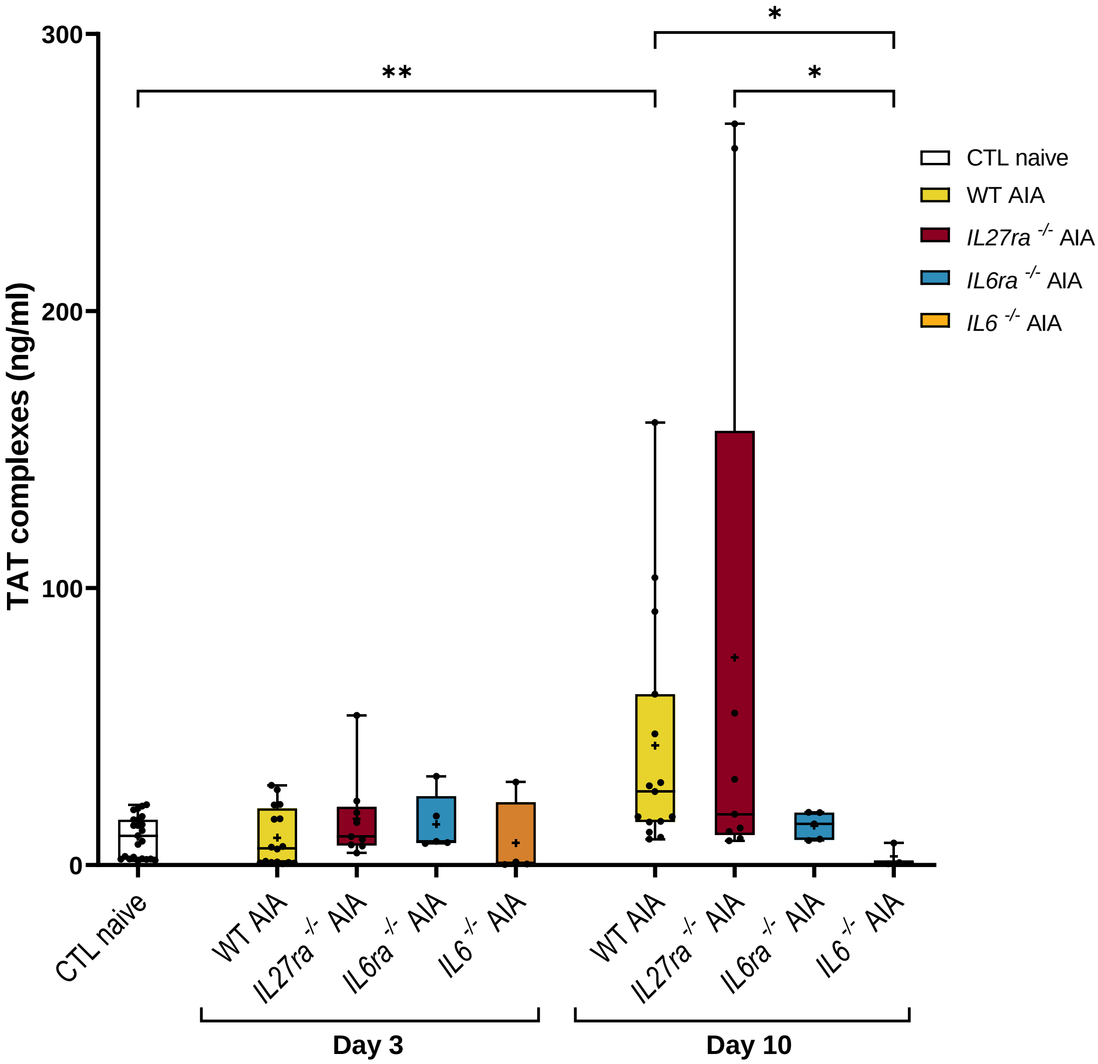

Figure 3.4: TAT complexes are increased in WT mice on day 10 of AIA development
AIA was induced in 9- to 12- week- old *WT* (n = 15), *IL27ra* $^{-/-}$ (n = 9), *IL6ra* $^{-/-}$ (n = 4) and *IL6* $^{-/-}$ (n = 4) male mice. Plasma TATs were measured by ELISA, on day 0 for controls (CTL), on day 3 and on day 10. Significance was tested using the Kruskal-Wallis test (p = 0.0008) and Dunn's multiple comparisons test (*p<0.05, ** p<0.001).

Prothrombin time (PT) is a common coagulation parameter responsive to the levels of coagulation factors II, VII, IX and X, and reflects the time it takes for plasma to clot, following the addition of a standard preparation of tissue factor-containing liposomes. Therefore, PT can indicate if coagulation is increased due to dysregulated coagulation factors. Thus, in this chapter, PT was also determined AIA model as described in Chapter 2, Section 2.2.17.

The Kruskal-Wallis test was once again used since the data was not normally distributed and a significant difference in PT between pathotypes was observed (column factor $p = 0.0434$). However, contrary to the other pathotypes, *IL6ra* $^{-/-}$, and *IL6* $^{-/-}$ mice displayed increased variability, which might ultimately be responsible for this result. The multiple comparison test indicated a significant difference on day 3 of AIA development, between *IL27ra* $^{-/-}$ and *IL6* $^{-/-}$ mice (Figure 3.5.A). This suggests that the different pathotypes might behave differently, however, PT levels are not significantly altered in the plasma of murine AIA. This indicated that coagulation factors dysfunction is not responsible for the previously observed TAT levels increase, especially on day 10.

Next, fibrinolysis was studied in the AIA model. D-dimers, a specific breakdown product of cross-linked fibrin fragments, frequently used as a clinical marker of thrombosis, have never been studied in murine arthritis models, despite elevated levels being found in both synovial fluid and plasma of these patients [142,147,148] Therefore, D-dimers were measured in plasma from *WT*, *IL27ra* $^{-/-}$, *IL6ra* $^{-/-}$, and *IL6* $^{-/-}$ mice, during AIA, as well as CTL naïve (Figure 3.5.B). Therefore, D-dimers were measured in plasma from *WT*, *IL27ra* $^{-/-}$, *IL6ra* $^{-/-}$, and *IL6* $^{-/-}$ mice, during the different AIA model experiments, as well as CTL naïve and pooled in order to compare between pathotypes (Figure 3.5.B). Considering that the data was normally distributed, a two-way ANOVA was performed. The two-way ANOVA test analyses two independent variables, and provides a p value for each variable, along with an p value for the interaction between both independent variables. As previously described, in this study the two-way ANOVA is limited to main effects only (row and column factors) due to the lack of CTLs for the transgenic mice. No significant difference was observed between the timepoints (row factor $p = 0.8400$). A significant difference between pathotypes (column factor $p = 0.0015$) was observed. However, post hoc tests, namely Tukey's multiple comparison test could not detect any significant difference between condition, including between *IL6ra* $^{-/-}$ and *IL6* $^{-/-}$ mice on day 3 of AIA development (p = 0.8166). This result was unanticipated since an increase during the acute-like phase was expected. D-dimers are described as being increased during high disease activity in human RA [236], therefore, a more marked difference was expected during the AIA model development. Nevertheless, some trends were noted. First, *IL6ra*$^{-/-}$ mice on day 3 of AIA displayed the highest levels of D-dimers, even when compared to WT mice at the same time point. In addition, D-dimers were higher on day 3 than on day 10 of AIA development for all analysed mouse strains.

These results suggest that fibrinolysis might be increased in *IL6ra*$^{-/-}$ mice on day 3 of AIA development, compared to other strains. Nevertheless, D-dimers exhibited high variability, which might be the reason no statistical difference was achieved between the pathotypes and CTL naïve mice. Therefore, no strong conclusions can be drawn without increasing numbers to reach statistical power.

In summary, coagulation markers were analysed in *WT*, *IL27ra* $^{-/-}$, *IL6ra* $^{-/-}$, and *IL6* $^{-/-}$ mice during AIA development and compared to CTL naïve, TAT complexes were increased in *WT* on day 10 of arthritis induction, while PT and D-dimers levels between each pathotype and timepoint did not exhibit significant differences. Collectively, this suggests that coagulation is increased, independently of coagulation factors levels, and fibrinolysis is unaffected, in *WT* mice during AIA development. It also suggests that coagulation is increased in an IL-6-dependent manner.

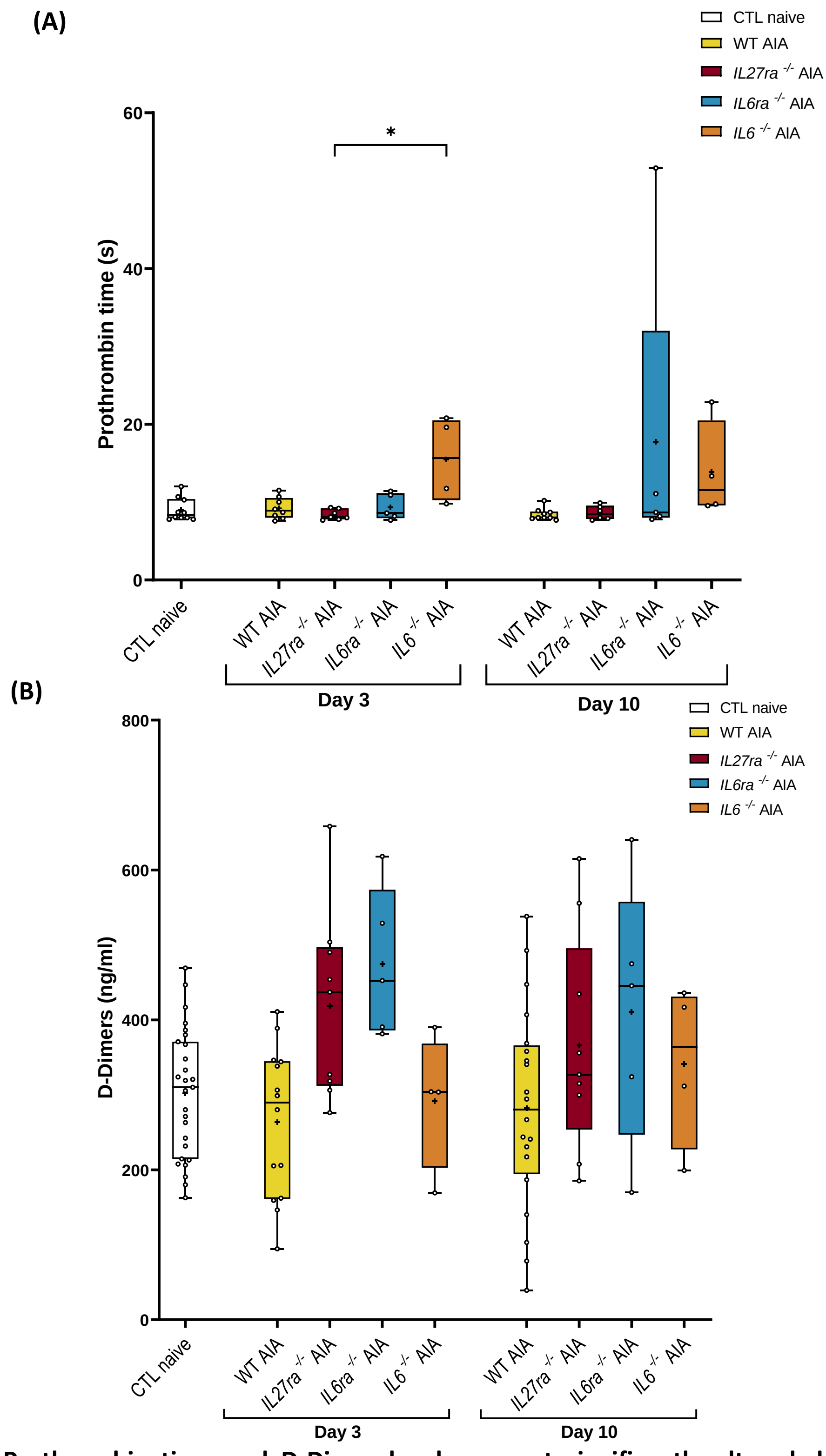

Figure 3.5: Prothrombin time and D-Dimer levels are not significantly altered during AIA development compared to CTL naïve mice.

AIA was induced in 9- to 12- week-old *WT* (n = 9), *IL27ra* $^{-/-}$ (n = 6), *IL6ra* $^{-/-}$ (n = 5) and *IL6* $^{-/-}$ (n = 4) male mice. Prothrombin time (Panel A), and D-Dimers (Panel B) were evaluated in plasma samples, as described in Methods, on day 0 for control (CTL) naïve (n=10), on day 3 and day 10. PT data was analysed using Kruskal-Wallis test and Dunn's multiple comparisons test, while D-dimers were analysed using two-way ANOVA and Tukey's multiple comparisons test. Data exhibits a significant difference between pathotypes, both for PT (column factor p = 0.0434) and D-dimers (column factor p = 0.0015), without reaching statistical significance between time points (row factor p = 0.8400 for D-dimers). (* p > 0.05)

3.2.5 Systemic inflammation is elevated in WT and *IL27ra* $^{-/-}$ mice during AIA development.

Systemic inflammatory markers have never been described in the AIA model. Considering that *IL-6* is one of the main stimulators of many acute-phase proteins (APPs)[237], a decreased in systemic inflammation was expected in both *IL6ra* $^{-/-}$and *IL6* $^{-/-}$ mice. However, the question is if, despite the localized nature of the AIA model, does any of the different pathotypes studied able to induce systemic inflammation. Thus, here I will analyse (APPs) in plasma from mice with AIA to test for systemic alterations in inflammation in the model.

Serum Amyloid A (SAA) is considered a major APP in both mice and humans. As expected, considering the acute inflammatory response still present in the joint on day 3 of AIA development, a clearly increase in SAA levels was found when compared to CTL, and to day 10, when the joint swelling is practically resolved (Figure.3.6).

Here, I found that the more severe phenotypes exhibited higher levels of SAA on day 3. Specifically, *WT* and *IL27ra* $^{-/-}$ mice exhibited significantly higher levels of SAA compared to CTL naïve, on day 3 of AIA. As expected, *IL6ra* $^{-/-}$ mice did not reach the same levels of SAA as *WT* and *IL27ra* $^{-/-}$ mice on day 3, displaying only a small non-significant increase. Interestingly, *IL6* $^{-/-}$ mice did not show any increase in SAA levels at any time point. Despite SAA levels diminishing, as expected on day 10 of AIA, *WT* and *IL27ra* $^{-/-}$ still displayed significantly elevated levels compared to *IL6ra* $^{-/-}$and *IL6* $^{-/-}$ mice on day 10.

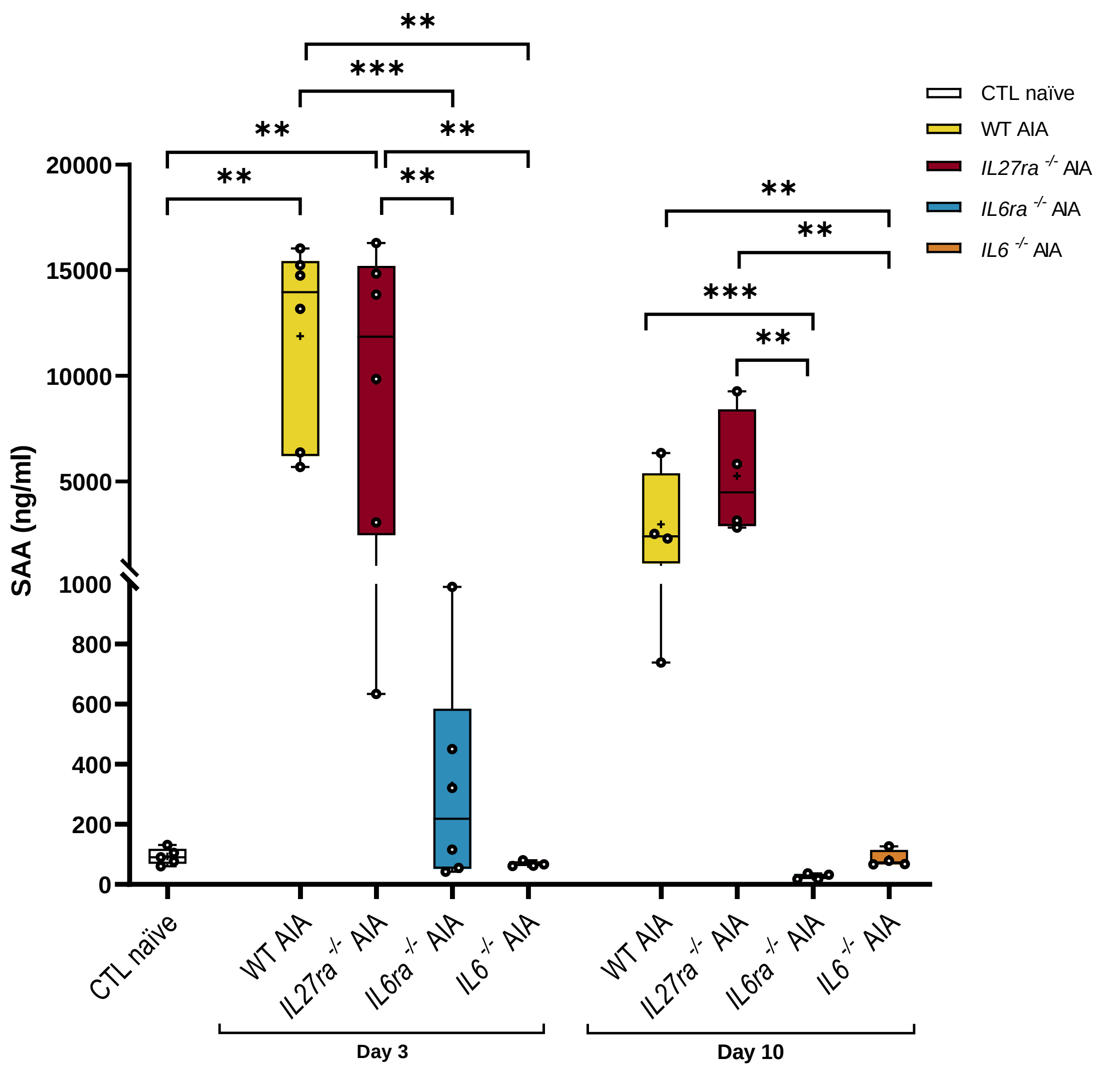

Figure.3.6: Systemic inflammation is highly increased in WT AIA and Il27ra$^{-/-}$ mice, but not in Il6ra$^{-/-}$ and Il6$^{-/-}$ AIA mice

AIA was induced in 9- to 12- week-old *WT* (n = 4), *IL27ra* $^{-/-}$(n = 4), *IL6ra* $^{-/-}$ (n = 4) and *IL6* $^{-/-}$ (n = 4) male mice. SAA in plasma was evaluated by ELISA on day 0 for control (CTL) naïve (n = 5), on day 3 and day 10. SAA data were analysed using two-way ANOVA (row and column factor p < 0.0001) and Tukey's multiple comparisons test (*p<0.05, **p<0.01, ***p<0.001, **** p<0.0001).

In addition, C-reactive protein (CRP) was also analysed. In contrast to SAA, CRP levels did not peak at day 3 of AIA development in any pathotypes analysed (Figure 3.7.A). Nevertheless, Kruskal-Wallis test displayed a significant difference ($p < 0.0001$), with Dunn's multiple comparison test showing this difference as an increase in both *IL27ra* $^{-/-}$ and *IL6ra* $^{-/-}$ mice on day 3 of AIA, compared to CTL naïve and even to *IL6* $^{-/-}$ mice during the same time point. Furthermore, *IL27ra* $^{-/-}$ mice on day 10 of AIA development also displayed a significant increase when compared to *IL6* $^{-/-}$ mice at the same time point. This indicates that CRP is not as good an APP in mice as SAA. Nevertheless, these results suggest that IL-6 cytokine is involved in the synthesis of the inflammatory response during AIA development.

To test a possible association between inflammation and coagulation, I undertook correlation studies between different markers, using simple linear regression. Here, I graphed values of all plasma samples where both D-dimers and CRP were determined from all experiments, (WT, *IL27ra* $^{-/-}$, *IL6ra* $^{-/-}$, *IL6* $^{-/-}$ mice during AIA development). Here, a significant positive correlation was seen between CRP levels and D-Dimers, with a Pearson correlation coefficient of 0.5966. Here, a significant positive correlation was seen between CRP levels with D-Dimers, with a Pearson correlation coefficient of 0.5966. Since the Pearson correlation coefficient value is above 0.5, along with a highly significant p-value for this linear regression ($p = 5.634 \times 10^{-5}$), this correlation can be considered moderate [238] (Figure 3.7.B).

No other significant correlations were found between coagulation and inflammatory markers in AIA. This suggests that D-dimers might also be considered an inflammatory marker, similar to CRP. Nevertheless, D-dimers did not display significant differences between the AIA pathotypes. Considering that both CRP and D-dimers were expected to display more dramatic differences, this result suggests that these biological markers would be of weak clinical value in AIA.

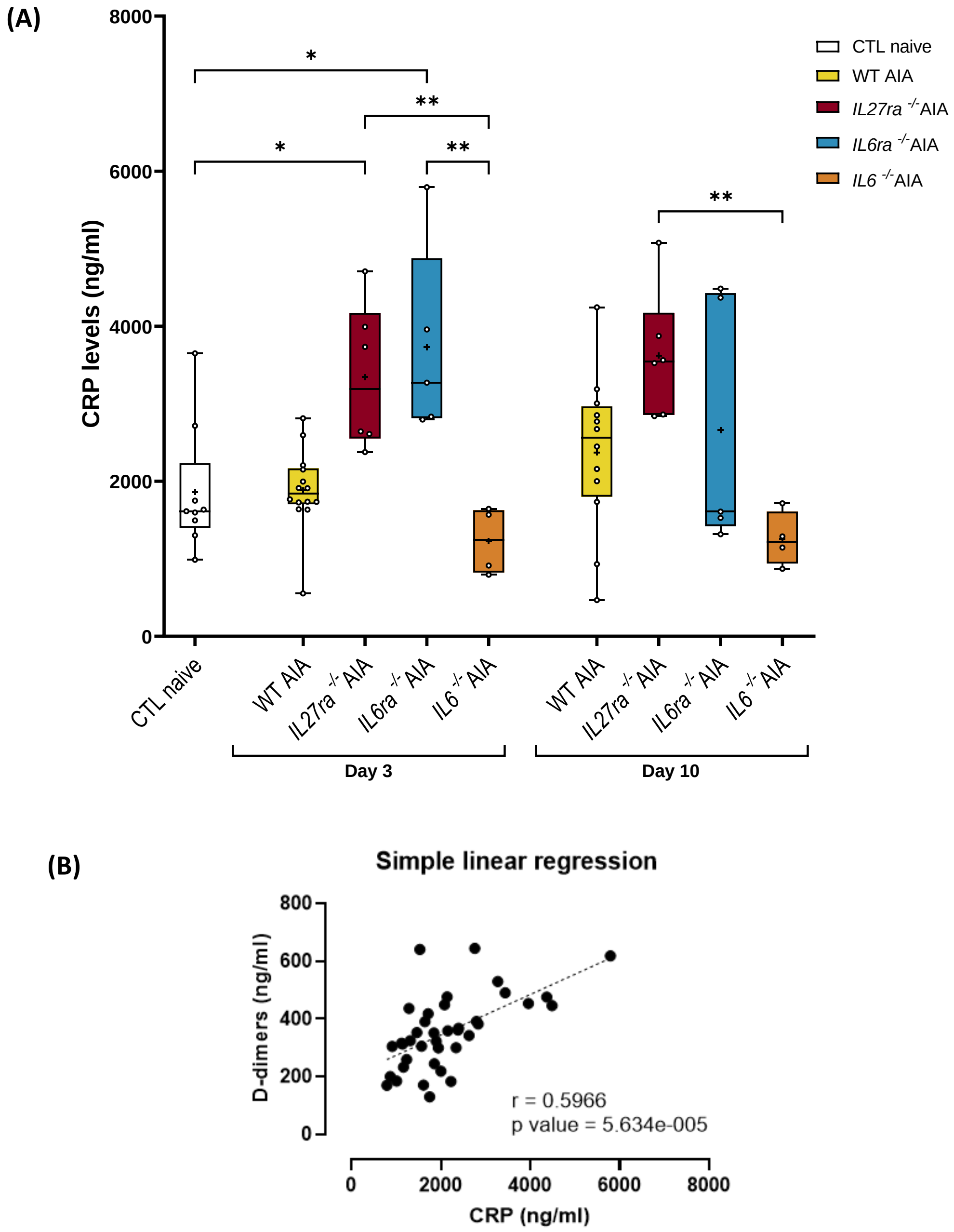

Figure 3.7: Plasma CRP levels of *IL27ra*$^{-/-}$ and *IL6ra*$^{-/-}$ mice on day 3 of AIA development are significantly higher to CTL naïve mice, with a positive correlation with D-dimers is observed. AIA was induced in 9- to 12- week-old *WT* (n = 12), *IL27ra*$^{-/-}$ (n = 6), *IL6ra*$^{-/-}$ (n = 5) and *IL6*$^{-/-}$ (n = 4) male mice. CRP levels (Panel A) were evaluated by ELISA on mouse plasma from day 0 for control (CTL) naïve (n = 9), on day 3 and day 10 of AIA development. CRP data was analysed using the Kruskal-Wallis test (p<0.0001) and Dunn's multiple comparison test (*p<0.05, **p<0.01, ***p<0.001, **** p<0.0001). (Panel B) Simple linear regression was generated between D-Dimer and CRP levels between the different analysed strains and time points (n = 26).

3.2.6 OxPLs are increased in *WT* and *IL27ra* $^{-/-}$ mice blood cells during AIA development.

Previously, I showed that coagulation was altered during AIA, especially on day 10. Here, to determine whether this is related to pro-coagulant membranes, I will analyse oxPL levels in circulating blood cells of mice during AIA development. Whole blood cells of control naïve mice, along with *WT*, *IL27ra* $^{-/-}$, *IL6ra* $^{-/-}$ and *IL6* $^{-/-}$ mice were harvested on day 3 and day 10 of AIA development. Lipids were extracted and profiled using LC/MS/MS, as described in Chapter 2, Section 2.2.28.

A distinct pattern of oxPLs was seen, especially when comparing *WT* and *IL27ra* $^{-/-}$ mice versus *IL6ra* $^{-/-}$ and *IL6* $^{-/-}$ mice during AIA (Figure 3.8). This is validated by the significant difference ($p < 0.0001$) observed in the Two-way ANOVA test. In the case of WT mice, a significant increase in total HETE-PEs is observed on day 3 of AIA, which then further heightened by day 10, when compared to CTL naïve (Figure 3.8.A). For *Il27ra*$^{-/-}$ mice, a similar pattern of increase was observed, however, there were considerably higher levels of oxPLs than for WT. In the case of *Il6ra*$^{-/-}$ and *Il6*$^{-/-}$ mice, regardless of the studied time point, the levels of HETE-PEs did not differ significantly from CTL naïve mice.

The strains that displayed higher levels of total HETE-PEs during AIA, namely WT and *Il27ra*$^{-/-}$ mice, were the same that exhibited elevated levels of SAA and increased TAT levels in Chapter 3. These results suggest a direct link between these lipids and coagulation and inflammation.

The heatmap shows 18:0a_12-HETE-PE as the most abundant oxPLs species in all analysed conditions, including in control naïve mice (Figure 3.8.B). Considering the similar timescale for the generation of free HETE and the HETE-PLs, along with the same substrate for the generation of the different positional isomers, these high levels of 18:0a_12-HETE-PE compared to the other HETE-PEs isomers suggest enzymatic oxidation. If HETE-PLs generation was non-enzymatic, the different oxPLs would be at relatively similar levels, since oxidation through ROS would generate all positional isomers at similar concentrations. Nevertheless, more analysis is required to prove the hypothesis, namely chiral analysis of these lipids. Furthermore, a distinct pattern of generated oxPLs is observed in both *WT* and *IL27ra* $^{-/-}$ during AIA development, which is not replicated in *IL6ra* $^{-/-}$ and *IL6* $^{-/-}$ mice.

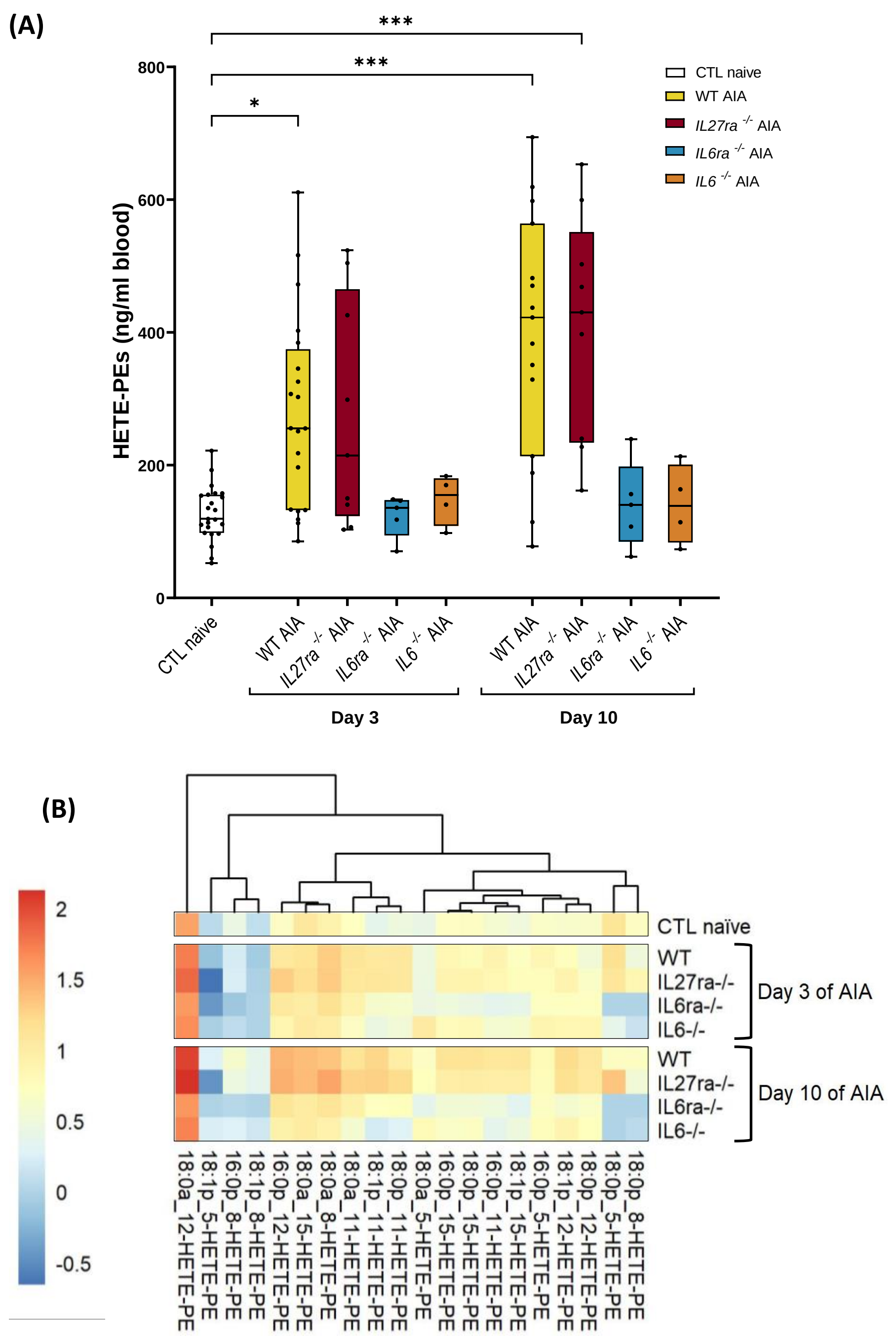

Figure 3.8: HETE-PEs are elevated in blood cells from WT and *Il27ra* $^{-/-}$ during AIA development, especially on day 10.

Antigen-induced arthritis was generated in 9- to 12- week-year-old *WT* (n = 17), *Il27ra* $^{-/-}$ (n = 10), *Il6ra* $^{-/-}$ (n = 5) and *Il6* $^{-/-}$ (n = 4) male mice. Whole blood was collected at day 0 for CTL naïve (n = 23), on day 3 and on day 10 of AIA. Lipids from whole blood cell pellets were analysed using LC/MS/MS. (Panel A) The sum of all the quantified HETE-PEs isomers (ng/ml) in blood was calculated. Data were analysed using the Two-way ANOVA test (row and column factor p <0.0001) and Tukey's multiple comparisons test (* p<0.05, ***p<0.001). (Panel B) Heatmap shows log10 values for analyte concentration (ng/ml).

The most abundant oxPLs detected in CTL naïve blood cells were 12-HETE-PEs, where a significant difference was observed between pathotypes (column factor p = 0.0002) and timepoints (row factor p<0.0001). Upon arthritis induction, 12-HETE-PEs demonstrated the largest elevations in WT and *Il27ra*$^{-/-}$ on day 3 of AIA when compared to CTL naïve mice, respectively. On day 10, the elevation in oxPLs was more pronounced, with both conditions highly increase compared to CTL naïve. In contrast, for both *Il6ra*$^{-/-}$ and *Il6*$^{-/-}$ mice, the AIA did not result in an increase in 12-HETE-PEs on day 3 of AIA, displaying a significant difference compared to both WT and *Il27ra*$^{-/-}$ in both day 3 and day 10. However, a small significant increase was observed on day 10 of AIA in both *Il6ra*$^{-/-}$ and *Il6*$^{-/-}$ mice, when compared to levels on day 3. These data suggest that platelet activation might be significantly higher in WT and *Il27ra*$^{-/-}$ mice during AIA development, especially on day 10, while in *Il6ra*$^{-/-}$ and *Il6*$^{-/-}$ mice the increase is attenuated (Figure 3.9.A).

In the case of 15-HETE-PEs levels, significant differences were also observed between pathotypes and throughout time points (p <0.0001). Tukey's multiple comparisons test exhibited a significant increase in WT on both day 3 and day 10 of AIA development. *Il27ra*$^{-/-}$ mice also presented an increase during AIA, but only achieved statistical significance on day 10. However, no difference in *Il6ra*$^{-/-}$ and *Il6*$^{-/-}$ mice was observed during AIA, maintaining similar levels to CTL naïve throughout the model, while displaying a significant difference compared to both WT and *Il27ra*$^{-/-}$ mice (Figure 3.9.B).

For 11-HETE-PEs, Two-way ANOVA presented significance between pathotypes and timepoints (p <0.0001), which most likely are generated through the action of COX-1. A significant increase was observed during AIA development in blood cells of WT and *Il27ra*$^{-/-}$ mice on both days 3 and 10 (Figure 3.9.C). Overall, the strains that showed low levels of SAA in Chapter 3, namely *Il6ra*$^{-/-}$ and *Il6*$^{-/-}$, did not show elevated 11-HETE-PEs during AIA development (Figure 3.9.C), suggesting a mechanistic link between inflammation, oxPLs generation and platelet activation.

A significant difference was achieved through a Two-way ANOVA test for 5-HETE-PEs between pathotypes (column factor p = 0.0196), but not between AIA time points (row factor p = 0.8510). Furthermore, Tukey's multiple comparisons test did not achieve any significant difference between specific pathotypes. In addition, a very low amount of 5-HETE-PEs was detected throughout the development of AIA in all strains and time points when compared to the previously analysed HETE-PEs (Figure 3.9.E).

Lastly, 8-HETE-PEs, which are generated non-enzymatically in whole blood, were seen to significantly differ between pathotypes (column factor p <0.0001) and time points (row factor p = 0.0003) (Figure 3.9.D). A significant increase in 8-HETE-PEs has observed on day 3 and day 10 of AIA developed in both WT and *Il27ra*$^{-/-}$ mice. Furthermore, no increase was observed in both *Il6ra*$^{-/-}$ and *Il6*$^{-/-}$ mice during AIA, exhibiting a significant difference when compared to WT and *Il27ra*$^{-/-}$ mice. Nevertheless, the amounts of 8-HETE-PEs detected were quite low when compared to 12-, 11- and 15-HETE-PEs. Considering that non-enzymatic oxidation would result in relatively similar concentrations between all positional isomers, these results suggest that these HETE-PEs are primarily generated enzymatically.

Given the low levels of 5-HETE-PEs, which were comparable to 8-HETE-PEs, a non-enzymatic generated HETE-PLs, it is more likely that these are also generated non-enzymatically in this model. Nevertheless, in order to confirm the enzymatic origin of these lipids, chiral chromatography will be used to test this hypothesis.

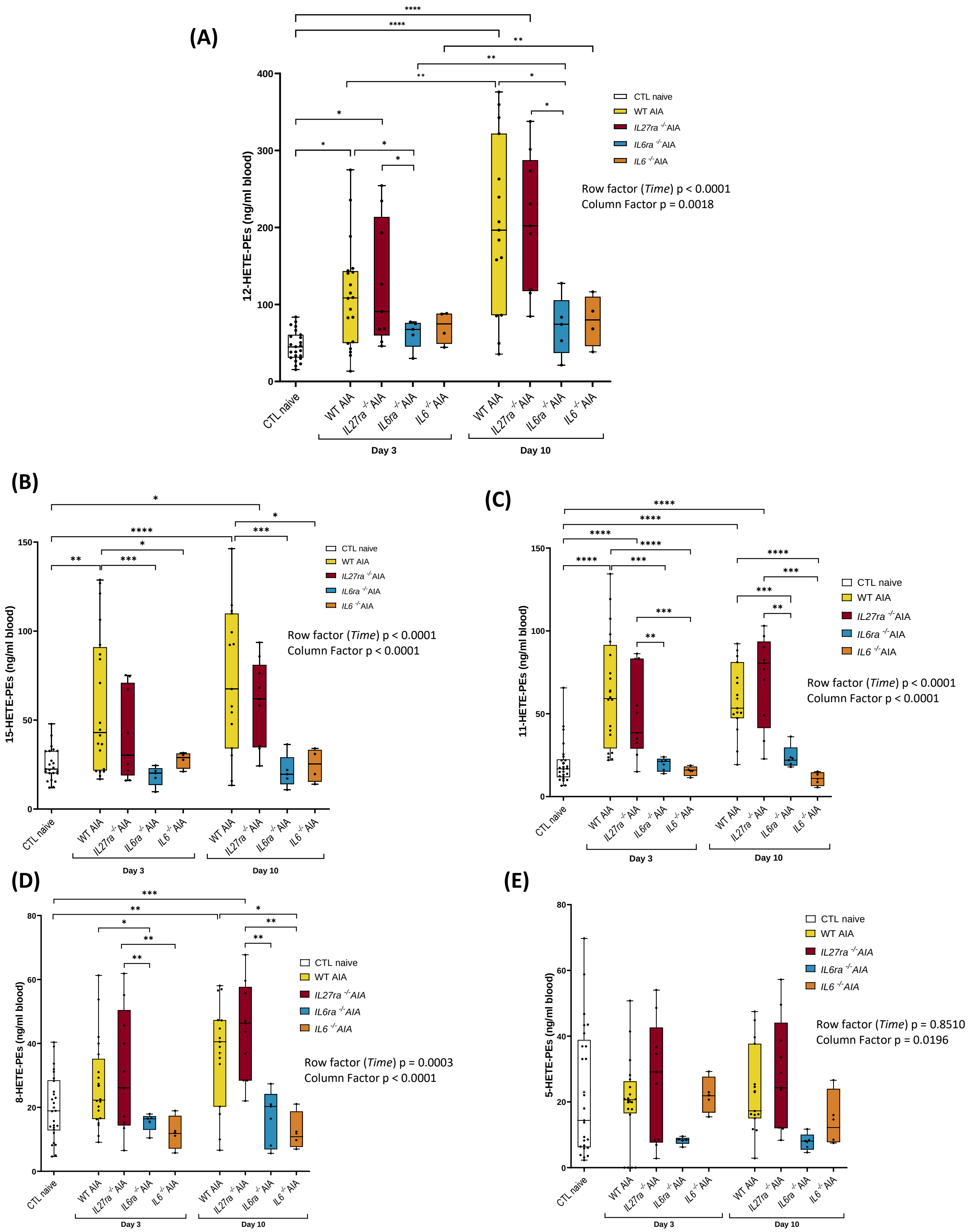

Figure 3.9: 12- and 11-HETE-PEs are the main isomers driving the increase of HETE-PEs observed in WT and *Il27ra*$^{-/-}$ during AIA development

Antigen-induced arthritis was generated in 9- to 12- week-year-old *WT* (n = 17), *Il27ra*$^{-/-}$ (n = 10), *Il6ra*$^{-/-}$ (n = 5) and *Il6*$^{-/-}$ (n = 4) male mice. Whole blood was collected at day 0 for CTL naïve (n = 23), on day 3 and on day 10 of AIA. Lipids from whole blood cell pellets were extracted as described in Methods. The sum of individual HETE-PEs positional isomers (ng/ml), namely 12-HETE-PEs (Panel A), 15-HETE-PEs (Panel B), 11-HETE-PEs (Panel C), 8-HETE-PEs (Panel D) and 5-HETE-PEs (Panel E) was calculated. Data were analysed using Two-way ANOVA and Tukey's multiple comparisons tests (*p<0.05, **p<0.01, *** p<0.001, **** p<0.0001).

3.2.7 Increase in oxPLs in whole blood cells during AIA development in *WT* and *IL27ra* $^{-/-}$ mice is mainly of enzymatic origin

Up to now, HETE-PE were analysed using reverse-phase chromatography, which doesn't provide any information on the chirality of the HETE-PEs isomers. It is important to confirm the enantiomeric composition because this provides information concerning the enzymatic origin of these lipids, depending on the S/R ratio composition. As previously described in Chapter 1, Section 1.1.3, LOX enzymes present in circulatory blood cells generate one specific product enantiomer of *S*-configuration. However, COX oxidation, as described in Section 1.1.4, generates mainly enantiomer of the R-configuration. Therefore, a high percentage of the S enantiomer for 12-HETE-PE, or R enantiomer for 11-HETE-PE, would indicate enzymatic generation, while a racemic mixture (50:50 ratio) would be indicative of non-enzymatic oxidation.

Therefore, I conducted chiral chromatography to determine the enantiomeric configuration of HETE-PLs. Firstly, as described in Chapter 2, in sections 2.2.29 and 2.2.30, HETEs from whole blood lipid extracts were separated by chiral chromatography using LC/MS/MS, before and after alkaline hydrolysis. This enables to subtract the free HETEs from the esterified HETE-PEs. This way, the S/R ratio of HETE-PLs was determined in whole blood cells from the different AIA mice. Considering the destructive effect of this analysis, only three samples of each pathotype and timepoint were analysed as used as a proof of concept. Unfortunately, one sample of *Il6* $^{-/-}$ mice during AIA development was found below the limit of detection in both 11-HETE-PEs and 15-HETE-PEs, therefore only two samples were displayed in Figure 3.10.B and Figure 3.10.C.

Esterified 12-HETE-PL displayed an S/R ratio > 85% in blood for all strains with AIA (Figure 3.10.A). No significant difference was found between pathotypes (column factor $p = 0.7558$) or between AIA time points (row factor $p = 0.4493$). Unlike humans, in mice, enzymatic 12-HETE-PLs can have two distinct origins: platelet-type 12-LOX (*Alox12*) or 12/15-LOX (*Alox15*), also known as leukocyte-type 12-LOX [51]. In order to confirm the specific enzymatic origin of the increased levels of 12-HETE-PEs during AIA development, as therefore the cell type responsible for tits synthesis, more studies are required. This will be addressed in Chapter 5, by analysing *Alox15*$^{-/-}$ mice.

When analysing 11-HETE-PLs, a significant difference was detected between pathotypes (column factor p<0.0001), but not between AIA time points (row factor p = 0.2572). Most samples showed an S/R ratio below 20% (Figure 3.10.B), indicating the predominance of R enantiomers, and therefore indicative of COX oxidation.[229] However, during AIA development, blood cells from *Il6*$^{-/-}$ mice showed a racemic mixture, displaying a 50% S/R ratio of 11-HETE-PLs, which was significantly higher when compared to the other pathotypes. These results have limitations due to the analysis of only 2 samples, nevertheless, the third analysed sample was below the limit of detection, plus the low 11-HETE-PEs found in the blood cell of these mice (Figure 3.9.C) suggests non-enzymatic oxidation, while the elevation of 11-HETE-PEs that was found in the other AIA pathotypes is a result of COX-1 or COX-2 activity. However, to fully test the enzymatic origin of 11-HETE-PEs, a non-selective COX inhibitor, such as indomethacin [239], should be given to the mice during AIA developments, and HETE-PEs re-analysis.

For 15-HETE-PLs species, the S/R ratio differs across different pathotypes (column factor p = 0.0012) and AIA time points (row factor p = 0.0473) (Figure 3.10.C). the average S/R ratio in both CTL naïve, WT and *Il6*$^{-/-}$ mice on both day 3 and day 10 of AIA development was around 50 %, which suggests a non-enzymatic origin. These ratios are not significantly different on day 10 of AIA. On the other hand, both *Il27ra*$^{-/-}$ and *Il6ra*$^{-/-}$ mice display elevated S/R ratio during AIA development, on both day 3 and day 10, indicating enzymatic oxidation. However, contrary to the other eoxPLs, 15- HETE-PEs can be generated through *Alox15* and/or *COX*, generating S- and R-enantiomers, respectively [229]. This complicates the interpretation of these results. To fully understand the enzyme responsible for the observed differences, specific inhibitors, such as indomethacin, a nonselective COX inhibitor, or genetic deletion, are required. In the case of 5-HETE-PEs and 8-HETE-PEs, it was not possible to determine chirality since the lipids were present in such low amounts, falling below the limits of detection of the LC/MS/MS.

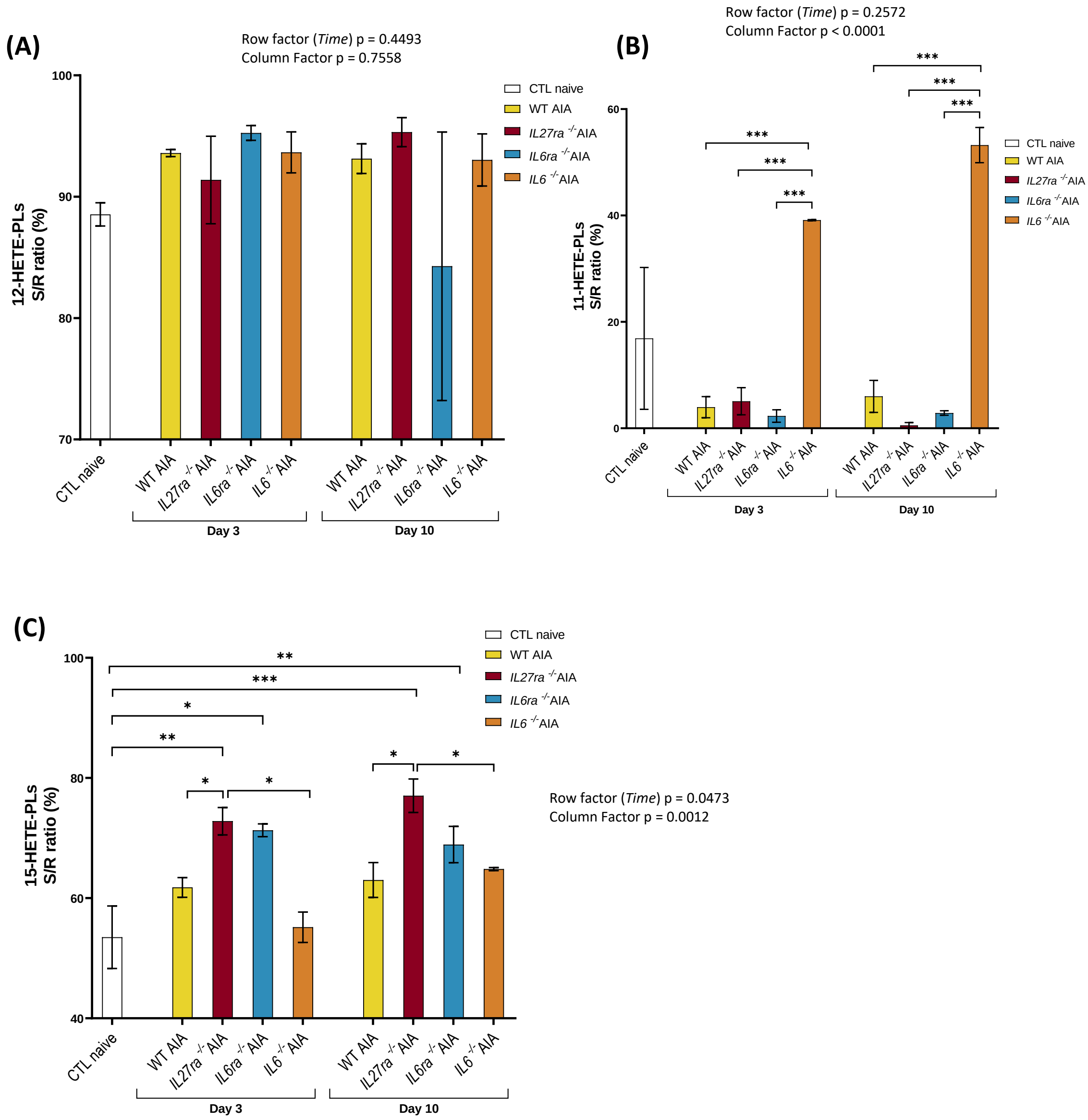

Figure 3.10: Increase of oxPLs in AIA mice is enzymatically generated

Antigen-induced arthritis was generated in 9- to 12- week-year-old *WT* (n = 3), *Il27ra*$^{-/-}$ (n = 3) *Il6ra*$^{-/-}$ (n = 3) and *Il6*$^{-/-}$ (n = 3 for Panel A, n = 2 for Panel B and C) male mice. Whole blood was collected on day 0 for CTL naïve (n = 4), and on day 3 and on day 10 of AIA development. Lipidomics of whole blood cells pellets was performed and the chirality of oxPLs was determined through LC/MS/MS. Lipid extracts were run before and after hydrolysis to determine the esterified HETEs enantiomers. 12-HETE-PEs (Panel A), 11- (Panel B) and 15- HETE-PEs (Panel C) show the S/R ration (%). Data represent mean values ± SEM. Data were analysed using two-way ANOVA and Tukey's multiple comparisons tests (*p<0.05, **p<0.01).

3.2.8 Free oxylipins differ depending on the mice strain during AIA development.

Free oxylipins are important immune modulators, that display both pro-and anti-inflammatory bioactivity. As precursors of the eoxPLs measured above, and derived from the same LOX and COX enzymes, it is relevant to analyse these lipids in AIA. Here, they will be analysed in whole blood cell pellets from the different strains during AIA. Although oxylipins are mainly secreted from cells, I will analyse whole blood cells since oxylipins in plasma could theoretically be generated from inflamed joints.

Lipids were hierarchically clustered through the complete linkage method, to group similar lipids, as well as to cluster pathotypes and AIA time points (Figure 3.11.A). WT and Il6$^{-/-}$ on day 3 clustered close to the CTL naïve oxylipin profile, while *Il27ra*$^{-/-}$ and *Il6ra*$^{-/-}$ clustered together. Unexpectedly, *Il6ra*$^{-/-}$ and Il6$^{-/-}$ did not cluster closely together during AIA development.

Contrary to expected, LTs, PGs and TXB2 were barely detected in the blood cells of mice with AIA at any time point, falling below the limit of detection in the majority of samples, preventing any further analysis. Furthermore, no specialized pro-resolving mediators were detected in the whole blood pellet of any strains or at any time points of AIA development, either by being absent or due to falling below the limit of detection. The most abundant oxylipin detected was 12-HETE, followed by 14-HDOHE and 13-HODE, therefore, these lipids were further analysed. All other lipids, such as 11-HETE and 15-HETE, exhibited very low levels and further analysis would just lead to speculation.

Both 12-HETE and 14-HDOHE can be generated by platelet 12-LOX, from AA and DHA, respectively. Similar to 12-HETE-PEs (Figure 3.9.A), a significant difference between conditions was found in 12-HETE levels ($p<0.0001$) (Figure 3.11.B). WT blood cells on day 3 showed an increase in 12-HETE compared to CTL naïve, while in *Il27ra*$^{-/-}$ mice this peak occurs on day 10. However, no elevation was observed in *Il6ra*$^{-/-}$ and Il6$^{-/-}$ mice. Likewise, the levels of 14-HDOHE were also significantly altered ($p<0.0001$) (Figure 3.11.C), exhibiting a peak on day 3 in whole blood cells of WT mice, which is significantly increased compared to CTL naïve, while for *Il27ra*$^{-/-}$, a significant increase was only observed on day 10.

In the case of 13-HODE which can be generated by 12/15-LOX, through the oxidation of linoleic acid, a significant difference was also found ($p<0.0001$). The levels of 13-HODE in blood cells from WT on day 3 increased compared to CTL naïve, with no elevation observed on day 10 (Figure 3.11.D). Additionally, 13-HODE peaked in Il27ra$^{-/-}$ blood on day 10, while, both Il6ra$^{-/-}$ and Il6$^{-/-}$ blood levels did not change during AIA development, compared to CTL naïve mice.

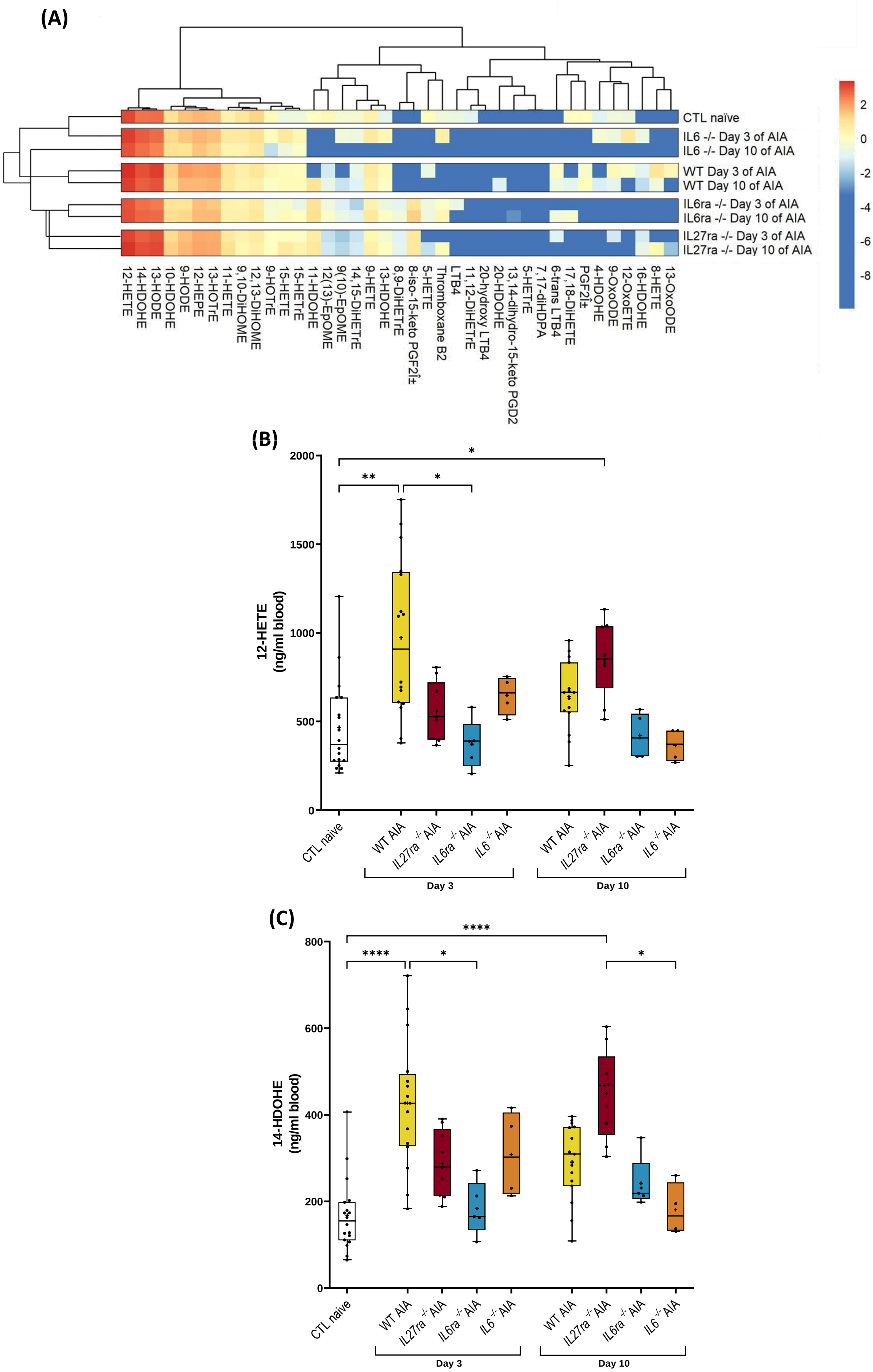

Figure continues into the next page

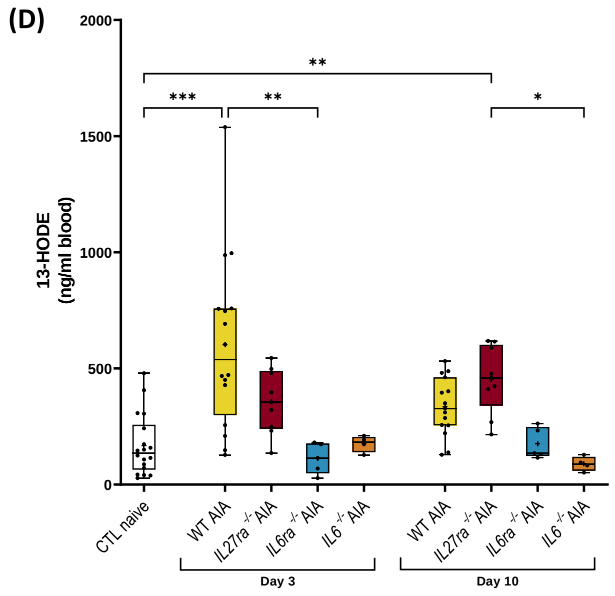

Figure 3.11: Eicosanoid profile is different among different strains, with WT mice displaying increased levels of 12-HETE, 14-HDOHE AND 13-HODE on day 3 of AIA development compared to other strains

Oxylipin levels in whole blood cells pellets from control naïve (n = 18), *WT* (n = 15), *Il27ra*$^{-/-}$ (n = 9), *Il6ra*$^{-/-}$ (n = 5) and *Il6*$^{-/-}$ (n = 5) male mice was analysed on day 3 and on day 10 of AIA development, using LC/MS/MS. (Panel A) Heatmap shows log10 values for analyte concentration (ng/ml). The most abundant lipids detected are represented in box plots, mainly the levels of 12-HETE (Panel B), 14-HDOHE (Panel C), and 13-HODE (Panel D) (ng/ml). Data were analysed using the Kruskal-Wallis test ($p < 0.0001$) and Dunn's multiple comparisons test (*p<0.05, **p<0.01, ***p<0.001, ****p<0.0001).

3.2.9 Blood cell counts are unchanged following the genetic deletion of *IL27ra, IL6ra* and *IL6* in mice.

In order to confirm the increase in both oxPLs and oxylipins is not due to an increase in blood cell numbers, platelets, red blood cells (RBC) and white blood cells (WBC) from *WT*, *IL27ra*$^{-/-}$, *IL6ra*$^{-/-}$ and *IL6*$^{-/-}$ mice were quantified basally, prior to AIA induction.

RBC and WBC were counted automatically using a haematology analyser (Yumizen H2500). However, as mouse platelets are significantly smaller than human platelets[240], the haematology analyser could not be used. Therefore, mouse platelets were isolated and counted manually using a haemocytometer. No significant difference in platelets (p = 0.9282), RBC (p = 0.2538) and WBCs (p = 0.1310) numbers between genotypes was observed, however genetically modified mice displayed a larger data variation in both platelet and WBC count (Figure 3.12). More cell counts should be done in order to properly visualize a possible count difference. Nevertheless, these results suggest that the differences in lipids are not due to differences in blood cell counts, but due to a change in cell composition.

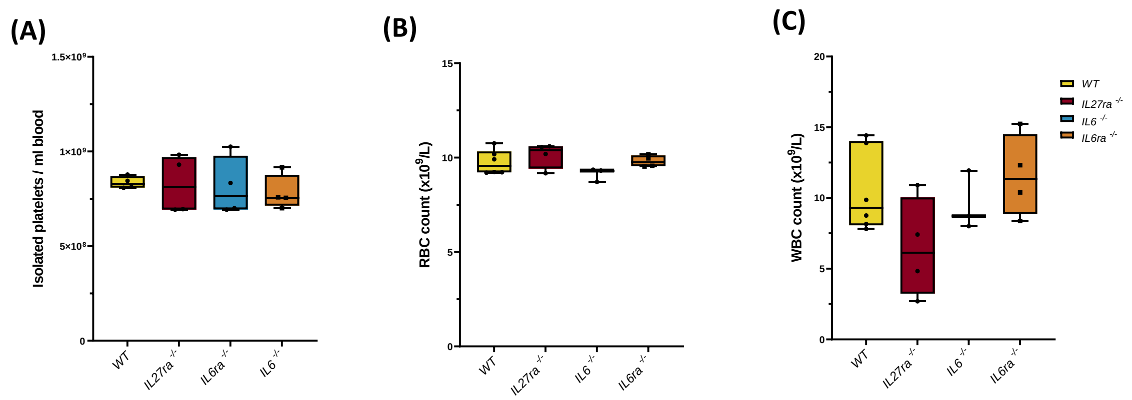

Figure 3.12: Blood cells numbers do not vary between the different mouse genotypes
(Panel A) Platelets (p = 0.9282), (Panel B) red blood cells (p = 0.2538) and (Panel C) white blood cells (p = 0.1310) were counted in whole blood obtained from WT (n = 4), *IL27ra*$^{-/-}$(n = 4), *IL6ra*$^{-/-}$(n=4) and *IL6*$^{-/-}$ (n = 4 (A); n = 3 (B-C)) mice. Platelets were counted after isolation, while RBC and WBC were counted using a haematology analyser (Yumizen H2500). Data are represented as box and whisker plots. Shapiro-Wilk test was used as a normality test and analysed using the ordinary one-way ANOVA test and Tukey's multiple comparison test.

However, thrombocytosis is a common finding in human RA[241], therefore is important to know if the development of AIA alters platelet numbers in this mouse model. This analysis will also answer if the increase in platelet derived lipids, such as 12-HETE-PEs, observed in arthritic WT mice is due to a possible increase of platelet numbers during AIA development. Considering the increase observed in 12-HETE-PEs in WT mice during AIA, but not in IL6ra$^{-/-}$ mice (Figure 3.9.A), platelets were isolated and counted on day 3 and day 10 of AIA of these two pathotypes and compared. In contrast to human RA, platelet numbers showed no significant difference between pathotypes (column factor p = 0.4137), and no interaction (interaction p = 0.4563), nevertheless a difference between time points was observed (row factor p = 0.0319), probably due to a small decrease for both WT and IL6ra$^{-/-}$ mice on day 3 of AIA, however, this difference was not significant in the post hoc test (Tukey's multiple comparison test). Nevertheless, both analysed strains showed the same changes throughout the course of the AIA model, indicating platelet numbers are not responsible for the difference in 12-HETE-PE previously observed.

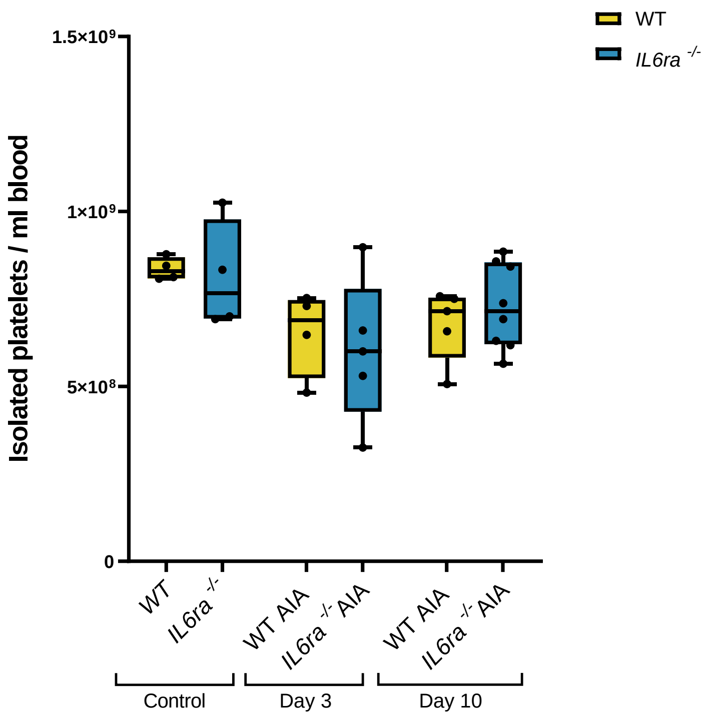

Figure 3.13: AIA model does not significantly alter the platelet count
Platelets from WT and *IL6ra*$^{-/-}$ mice were counted at various stages of AIA development. Data are represented as box and whiskers plots (n = 5). Data were analysed using the ordinary two-way ANOVA test (column factor p = 0.4137; interaction p = 0.4563; row factor (*time*) p = 0.0319) and Tukey's multiple comparison test.

3.3 Discussion

To gain a mechanistic understanding of coagulation in human RA, the AIA mouse model was applied to a series of knockout mice resulting in four distinct pathotypes: myeloid (WT), lymphoid (*IL27ra*$^{-/-}$), and fibroid-rich (*IL6ra*$^{-/-}$), and low inflammatory (*IL6*$^{-/-}$) arthritis. Furthermore, this model was studied at two different time points, early disease on day 3, and established disease on day 10[193,206].

Here I found that the immunization process did not impact either coagulation or inflammation. Furthermore, no significant difference was observed in HETE-PEs due to immunization, therefore, these oxPLs were also analysed in different AIA pathotypes.

First, in order to study the coagulation process in AIA, TAT complexes were analysed. An increase in WT mice on day 10 of AIA development was observed. This is consistent with human RA, where increased levels of TAT have been described[142]. However, neither *Il6ra*$^{-/-}$ nor *Il6*$^{-/-}$ mice showed this increase, suggesting IL-6 is required. Similarly, *Il27ra*$^{-/-}$ mice displayed an increase at day 10 of AIA development when compared to *Il6*$^{-/-}$ mice on the same time point. Interestingly, IL-6 was previously shown to increase coagulation by stimulating antithrombin production, the main inhibitor of thrombin, along with fibrinogen *in vitro*[242], as well as increasing TAT complexes in human plasma[243].

In contrast, PT was not found to increase in WT and *Il27ra*$^{-/-}$ mice during AIA development. This is similar to what is described in human RA, where no alteration to either prothrombin or partial thromboplastin times has been observed[148]."These results suggest the increase in coagulation observed in these mice during AIA is independent of coagulation factors. Surprisingly, an increase in Il*6*$^{-/-}$ mice on day 3 of AIA development was observed. Nevertheless, the elevation was small and not necessarily indicative of a coagulation issue.

Fibrinolysis was studied through the analysis of D-Dimers, however, no significant differences between conditions were observed. This was unexpected considering the high levels of D-dimers described in human RA [91].

In summary, since TATs were elevated, but there were no major differences in PT and D-dimers during AIA overall, I propose that both WT and *Il27ra*$^{-/-}$ mice have an increased thrombin generation, independent of coagulation factors, while maintaining a normal fibrinolysis.

In parallel to the coagulation study, systemic inflammation was also evaluated through the analysis of SAA and CRP during AIA development. An increase in SAA in both WT and *Il27ra*$^{-/-}$ mice was seen on day 3 of AIA. This is consistent with both WT and *Il27ra*$^{-/-}$ mice developing a more severe joint inflammation during AIA. This elevation indicates that WT and *Il27ra*$^{-/-}$ mice induce systemic inflammation during AIA development. As expected, *Il6ra*$^{-/-}$ and *Il6*$^{-/-}$ mice developed low levels of systemic inflammation, as reflected by SAA levels. As a stimulator of APP synthesis by the liver, deletion of *IL-6* signalling was expected to prevent the increase of SAA during AIA development. Interestingly, WT and *Il27ra*$^{-/-}$ mice, were the same pathotypes that also displayed higher levels of TAT complexes during AIA development, suggesting that increased inflammation seen in RA may be linked to coagulation. Elevated SAA in human plasma has been previously shown to be a useful biomarker for venous thromboembolism, independently of CRP, which was shown to be inconsistent [244]. In addition, SAA was previously shown to escalate the progression of atherosclerosis in apolipoprotein E–deficient mice [245]. In cardiovascular diseases, SAA is known to induce tissue factor and pro-inflammatory cytokines, including *IL-6* and TNF-α [245,246]. Therefore, increased coagulation in WT and *Il27ra*$^{-/-}$ mice during AIA could be tissue factor (TF) dependent, but this remains to be determined experimentally. Consequently, TF should also be analysed during AIA, as well as IL-6 levels, to further understand the relationship between inflammation and increased coagulation in this murine arthritis model.

CRP levels were also analysed as an APP during AIA. *Il27ra*$^{-/-}$ mice on day 3 of AIA development displayed an increase in CRP level compared to CTL naïve, while WT mice maintained basal levels throughout the model. This was unexpected, considering that IL27 has been reported to correlate with CRP in human diseases such as Crohn's disease [247], and in auto-immune disease such as RA, and neonatal sepsis[248]. In contrast to SAA, *Il6ra*$^{-/-}$ mice displayed an elevation in CRP on day 3 of AIA development. However, despite being used as a clinical biomarker in humans, in mice, CRP is considered only a moderate inflammatory marker, with SAA being considered more useful marker in this species [249]. Nevertheless, IL-6 induces CRP synthesis[250], and hence, was expected to be diminished in *Il6ra*$^{-/-}$ mice. Furthermore, antagonization of *IL6ra* is currently employed as therapy in RA[251], therefore, *Il6ra*$^{-/-}$ mice were expected to have a reduced CRP similar to *Il6*$^{-/-}$ during AIA development. In humans, IL-6 induces CRP synthesis in the liver[252]. However, these results suggest that, in mice, the CRP synthesis is being induced by a different pathway. In fact, an IL-6 independent CRP regulation has been previously described in hCRP transgenic mice through other cytokines such as IL-1β and other IL-6 class cytokines, namely leukaemia inhibitory factor and oncostatin M[249,253,254]. Therefore, an alternative CRP synthesis pathway, independent of IL-6 might be responsible in these mice. To confirm this, in future directions, IL-1β plasma levels should be measured.

CRP levels significantly correlated with D-dimers, exhibiting a moderate correlation with a Pearson correlation coefficient of 0.5966 [238]. This suggests that inflammation and fibrinolysis, are linked in mice. Interestingly, D-dimers are commonly used in clinical practice as a disease activity marker and are often associated with acute inflammation and disease flares[142,255]. In fact, these correlation has been previously described in synovial fluid of human RA [142]. However, the mechanism behind the association of this fibrinolytic marker and inflammation is currently unknown. Nevertheless, no significant difference was observed in either D-dimers or CRP levels between the different strains during AIA development and CTL naïve, which indicates that they are not directly involved in the AIA model.

These data suggest that IL-6 plays a role in the elevated systemic coagulation observed. However, the mechanism behind the increase of coagulation in these mice is still unknown, as well as the of IL-6 role in this process. Nevertheless, this confirms the influence of cytokines in coagulation previously described in the literature. The deletion of IL-6 prevented the increase of coagulation, more specifically of TAT complexes. This has been previously described in chimpanzees, whereupon receiving an anti-IL-6 antibody, the increase of TAT complexes was prevented following *Escherichia coli* endotoxin injection [256]. Furthermore, in patients with renal cell carcinoma, administration of IL-6 resulted in the increase of TAT complexes, without affecting fibrinolysis.[243]

Coagulation is driven *in vivo* through several mechanisms including TF and pro-coagulant membranes of circulating blood cells and platelets. PT was overall unaltered in *WT* and *IL27ra*$^{-/-}$ mice during AIA development, ruling out altered coagulation factors levels as being responsible. Instead, the increase in TAT complexes seen in the plasma of these mice, indicative of increased coagulation, might be driven by alteration in the pro-coagulant phospholipid composition of blood cells during AIA development. Thus, I considered the impact of phospholipids on arthritis. Pro-coagulant phospholipids termed oxPLs were measured, along with their oxylipin precursors, in whole blood cell pellets from mice during the development of AIA.

OxPLs are thought to be important lipid mediators during innate immunity, for example, by limiting bleeding[257]. Studies have quantified oxPLs in human diseases such as antiphospholipid syndrome and abdominal aortic aneurysms[125,212]. However, their analysis in arthritis is non-existent. Here, similar to the TAT levels, oxPLs were significantly increased in WT and *Il27ra*$^{-/-}$ mice, especially on day 10 of AIA, while in *Il6ra*$^{-/-}$ and *Il6*$^{-/-}$ oxPLs levels were identical to the basal values of CTL naïve mice.

The observed increase in total HETE-PEs was mainly driven by the elevated amounts of 12-HETE-PEs, with 11-HETE-PEs levels also raised. An increase in 15-HETE-PEs was also observed on day 10 of AIA, especially in WT mice. Both WT and *Il27ra*$^{-/-}$ mice have been described to develop a myeloid-rich and lymphoid-rich phenotype, respectively, while both *Il6ra*$^{-/-}$ and *Il6*$^{-/-}$ develop a fibroblastic-rich phenotype[200,202,206]. Therefore, the increase of total HETE-PEs in both WT and *Il27ra*$^{-/-}$ mice during AIA, might be a result of the increase in circulatory immune cells consequence of their specific arthritis pathotype.

Therefore, circulatory blood cells, specifically platelets, WBC and RBC, were counted in the different strains before the development of AIA. No significant difference in cell numbers was observed basally between the different strains, despite the large variability displayed. Furthermore, despite thrombocytosis being commonly found in human RA[241], both WT and *Il6ra*$^{-/-}$ mice platelet counts did not significantly change during the development of AIA. Indeed, Il-6 deletion has been previously shown to not affect platelet numbers[152]. This suggests that the systemic differences observed between the analysed strains during AIA are not due to altered cell counts. Moreover, this indicates that the cells are being activated during arthritis development, generating more oxPLs.

Considering the increase in HETE-PEs, oxPLs origin was further investigated. The low 8-HETE-PEs levels, which is considered a non-enzymatic HETE-PEs since no enzyme can generate it in circulatory blood cells, along with chiral chromatography, confirmed the increase in oxPLs to be mainly enzymatic (Figure 4.2.4). Higher eoxPLs generation and associated coagulation have been previously suggested to contribute to atherosclerosis and abdominal aortic aneurysm since *Alox12*$^{-/-}$ and *Alox15*$^{-/-}$ mice[212,258].

The increase of these specific eoxPLs, namely 12- and 11-HETE-PEs, suggests platelets as potential players responsible for the increased coagulation in WT and *Il27ra*$^{-/-}$ mice during AIA. Nevertheless, 12(S)-HETE-PEs can also be generated through the 12/15-LOX expressed in monocytes/macrophages, and in circulating blood eosinophils[259]. As previously described in Chapter 1, Section 1.1.3, while platelet 12-LOX generates 12(S)-HETE-PE, murine *Alox15* gene, also termed 12/15-LOX, produces primarily 12(S)-HETE-PE, as well as a small amounts of 15(S)-HETE-PE, in a 3:1 ratio[259]. Therefore, to determine whether platelets or myeloid cells are responsible for the elevation of 12-HETE-PLs, the AIA model will be induced in *Alox15*$^{-/-}$ mice and coagulation and eoxPLs will be analysed in the next chapters.

The absence of HETE-PE increase in *Il6ra*$^{-/-}$ and *Il6*$^{-/-}$ mice further supports the idea of a role of *IL-6* signalling in the increase of both coagulation[243], and consequently venous thromboembolism, as well as atherosclerosis[260], in RA patients. Specifically, deletion of IL-6, or its receptor, might result in less reactive platelets. The role of IL-6 in platelet activation has been previously shown *in vitro,* where an increase in platelet aggregation and secretion was observed upon IL-6 incubation of human platelet-rich plasma[261]. However, the mechanism for this is far from known. Interestingly, blockade of IL-6 trans-signalling *in vivo* in the collagen-induced arthritis model results in the improvement of vascular function, which ultimately led to a diminished cardiovascular dysfunction.[262] This suggests that IL-6 might regulate both coagulation, platelet activation and vascular responses, offering a new mechanistic view on the increase of cardiovascular risk in RA patients.

Finally, I also analysed oxylipins in blood pellets from *WT*, *IL27ra* $^{-/-}$, *IL6ra* $^{-/-}$ and *IL6* $^{-/-}$ mice during AIA development. Two oxylipins that were found elevated in the AIA model are considered pro-inflammatory. 13-HODE has been previously described as increased in LDL and HDL from patients with active RA[263], while, along with 12-HETE, is considered a chemoattractant for immune cells[264,265] and both lipids are commonly found in aortal atheroma plaques[266]. However, 13-HODE is also a known PPARγ ligand, therefore, it also activates anti-inflammatory processes. In addition, 14-HDOHE was also a prominent oxylipin detected in the blood cells of these mice and is considered to have anti-inflammatory properties[267]. Interestingly, both *Il6ra*$^{-/-}$ and *Il6*$^{-/-}$ mice did not exhibit significant differences in free oxylipins during AIA development. Plus, 12-HETE peaked on day 3 in WT mice in contrast with the 12-HETE-PEs, where the highest levels were found on day 10. This suggests a possible increase in esterification rates for 12-HETE into 12-HETE-PEs later on, during the development of established disease at day 10 of AIA, while free oxylipins are more prevalent during early stages, where the peak of inflammation is observed.

Overall, assuming that eoxPLs contribute to the elevated coagulation markers detected, these results suggest that IL-6 plays a role in the increased coagulation observed in the AIA model, with platelets potentially playing a role in the elevated systemic coagulation observed. Next, to further investigate the cell origin of the eoxPLs, as well as their potential roles in coagulation and inflammation, in the next chapters, the AIA model will be induced and studied in *Alox15*$^{-/-}$ mice.

Alox15 deletion is not associated with altered coagulation in AIA

Chapter 4

4.1 Introduction

The ability of eoxPls to support coagulation has been observed in a multitude of *in vitro* and *in vivo* models. For example, *Alox15*$^{-/-}$ and *Alox12*$^{-/-}$ mice display a bleeding phenotype[212]. Furthermore, in healthy WT mice, HETE-PL administration enhances coagulation*,* increased circulating TAT complexes, and reduced tail bleeding time, which is driven by coagulation factor activities[125]. Moreover, *Alox15* deletion displayed fewer oxPLs when compared to WT mice basally, and resulted in reduced development of abdominal aortic aneurysms through the infusion of angiotensin II / ApoE$^{-/-}$ mouse model [212]. In a separate study, selective inhibition of 12-LOX impaired thrombus formation and vein occlusion[268]. The bleeding phenotype in Factor VIII-deficient mice was prevented through the administration of liposomes containing 12-HETE-PLs, and thrombin generation was improved in Factor VIII-deficient human plasma[68].

While LOX enzymes generate one specific product enantiomer, commonly an *S*-hydroperoxide, non-enzymatic lipid oxidation produces a racemic mixture of 50/50 *R*- and *S*- enantiomers. Also, non-enzymatic oxidation generates the same relative amounts of all positional isomers, contrasting with the positional isomeric specificity of enzymatic oxidation [5]. Therefore, by measuring the relative levels of all positional isomers, combined with chiral analysis of enantiomers, and confirmed by the deletion of the suspected enzyme, we can deduce the likely enzymatic origin of HETE-PEs in many tissue samples.

Nevertheless, non-enzymatically generated oxPLs were previously shown to play a role in coagulation. For example, OxPAPC, a non-enzymatic oxPL, up-regulated TF *in vitro*, a reaction not observed for native phospholipids[126]. These findings prompted me to examine whether mice lacking eoxPL show reduced coagulation in AIA.

As previously described in Chapter 1, Section 1.1.3, the murine *Alox15* gene, present in eosinophils and monocytes/macrophages, mainly generates 12(*S*)-HETE, along with small amounts of 15(*S*)-HETE, in a 3:1 ratio. This contrasts with human *ALOX15*, which generates primarily 15(*S*)- HETE-PE, along with small amounts of 12(*S*)-HETE-PE, in a 9:1 ratio [53–55]. In the case of *Alox12*, present in platelets, both human and murine 12-LOX generate exclusively 12(*S*)-HETE-PEs [269]. Therefore, both *Alox12,* implicating platelets*,* and *Alox15,* which is expressed by eosinophils and monocytes/macrophages, are responsible for the generation of 12-HETE-PLs in mice. Hence, in order to fully understand the origin of the elevated 12-HETE-PEs I found in mouse blood during arthritis (Chapter 3), the AIA model will be generated in *Alox15*$^{-/-}$ mice, and oxPLs analysed. Unfortunately, due to time restrictions, I was not able to test *Alox12*$^{-/-}$ mice.

Furthermore, to investigate the impact of eoxPLs in RA, coagulation markers will be analysed in *Alox15*$^{-/-}$mice during AIA development. The generation of several oxylipins, such as 13-HODE and 14-HDOHE, can also be dependent on 12/15-LOX. Since, in Chapter 3, I found these lipids increased in whole blood cells of mice developing AIA, I will measure them in *Alox15*$^{-/-}$mice in order to explore their enzymatic origin.

4.1.1 Aims

Here, I will characterize the impact of *Alox15* gene deletion on coagulation in AIA, by inducing arthritis, in parallel, in both WT and *Alox15*$^{-/-}$ mice:

- Characterise coagulation markers in *WT*, *Alox15*$^{-/-}$ mice during AIA development, namely TAT complexes, D-dimers and PT.
- Analyse whole blood cells from AIA mice for oxPLs and oxylipins using LC/MS/MS.

4.2 Results

4.2.1 Genetic deletion of *Alox15* does not influence TAT levels during the development of AIA.

Firstly, these mice were confirmed to be *Alox15*$^{-/-}$ mice, thorough genotyping, as described in Chapter 2, Section 2.2.2. An exemplar picture of the gel proving the genotype can be seen in the appendix of this thesis (Chapter 10) (Figure 10.1).

I then analysed TAT levels in both WT and *Alox15*$^{-/-}$ mice, as well as during AIA development, on day 3 and on day 10, which represent early and established disease, respectively. No significant difference was observed between WT and *Alox15*$^{-/-}$ mice ($p = 0.4826$). In fact, both WT and *Alox15*$^{-/-}$ mice control mice, as well as on day 3 of AIA displayed no significant difference between each other (Figure 4.1.A). However, TAT levels rose on day 10 of AIA in both WT and *Alox15*$^{-/-}$ mice compared to their respective CTL. This is indicative of a significant change during the time points (row factor $p < 0.0001$). Nevertheless, no significant difference was observed between WT and *Alox15*$^{-/-}$ mice, as indicated by the two-way ANOVA interaction test (interaction $p = 0.4663$). This suggests that *Alox15* has little or no impact on systemic levels of TAT complexes during the development of AIA

PT was also not significantly altered between WT and *Alox15*$^{-/-}$ mice, or between AIA time points (row factor $p = 0.1311$) (Figure 5.1.B). Despite the apparent increase of PT in *Alox15*$^{-/-}$ AIA mice on day 10 of AIA, this is mainly due to one failed data point, where the plasma analysed was unable to clot until the cut-off time of 120 s. Nevertheless, the overall difference was not significant.

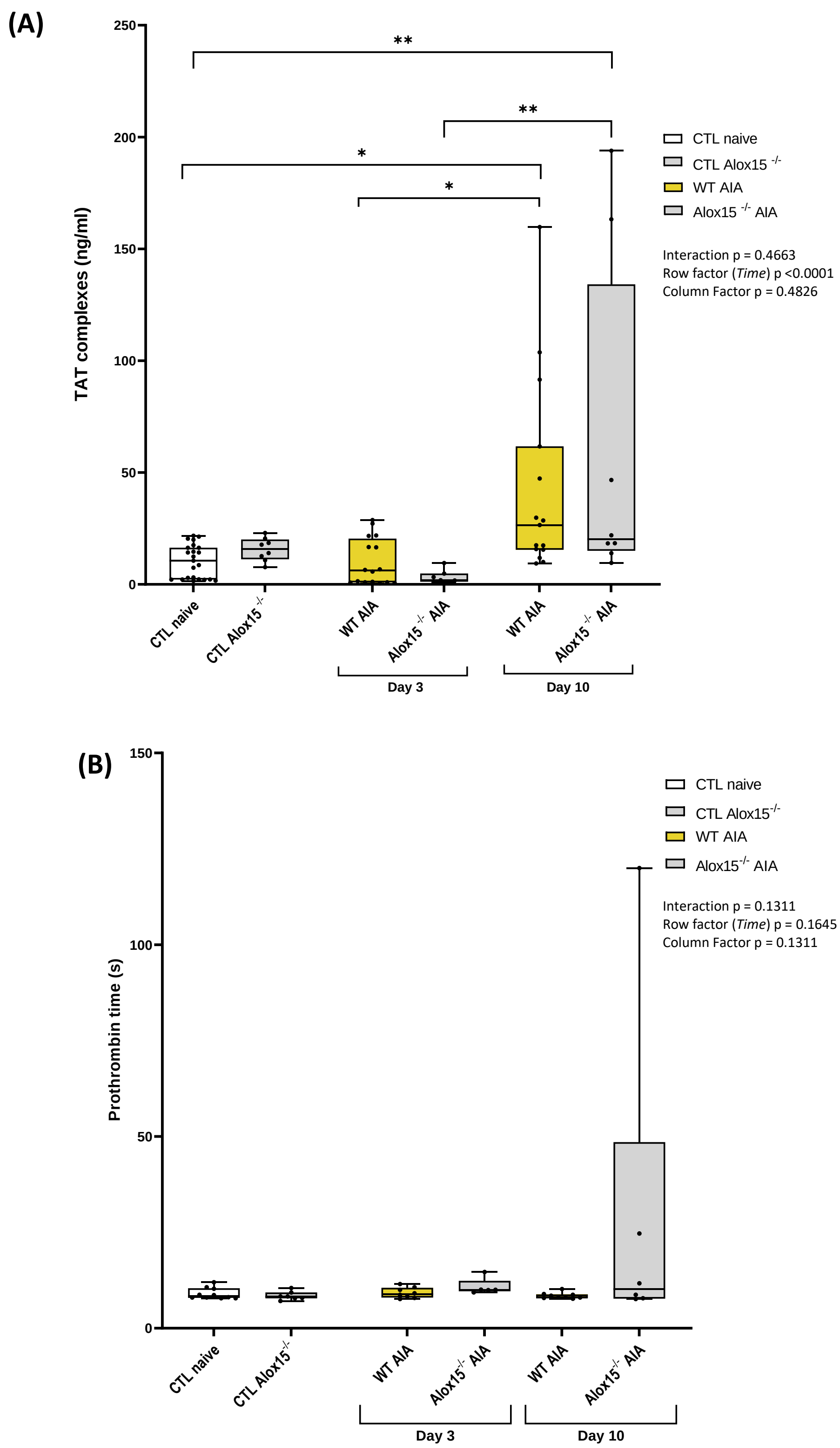

Figure 4.1: *Alox15* deletion does not significantly impact coagulation in AIA mice
AIA model was generated in 9- to 12- week-year-old WT (n = 15) and *Alox15*$^{-/-}$ (n = 7) male mice. Plasma levels of TAT complexes (Panel A) were evaluated on day 0 as CTL naïve (n = 25), on day 3 and on day 10 of AIA. (Panel B) PT was also evaluated in WT (n = 8) and *Alox15*$^{-/-}$ (n = 5) male mice during AIA development, as well as CTL naïve (n = 10) and CTL *Alox15*$^{-/-}$ (n = 7). Data is represented in box and whisker plot. Data were analysed using two-way ANOVA and Tukey's multiple comparisons test (*p <0.05, **p <0.01).

4.2.2 Genetic deletion of *Alox15* increases D-dimers during the development of AIA.

Next, fibrinolysis was analysed. Here, D-dimers were interacting significantly (interaction p = 0.0067) when analysed through a Two-way ANOVA test, displaying a significant difference between time points (row factor p = 0.0060) and genotypes (column factor p = 0.0071). Furthermore, through Tukey's multiple comparison test, a significant increase was observed on day 3 of AIA in *Alox15*$^{-/-}$ mice when compared to CTL naïve and WT mice on the same AIA time point (Figure 4.2). On day 10 of AIA development, this difference was not evident, with both WT and *Alox15*$^{-/-}$ displaying similar D-Dimer levels, and no significant difference when CTL naïve mice. This shows that *Alox15*$^{-/-}$ mice suffered a transient increase on day 3 during AIA development, which was lacking in WT mice.

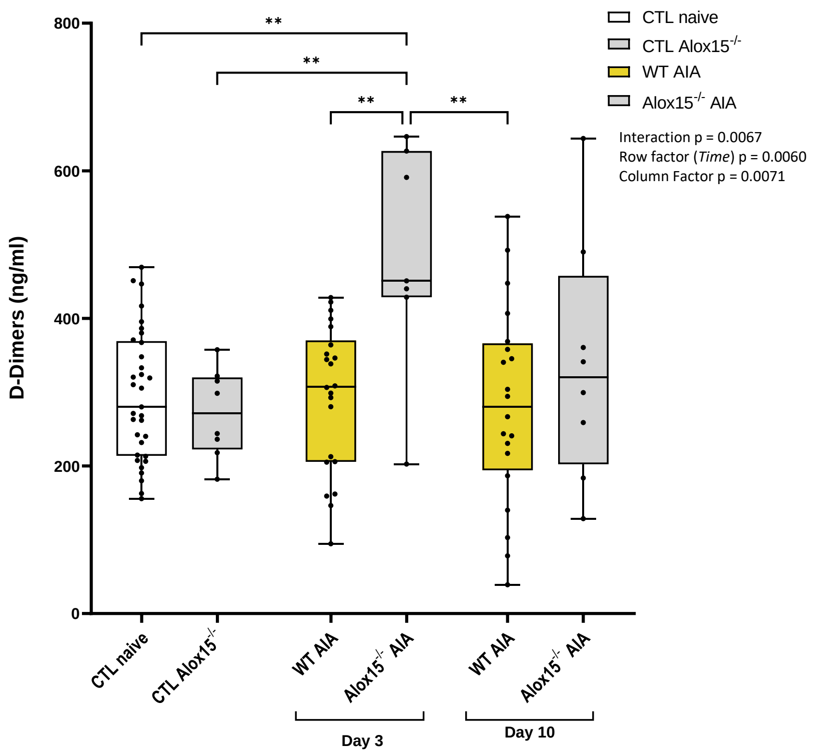

Figure 4.2: *Alox15* deletion increases D-Dimer levels
AIA model was generated in 9- to 12- week-year-old WT (n = 20) and Alox15 $^{-/-}$ (n = 8) male mice. Plasma levels of D-dimers were evaluated on day 0 for CTLs, and on day 3 and on day 10 of AIA. Data is represented in box and whisker plot. Data were analysed using the Two-Way ANOVA and Tukey's multiple comparisons test (** p <0.01).

4.2.3 Blood cell levels of oxPLs are not altered during AIA development by deletion of *Alox15*.

Next, HETE-PEs levels were next analysed through LC/MS/MS in whole blood cells from WT and *Alox15*$^{-/-}$ mice during AIA development. Here I found that HETE-PEs present were similar between WT and *Alox15*$^{-/-}$ mice. 18:0a_12-HETE-PE remains the most abundant oxPLs (Figure 4.3.A). Unexpectedly, total oxPLs levels in *Alox15*$^{-/-}$ mice were highly increased compared to WT basally (Figure 4.3). In summary, during AIA, *Alox15*$^{-/-}$ mice HETE-PE levels were significantly higher compared to CTL naïve, without, however, displaying any significant difference with WT mice at the same time point.

Individual isomers were next analysed separately. Here I found high basal levels of 12-HETE-PEs, 11-HETE-PEs, 15-HETE-PEs and 8-HETE-PEs in *Alox15*$^{-/-}$ compared to CTL naïve mice (Figure 4.4). However, no significant differences were observed between CTL *Alox15*$^{-/-}$ and *Alox15*$^{-/-}$ mice during AIA, both on day 3 and day 10, except for 11-HETE-PEs, which peaked on day 3 of this model. In addition, the 12-HETE-PE isomer remained the most abundant oxPLs generated during the AIA model, even after *Alox15* deletion (Figure 4.4.A). This result suggests that 12-HETE-PEs in these mice is not from *Alox15.*

The same pattern is observed when analysing 15-HETE-PEs (Figure 4.4.B), which were significantly increased in CTL *Alox15*$^{-/-}$ versus CTL naïve and are then maintained during AIA development. This suggests that the deletion of *Alox15* does not impact the levels of these blood oxPLs. A significant decrease in 11-HETE-PEs was seen from day 3 to day 10 of AIA in *Alox15*$^{-/-}$ mice. However, analysis of the 8-HETE-PEs levels also suggests a non-enzymatic generation of some HETE-PEs (Figure 4.4.E). In fact, the levels of 8-HETE-PEs are increased in the same pattern as 12- and 15-HETE-PEs (Figure 4.4.B-C), suggesting at least a fraction is of non-enzymatic origin. However, the high levels of 12-HETE-PEs, suggest that a large amount of these lipids are formed by enzymes, and most likely from *Alox12*.

Interestingly, 5-HETE-PE levels were found to be lower than 8-HETE-PEs (Figure 4.4.D-E). Despite not reaching a statistically significant difference, 5-HETE-PEs were detected at reduced levels in *Alox15*$^{-/-}$ compared to WT mice during AIA development, on both day 3 and day 10.

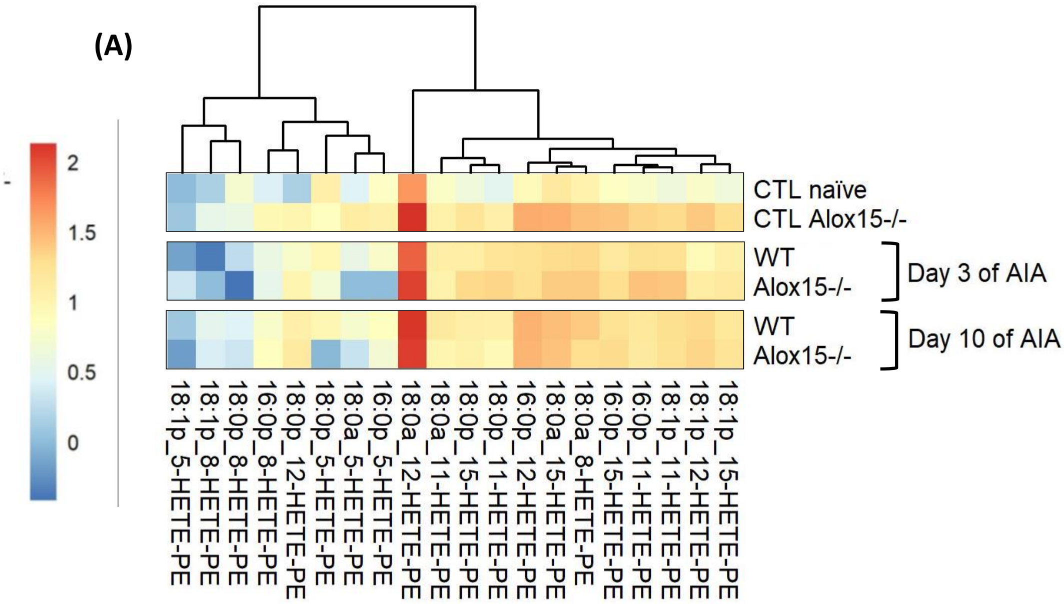

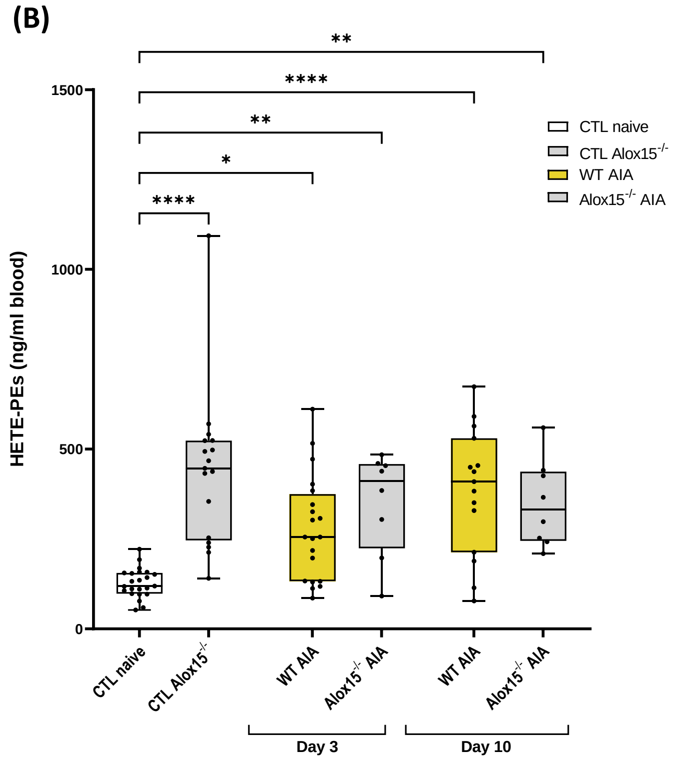

Figure 4.3: ***Alox15*** **deletion does not prevent elevated levels of HETE-PEs in mouse blood during AIA development.**

Antigen-induced arthritis was generated in 8- to 11- week-year-old *WT* (n = 20) and *Alox15*$^{-/-}$ (n = 8) male mice. Whole blood was collected on day 0 for CTLs (n = 20), on day 3 and on day 10 of AIA. Whole blood cell pellets were analysed through LC/MS/MS. (Panel A) Heatmap shows log10 values for analyte concentration (ng/ml). (Panel B) The sum of all the quantified HETE-PEs isomers (ng/ml) in blood was calculated. Data were analysed using the Kruskal-Wallis test (p <0.0001) and Tukey’s multiple comparisons test (*p<0.05, **p<0.01, ****p<0.0001).

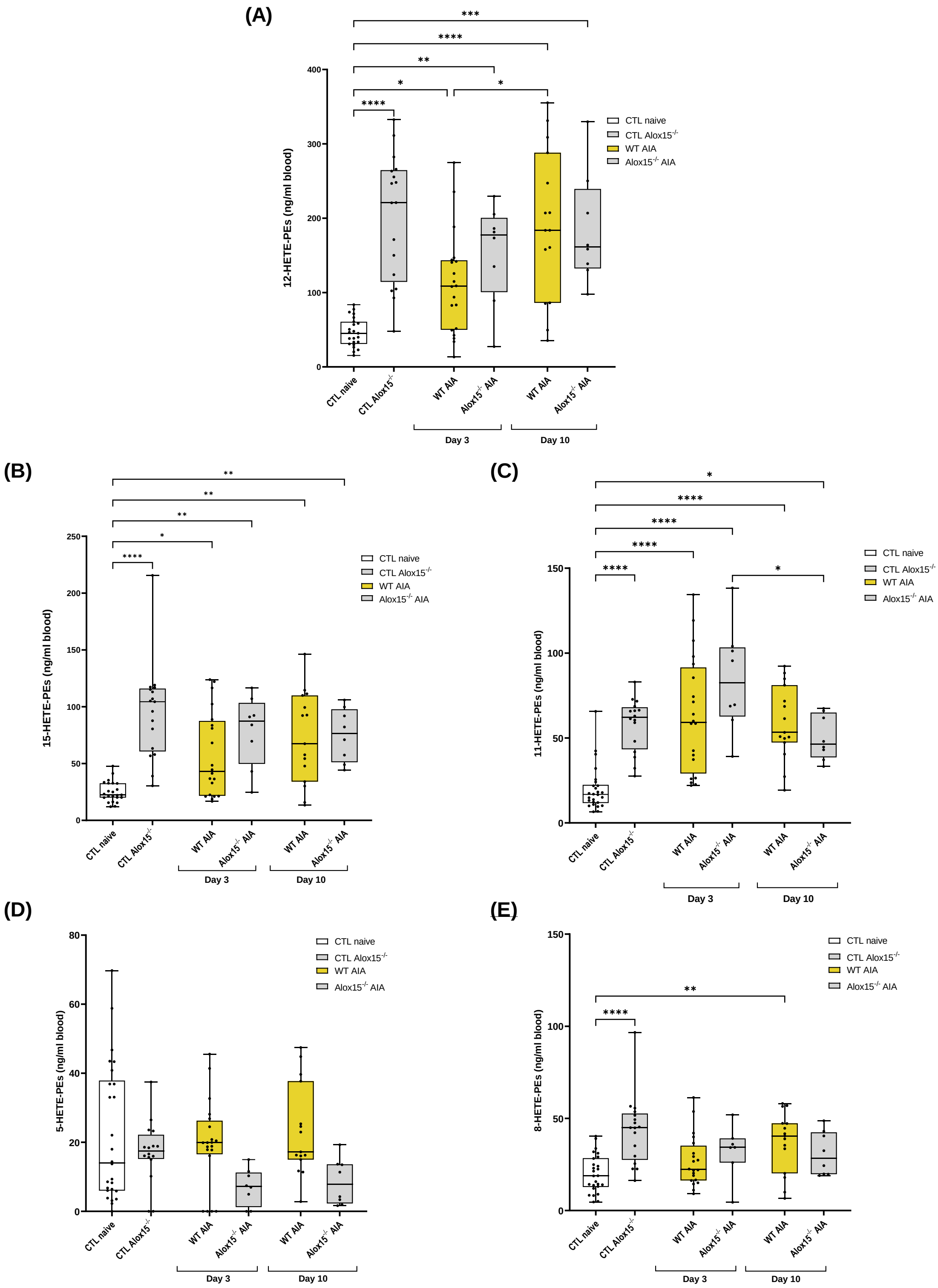

Figure 4.4: HETE-PEs levels are increased, partially, due to non-enzymatic oxidation in Alox15$^{-/-}$ mice during AIA

Antigen-induced arthritis was generated in 8- to 11- week-year-old *WT* (n = 20) and *Alox15$^{-/-}$* (n = 8) male mice. Whole blood was collected on day 0 for CTLs (n = 20), on day 3 and on day 10 of AIA. HETE-PE positional isomers (ng/ml) were determined in whole blood cells, analysed using LC/MS/MS. Data are shown for 12-HETE-PEs (p<0.0001) (Panel A), 15-HETE-PEs (p <0.0001) (Panel B), 11-HETE-PEs (p <0.0001) (Panel C), 5-HETE-PEs (p = 0.0131) (Panel D) and 8-HETE-PEs (p <0.0001) (Panel E). Data were analysed using Kruskal-Wallis and Tukey's multiple comparisons tests (*p<0.05, **p<0.01, **** p<0.0001).

4.2.4 *Alox15*$^{-/-}$ mice show similar levels of whole blood oxylipins as WT during the development of AIA.

Several oxylipins are generated by 12/15-LOX oxidation, including HETEs and HODEs, and it is important to discern their enzymatic origin, along with their impact on this inflammatory arthritis model. Therefore, here I analysed the oxylipin profile from WT and *Alox15*$^{-/-}$ mice during AIA development.

Genetic loss of *Alox15* did not result in a major reduction of oxylipin levels (Figure 4.5.A). The species present in the highest amounts in blood were 12-HETE, 14-HDOHE and 13-HODE, regardless of *Alox15* deletion. However, *Alox15*$^{-/-}$ mice exhibit basally an overall rise in oxylipins compared to CTL naïve. However, this basal increase in oxylipins present in *Alox15*$^{-/-}$ mice, did not significantly change upon AIA development. This is particularly evident for 12-HETE (Figure 4.5.B), where *Alox15*$^{-/-}$ mice display increased levels basally, which were maintained upon AIA development. This contrast with WT mice, where a peak is observed on day 3 of AIA development.

Furthermore, 11-HDOHE, another product of platelet *Alox12*[270], through oxidation of docosahexaenoic Acid (22:6), is basally increased in *Alox15*$^{-/-}$ mice compared to CTL naïve (Figure 4.5.C). This suggests that *Alox12* might have higher levels of expression upon *Alox15* deletion. Upon AIA development, 11-HDOHE fell below the limit of detection on day 3 in both WT and *Alox15*$^{-/-}$ mice. Falling below the limit of detection does not necessary the absence of this lipid, nevertheless, it increases variability within the dataset when the concentration cannot be accessed through LC/MS/MS. However, when analysing day 10 of AIA development, an increase in 11-HDOHE above detection limits was observed, with *Alox15*$^{-/-}$ mice exhibiting the same level present basally, while the WT mice suffered an increase compared to CTL naïve.

In the case of 15-HETrE (Figure 4.5.D), an oxylipin that can be generated either by 12/15-LOX or non-enzymatically, *Alox15*$^{-/-}$ mice displayed lower levels when compared to WT during AIA development, despite the non-statistical significance, suggesting it may arise from via enzymatic biosynthesis. Similar to the previously analysed lipids, *Alox15*$^{-/-}$ mice exhibit elevated basal levels of 15-HETrE compared to CTL naïve, further suggesting a non-enzymatic origin.

In contrast, 13-HODE peaked in both WT and *Alox15*$^{-/-}$ mice on day 3 of AIA compared to the respective control and day 10 of AIA development (Figure 4.5.E). However, similar to other oxylipins *Alox15*$^{-/-}$ mice exhibit high basal levels of 13-HODE compared to CTL naïve. In summary, the deletion of *Alox15* did not massively alter the oxylipin profile of these mice during AIA development.

(A)

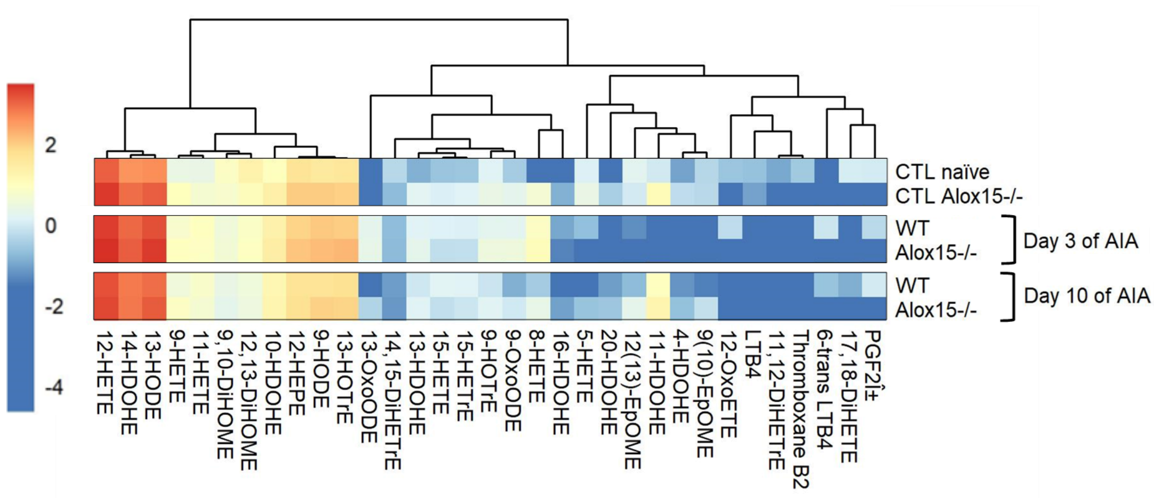

Figure continues into the next page

(B)

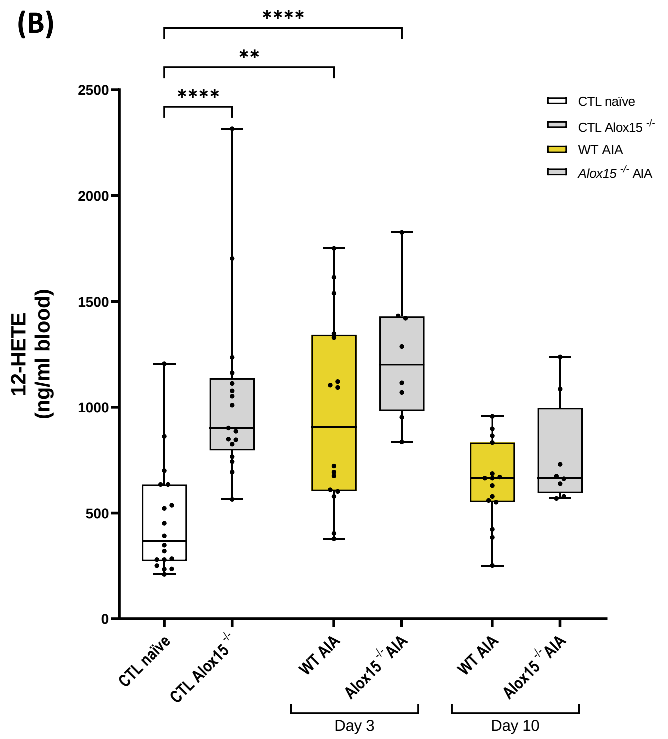

(C)

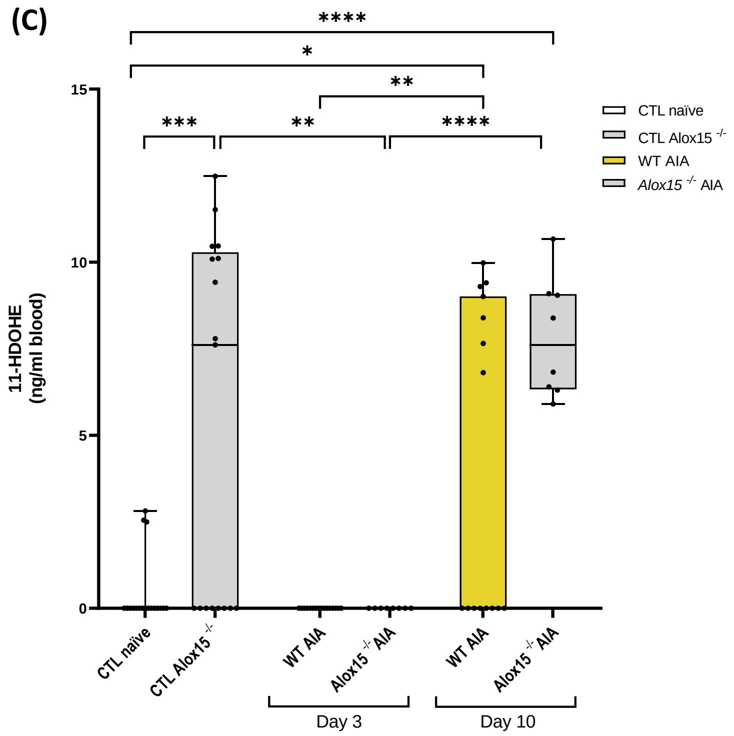

Figure continues into the next page

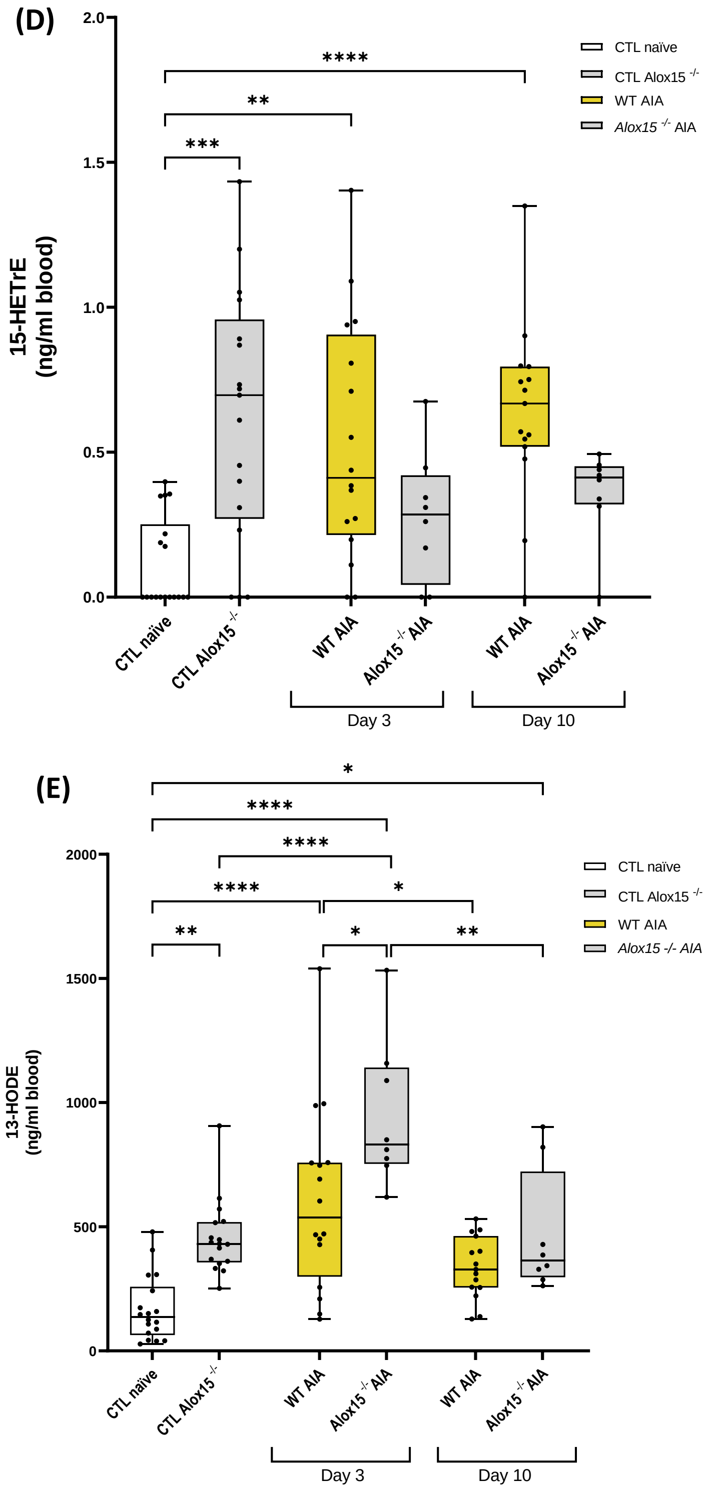

Figure 4.5: Oxylipins synthesis is increased in *Alox15*$^{-/-}$ mice basally, however AIA development does not significantly differ oxylipin production.

Oxylipin levels in whole blood cells pellets from *WT* (n = 16) and *Alox15*$^{-/-}$ (n = 8) male mice, along with respective controls, were analysed on day 3 and on day 10 of AIA development, using LC/MS/MS. (Panel A) Heatmap shows log10 values for analyte concentration (ng/ml). Whole blood levels of 12-HETE (p <0.0001) (Panel B), 11-HDOHE (p<0.0001) (Panel C), 15-HETrE (p<0.0001) (Panel D) and 13-HODE (p<0.0001) (Panel E) were calculated (ng/ml). Data were analysed using Kruskal-Wallis and Tukey's multiple comparisons tests (*p<0.05, **p<0.01, ***p<0.001, ****p<0.0001).

4.3 Discussion

As previously shown in Chapter 3, AIA development in WT mice elevated systemic coagulation, as shown by the increased levels of TAT complexes. However, the molecular mechanism behind this is still unknown. The observed increase in eoxPL in these mice suggests a possible mechanism for this increase. However, the enzymatic origin of increased levels of 12-HETE-PEs present in these mice might be by 12-LOX or 12/15-LOX oxidation. In order to probe the potential cellular origin of these eoxPLs, the AIA model was induced in *Alox15*$^{-/-}$ mice, where no oxidation by 12/15-LOX occurs.

Expressed mainly in eosinophils and macrophages, the 12/15-LOX enzyme is responsible for the generation of numerous lipid mediators that play a role in coagulation and inflammation. However, the deletion of *Alox15* resulted in no differences in TAT levels compared to WT mice, with a significant increase still observed on day 10 of AIA development in these mice. Interestingly, a high variability in TAT complexes is observed on day 10 of AIA development, which can be a consequence of the increased coagulation. In fact, variability between mice, specially during the model, was expected considering the slight inherent changes in blood taking, despite being minimised through a careful and fast drawing protocol.

Nevertheless, no significant difference was found in PT between conditions. This contrasts with a previous study, where TAT levels and PT were observed to be elevated in *Alox15*$^{-/-}$ compared to WT mice.[212] However, there are methodological differences between my experiments and these. In particular, the mice used in the previous study were older, at 19 weeks old, while in my analysis the mice were exclusively males of 12-14 weeks of age. Second, the blood collection protocol I used, described in Chapter 2, employs CTI as an anticoagulant, contrary to the published paper. This will have the effect of further stabilising the blood and dampening down coagulation activity *in vitro*, potentially explaining why no difference was found in my study.

Contrary to WT mice, D-dimers were increased in *Alox15*$^{-/-}$ mice on day 3 of AIA development. As previously discussed in Chapter 3, Section 3.3, D-dimers significantly correlated with CRP, an important inflammation marker. In fact, D-dimers are considered a disease activity marker, commonly used in clinical practice as a disease activity marker and are often associated with peaks of inflammation [142,255]. Therefore, an increase of D-dimers on day 3 of AIA development, which is when the peak of swelling and inflammation occurs was not unexpected. On day 10, following the resolution of the swelling, a significant decrease of D-dimers compared to day 3 would also be expected. Nevertheless, the non-replication by WT mice during AIA suggests that *Alox15*$^{-/-}$ mice might develop a more severe AIA phenotype compared to WT. In order to determine the severity of the phenotype developed, *Alox15*$^{-/-}$ will be induced to develop AIA in the next chapter, and joints will be analysed.

In addition, blood oxPLs were higher basally in *Alox15*$^{-/-}$ blood cells and they were unaffected upon induction of inflammatory arthritis. These results differ from the gradual increase of eoxPL observed in WT mice during AIA development. Interestingly, high levels of 12-HETE-PEs were observed in *Alox15*$^{-/-}$ mice during AIA development. This suggests that a large amount of these lipids is formed by enzymes, therefore, indicating platelet *Alox12* as the primary source of elevated 12-HETE-PEs during AIA development in mice. Nevertheless, in order to exclude the possibility of a non-enzymatic origin, the AIA model should be induced in *Alox12*$^{-/-}$ mice and 12-HETE-PEs levels determined.

In addition, a significant decrease in 11-HETE-PEs was seen from day 3 to day 10 of AIA development in *Alox15*$^{-/-}$ mice, which suggests at least a higher COX activation in *Alox15*$^{-/-}$ mice. Considering the importance of COX in platelet, where an acute synthesis of oxylipins and oxPLs is observed upon the activation of these cells [271], these results suggest a possible increase in platelets activation upon AIA development in *Alox15*$^{-/-}$ mice compared to WT. Furthermore, elevated levels of 8-HETE-PEs also suggest a non-enzymatic oxidation present basally in these mice, which might be a result of increased systemic oxidative stress. However, the increased level of eoxPLs might also be a result of a feedback mechanism by 12-LOX to compensate for the lack of enzymatically generated oxPLs due to the absence of 12/15-LOX. This hypothesis is further supported by the 11-HETE-PEs results previously discussed, which further indicates that platelets from *Alox15*$^{-/-}$ might be more basally active than in WT mice. However, chiral chromatography, or the analysis of these lipids in *Alox12*$^{-/-}$ mice during the AIA development, would need to be performed to understand if the origin of the increased oxPL present basally in *Alox15*$^{-/-}$ mice is from platelet 12-LOX, or simply due to an increase in oxidative stress.

Interestingly, 5-HETE-PE levels were found to be relatively lower than the remaining HETE-PEs isomers. The deletion of *Alox15* should not affect the generation of 5-HETE-PEs, considering that this HETE-PE isomer is either generated through non-enzymatic oxidation or enzymatically oxidised by *Alox5* present neutrophils. Nevertheless, 5-HETE levels were described as slightly increased in *Alox15*$^{-/-}$ mice during a peritonitis mice model in *Dioszeghy et al*.[272] Therefore, an increase in 5-LOX expression might occurs due to *Alox15* ablation, possibly as a compensatory mechanism, however this was not observed in this analysis. More studies are necessary to understand if and how 5-LOX expression is affected in *Alox15*$^{-/-}$ mice.

Whole blood cell levels of 12-HETE, 14-HDOHE and 13-HODE were also elevated basally in *Alox15*$^{-/-}$ mice, compared to CTL naive. This suggests that their blood levels may originate from platelet 12-LOX, which is substantially activated in these mice when compared to WT. To test this, AIA should be induced in *Alox12*$^{-/-}$ mice and a lipidomic analysis performed. This would show if platelet 12-LOX is responsible for the generation of these oxylipins and eoxPLs, or if the increase of these lipids in *Alox15*$^{-/-}$ mice is due to an increase in non-enzymatic oxidation.

In contrast to WT mice, 15-HETrE levels in *Alox15*$^{-/-}$ mice during AIA decreased on day 3, although this was not significant. This result was expected since its generation can be through 12/15-LOX oxidation. In spite of being mainly studied in the skin, 15-HETrE has been described as a potent inhibitor of LTB_4, and is usually described as a potential anti-inflammatory lipid.[273] This, along with the increased levels of oxylipins generally considered pro-inflammatory, suggest that the deletion of *Alox15* might develop a worse inflammatory arthritis phenotype. Next, to test this, joint histology, joint lipidomics and clinical assessment of the mice during AIA development will be performed.

Overall, the increase in TATs and eoxPLs rise during AIA development was not prevented upon genetic deletion of *Alox15*. This suggests that *Alox15* is not involved in the increased coagulation observed in WT mice during AIA development. Instead, it is possible that platelet *Alox12* might be responsible. To further understand the impact of platelets in enzymatically generated oxPLs, the AIA model should be induced in *Alox12*$^{-/-}$ mice and systemic coagulation, along with oxylipidomics, analysed.

Alox15-deficient mice show elevated inflammation and swelling during AIA development

---

Chapter 5

5.1 Introduction

Several arthritis mice models have been used to study the impact of *Alox15* deletion on disease, however, contradictory results have been published[89,189]. As previously described in Chapter 1, Section 1.4, TNF- α Tg mice model and K/BxN serum-induced arthritis model in *Alox15*$^{-/-}$ mice resulted in a more pronounced inflammatory state when compared to the respective WT mice [189]. However, when using the adjuvant-induced arthritis model in *Alox15*$^{-/-}$ mice, a reduced paw swelling was described [89].

Nevertheless, no *in vivo* arthritis model is 100 % reflective of human disease, with each model displaying a distinct pathological mechanism of RA, which might result in different outcomes upon LOX modulation. The limitation of the TNF- α Tg mice model is the lack of cure in human RA using anti-TNF-α therapies, such as Infliximab. Similarly, the antigen-induced arthritis model does not mirror human arthritis, as it is effectively cured through the use of COX inhibitors [192]. Meanwhile, the K/BxN serum-induced arthritis model is exclusively mediated by antibodies [191], which also does not reflect the mechanisms of human RA. In addition, none of the studies did measure LOX products using LC/MS/MS, but by ELISA, which can be considered a controversial method of lipid analysis, as described in Chapter 1, Section 1.1.2.1.

The AIA model, despite being one of the most commonly used inflammatory arthritis murine model [193], has not yet tested for an involvement of 12/15-LOX. Plus, in Chapter 4, increased D-dimers was observed systemically on day 3 of AIA development, along increased pro-inflammatory oxylipins in whole blood cells. This suggests that *Alox15* deletion might result in elevated systemic inflammation. Therefore, in order to understand if *Alox15* is involved in the resolution of inflammation, in this chapter, the impact of *Alox15* deletion on systemic inflammation and joint pathology, along with lipid analysis of joint tissue, will be studied.

5.1.1 Aims

This chapter will further characterize the impact of *Alox15* gene deletion in the AIA model and investigate the importance of 12/15-LOX products in inflammatory arthritis *in vivo*. In this regard, AIA was induced in parallel in WT and *Alox15*$^{-/-}$ mice, and day 3 and day 10 studied, as follow:

- Clinically assessment of *WT* and *Alox15*$^{-/-}$ mice during AIA development, namely evaluate knee swelling, weight, joint histology and mBSA antibody titre.
- Characterisation of inflammatory markers in *WT* and *Alox15*$^{-/-}$ mice during AIA development, namely CRP and SAA.
- Analyse joint extracts from *WT* and *Alox15*$^{-/-}$ mice during AIA for oxPLs and oxylipins through LC/MS/MS.

5.2 Results

5.2.1 *Alox15* deletion is associated with slower resolution of synovial inflammation in AIA.

AIA was induced in both WT and *Alox15*$^{-/-}$ mice, and early and established arthritis time points, representing day 3 and day 10 of AIA development respectively, were analysed.

As described in Chapter 2, Section 2.2.3, joint swelling was measured with a POCO 2T micrometer (Kroeplin) and compared to joint diameter before arthritis induction (Figure 5.1.A). A significant difference through time was found using the two-way ANOVA test (row factor $p<0.0001$), however, no significant overall difference was detected between conditions (column factor $p = 0.1092$). Nevertheless, when comparing each time point between WT and *Alox15*$^{-/-}$ mice through the student t-test test, Alox*15*$^{-/-}$ mice showed a significant increase in swelling on day 7 of AIA. In fact, overall, a higher degree of swelling was displayed in Alox*15*$^{-/-}$ mice throughout the AIA model, suggesting a more severe AIA phenotype occurs upon *Alox15* deletion.

The clinical response against mBSA was also analysed in both strains, as described in Chapter 2, Section 2.2.17. As the antigen used to induce arthritis, mBSA antibodies are produced as an immunological response to immunization. mBSA-specific IgG in murine plasma was detected using anti-mouse IgG conjugated to HRP which was quantified using a chromogenic peroxidase substrate by measuring optical density at 450 nm (OD_{450}), which reflect the amount of mBSA-specific IgG. *Alox15* deletion did not alter the immune response to BSA compared to WT mice during AIA. No significant changes were observed in mBSA-specific antibody titres in plasma, at both days 3 ($p = 0.1404$) and day 10 ($p = 0.9419$) of AIA upon Alox*15* deletion (Figure 5.1.B-C).

Weights were also recorded throughout AIA development, as a parameter for wellbeing, despite not being a direct assessment of inflammatory arthritis severity. Due to the length of the model, weight gain during a 31-day period was also measured in an aged-matched group of healthy mice from both studied strains, as controls. A significant difference was observed through AIA development (row factor p <0.0001), without affecting the genotypes (column factor p = 0.7172). This is further reflected by the lack of weight differences between WT mice and their respective controls throughout the progression of the model, with both showing normal weight gain in line with age (Figure 5.1.D).In contrast with their respective controls, *Alox15* $^{-/-}$ mice failed to gain weight during AIA development, displaying a significant decrease compared to the respective control on day 4 and day 10 of AIA development.

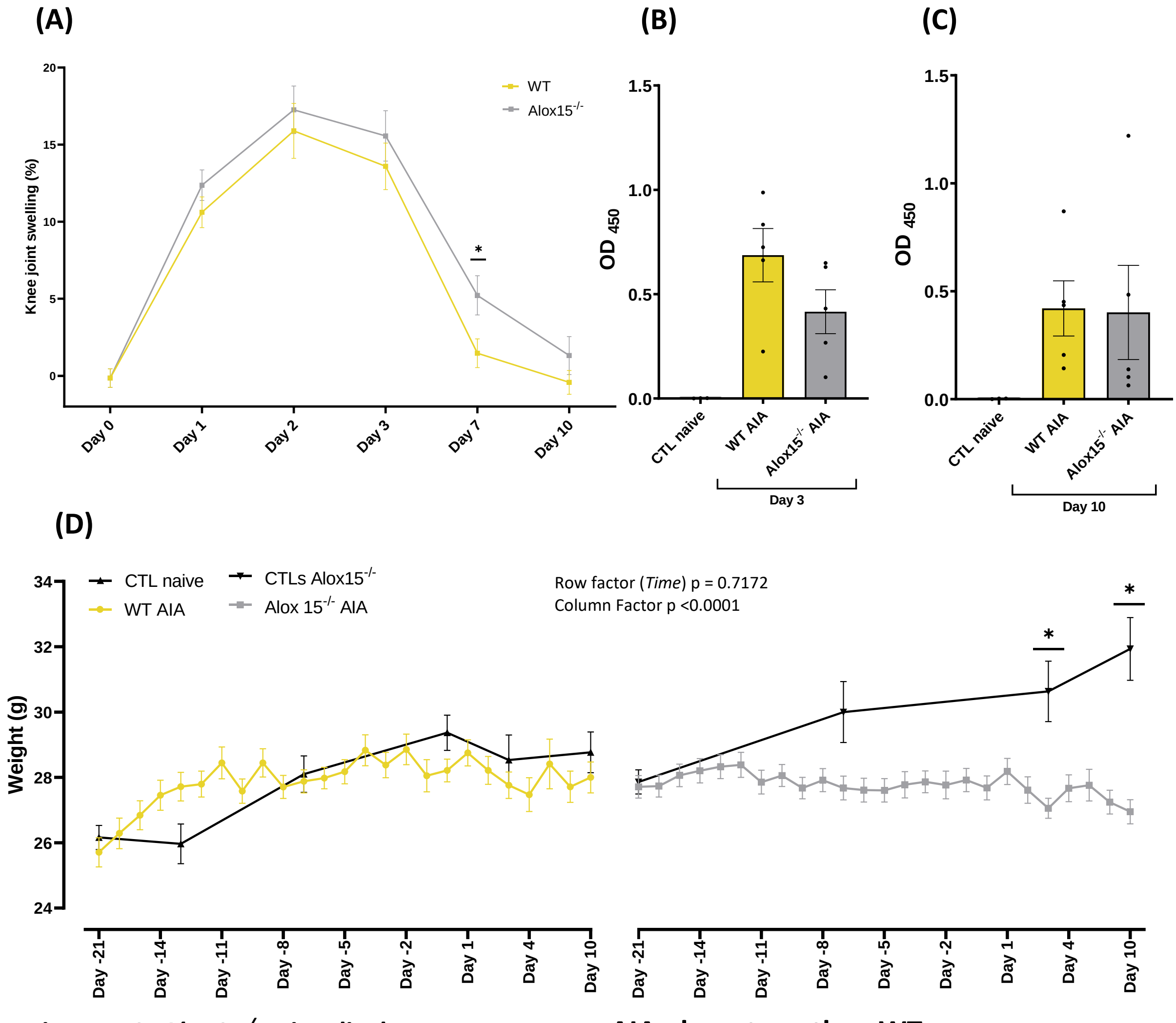

Figure 5.1: *Alox15*$^{-/-}$ mice display a more severe AIA phenotype than WT.
(Panel A) Knee diameter was measured every 1-2 days and knee joint swelling was calculated as a percentage relative to knee diameter at day 0 (before arthritis induction). Average knee joint swelling percentages and SEM are represented from day 0 to day 10, the last day of the performed model. Data represent mean ± SEM, and statistical analysis was performed using a student t-test (*p < 0.05) (n ≥ 16). (Panel B) mBSA specific antibody titres in mice plasma on day 3 and (Panel C) day 10 post arthritis induction were determined through ELISA. Data represents mean ± SEM (n = 5) and statistical analysis was performed using a student t-test (p = 0.1404 for day 3 and p = 0.9419 for day 10). (Panel D) Mice were weighted every week, in the case of CTLs, or every 1-2 days, in the case of the AIA mice, respectively. Average values, along with SEM, are represented from day 0 to day 10, the last day of the performed model. Data was analysed using the Two-Way ANOVA and Tukey's multiple comparisons test (* p < 0.05).

5.2.2 Synovial inflammatory infiltrations are elevated in Alox15$^{-/-}$ mice during AIA development.

Next, as described in Chapter 2, Section 2.2.9, I sliced parasagittal serial sections. This was followed by staining with haematoxylin, eosin and safranin O staining, in order to histologically assess joint pathology, as described in Chapter 2, section 2.2.10 (Table 2.4). Haematoxylin staining indicates cellular infiltration, by staining the nucleus blue and cytoplasm pink, while safranin-O stains cartilage red, indicating cartilage erosion. As an example of different scoring is represented in Figure 2.2. This assessment was performed blindly by Gareth Jones, PhD and David Hill, PhD from Bristol University, and Aisling Morin, PhD from Cardiff University, to evaluate synovial exudate, synovial inflammation and hyperplasia and cartilage and bone erosion, and overall joint damage in both WT and *Alox15*$^{-/-}$ mice, as described in Chapter 2, section 2.2.11.

The overall arthritic index was calculated through the sum of all analysed parameters, namely synovial infiltrate, synovial exudate, synovial hyperplasia and pannus formation and cartilage and bone erosion. These parameters were compared between WT and *Alox15*$^{-/-}$ mice during AIA development, within the same timepoint, therefore, the statistical analysis was performed through the student's t-test. No significant difference was found between WT and *Alox15*$^{-/-}$ mice during AIA development, although *Alox15*$^{-/-}$ mice showed a tendency to increase compared to WT on day 10 (Figure 5.2.B).

When analysing individual parameters of the arthritic index, a significant increase in synovial infiltrate was observed in *Alox15*$^{-/-}$ mice knee joint compared to WT on day 10 (Figure 5.2.C). An increase in cartilage and bone erosion was also observed in *Alox15*$^{-/-}$ mice on day 10, however, this was not statistically significant (Figure 5.2.F). The other analysed criteria, namely synovial hyperplasia and pannus formation, and synovial exudate displayed no difference in scoring (Figure 652.D-E). Overall, these results indicate that the increased swelling observed in *Alox15*$^{-/-}$ mice, compared to WT, is due to a greater synovial infiltration.

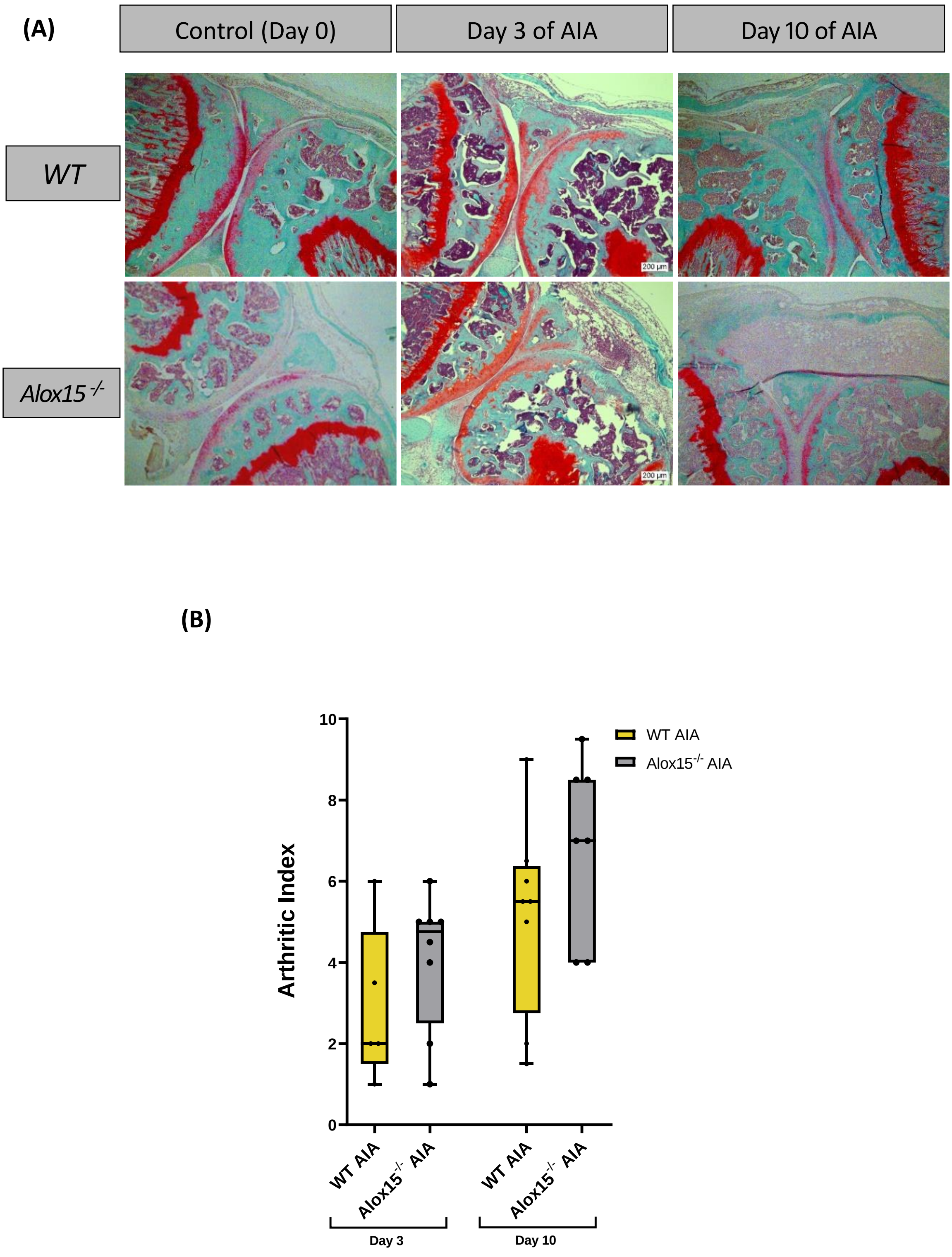

Figure continues into the next page

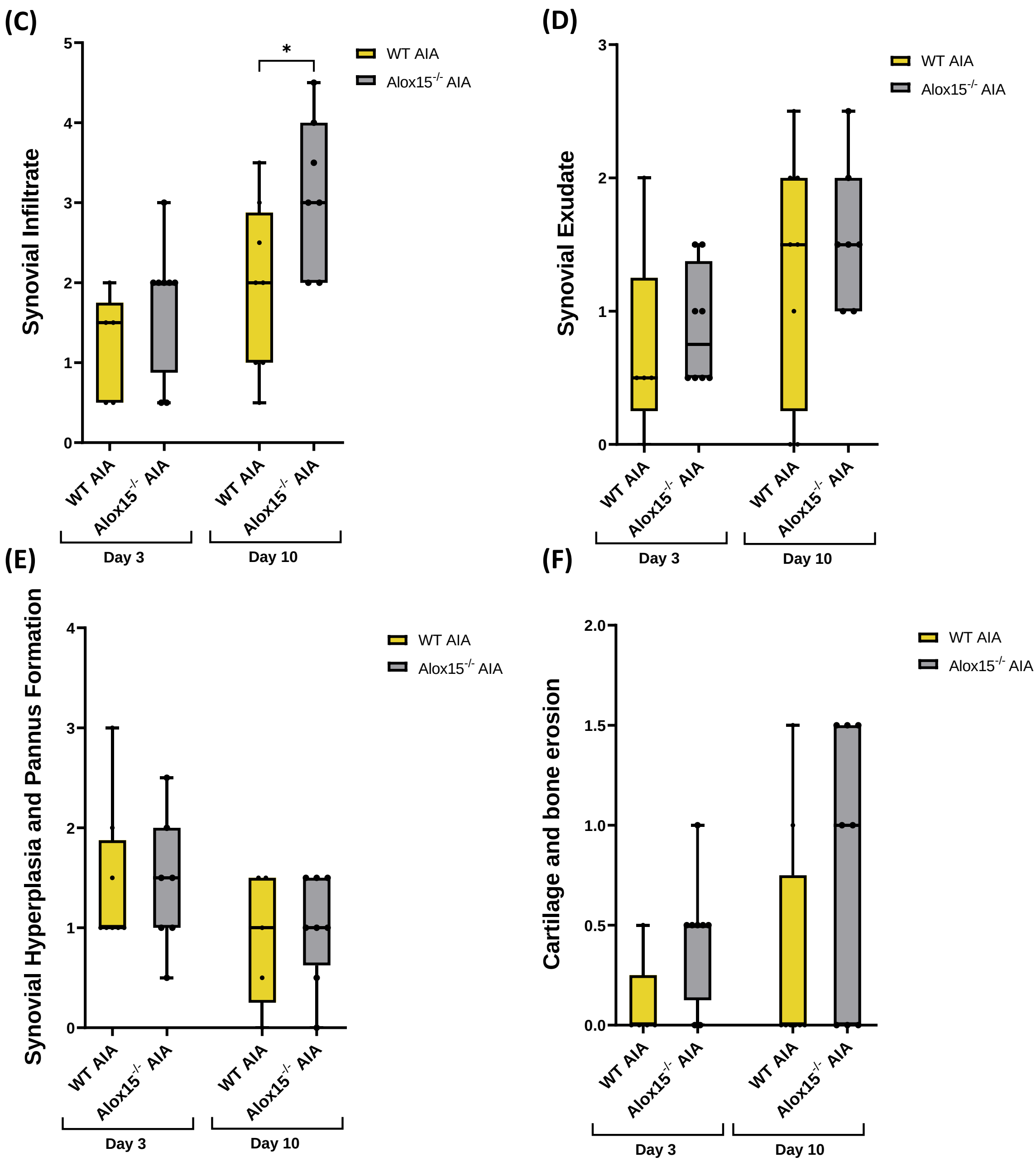

Figure 5.2: AIA development in *Alox15$^{-/-}$* mice results in an increase in synovial infiltration of immune cells

AIA was induced in 9- to 12- week-year-old WT *and Alox15$^{-/-}$* mice, and joints collected on day 0 (n = 3 - 5), as controls, on day 3 (n = 5 - 8) and day 10 (n = 7 - 8) of AIA for histological staining and assessment, as described in Section 2.2.11 in the Methods chapter. (Panel A) Representative images of haematoxylin, fast green, and safranin O staining of WT (top) and Alox15$^{-/-}$ (bottom) mouse knee joints at day 3 (centre) and day 10 (right) post-arthritis induction, as well as controls (left). Histopathology scoring of AIA was performed and (Panel B) Arthritic score, (Panel C) Synovial infiltration, (Panel D) Synovial exudate, (Panel E) Synovial Hyperplasia and Pannus formation, and (Panel F) cartilage and bone erosion were evaluated. Data were analysed Student's t-test, according to time point (*$p < 0.05$).

5.2.3 *Alox15*$^{-/-}$ mice show a higher elevation in SAA than WT at the earlier disease time point of AIA development.

Next, systemic inflammation was compared between WT and *Alox15*$^{-/-}$ mice during AIA development, by analysing SAA levels. Since the levels are being analysed through time in different genotypes, two-way ANOVA was used, where a significant interaction was found (interaction $p = 0.0174$). Furthermore, a significant difference was found between time points (row factor $p<0.0001$), however, no overall difference was found between genotypes (column factor $p = 0.4396$).

Nevertheless, when using Tukey's multiple comparison test, SAA levels were found significantly increased on day 3 of AIA development in *Alox15*$^{-/-}$ mice when compared to WT mice at the same time point (Figure 5.3.A). As previously observed in Chapter 3, SAA levels peaked on day 3 of AIA development, followed by a significant decrease on day 10 of AIA development in the plasma of both analysed genotypes. Therefore, as expected, SAA levels drop significantly for both WT and *Alox15*$^{-/-}$ mice, from day 3 to day 10 of AIA development, respectively. When comparing both mice at this time point, SAA levels appear to drop lower in *Alox15*$^{-/-}$ than in WT mice, however, the difference wasn't significant.

A large variation of data was observed in WT on day 3 of AIA ($n = 13$) when compared to *Alox15*$^{-/-}$ mice ($n = 7$) at the same time point. This variation might be a result of the distinct n numbers analysed between WT and *Alox15*$^{-/-}$mice. Furthermore, WT mice were order in, while *Alox15*$^{-/-}$ mice were bred in house, which might reduce inherent differences between mice. Plus, as previously described, the blood drawing protocol might provoke inherent differences between mice.

Overall, these data suggest that deleting Alox15$^{-/-}$ results in a worsened acute phenotype of inflammatory arthritis during AIA development.

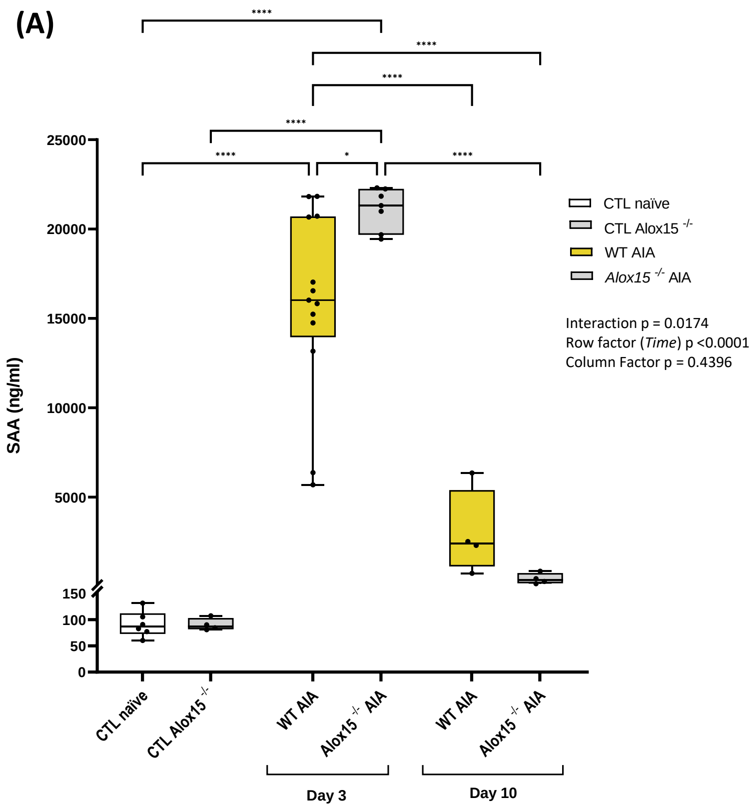

Figure 5.3: **SAA levels are higher in *Alox15*$^{-/-}$ mice compared to WT on day 3 of AIA development**
AIA model was generated in 9- to 12- week-year-old WT and *Alox15*$^{-/-}$ male mice. SAA levels in plasma were evaluated on day 0 for control (CTL) (n = 6 for naïve and 4 for *Alox15*$^{-/-}$ mice), on day 3 (n = 13 for WT and 7 for *Alox15*$^{-/-}$ mice), and on day 10 (n = 4) of AIA. Data were analysed using Two-way ANOVA and Tukey's multiple comparisons tests (*p<0.05, **** p<0.0001).

5.2.4 OxPLs are increased in WT mice joints during AIA development.

Next, I measured oxPLs in synovial tissue in WT and *Alox15*$^{-/-}$ mice during AIA development, and respective controls. To provide sufficient tissue for analysis, joints from each condition were pooled to reach around 10 mg wet weight per sample, with tissue from at least 3 mice (6 joints) pooled to generate each data point (each n). Due to the large number of mice required for each analysis, only a total n of 3 was analysed. This reduced n number is an obvious limitation in the conclusions of the following sections. Increasing the number would provide increase power and it may reduce variability, nevertheless, the pooling would have induced a reduction in data variability.

As expected, relating to HETE-PEs, synovial tissue exhibits a different pattern to whole blood cells, considering that they have a different cell composition. For example, platelets were the major contributor to HETE-PL levels in whole blood. When analysing the HETE-PEs data through Two-way ANOVA, a significant interaction was found (interaction p = 0.0227), along with a significant overall difference between WT and *Alox15*$^{-/-}$ mice (column factor p = 0.0230), and time points (row factor p = 0.0003) (Figure 5.4.B).

Here, joint levels of oxPLs were overall reduced in *Alox15*$^{-/-}$ mice, compared to WT, both basally, and during AIA development (Figure 5.4.A). This suggests that the oxPLs are of enzymatic origin. The deletion of *Alox15* results in a decrease in eoxPLs, indicating that oxPLs present in synovial tissue is dependent on 12/15-LOX activity. This clearly contrasts with the results described in whole blood cells, where deletion of *Alox15* did not result in a significant reduction, probably due to either increase in non-enzymatic oxidation, or due to platelet-12-LOX activity.

Furthermore, HETE-PEs peaked in WT joints on day 10 of AIA development (Figure 5.4.B). However, this was not observed in joints from *Alox15*$^{-/-}$ mice, where the elevation was small and non-significant. These results further indicate that WT joints generate significant amounts of eoxPL in arthritic joints via 12/15-LOX during AIA development.

As in whole blood cells, 12-HETE-PEs were the main oxPL detected in joint tissue in WT mice on day 10. A significant interaction was observed (interaction $p < 0.0001$), as well as a significant difference between time points and genotypes (row factor $p < 0.0001$ and column factor $p < 0.0001$, respectively) (Figure 6.5.A). Interestingly, these lipids did not elevate significantly in *Alox15*$^{-/-}$ mice. This indicates that the increased 12-HETE-PEs generated during AIA are from 12/15-LOX (leukocyte 12-LOX), potentially expressed by monocytes/macrophages.

Interestingly, 15-HETE-PEs showed no significant interaction (interaction $p = 0.2711$), but a significant difference considering the time (row factor $p = 0.0008$) and an overall difference between genotypes (column factor $p = 0.0435$). This is further reflected in the Tukey's multiple comparison test where a significant increase in WT mice joints on day 10 of AIA development was observed, but not in *Alox15*$^{-/-}$ mice (Figure 5.5.B).

The remaining 11-HETE-PEs, 5-HETE-PEs and 8-HETE-PEs showed no significant differences according to the Tukey's multiple comparisons tests. In fact, their levels were relatively similar amounts within the joints between WT and *Alox15*$^{-/-}$ mice, exhibiting no significant impact by *Alox15* deletion. Interestingly, *Alox15*$^{-/-}$ mice presented relatively similar amounts of 12-, 15-, 11-, 5- and 8-HETE-PEs within the joints. Considering that the different positional HETE-PEs isomers are generated at similar concentrations when their generation is of non-enzymatic origin, these results suggest that some oxidation through ROS was involved in the production of HETE-PEs in these mice Therefore, no compensation process for the lack of 12/15-LOX oxidation is present. Nevertheless, chiral analysis is required to prove this hypothesis (Figure 5.5.C-E).

As previously mentioned, the restricted number of analysed samples, even if representing pooled mice, limits the possible conclusion. More analysis would be necessary, however, the number of mice required makes it extremely difficult.

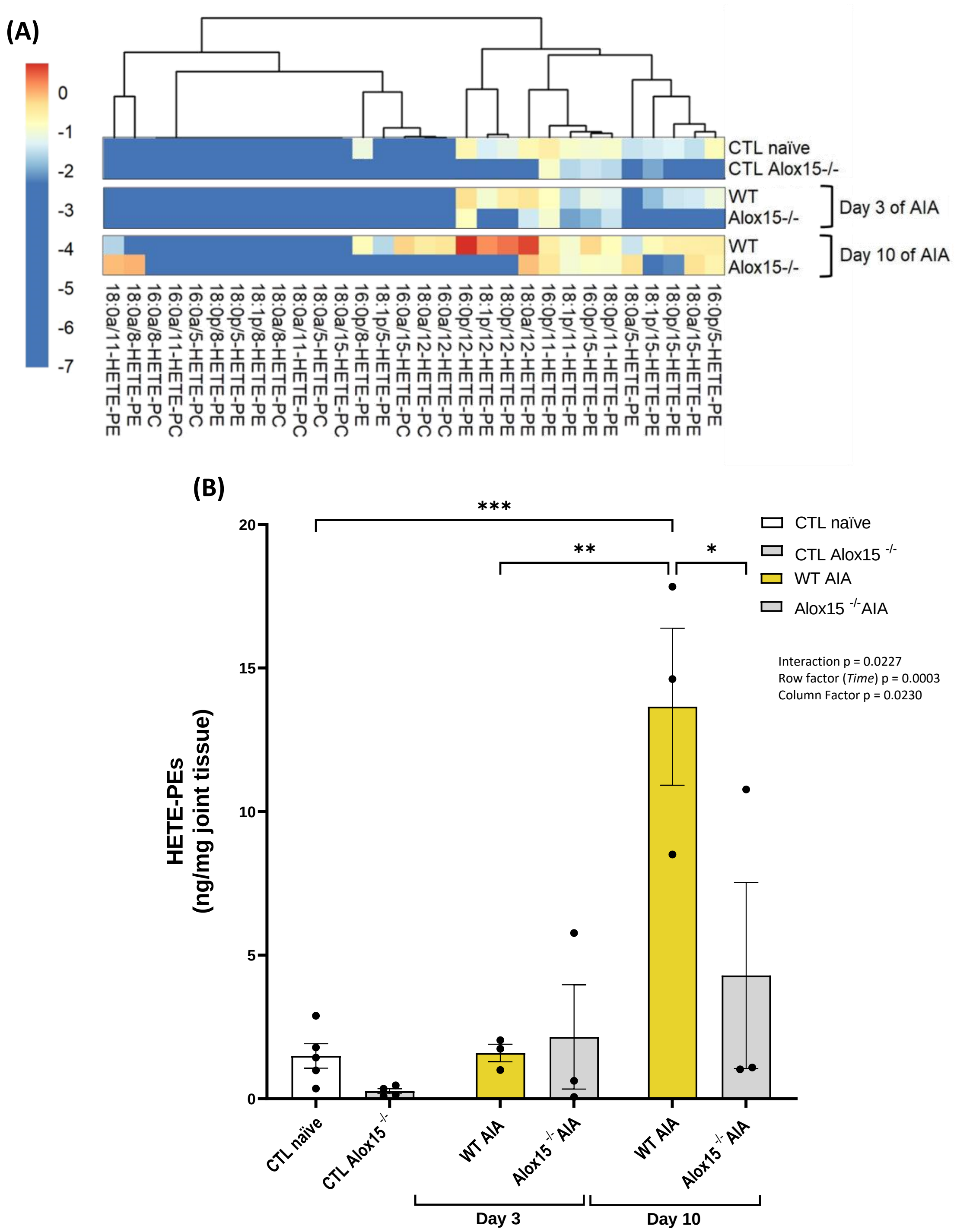

Figure 5.4: OxPLs are significantly increased in WT on day 10 of AIA, but not in Alox15$^{-/-}$ mice
Antigen-induced arthritis was generated in 8- to 11- week-year-old *WT* and *Alox15$^{-/-}$* C57B6J male mice, simultaneously. Joint tissue was collected, and pooled, on day 0 for CTL (n = 4 - 5), on day 3 (n = 3), and on day 10 (n = 3) of AIA. Pooled joint tissue was analysed through LC/MS/MS. (Panel A) Heatmap shows log10 values for analyte concentration [ng/mg (wet weight)]. (Panel B) The sum of all the quantified HETE-PEs isomers [ng/mg (wet weight)] in joint tissue was calculated. Data represent mean values ± SEM, along with the respective scatter plot displaying individual values. Data were analysed using the Two-Way ANOVA and Tukey's multiple comparisons test (***p < 0.001).

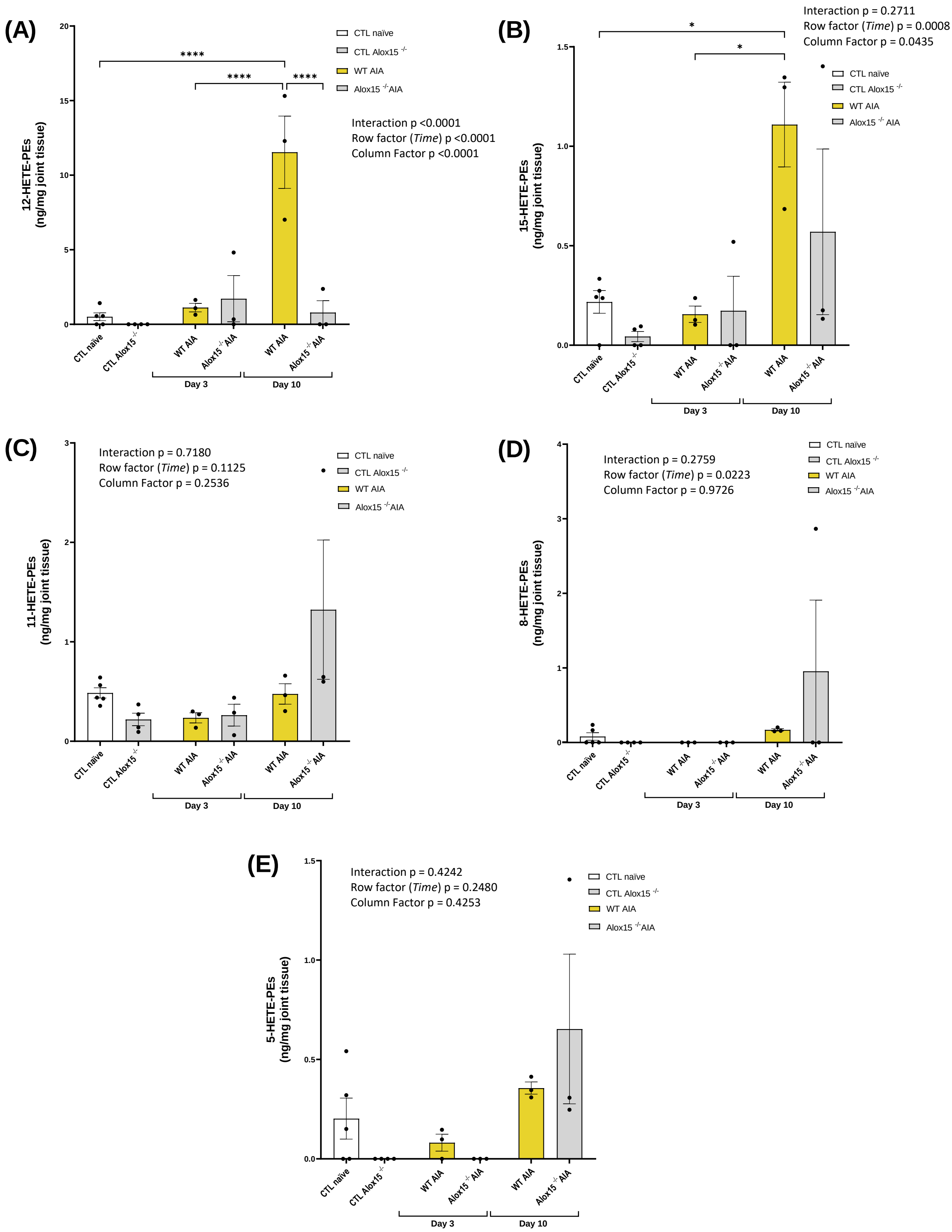

Figure 5.5: Enzymatic 12- and 15-HETE-PE are the main oxPLs increased in WT knee joints on day 10 of AIA development

The sum of individual HETE-PEs isomers [ng/mg (wet weight)] in joint tissue, namely 12-HETE-PEs (Panel A), 15-HETE-PEs (Panel B), 11-HETE-PEs (Panel C), 8-HETE-PEs (Panel D) and 5-HETE-PEs (Panel E), were analysed through LC/MS/MS. Data represent mean values ± SEM, along with the respective scatter plot displaying individual values. Sample numbers were as listed in Figure 5.4 above. Data were analysed using Two-way ANOVA and Tukey's multiple comparisons tests (*p < 0.05, **** p < 0.0001).

5.2.5 Synthesis of oxylipins in mouse joints during AIA is largely dependent on *Alox15.*

Next, oxylipins were analysed in the joint tissue of WT and *Alox15*$^{-/-}$ mice during AIA development. AIA induced an increase in many oxylipins in the joints of WT mice, but not *Alox15*$^{-/-}$ (Figure 5.6.A). When analysing LOX products, significant changes were observed. WT mice, on day 10 of AIA development, displayed increased levels of 15-HETE, 12-HETE and 13-HODE, which upon the loss of 12/15-LOX were not detected (Figure 5.6.B-D).

The two-way ANOVA test was chosen as the correct statistical analysis test considering that two variables, genotypes, represented as WT and *Alox15*$^{-/-}$ mice, as well as time, with day 0 as controls, day 3 as early disease and day 10 as established disease, were present. While 15-HETE levels displayed a significant interaction between genotypes and time points (interaction $p<0.0001$), while presenting a significant difference between each (column and row factor $p<0.0001$), 12-HETE levels, only presented a significant difference between genotypes (column factor $p = 0.0047$) and time points (row factor $p = 0.0420$), without presenting a significant interaction between them (Figure 5.6.B-C).

As expected, both 12- and 15-HETE, which can be generated by 12/15-LOX, were maintained at basal levels in *Alox15*$^{-/-}$ mice throughout AIA development. In contrast, WT mice exhibited a significant increase compared to CTL naïve on day 10 (Figure 5.6.B-C). Furthermore, and as expected, 13-HODE, which can also be generated by 12/15-LOX, through oxidation of linoleic acid, the same trend was observed (Figure 5.6.D). A significant interaction was observed (interaction $p = 0.0060$), along with significant differences between time and genotypes (row and column factor $p = 0.0009$). These results indicate that 15-HETE, 12-HETE and 13-HODE, are derived from enzymatic oxidation from 12/15-LOX. This indicates that oxylipin composition within the joint is different to the blood, suggesting a compartmentalization of these lipids.

PGD_2 and PGE_2, as products of COX oxidation, were significantly increased in both WT and *Alox15*$^{-/-}$ mice, on day 10 of AIA, with no impact of *Alox15* deletion (Figure 5.6.E-

F). PGD2, despite not presenting a significant interaction (interaction $p = 0.1086$) or difference between genotypes (column factor $p = 0.8567$), did present a significant difference along time (row factor $p<0.0001$). In the case of PGE_2, only a significant difference between time points was observed (row factor $p<0.0001$). This further confirms the lack of impact upon *Alox15* deletion, while indicating that the AIA development into an established disease (day 10) is responsible for the increase of both PGD_2 and PGE_2.

Unexpectedly, in the case of PGE_1, deletion of *Alox15* resulted in a drop, when compared to WT mice on day 10 of AIA development, despite also being a COX product (Figure 5.6.G). However, these results might be a consequence of the low concentrations present boarding on the limits of detection of the LC/MS/MS. Nevertheless, similar to PGE_2 and PGD_2, no significant interaction or difference between genotypes was observed through the two-way ANOVA test (interaction $p = 0.0773$ and column factor $p = 0.0938$), with a significant difference observed throughout the AIA development (row factor $p = 0.0087$).

No specialized pro-resolving mediators were detected apart from a small chromatographic peak in one single WT mice joint sample which co-eluted with the RvD5 standard. However, due to the small peak detected, it was impossible to perform an EPI scan or chiral chromatography to determine the structure of this lipid. Therefore, this lipid was designated as 7,17-diHDHA, which doesn’t assume the enantiomeric structure of RvD5. Notably, since it was only present in one sample, it was not reproducibly detected.

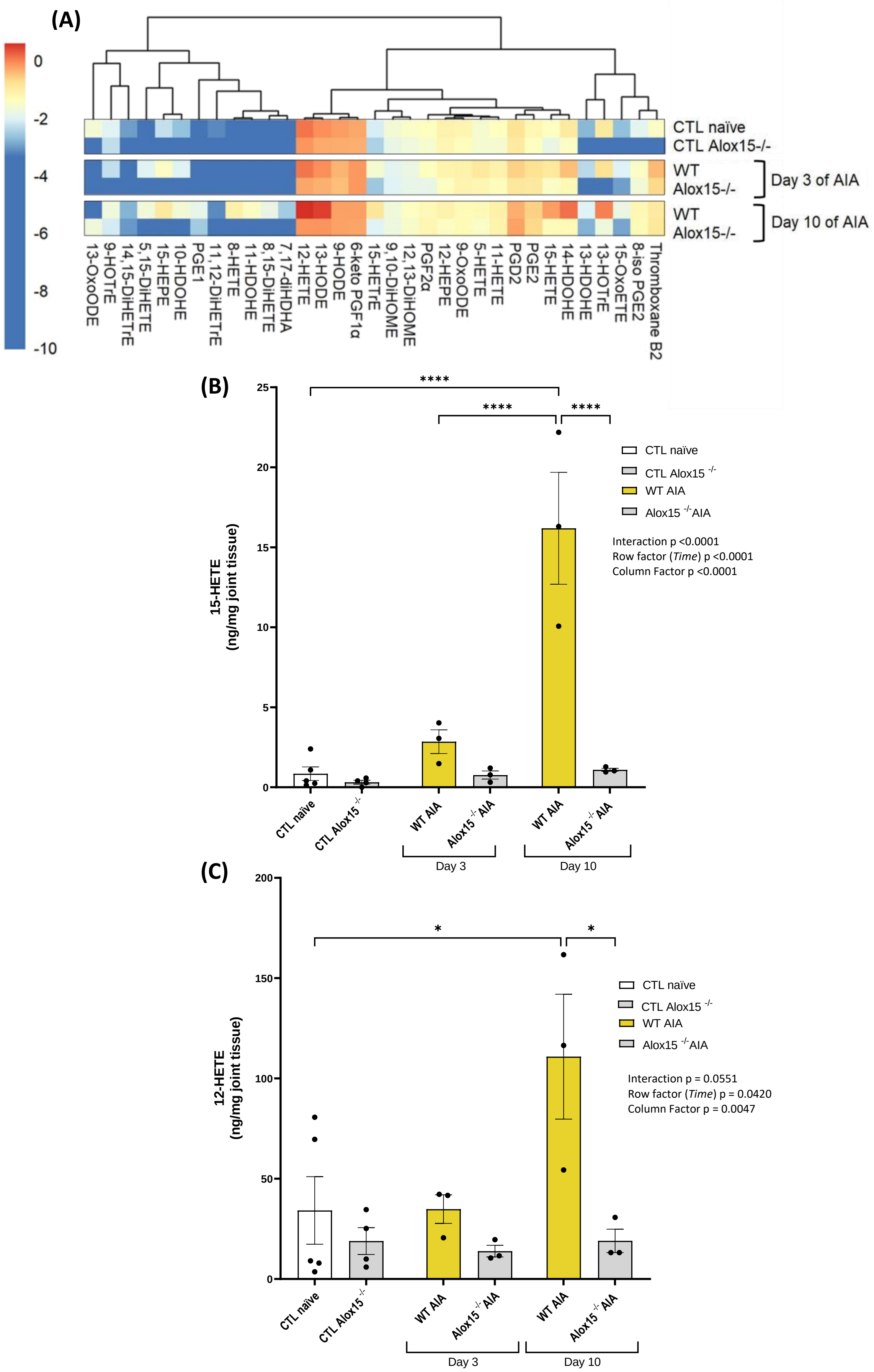

Figure continues into the next page

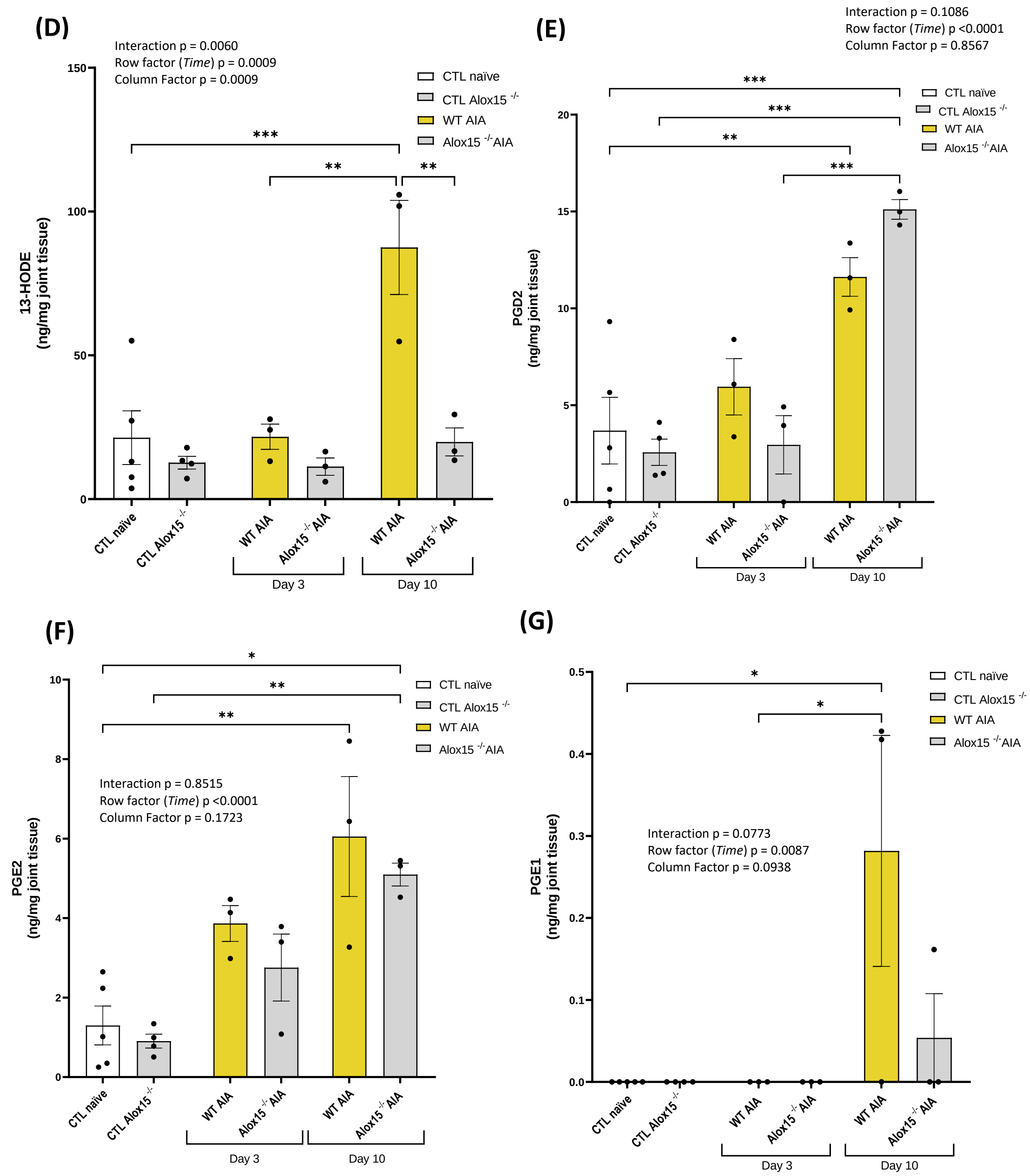

Figure 5.6: *Alox15* deletion alters the joint oxylipin profile on day 10 of AIA development
Antigen-induced arthritis was generated in 8- to 11- week-year-old *WT* and *Alox15*$^{-/-}$ male mice, simultaneously. Joint tissue was collected, and pooled, on day 0 for controls (CTL) (n = 4 - 5), on day 3 (n = 3) and on day 10 (n = 3) of AIA. Pooled joint tissue was analysed through LC/MS/MS. (Panel A) Heatmap shows log10 values for analyte concentration [ng/mg (wet weight)]. Lipids of interest were represented in bar graphs, namely 15-HETE (Panel B), 12-HETE (Panel C), 13-HODE (Panel D), PGD2 (Panel E), PGE2 (Panel F) and PGE1 (Panel G). Data represent mean values ± SEM, along with the respective scatter plot displaying individual values. Data were analysed using the Two-way ANOVA and Tukey's multiple comparisons test (*p < 0.05, **p < 0.01, ***p < 0.001, ****p < 0.0001).

5.3 Discussion

12/15-LOX is expressed mainly in monocytes/macrophages and eosinophils and is responsible for the generation of numerous lipid mediators involved in inflammation. In fact, *Alox15*$^{-/-}$ mice have been previously shown to be protected against atherosclerosis, abdominal aortic aneurysm, and even diabetes [212,258,274]. However, in the case of inflammatory arthritis, specifically AIA, I found that *Alox15*$^{-/-}$ mice develop increased joint swelling and inflammatory synovial infiltration, suggesting a protective response of 12/15-LOX.

Multiple studies have been conducted in arthritis *in vivo* models in order to understand the impact of *Alox15* products. As described in Chapter 1, Section 1.4, both the TNF- α Tg and the K/BxN serum-induced arthritis mice model resulted in a worsening of inflammatory arthritis in *Alox15*$^{-/-}$ mice compared to WT [189]. However, the opposite was described in the adjuvant-induced arthritis model, where the *Alox15*$^{-/-}$ mice developed a reduced paw swelling [89] compared to WT mice.

Despite the AIA model being one of the most commonly used inflammatory arthritis murine models, as well as offering two different time points of disease, early (day 3) and established (day 10) arthritis [193], this model had not been tested in *Alox15*$^{-/-}$ mice. Furthermore, the role of oxPLs, and their impact on inflammation and resolution had not yet been tested in any arthritis model.

In AIA, deletion of *Alox15* appeared to result in a slower resolution of knee swelling. A significant reduction in weight gain was also observed for *Alox15*$^{-/-}$ mice during AIA development. This might be explained by the different progression of inflammation, reflecting an increased burden. In addition, mBSA-specific antibody titres were also measured, however, no significant differences were observed. Resident macrophages expressing *Alox15* were shown to inhibit antigen presentation of apoptotic cells[75]. Nevertheless, mBSA is not an endogenous antigen, and the adaptive immune response appears to remain unaltered upon *Alox15* deletion.

Elevated joint swelling was further confirmed by histology staining, where an increase in synovial infiltration in *Alox15*$^{-/-}$ joints was seen, however, no significant difference was overall observed in the arthritis index. Nevertheless, I previously showed that plasma SAA levels are higher in *Alox15*$^{-/-}$ mice on day 3 of AIA development when compared to WT mice. In fact, SAA plasma levels appear to replicate the joint swelling curve. Furthermore, in the previous Chapter 4, I showed that plasma D-dimer levels were also higher in *Alox15*$^{-/-}$ mice on day 3 of AIA than in WT. This fibrinolysis marker is often used as an activity marker of disease, which further suggests *Alox15*$^{-/-}$ mice develop a heightened inflammatory response to AIA development when compared to WT mice.

Lipidomic data shows that oxPLs are significantly increased in the joint tissue of WT mice on day 10 but not in *Alox15*$^{-/-}$ mice. These results contrast with the previously discussed results of Chapter 4, where the whole blood cells of these mice showed increased levels of HETE-PEs in *Alox15*$^{-/-}$ mice throughout the AIA model. This most likely reflects the fact that blood and synovial tissue have a different cell composition, with a different profile of LOX enzyme expression and therefore, this difference was not unexpected.

Alox15 expression, as well as PLA_2, was been previously described as increased in both RA and OA human joints[183], nevertheless, this is the first time oxPLs have been measured in any arthritis murine models. My data showed that *Alox15* appeared to be responsible for the generation of multiple oxPLs in the joint tissue during the AIA model. An increase in 12-HETE-PEs and 15-HETE-PEs in WT and not in *Alox15*$^{-/-}$ mice during AIA development indicates an enzymatic origin due to oxidation by 15-LOX. This might be a result of monocytes/macrophages since a rise in total macrophages in the WT mice joints during AIA has been described in the literature [275]. Furthermore, the composition of oxPLs measured in *Alox15*$^{-/-}$ mice joints during AIA suggests a non-enzymatic origin, probably generated by ROS, as a consequence of oxidative stress. This is reflected by the relatively similar amounts of the positional isomers, namely 12-, 11-, 15-, 8- and 5-HETE-PEs in *Alox15*$^{-/-}$ mice during AIA development within the synovial tissue. This could be further confirmed by conducting chiral chromatography of oxPLs.

Furthermore, elevated oxPLs levels were found both in whole blood cells, as described in Chapter 3, and in joint tissue in WT mice on day 10 of AIA development. This shows that the AIA model, despite being considered a local inflammatory arthritis model, induces systemic effects similar to the ones observed in human RA.

EoxPLs can regulate immunity. Specifically, 12/15-LOX-derived HETE-PEs, when exposed to resident macrophages, block phagocytosis by inflammatory monocytes, and this can prevent the generation of autoantibodies by B-cells[75]. However, in this study, no difference was observed in mBSA-specific antibody titres between *WT* and *Alox15*$^{-/-}$ mice, which might be due to the non-endogenous nature of mBSA. In addition, oxPLs can induce an anti-oxidative response through the activation of Nuclear factor-erythroid factor 2-related factor 2 (NRF2)[276]. This transcription factor is well known for its function in antioxidant defence, as well as inflammatory responses and autophagic degradation[277]. In fact, NRF2 deficient mice showed a worse arthritis phenotype[278], similar to the phenotype described in *Alox15*$^{-/-}$ mice.

12/15-LOX derived oxylipins, such as 12-HETE,15-HETE, and 13-HODE, are known peroxisome proliferator-activated receptor gamma (PPARγ) ligands. Known as an immune modulator, PPARγ is responsible for regulating macrophage polarization into an anti-inflammatory phenotype, which suppresses cytokine production, including IL-6 and TNFα[279,280]. Furthermore, 12-HETE and 15-HETE can be neuroprotective by activating PPARγ, reducing the expression of IL-1 β and COX-2[281]. In addition, 13-HODE and 15-HETE suppress inflammatory responses in *ex vivo* cartilages by decreasing the production of pro-inflammatory lipids, such as PGE_2[282]. Furthermore, PPARγ activation can decrease leukocyte recruitment [283]. Overall, a deficit in PPARγ ligands, which might explain the increased synovial infiltrate observed in *Alox15*$^{-/-}$ mice during AIA compared to WT.

The reduced levels of 12-HETE, 15-HETE, 13-HODE and oxPLs in mice upon *Alox15*$^{-/-}$ deletion during AIA development, suggest both PPARγ and NRF2 as possible transcriptional pathways involved in the heightened swelling and inflammation during AIA development in *Alox15*$^{-/-}$ mice. Both these transcription factors are upstream promotors for antioxidant genes, such as heme oxygenase-1 and catalase that present anti-oxidative and anti-inflammatory functions [284]. An increase in antioxidant gene expression might lead to reduced inflammation observed in WT mice when compared to *Alox15*$^{-/-}$ during AIA development. However, to confirm this, more studies are necessary. Joint tissue from both WT and *Alox15*$^{-/-}$ mice during AIA development could be analysed for PPARγ and NRF2 activity, using DNA binding immunoassays[285]. Furthermore, cytokine levels, as well as oxidative stress markers, such as heme oxygenase-1, which represent an important antioxidant enzyme [284], could be measured in the systemic circulation and synovium tissue.

Overall, these results suggest that 12/15-LOX products might be responsible for attenuating inflammation in the AIA model. Furthermore, I described for the first time the increased presence of eoxPLs during AIA development, which might have a role in the resolution of inflammation. These findings suggest that eoxPLs, more specifically oxPLs derived from *Alox15,* might have a positive impact on human RA, possibly by stimulating an anti-inflammatory pathway within the joint. However, more studies including the introduction of these lipids during the course of inflammatory arthritis are required to fully understand the benefits of eoxPLs in arthritis. In the next Chapters, immune cells from RA patients and healthy controls will be studied, focusing on oxPLs and their role in coagulation.

Total oxPLs in rheumatoid arthritis patients' blood cells are elevated, resulting in immunological consequences and increase thrombin generation

Chapter 6

6.1 Introduction

Plasma from RA patients displays high levels of molecular markers indicative of thrombin activation along with increased fibrinolysis[142]. As described in Chapter 1, Section 1.3.4, plasma from RA patients displays high levels of TAT complexes [142,146], similar to what was observed in the AIA model described in Chapter 3 of this thesis. Furthermore, human RA displays an elevation of D-dimers both in synovial fluid and in plasma[142,147,148], although this was not reflected in the AIA model. In addition, platelets from RA patients have been described as altered, with a different activation and reactivity state, more specifically an increase in mean platelet count, along with an increased platelet volume[150–152].

Nevertheless, despite all these increased markers, the mechanisms for increased coagulation are unknown. Considering the elevated levels of oxPLs observed in the AIA model, as shown in the previous chapters, I propose that the PL membrane composition may play an important role in coagulation in human RA. This idea will be tested in this Chapter using blood cells, namely platelets and white blood cells (WBCs), as well as extracellular vesicles enriched plasma (EVs), from an RA clinical cohort. The process of thrombin generation requires the assembly of the prothrombinase complex on the negatively charged PL surface of activated platelets or WBCs or even EVs.[286]

Platelets and white blood cells were chosen considering they are possessing a lipid membrane where this assembly might take place. Furthermore, as cell-derived membranous structures, EVs were also analysed. EVs include exosomes, apoptotic bodies and microvesicles, which can be shed from the plasma membrane of different cells. This results in a highly heterogeneous composition [287,288]. Nevertheless, EVs own a lipid membrane where the assembly of coagulation factors might take place.

The process of thrombin generation requires the assembly of the prothrombinase complex on the negatively charged PL surface of activated platelets or blood cells or even extracellular vesicles.[286] The influence of these different membranes on this process is not very well understood, and the number of EVs changes in disease.[287], including RA[289], so their relative contribution may vary. Therefore, it is imperative to understand whether these lipid membranes contribute to the increased thrombosis seen in arthritis. The prothrombinase assay measures thrombin generated by cell membranes, namely platelets and WBCs, along with EVs, independently from coagulation factors, inhibitors, and tissue factor expression.

In RA, EVs have been shown not only to be altered, with increased TNF-α and citrullinated proteins, as well as present in heightened numbers. This increase in EVs numbers originate from the different cell types present in the synovial fluid of these patients, and can form immune complexes, which increases inflammation[290,291]. Furthermore, increased EVs in RA patients have been associated with coagulation activation [292], however, the role of oxPLs in this increased coagulation has never been studied.

Here, I will analyse blood cells from patients recruited from the *Cardiff Regional Experimental Arthritis Treatment and Evaluation Centre* clinical cohort using the prothrombinase assay, to determine the procoagulant potential of platelets, white blood cells (WBC) and EVs, as described in chapter 2, in section 2.2.25. Due to the limitation within of laboratory facility, namely an absence of an ultracentrifuge, EVs were obtained as plasma-enriched EVs as described in Chapter 2, Section 2.2.23.

EoxPLs can be generated by cells, including platelets, monocytes and neutrophils[5,68]. Both eoxPLs and oxPLs, as described in Chapter 1, Section 1.2.4, can enhance the binding of coagulation factors to membranes, therefore contributing to blood clotting[5] (Figure 1.6). Therefore, I will also analyse oxPL levels in platelets, WBC and EVs from RA patients and healthy controls.

In addition, I will analyse whether RA patients have experienced an immune response to these lipids, as previously shown in anti-phospholipid syndrome[125]. Despite being an auto-immune disease and exhibiting a raised level of auto-antibodies against phospholipids such as cardiolipin [293], the immune response of these patients against oxPLs has never been analysed. Osteoarthritis, as previously described in Chapter 1, Section 1.3.1, is often considered a non-auto-immune disease, which shows a low percentage of circulating autoantibodies against rheumatoid factor and CCP, contrary to RA. Therefore, it will be considered a control for immunological recognition of HETE-PLs, along with a group of healthy volunteers.

6.1.1 Aims

The aims of this chapter are to:

- Analyse the procoagulant potential of platelets, WBCs and EVs from blood from RA patients and healthy volunteers.
- Characterize and compare HETE-PL levels in platelets and WBCs from blood from RA patients and healthy volunteers both basally and following *in vitro* activation.
- Characterise HETE-PL composition in EVs from RA patients and healthy controls.
- Investigate the presence of autoantibodies against HETE-PLs in plasma from RA and OA patients, using the *Early Arthritis Cohort* from Leiden Medical Center, and healthy volunteers from Cardiff, through the *Study of autoantibodies against lipids relevant in coagulation.*

6.2 Results

6.2.1 Participant baseline characteristics of the Cardiff cohort

The *Cardiff Regional Experimental Arthritis Treatment and Evaluation Centre* clinical cohort involved fifty participants, recruited over a period of 26 months, totalling 25 healthy controls (HC) and 26 RA patients. The mean age of patients was 61 ± 16.5 SD years, with 88 % females while the mean age for healthy controls was 51 ± 8.7 SD, with an overall higher proportion of females (84 %). Disease score activity (DAS) was evaluated using the DAS28 score system. This clinical assessment of RA disease activity can be calculated based on tender joint count (TJC) and swollen joint count (SJC) of 28 specific joints, along with overall health assessment of the patient and serum inflammatory markers, which in this particular case was calculated using CRP values. The mean DAS28 of RA patients was 2.68 ± 1.45, indicating a low disease activity[294]. The baseline clinical characteristics of all participants are shown in Table 6.1.

Exclusion criteria for healthy individuals were a history of arterial or venous thrombosis, any other chronic inflammatory diseases or auto-immune diseases such as RA, SLE, diabetes, high cholesterol, abnormal renal or liver function, or other diseases that may conflict with the study parameters. Healthy volunteers were instructed to not ingest aspirin, non-steroidal anti-inflammatory drugs, or any other medication, such as paracetamol, in the 14 days preceding blood collection. Since RA is a cardiovascular risk factor, differences in baseline cardiovascular risk were expected as a study limitation, as well as the usage of aspirin (8 % of RA patients) and other NSAIDs (Naproxen: 30 % and Ibuprofen: 3 % of RA patients). No patients were taking paracetamol.

Variable	Healthy control (HC) [n=25]	Rheumatoid Arthritis (RA) [n=26]	p
Age, Mean ± SD	51.69 ± 8.74	61.08 ± 16.51	0.0066 (b)
Female gender	21 (84%)	23 (88%)	0.6514 (a)
DAS28 mean ± SD	–	2.68 ± 1.45	–
Disease duration (years), Mean ± SD	–	7.58 ± 8.43	–
Rheumatoid Factor (+)	–	60%	–
Anti-CCP (+)	–	64%	–
Erythrocyte sedimentation rate (mm/hour ± SD)	-	14.12 ± 12.9	-
CRP (mg/L, Mean ± SD)	-	4.8 ± 7.37	-
Aspirin use	0	8%	–
NSAIDs use	0	30%	–
Smoker	0		–
Osteoarthritis	0	23%	–
Hypertension	0	19%	–
Diabetes	0	0	–
Hypothyroidism	0	12%	–
Statin use	0	0	–

Table 6.1: Baseline clinical characteristics of recruited volunteers in the clinical cohort (CCP: Cyclic Citrullinated Peptide, CRP: c-reactive protein, DAS: disease score activity, p-value tests: Fisher exact for categorical (a) or student's t-test for continuous variables (b))

6.2.2 Rheumatoid arthritis patients have an increased platelet count but no change in white blood cell numbers.

Washed platelets, EVs and WBC were isolated from patients and controls as outlined in Chapter 2, section 2.2.22, 2.2.23 and 2.2.24, respectively. As previously mentioned, EVs were studied as plasma-enriched EV, therefore, EV count was possible due to the isolation protocol used. Furthermore, purity analysis was also not possible. This represents a limitation of this study. A total of 6 ml of plasma from each sample was used to obtain an EV-enriched plasma, which was not purified or counted. Isolated platelets and WBCs were counted, and numbers were standardised in the assay to match the normal concentration present in healthy humans. Specifically, platelets were resuspended at 2 x 10^8 cells/ml, while WBCs were resuspended at 4 x 10^6 cells/ml.

During the platelet isolation protocol, platelet clumping occurred in four healthy controls and one RA patient, which prevented the correct counting of these cells. This can occur for a multitude of reasons, from pre-analytic errors, and delay between collection and analyses, to possible infections[295]. Nevertheless, WBC and EVs samples were still analysed, and therefore, these samples were not excluded from the cohort, contrary to the platelet samples. Based on the yield of cells obtained, platelet numbers from RA patients were 1.21-fold higher than healthy controls (Figure 6.1.A). The fold change was calculated using the ratio between the median of the platelet number of RA patients and the median of the platelet number of healthy controls.

In the case of WBC, no significant difference was found between RA patients and healthy controls (Figure 6.1.B).

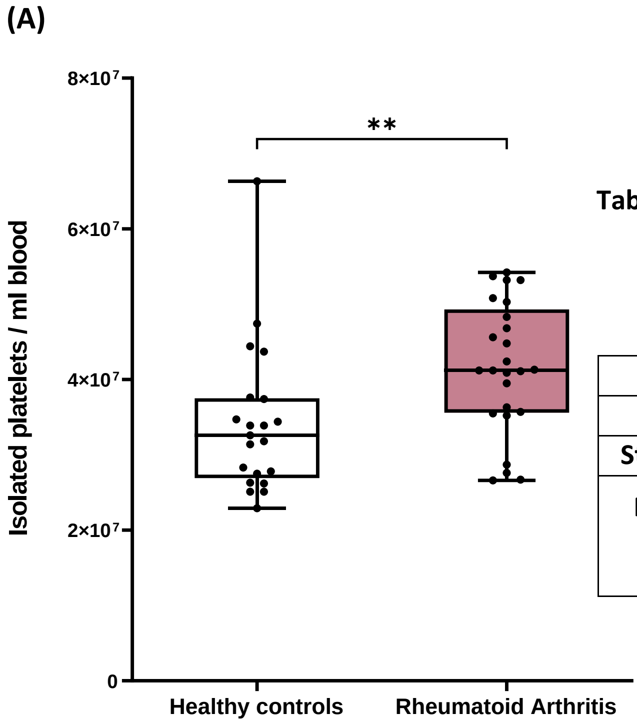

Table 6.2. Descriptive statistic of Figure 6.1.A

	Healthy controls	Rheumatoid arthritis
Mean	3.4×10^7	4.1×10^7
Median	3.2×10^7	4.1×10^7
Std. Deviation	9.9×10^6	8.6×10^6
Fold change (According to median)	1.21-fold change 21% increase in RA ($p = 0.0097$)	

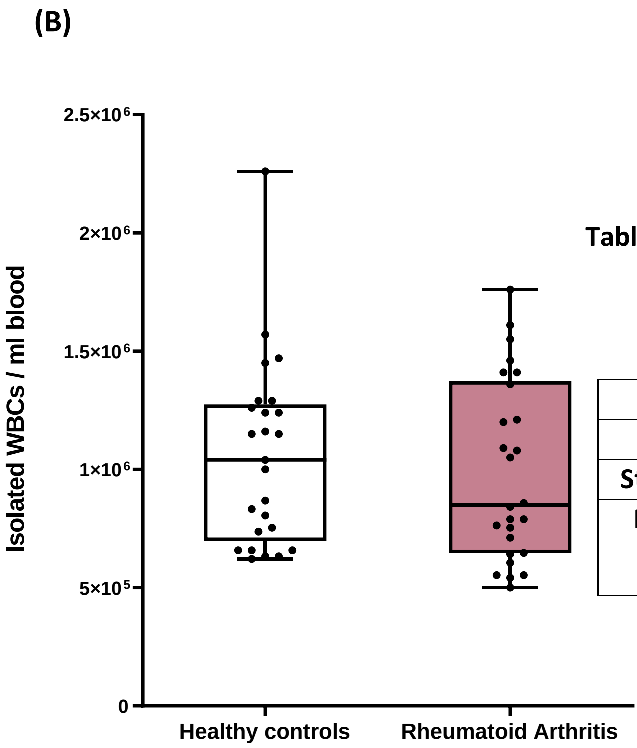

Table 6.3. Descriptive statistic of Figure 6.1.B

	Healthy controls	Rheumatoid arthritis
Mean	1.05×10^6	9.8×10^6
Median	1.04×10^6	8.5×10^6
Std. Deviation	3.9×10^5	3.8×10^5
Fold change (According to median)	Non-significant ($p = 0.5218$)	

Figure 6.1: Platelet count is significantly elevated in blood from patients with rheumatoid arthritis

Platelets (Panel A) and white blood cells (Panel B) were isolated, as described in Methods, from healthy controls (n = 21 for Panel A and n = 25 for Panel B) and RA patients (n = 25 for Panel A and n = 26 for Panel B). Isolated cells were counted and calculated back to give the equivalent of 1 ml of blood. A table with descriptive statistic of each graph was also provided next to each graph. Data was analysed using Mann-Whitney test (** $p < 0.0001$).

6.2.3 Extracellular vesicles, but not platelets or white blood cells, from RA patients, support higher thrombin generation.

Thrombin generation was measured by adapting previously described chromogenic prothrombinase assays[209,210]. In the presence of the PL surface provided by platelets, WBC or EVs, a mixture of purified FXa, FVa, FII and Ca^{2+} was added and thrombin was generated. Thrombin generation was quantified through a chromogenic assay, using a standard curve of human thrombin with amounts between 3 nM to 400 nM.

No difference was observed between RA patients and healthy controls, for either platelets or WBCs (Figure 6.2.A-B). For this assay, thrombin generation was performed in standardized cell numbers. However, I noted that platelet numbers are 21 % higher for RA patients (Figure 6.1.A). Thus, in RA this significantly higher circulating platelet count could theoretically lead to greater availability of platelet membranes for thrombin generation, and therefore, contribute to the elevated thrombotic risk seen in RA.

In the case of EVs, significantly higher levels of thrombin generation were observed in RA patient samples, compared to those from healthy controls, displaying a 1.28-fold increase (Figure 6.2.C). However, contrary to platelets and WBC, EV count was not performed, therefore EV numbers are not known. Instead, each analysed sample represents the total amount of EV isolated from 6 ml of plasma from each volunteer.

Thus, considering the description in the literature that RA patients' blood has higher EV counts[296], then this could explain the higher thrombin generation observed. Regardless of the mechanism, my data show that circulating EV membranes in RA plasma can promote higher levels of thrombin generation, and thus they could direct contribute to the increased thrombosis risk experienced by these patients.

(A)

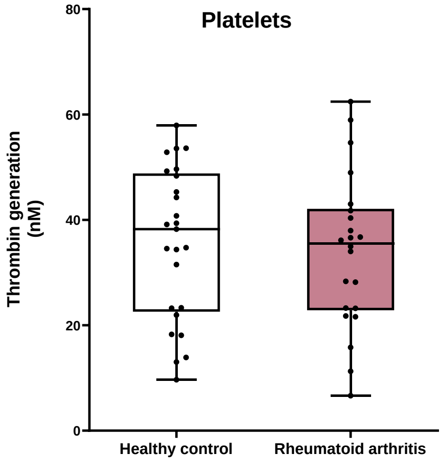

Table 6.4. Descriptive statistic of Figure 6.2.A.

	Healthy controls	Rheumatoid arthritis
Mean	35.56	34.31
Median	38.24	36.14
Std. Deviation	14.42	14.41
Fold change (According to median)	Non-significant (p = 0.7668)	

(B)

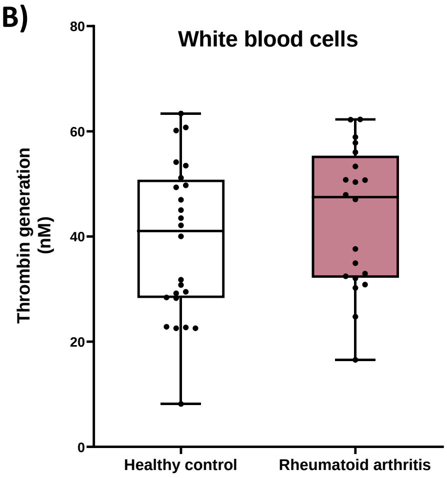

Table 6.5. Descriptive statistic of Figure 6.2.B.

	Healthy controls	Rheumatoid arthritis
Mean	39.02	43.48
Median	41.06	47.49
Std. Deviation	14.75	13.51
Fold change (According to median)	Non-significant (p = 0.3050)	

(C)

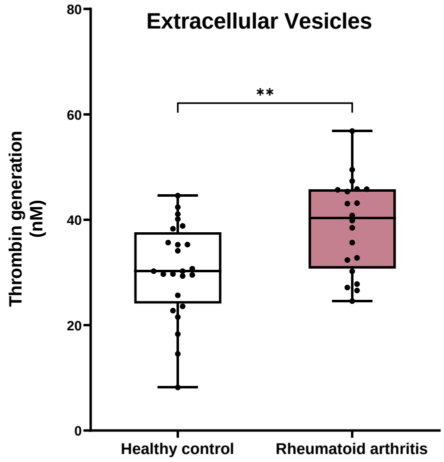

Table 6.6. Descriptive statistic of Figure 6.2.C.

	Healthy controls	Rheumatoid arthritis
Mean	30.26	40.81
Median	30.40	39.09
Std. Deviation	8.7	9.0
Fold change (According to median)	1.28-fold change 28% increase in RA (p = 0.0021)	

Figure 6.2: Extracellular vesicles but not platelets or white blood cells from RA patients generate higher amounts of thrombin than healthy controls in an *in vitro* prothrombinase assay

The ability of platelets (Panel A), WBC (Panel B), and EV (Panel C) membranes to support coagulation reactions was assessed using the prothrombinase assay, as described in Methods, between healthy controls (n = 20) and RA patients (n = 24). A table of descriptive statistic of each graph was also provided next to each graph. Data were analysed using the student's t-test (** $p < 0.001$).

6.2.4 Activated platelets from RA patients have similar levels of HETE-PL to control basally but generate less upon thrombin activation

First, HETE-PLs were quantified in both resting and thrombin-activated platelets, obtained from patients enrolled in the *Cardiff Regional Experimental Arthritis Treatment and Evaluation Centre* cohort described previously in this Chapter, Section 6.2.1.

Washed platelets were isolated, counted, and resuspended at 2 x 10^8 cells/ml, followed by lipid extraction and analysis using LC/MS/MS, as described in section 2.2.28. Platelets were either analysed basally or following activation using 0.2 U/ml thrombin, at 37 °C, in the presence of 1 mM calcium.

As described in Chapter 1, Section 1.1.1, phospholipids have different fatty acids in the *sn1* position linked by either acyl (a), alkyl ether or plasmalogen (p) bonds[9]. Therefore, firstly, the different HETE-PLs species were analysed, and oxPLs with different *sn1* compositions were compared. The most abundant HETE-PLs measured were 18:0a_12-HETE-PC, 18:0a_12-HETE-PE (stearic acid on the *sn1* position with an acyl bond) and 16:0a_12-HETE-PC (palmitic acid on the *sn1* position with an acyl bond), although many others were also detected in lower amounts (Figure 6.3.A). This is consistent with low levels of 12-LOX activity basally. No statistical testing was displayed in the heatmaps of this Chapter. The statistical analysis was performed as described in Chapter 2, Section 2.2.36, where the amount of HETE-PLs positional isomers was analysed.

As the data was not normally distributed, and I was testing for statistical differences between healthy controls and RA for each positional isomer of HETE-PLs, Mann-Whitney test was performed for each individual lipid. This procedure can also be termed multiple Mann-Whitney tests. Nevertheless, resting platelets did not exhibit significant differences between RA patients and healthy controls when analysing the different HETE-PLs isomers in resting platelets (Figure 6.3.B).

Thrombin is one of the most efficient and physiological activators of platelets [297]. Upon activation, calcium is released within the platelet, which activates phospholipase A2, therefore releasing increased levels of AA. The increase of AA is utilized by platelet COX-1, generating increased levels of oxylipins, including thromboxane A_2, which further induces platelet activation and aggregation [298]. Thrombin stimulated platelets also generate HETE-PL. Along with several 12-HETE-PLs, both 11- and 15-HETE-PLs were also detected. As described in Chapter 1, Section 1.1.4, both COX-1 and COX-2, generate 11- and 15-HETE-PE, however considering that COX-1 is the main isoform present in platelets, the generation of these isoforms is most likely via COX-1.

RA patients' platelets generated lower levels of HETE-PLs than platelets from healthy volunteers upon thrombin activation. (Figure 6.4). This was significant for 5-, 15- and 11-HETE-PLs, as well as in the total sum of all HETE-PLs. For 15- and 11-HETE-PLs, this difference could potentially be explained by NSAIDs usage by 30% of RA patients in the cohort, since NSAIDs will inhibit COX-1 in platelets (Table 6.1). This idea will be tested in the next section.

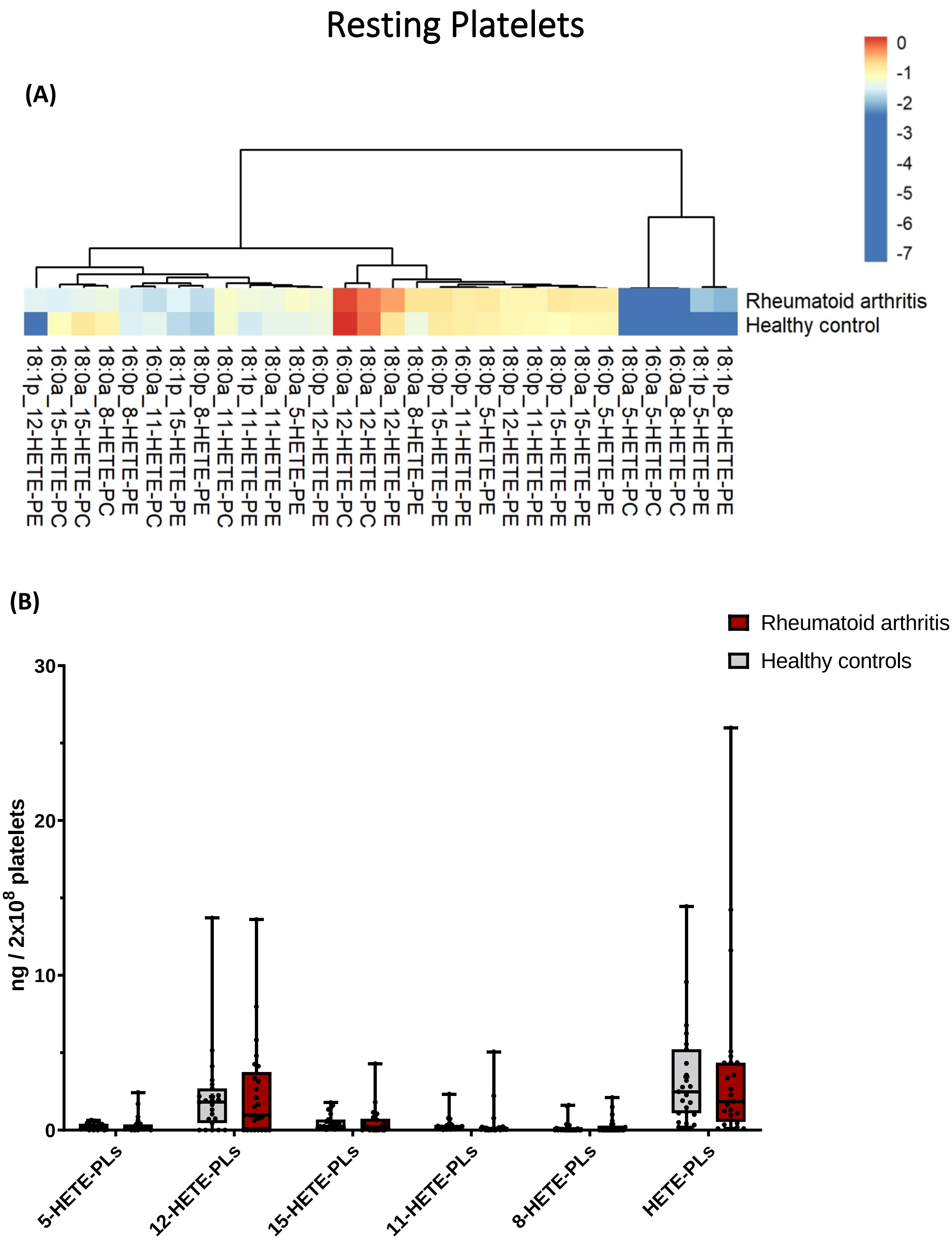

Figure 6.3: Resting platelets from RA and healthy controls contain similar levels of HETE-PLs
Washed platelets from RA patients (n = 25) and healthy controls (n = 23) were isolated as described in Methods, and eoxPLs were analysed by LC/MS/MS. (Panel A) Heatmap shows log10 values for analyte amount (ng/2x10^8 platelets). (Panel B) The sum of all the quantified HETE-PLs isomers (ng/2x10^8 platelets) was calculated. Data were analysed using the multiple Mann-Whitney test.

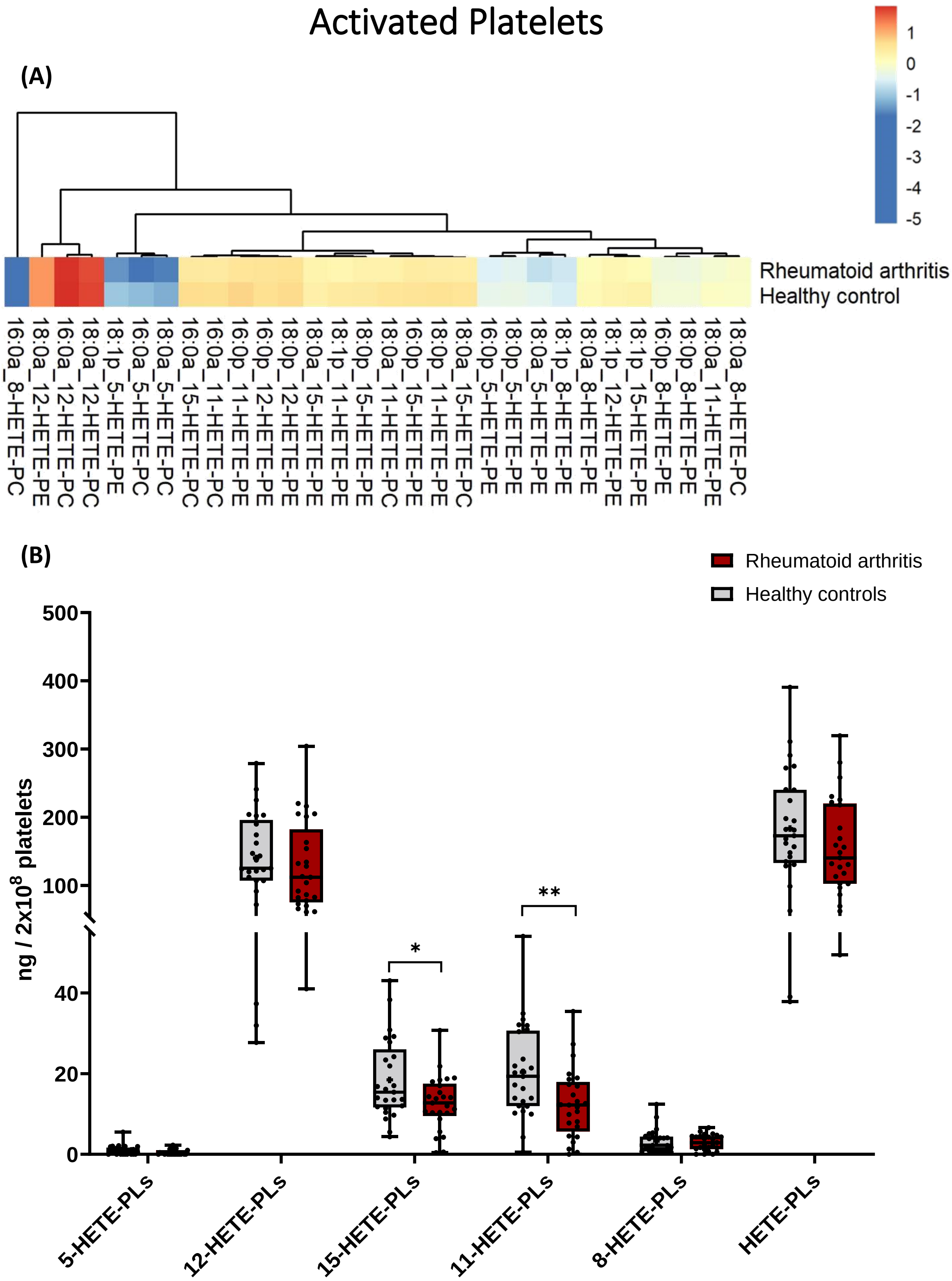

Figure 6.4: Activated platelets from RA patients generate less HETE-PLs than healthy controls

Washed platelets from RA patients (n = 25) and healthy controls (n = 25) were isolated and activated with 0.2 U/ml thrombin and 1 mM $CaCl_2$, as described in Methods. OxPLs were analysed by LC/MS/MS. (Panel A) Heatmap shows log10 values for analyte amount (ng/$2x10^8$ platelets). (Panel B) The sum of all the quantified HETE-PLs isomers (ng/$2x10^8$ platelets) was calculated. Data were analysed using the multiple Mann-Whitney test (* p<0.05, **p<0.01, ***p<0.001).

6.2.4 Reduced generation of HETE-PLs by activated platelets of RA patients may be partially due to NSAID administration

Many patients with RA are routinely taking aspirin or other NSAIDs for their anti-inflammatory effects. However, these drugs are also known for their antithrombotic proprieties, which derives from inactivating COX-1. For instance, aspirin, permanently inactivates COX-1, inhibiting the formation of thromboxane A_2, preventing platelet aggregation, a vital step in thrombosis [299]. However, the impact of NSAIDs in eoxPLs generation, and respective consequences in coagulation, is not very well known. Therefore, to understand whether this impacts eoxPL generation, I next compared levels of these lipids with those on or off this class of drugs.

Here, patients were taking aspirin (n = 2), Ibuprofen (n = 1), and naproxen (n = 8), all nonselective COX inhibitors, blocking both COX-1 and COX-2, depending on the dose. Paracetamol also inhibits COX, however, it is generally not considered an NSAID as it does not share the same anti-inflammatory properties [300]. Nevertheless, no patient or healthy volunteer was taking paracetamol at the time of the blood draw.

Generation of 11-HETE-PLs was significantly reduced in RA platelets from patients using NSAIDs, however, a non-significant reduction was also observed in RA platelets from patients not using NSAIDs (Figure 6.5). The same trend was observed for 15-HETE-PLs, without reaching statistical significance. These differences were not observed in total HETE-PLs, since the overall high abundance of 12-HETE-PLs masked the reduction when measuring the total amounts.

This suggests that NSAIDs partially dampen the production of 15- and 11-HETE-PLs in thrombin-activated platelets of RA patients, and another mechanism must also be involved.

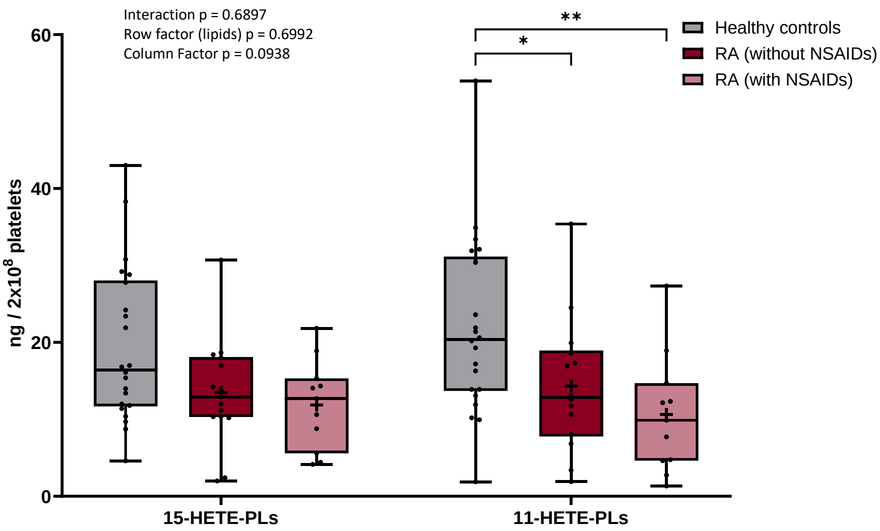

Figure 6.5: NSAIDs usage by RA patients is partially responsible for the reduced generation of 15- and 11-HETE-PLs in activated platelets

Washed platelets from RA patients taking NSAIDs (n = 11), and without (n = 14), along with healthy controls (n = 25) were isolated and activated with 0.2 U/ml thrombin and 1 mM $CaCl_2$, as described in Methods. OxPLs were analysed by LC/MS/MS. The sum of all quantified HETE-PLs isomers (ng/2x10^8 platelets) was calculated. Data were analysed using the two-way ANOVA test (* p<0.05, **p<0.01).

6.2.5 Elevated HETE-PLs are detected in resting white blood cells in RA patients compared to healthy volunteers

Next WBCs were isolated as described in Chapter 2, Section 2.2.24, and HETE-PLs were analysed either in a resting state or following activation using 10 µM Ca^{2+} Ionophore A23187 and 1 mM $CaCl_2$.

Once again, a heatmap was generated with the analysed oxPLs species (Figure 6.6.A). Few HETE-PLs were detected in resting WBC, with 16:0a_8-HETE-PC the most abundant, followed by a low amount of 15-HETE-PLs.

The data was not normally distributed, so multiple Mann-Whitney tests were performed. This confirmed that 15-HETE-PLs were significantly increased in RA patients compared to healthy controls (Figure 6.6.B), with 18:0a_15-HETE-PC, 16:0a_15-HETE-PC and 18:0a_15-HETE-PE, driving this elevation.

Upon ionophore activation, HETE-PL levels dramatically increased (Figure 6.7.A), with 5-, 15- and 12-HETE-PLs detected in high amounts (Figure 6.7.B). This is consistent with 5-LOX and 15-LOX present in different WBC populations. However, the increase in 12-HETE-PLs was unexpected and suggests the presence of some contaminating platelets. No difference was observed in oxPL levels between activated WBC from RA patients versus healthy controls.

Overall, very low levels of HETE-PLs were detected basally in WBCs, with only 15-HETE-PLs levels slightly increased in WBCs from RA patients, compared to healthy controls. However, the high level of variation in the data prevents making strong conclusions. No other significant differences were found for HETE-PL levels, in either resting or activated states.

HETE-PL levels were below the limit of detection in EVs isolated from either RA patients or healthy volunteers.

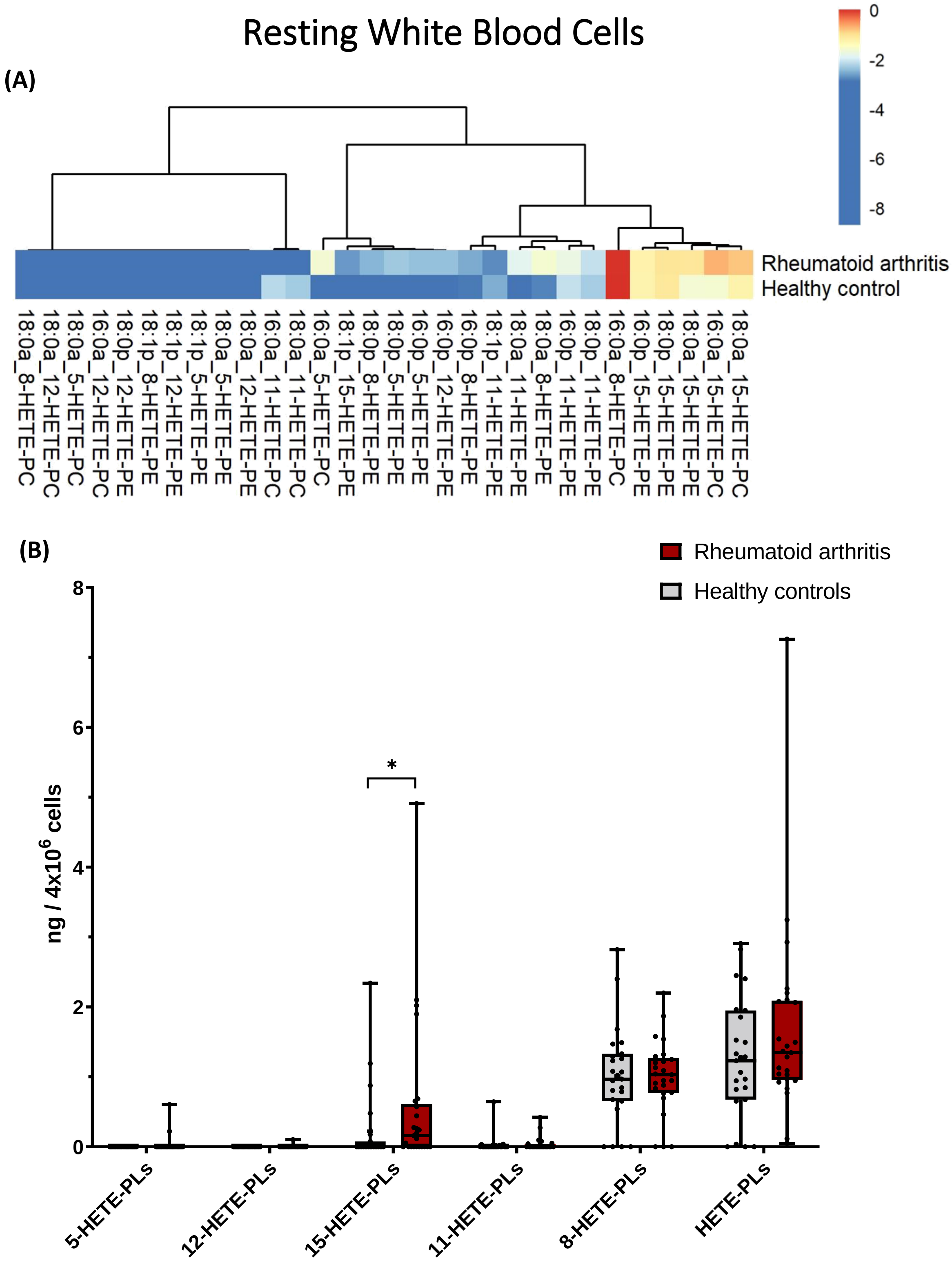

Figure 6.6: Only 15-HETE-PLs were elevated in resting WBCs of RA patients compared to healthy controls

Resting WBCs from RA patients (n = 25) and healthy controls (n = 25) were isolated as described in Methods, and oxPLs were analysed by LC/MS/MS. (Panel A) Heatmap shows log10 values for analyte amount (ng/4x10^6 WBCs). (Panel B) The sum of all the HETE-PLs isomers (ng/4x10^6 WBCs) was calculated. Data were analysed using the multiple Mann-Whitney test (* p<0.05).

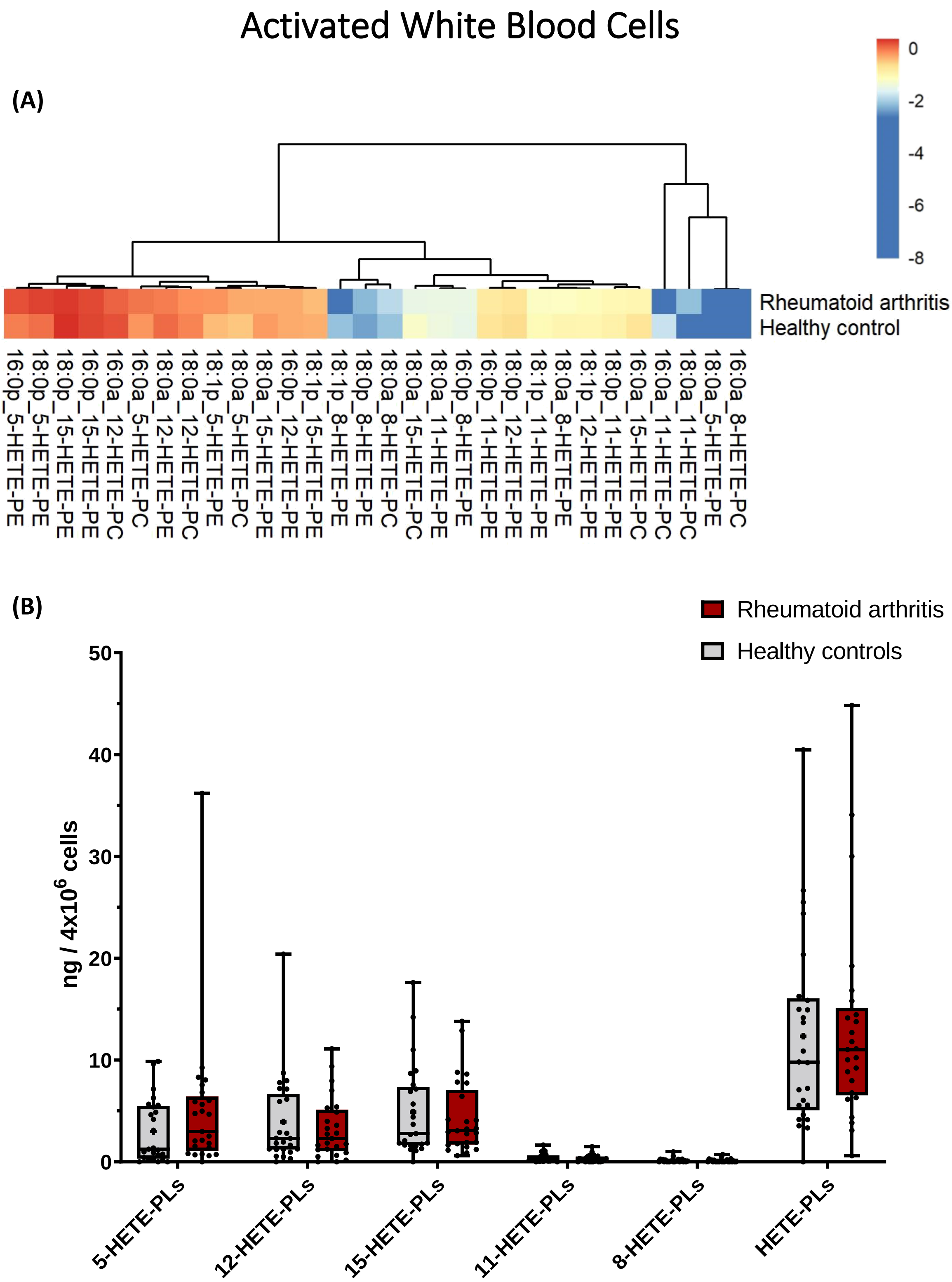

Figure 6.7: No difference in HETE-PLs were observed in activated WBC between RA and healthy controls.

Activated WBCs from RA patients (n = 25) and healthy controls (n = 25) were isolated as described in Methods, and oxPLs were analysed by LC/MS/MS.(A) Heatmap shows log10 values for analyte amount (ng/4x10^6 WBCs). (B) The sum of all the HETE-PLs isomers (ng/4x10^6 WBCs) was calculated. Data were analysed using the multiple Mann-Whitney test.

6.2.4 Participant baseline characteristics of Leiden cohort, plus healthy volunteers from Cardiff.

Next, I analysed the immunological response against oxPLs, by evaluating IgG responses against individual HETE-PLs positional isomers. For this, serum samples from the *Early Arthritis Cohort* Biobank, Leiden University Medical Centre (n =25 OA, 25 RA) were sent to Cardiff on dry ice. Since this cohort did not include healthy volunteers, I next recruited 8 healthy controls from Cardiff under the *Study of autoantibodies against lipids relevant in coagulation.*

Both clinical groups from the *Early Arthritis Cohort* were age, and gender-matched, with an average age of 59 ± 11 (mean ± SD) years for OA and 57 ± 10 (mean ± SD) years for RA patients, and a higher proportion of females, which represented 72 % and 60 % of OA and RA patients recruited, respectively. The DAS28 -ESR, as a clinical assessment of RA patient, shows an average value higher than 3.2, therefore indicative of a disease with moderate activity[294]. DAS28 -ESR was calculated based on 3 variables, erythrocyte sedimentation rate (ESR), tender joint count (TJC) and swollen joint count (SJC) of 28 specific joints, using the following formula:

Equation 2: DAS28-ESR formula

$$DAS28 - ESR = \left[\left(0.56 \times \sqrt{TJC}\right) + \left(0.28 \times \sqrt{SJC}\right) + (0.70 \ln ERS)\right] \times 1.08 + 0.16$$

As expected, RA patients displayed a higher DAS28-ESR score than OA patients, reflecting the high inflammatory nature of RA [301]. For the evaluation of IgG reactivity against HETE-PCs, only this clinical cohort was used, analysing RA serum, and comparing it to OA samples, which represent an immunological control.

Healthy controls from the *Study of autoantibodies against lipids relevant in coagulation*, were age- and gender-matched to the clinical groups, with an average of 51 ± 7 (mean ± SD) years, and 75 % of females. These samples were used to test IgG reactivity against HETE-PEs, in addition to the clinical cohort samples, consisting of both RA and OA patients.

Healthy individuals were excluded if they had a history of arterial or venous thrombosis, as well as any other chronic inflammatory diseases or auto-immune diseases such as RA, SLE, diabetes, high cholesterol, and abnormal renal or liver function. Plus, healthy volunteers did not intake aspirin, non-steroidal anti-inflammatory drugs, or any other medication, such as paracetamol, in the 14 days preceding the blood collection. The baseline clinical characteristics of all participants of the clinical cohort are presented in (Table 6.2).

Variable	Healthy control (HC) [n=8]	Osteoarthritis (OA) [n=25]	Rheumatoid Arthritis (RA) [n=25]	p
Age, Mean ± SD	51.2 ± 6.81	59.3 ± 11.23	57.5 ± 9.81	0.1269 (b)
Female gender	6 (75%)	18 (72%)	15 (60%)	0.5854 (a)
Disease duration (years), Mean ± SD	–	1.17 ± 0.37	1.03 ± 0.25	0.1177 (c)
DAS28- ESR, means ± SD	–	3.61 ± 1.08	4.47 ± 1.095	0.0089 (b)
Rheumatoid Factor (+)	–	16%	84%	<0.0001 (a)
Anti-CCP (+)	–	4%	100%	<0.0001 (a)
CRP (mg/L, Mean ± SD)	–	10.24 ± 18.52	12.61 ± 11.95	0.5924 (b)
Creatinine (µmol/L, Mean ± SD)	–	75.58 ± 22.17	65.88 ± 9.24	0.0497 (b)
Haemoglobin (g/dL, Mean ± SD)	–	8.433 ± 1.083	8.276 ± 0.7907	0.5631 (b)
WCC (x 10^9/L, Mean ± SD)	–	7.542 ± 2.395	8.040 ± 2.071	0.4393 (b)
Smokers (former smokers)	13% (0)	36% (24%)	36% (40%)	0.4351 (a)

Table 6.7: Baseline clinical characteristics of participants in the immunological clinical cohort
Data from RA and OA patients were provided by Leiden University Medical Centre.
(WCC: white cell count, ESR: Erythrocyte sedimentation rate, SD: standard deviation, p-value tests: (a) Chi-square test for categorical and (b) ANOVA test or Mann-Whitney (c) for continuous variables)

6.2.5 Rheumatoid Arthritis patients display an autoimmune response against oxPL.

Here, I analysed whether oxPLs are recognised by circulating autoantibodies in RA serum. For this, I evaluated the IgG reactivity towards the different positional isomers, including both PE and PC phospholipids. First, I generated, isolated and purified different HETE-PLs positional isomers, as described in Chapter 2, Section 2.2.26. These were generated from 1-Stearoyl-2-arachidonoyl-phosphatidylethanolamine (SAPE) and -phosphatidylserine (SAPS), which will be used as non-oxidized phospholipid controls. The purity of each positional isomer was confirmed through a Q1 ion scan, while the identity of the isolated HETE-PLs isomers was confirmed through an enhanced product ion (EPI) scan by monitoring the precursor ion to product ion transitions (Table 2.5). This, along with the use of blocker buffer during the ELISA, ensures antibody specificity for each HETE-PLs positional isomer.

HETE-PL autoantibody titres were then determined by chemiluminescent ELISA assay as previously described.[125] Firstly, I tested 18:0a_HETE-PCs positional isomers, namely, using serum from RA and OA patients in a chemiluminescent ELISA assay, as described in Section 2.2.21. The initial experimental design used samples from OA, a non-autoimmune arthritic disease, as an immunological control for RA when analysing IgG reactivity. Consequently, in this experiment, no healthy controls were analysed for HETE-PCs IgG recognition. As controls for HETE-PC IgG reactivity towards unoxidized PCs, I also included SAPC (PC 18:0_20:4) as a control non-oxidised lipid.

A two-way ANOVA test was used, since both oxidised and non-oxidised, along with OA and RA conditions were compared. No significant interaction in IgG reactivity towards the 12- (interaction $p = 0.4921$), 11- (interaction $p = 0.2174$), 15- (interaction $p = 0.9134$), 8- (interaction $p = 0.2652$) and 5-HETE-PCs (interaction $p = 0.0746$) was observed between OA and RA patients (Figure 6.8). However, IgG reactivity towards 11- and 5-HETE-PCs was found significantly altered (row factor $p = 0.0063$ and row factor $p = 0.0003$, respectively) when analysing oxidised versus non-oxidised lipids. Upon Tuke’s multiple comparison test, a significant increase was found in both 11- and 5-HETE-PCs when compared to reactivity towards SAPC (non-oxidised PLs) in RA serum (Figure 6.8.B and E). In the case of OA, a similar results significant difference was observed (column factor p = 0.0010), with a significant increase found for IgG levels against 8-HETE-PCs (Figure 6.8.D). This was unexpected given the non-auto-immune nature of OA. Nevertheless, it is not uncommon to find auto-antibodies in OA. In fact, as described in Table 6.2, 16 % of OA patients were Rheumatoid factor positive (RF +), while 4 % displayed auto-antibodies against the cyclic citrullinated peptide (anti-CCP +). Therefore, healthy volunteers' serum would represent a better control compared to OA patients. However, the *Early Arthritis Cohort* Biobank, Leiden University Medical Centre did not include healthy volunteers, therefore, healthy controls were recruited at Cardiff. Unfortunately, healthy control sera could not be analysed for IgG reactivity towards HETE-PCs positional isomers since I had recruited these volunteers after the HETE-PC IgG reactivity analysis had already been completed. The geographic difference between arthritis patients and healthy controls represents a limitation of this study.

After the recruitment of healthy controls, I analysed IgG reactivity towards HETE-PEs positional isomers, in RA, OA and healthy control serum. The two-way ANOVA tests were used, where once again no significant interactions were found in IgG reactivity towards the 12- (interaction p = 0.4205), 11- (interaction p = 0.3824),15- (interaction p = 0.2173), 8- (interaction p = 0.4385) and 5-HETE-PEs (interaction p = 0.6944) was observed between healthy controls, OA and RA patients (Figure 6.8). However, significant differences were found between 12- (row factor p<0.0001), 11- (row factor p < 0.0001),15- (row factor p <0.0001), 8- (row factor p <0.0001) and 5-HETE-PEs (row factor p = 0.0065) and non-oxidised PEs (SAPE). Upon Tukey's multiple comparison test, both 12- and 8-HETE-PEs displayed significantly higher IgG recognition in RA serum than in healthy controls (Figure 6.9.A-B). This increase was also present in RA patients when compared to OA, despite the difference not being statistically significant. In addition, the IgG response towards HETE-PEs was stronger than towards SAPE (PE 18:0_20:4) in both OA and RA patients. This elevated IgG response toward the oxPLs compared to the native PE was also observed in OA and RA patients for 11-, 8- and 15-HETE-PEs, but not for 5-HETE-PEs, where no statistical difference was seen. Interestingly, healthy controls also displayed an increase in IgG reactivity towards 11- and 15-HETE-PEs compared to the unoxidized SAPE. Nevertheless, the IgG response towards these HETE-PEs in healthy controls was small when compared to both OA and RA patients. Overall, these data suggest that RA patients mounted the highest immune response to HETE-PLs.

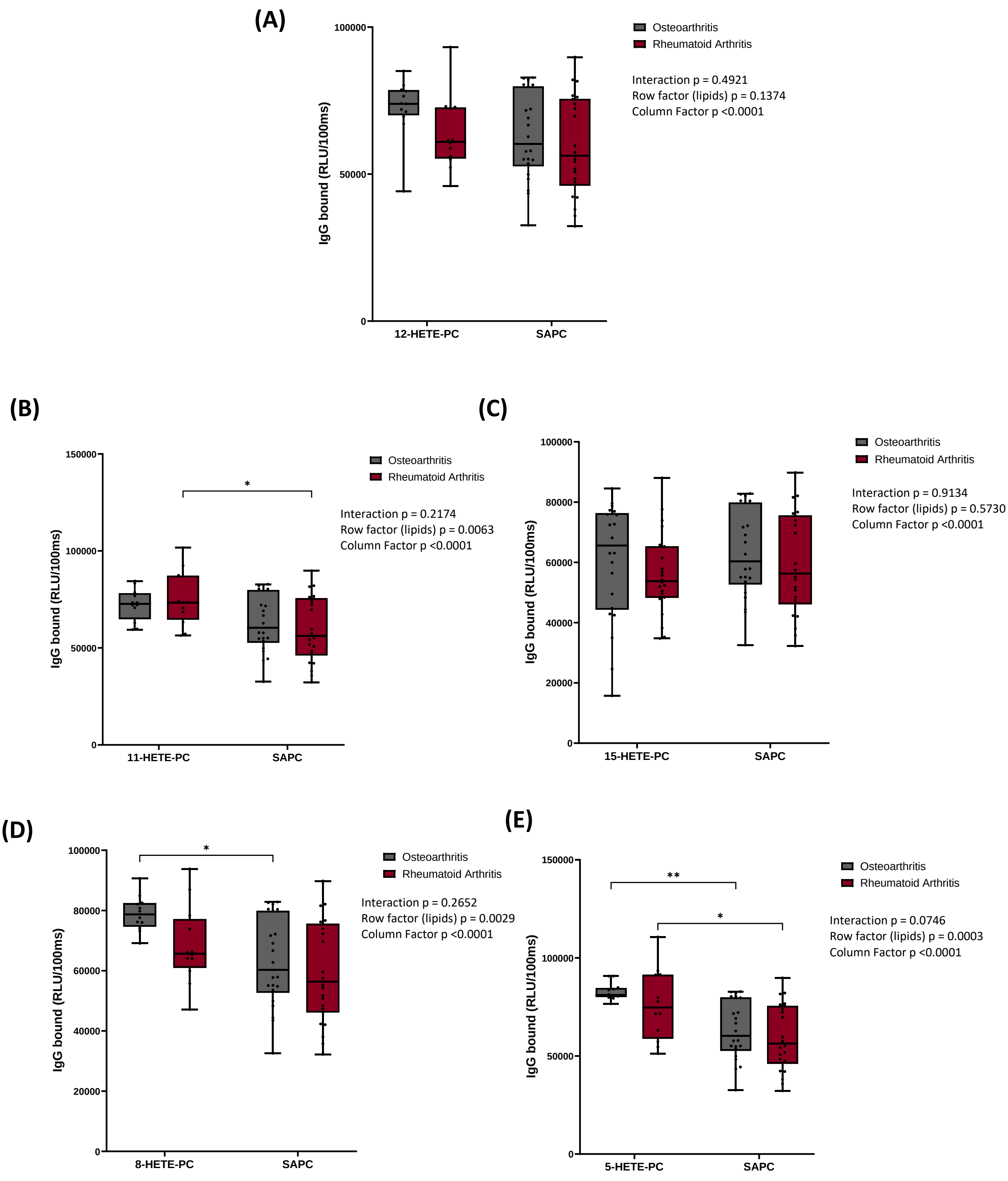

Figure 6.8:Circulating IgG against HETE-PCs are increased in both RA and OA
IgG levels against 12-HETE-PC (Panel A), 11-HETE-PC (Panel B), 15-HETE-PC (Panel C), 8-HETE-PC (Panel D) and 5-HETE-PC (Panel E) (n = 12) compared to SAPC (n = 24), in OA and RA patients, as described in Methods. Data were analysed using two-way ANOVA and Tukey's multiple comparisons tests (*p<0.05, ***p<0.001, **** p<0.0001).

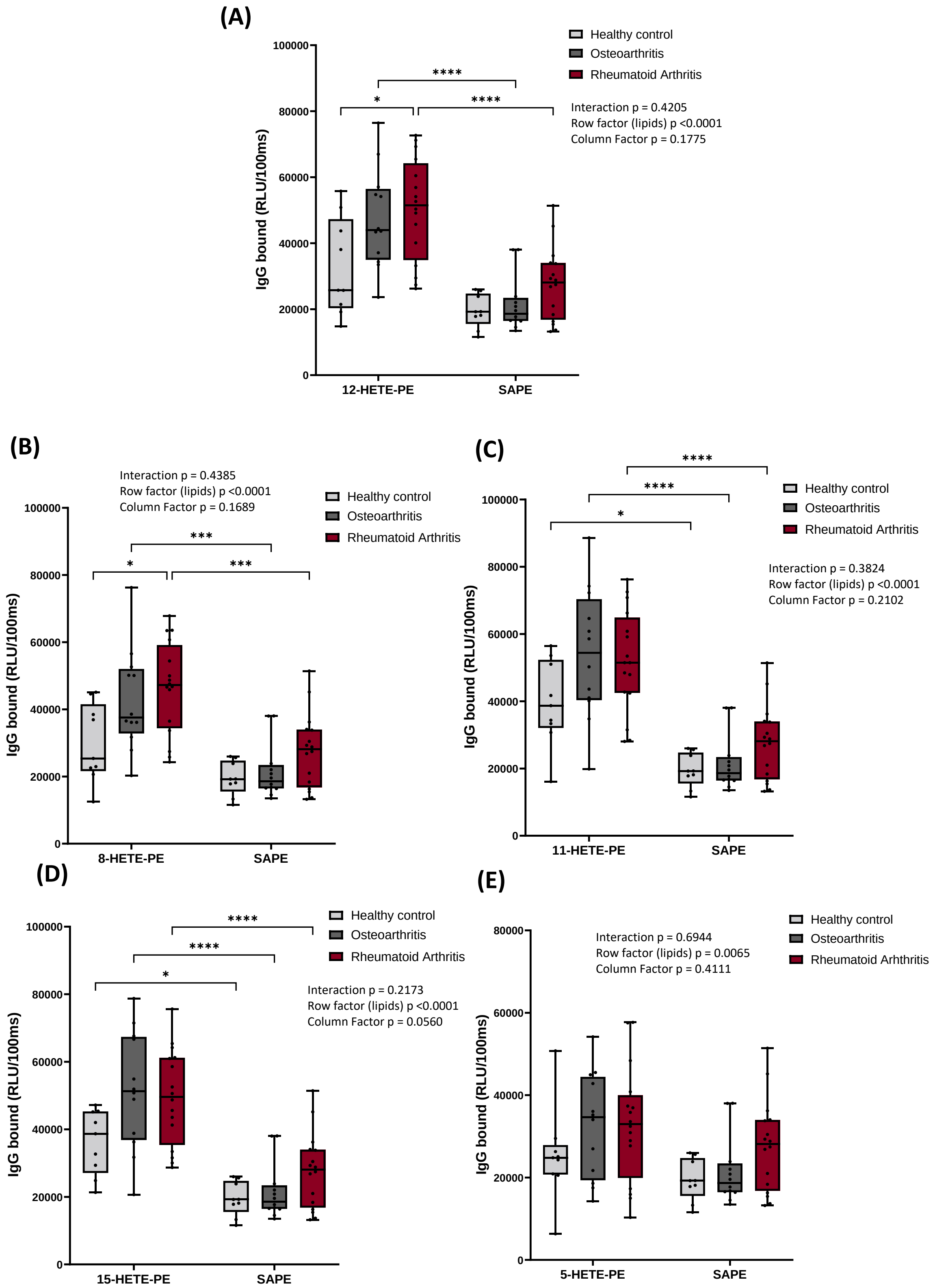

Figure 6.9: Circulating IgG against HETE-PEs are increased in both RA and OA

IgG levels against 12-HETE-PE (A), 8-HETE-PE (B), 11-HETE-PE (C), 15-HETE-PE (D) and 5-HETE-PE (E) (n = 12) compared to SAPE (n = 24), in healthy controls, OA and RA patients, as described in Methods. Data were analysed using two-way ANOVA and Tukey's multiple comparisons tests (*p<0.05, ***p<0.001, **** p<0.0001).

6.3 Discussion

In this chapter, I analysed the procoagulant potential of blood cells from RA patients and healthy controls from the *Cardiff Regional Experimental Arthritis Treatment and Evaluation Centre* clinical cohort. Two limitations were found in this cohort: the significant difference in the ages of both groups, and the use of NSAIDs or aspirin by 38% of RA patients.

Here, I found that platelet count was 20 % higher in RA patients. This agrees with a vast majority of other studies that show an increase in platelet numbers in the disease[150–152]. Importantly, pathological thrombopoiesis is widely known in arthritis and is commonly linked to increased thrombosis, although the mechanism is currently unknown. My findings may provide a partial explanation for this since the observed increase in platelet number could result in an overall increase in coagulation due to the greater availability of membrane for the assembly of coagulation factors. To test this, the prothrombinase assay could be performed using platelets at their original blood count level for each patient, instead of using the same number of platelets per assay.

No difference was observed in the WBC count between RA patients and healthy controls. This was expected since leucocytosis is not commonly observed among patients under DMARDs treatment or even under NSAIDs [302,303], which was the case of all studied patients in the cohort, although it can be seen in patients with corticosteroid therapy. As previously described in Chapter 1, Section 1.3.5, DMARDs are medication used to achieve remission in RA. In fact, conventional DMARDs such as methotrexate, are the first-line treatment of RA. NSAIDs, on the other hand, and anti-inflammatory drugs, commonly used for pain management in RA. Furthermore, no difference in thrombin generation was found between RA patients and healthy controls. This suggests that the WBCs membrane is not involved in the increased coagulation observed in these patients.

Activated blood cells can generate EVs from their membrane, which includes microparticles (MPs), exosomes, and apoptotic bodies. In the case of MPs, their increase is associated with inflammatory states like infection and auto-immune disease.[304,305]

Here, I was not able to count EV numbers due to time and facility limitations, which conditions the power of these conclusions. However, MPs have been shown to be highly increased in RA [152,296,306] and to originate mainly from platelets[296]. Platelet-derived microparticles (PMPs) share their parent procoagulant surface, exposing an anionic phospholipid-rich monolayer, therefore playing an important role in coagulation.[307] In addition, circulating PMPs in systemic lupus, another auto-immune disease affected by increased coagulation, have been shown to correlate with thrombin generation[308.] Furthermore, PMPs were shown to augment fibrin and platelet deposition in damaged arterial walls, which promotes arteriosclerosis[309.]

This is consistent with my findings, where an increase in thrombin generation was found in EV preparations from RA patients compared to healthy controls. This elevation might be a result of the increased EV numbers in these patients, or through a more procoagulant membrane present in these particles. To answer this question, EVs should be counted, and an equal number of EVs between healthy controls and RA patients should be analysed through the prothrombinase assay. Furthermore, the origin of these EVs should be analysed to understand the role of PMPs, along with platelets, in the increased coagulation in these patients. As previously described in Chapter 1, section 1.2.4, MPs derived from monocytes can bear TF which supports the extrinsic tenase complex constituted of TF, factor VIIa and calcium, which initiates the thrombin generation process[101]. Along with this, the PL membrane of these EVs can be considered a key player in the rise of thrombosis present arthritis, independently of TF presence.

Considering the difference observed in the coagulation of different AIA pathotypes, this human study was limited by the lack of information regarding the synovial disease. In order to properly correlate these results, these patients' phenotypes should have been determined.

Overall, platelets and EVs appear to play important roles in the elevated coagulation observed in RA patients, due to an increase in thrombin generation, possibly owing to their pro-coagulant phospholipid membrane. Therefore, in the next chapters, to examine this further, phospholipids from platelets, WBC and EVs from RA patients and healthy controls from the *Cardiff Regional Experimental Arthritis Treatment and Evaluation Centre* clinical cohort will be analysed.

In addition to analysing thrombin generation, oxPLs were also measured in these cells and EVs. Here, I first measured oxPLs in platelets and WBCs, in both resting and activated states, as well as EVs, isolated from peripheral blood from RA and healthy volunteers, recruited from the *Cardiff Regional Experimental Arthritis Treatment and Evaluation Centre* clinical cohort, described in this Chapter, section 6.2.1.

No difference was observed for HETE-PLs levels in resting platelets, which is consistent with the lack of difference in thrombin generation seen in platelets. However, considering the elevated numbers of platelets in RA patients, higher levels of platelet oxPL are likely to be found in the circulation in these patients, potentially contributing to the higher thrombotic risk seen in RA.

As previously shown, HETE-PL were generated by platelets upon thrombin activation[228]. Overall, total platelet HETE-PL were unchanged in RA, with this being mainly driven by 12-HETE-PLs, the most abundant isomer. However, activated platelets from RA patients generated significantly lower levels of 5-, 11- and 15-HETE-PLs compared to healthy volunteers. Nevertheless, data from resting platelets is more relevant than in a fully activated state since it is only achieved *in vivo* upon a great challenge.

As free 15- and 11-HETEs can be generated via COX-1 oxygenation of arachidonate in platelets, I proposed that the reduced levels of 15- and 11-HETE-PLs seen in RA platelets could be related to NSAIDs, which inhibit this enzyme. While most NSAIDs, only temporarily inhibit COX activity, aspirin irreversibly acetylates COX, inhibiting it; therefore, its effect will last for ≈ 10 days, the life duration of a platelet [310]. Consequently, an impact of NSAIDs, especially of aspirin, in these patients on COX derived lipids is very likely. To test this hypothesis, I analysed the impact of NSAID administration and observed a significant decrease in these oxPLs. However, this was not fully explained by NSAIDs since a decrease in 11-HETE-PLs was still observed in activated platelets from RA patients not using NSAIDs. This suggests COX inhibition by NSAIDs is partially responsible for the lower levels of 15- and 11-HETE-PLs observed. Interestingly, methotrexate has been described as a selective COX-2 inhibitor in *ex vivo* studies using blood from RA patients taking this conventional DMARD[311]. Considering that the majority of RA patients in this cohort were on methotrexate, a DMARD used as a first-line treatment for active disease[312], this therapy could be responsible for the observed reduced generation of 11- and 15-HETE-PLs by activated platelets in these patients. Nevertheless, other studies contradict these findings, describing no impact of methotrexate on COX metabolism[313]. Furthermore, TNF-α antagonists have also been described as preventing platelet activation *in vitro*, as well as a significant reduction in platelet activation in RA patients[314], however, only 8 % of recruited patients were undertaking this medication. In order to further understand platelet activity status, naïve RA patients, which haven't received any DMARD medication, should be recruited and compared to patients on these drugs.

Resting WBCs from RA patients showed significantly higher 15-HETE-PLs. In addition, raised levels of 8-HETE-PLs were observed in both RA patients and healthy controls when compared to the other HETE-PLs positional isomers. 8-HETE-PLs are considered to be generated non-enzymatically, as described in Chapter 1, Section 1.2.3, an 8-lipoxygenating enzyme has only been described in murine epidermis [53]. Hence, it was unexpected to see this non-enzymatic generated positional isomer be higher than other HETE-PLs, considering that oxidative stress, would result in similar levels of all HETE-PLs positional isomers. Nevertheless, no difference was observed between health and disease.

As expected, activation of WBCs with Ca^{2+} ionophore resulted in a large generation of oxPLs.[125,228] However, no significant differences were observed between activated WBCs from RA patients and healthy controls. However, activation with ionophore is not physiological, and thus this simply represents the capacity of cells to generate eoxPLs with maximal stimulation. Detection of 12-HETE-PL in activated WBCs was unexpected since WBC do not possess 12-LOX. Nevertheless, its presence has been previously described in a similar study.[125] These could potentially be present due to contaminating platelets, platelet-derived EVs or platelet-WBC aggregates present in the samples.

This lack of difference in oxPLs generation in activated WBCs suggests no difference in 5- and 15-LOX activity. However, oxPLs do not only depend on LOX but also substrate availability, as well as re-esterification rates. Furthermore, methotrexate, which represents 65% of the therapeutic RA patients in this cohort, could impact the activation potential of WBCs. However, several studies indicate no impact of methotrexate on 5-LOX metabolism[313,315,316], however, no studies were found describing the effect of DMARDs on 15-LOX activity. Nevertheless, my findings suggest that WBCs are not the major players in the increased coagulation in RA.

No oxPLs were detected in EV samples from any groups, suggesting that, HETE-PLs are not a major constituent of plasma EV membranes. Overall, these results suggest that in EVs, HETE-PLs do not contribute to the increase in thrombin generation observed in RA patients, described in Chapter 7.

The lack of difference in thrombin generation seen in platelets and WBCs from RA patients versus healthy volunteers is consistent with the similar HETE-PLs profile found in these cells. However, the increase in platelet count could contribute to an overall increase in eoxPLs in circulation in these patients, consistent with elevated thrombotic risk. This chronic exposure to circulating eoxPLs might result in increased IgG recognition. Therefore, to further understand the impact of a possible increase in oxPLs in circulation, I also analysed HETE-PLs as possible targets for autoantibodies in RA, OA and healthy controls.

As an auto-immune disease, RA is responsible for the production of self-antibodies, which can include auto-antibodies that recognise oxPLs. Increased immune recognition of 12-HETE-PE was found in RA serum, in comparison with healthy controls. This agrees with the hypothesis of increased 12-HETE-PLs levels in the circulation in these patients, which leads to an increase in immune recognition. Therefore, these results suggest that these patients experience a higher chronic exposure to 12-HETE-PLs in circulation, which can ultimately lead to increased TATs and elevated thrombotic risk. Interestingly, increased immune recognition towards HETE-PLs was not exclusive to RA, with OA patients also exhibiting higher IgG reactivity towards 8-HETE-PLs, 11-HETE-PEs, 12-HETE-PEs and 15-HETE-PEs, compared to the non-oxidised phospholipid analogue (SAPE and SAPC). This was unexpected, since OA is not an autoimmune disease, and self-reactivity was not expected. However, an increase in thromboembolism incidence in these patients has been described, although, contradicting studies have also reported no increase in thrombotic risk[135,317]. Nevertheless, increasing reports of autoantibodies in OA suggest adaptive immunity involvement. This autoimmune response is mainly against cartilage-related components, namely collagen[318] and osteopontin[319], as well as glycolytic enzymes, such as triosephosphate isomerase[320]. In fact, some OA patients studied in this Chapter presented auto-antibodies against cyclic citrullinated peptide (CCP) and rheumatoid factors (RF).

Despite OxPLs being described to have an important role in signalling the innate immune system for oxidative stress [5], the adaptative immune system has also been previously described to respond to oxPLs in anti-phospholipid syndrome [125]. Furthermore, in auto-immune diseases such as systemic lupus erythematosus[321] and RA[322], oxidised lipids, more specifically oxidised low-density lipoprotein (LDL) were described to be recognized by the humoral adaptive immune system, generating both IgG and IgM antibodies against oxPLs. This was also observed in atherosclerosis [323], where the titres of these auto-antibodies correlated with both disease progression and lipid peroxidation [324]. Considering the correlation with lipid peroxidation, this increase of autoantibodies against oxidised lipid is probably also due to an increase in lipid oxidation, not only due to an increase of the adaptative immune system response. In fact, T- [325]and B-cells [326] have only been described to express 5-LOX, however, production of LOX derived lipids by these cells was only been described after a non-physiological *in vitro* activation and in very low amounts compared to the production of these lipids by other immune cells. Therefore, the elevated numbers of these lymphocytes during the activation of the adaptative immune system would most likely not result in an increase of LOX derived eoxPLs. Nevertheless, COX expression might partially mediate the increase of eoxPLs, however, this has not analysed yet.

Overall, these results suggest that RA patients will have higher levels of oxPLs in their blood circulation, not due to a change in the individual membrane phospholipid composition, but as a result of higher circulating platelet levels. This supports the idea that eoxPLs could contribute to the elevated thrombotic risk seen in RA.

Aminophospholipid exposure in rheumatoid arthritis patients' blood cells is similar to healthy volunteers

Chapter 7

7.1 Introduction

The plasma membrane is asymmetrically organized, being externally comprised mainly of neutral phospholipids, such as phosphatidylcholine (PC) and sphingomyelin, while aminophospholipids (aminoPLs) such as phosphatidylserine (PS) and phosphatidylethanolamine (PE) are mostly distributed on the inner face.[327] As previously described in Chapter 1, Section 1.2.4, not only oxPLs are involved in coagulation. While the oxidation of any phospholipids will generate a charged surface for the binding of phospholipids, aminophospholipids (aminoPLs) also play a role in thrombosis, by providing these binding sites for the assembly of coagulation factors, without further oxidation. AminoPLs are phospholipids with an amine group (NH_2), namely PS and PE (Figure 1.1). While PS is essential to support coagulation, PE boosts PS activity[123,328,329].

In resting cells, aminoPLs are maintained on the inner leaflet of the plasma membrane, via ATP-dependent flippase enzymes, therefore exhibiting extremely low levels of externalisation. However, upon activation, a loss of asymmetry occurs, and aminoPLs are relocated to the outer leaflet, increasing externalization levels. This exposure of aminoPLs in platelet activation is a key event for coagulation[330]. In the case of EVs, they are generated by activated blood cells, and their membrane partially resembles the parent cell, without however being the same. Published lipidomic analysis in EVs is limited, nevertheless, they describe an enriched aminophospholipids when compared to cells [331]. Therefore, the externalisation of PEs and PCs will be analysed in platelets, WBC and plasma-enriched EVs, since they will be at higher levels than HETE-PEs analysed in the previous Chapter 6.

Auto-immune diseases are associated with a rise in immune cell activation, as shown by an increase in PS exposure in platelets and EVs from RA patients analysed through annexin V binding assay[332,333]. AminoPL externalisation can also result from apoptosis and cell stress, being often associated with diseases with high cardiovascular risk, establishing a bridge between coagulation and RA[330]. However, to date, no studies have directly measured aminoPL externalization, namely the amount of molecular species of PE and PS on the outside, through LC/MS/MS in blood cells from patients with RA.

In the previous Chapter, I demonstrated that thrombin generation was elevated in EVs from RA patient plasma, as well as observed an increase in platelet count in these patients. Furthermore, I investigated the presence of oxPLs in the blood cells of RA versus healthy controls. Next, in this chapter, I will study aminoPL in circulating blood cells in RA, including their externalization, in order to determine whether they could also contribute to the increased thrombosis observed.

7.1.1 Aims

In this chapter, I will quantify the external facing aminoPL in platelets, WBCs and plasma EV in RA patients and healthy controls using LC/MS/MS. By profiling the aminoPLs in the membranes of cells from these patients, I will aim to establish their possible relevance to the increased thrombotic risk observed in RA.

7.2 Results

7.2.1 Resting platelets from RA patients externalize aminoPLs similar to healthy volunteers.

AminoPLs are mainly located in the inner leaflet of the plasma membrane, however, upon activation, this asymmetry is lost, which exposes them to the outer leaflet, enabling coagulation[121,334]. Here, both the percentage of aminoPL externalised, calculated as ng externalised (outer leaflet) ÷ ng total (both outer and inner membrane) in percentage (%), and the amount (ng/2x10^8 platelets) was determined in platelets.

The LC/MS/MS method for derivatisation and analysis of external PE/PS is described in Chapter 2, Sections 2.2.33 and 2.2.34. Here, washed cells and EVs were incubated with SNB for a short time, which is not permeable to plasma membranes, therefore biotinylating only external-facing aminoPLs. For total aminoPLs, NHS-biotin was instead used, since it is permeable to PL membranes. To calculate the percentage externalised, the outer facing amount was divided by the total.

Here, platelets were isolated from peripheral blood from RA patients and healthy volunteers, and externalisation of aminoPLs was determined in unstimulated platelets, as described in Methods. Resting platelets from RA patients showed a trend towards an increase in the percentage of PE/PS on the outside, in particular for 18:0a_20:4-PE, but the differences were not significant, and there was an extremely high level of inter-individual variation (Figure 7.1.A).

However, when looking at ng levels, I observed higher amounts of amount of externalized PLs on the outside of platelets from healthy volunteers, but as for resting cells, this was not significantly different (Figure 7.1.B). Overall, the most abundant aminoPL externalized in resting platelets was 18:0a_20:4-PE, as well as being the lipid with the highest percentage of externalization.

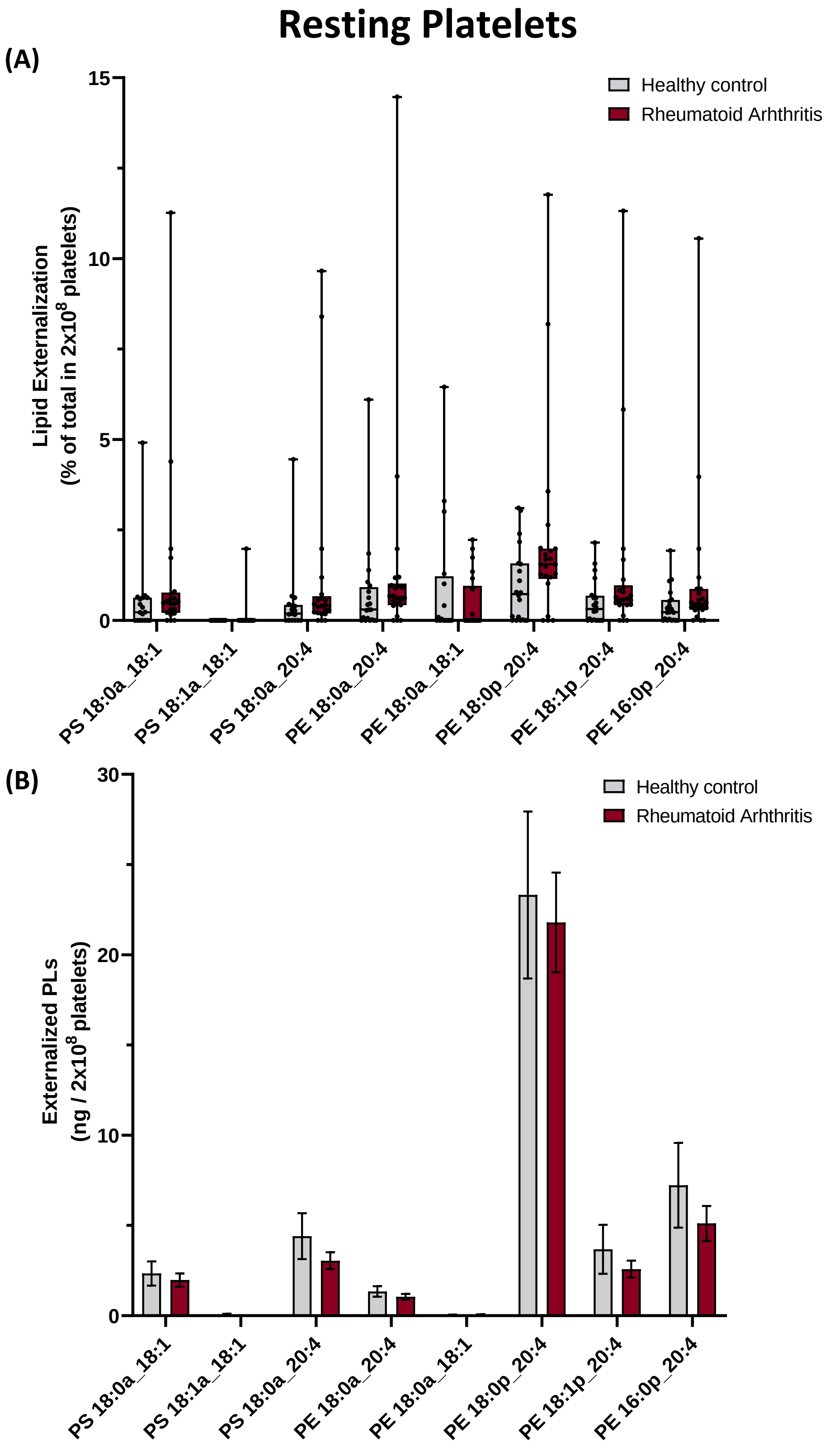

Figure 7.1: Percentage and amount of externalised aminoPLs in resting platelets is similar between healthy controls and RA patients

Lipids were extracted from resting platelets isolated from healthy volunteers (n = 25) and RA patients (n = 26), as described in Methods, and analysed by LC/MS/MS. The percentage of externalised PS and PE were calculated for each sample (ng externalised ÷ ng total) (Panel A), as well as amount externalized (ng/2x10^8 platelets) (Panel B). Data are represented as box and whiskers plot and analysed through multiple unpaired t tests (Panel A) and Mann-Whitney tests (Panel B).

7.2.2 The percentage of aminoPLs externalised is increased in RA patients' activated platelets, although overall amounts are unchanged.

Next, thrombin-activated platelets from both RA patients and healthy controls were analysed. Activation-induced an overall increase in aminoPL externalization from approximately 0.8% in resting platelets to 7 % upon stimulation, as expected due to scramblase activation[335]. Similar to resting cells, activated platelets showed a non-significant change in percentage of externalised aminoPL in RA compared to healthy volunteers, and there was a high degree of variation (Figure 7.2.A). The aminoPL with the highest % externalization was 18:0p_20:4-PE, closely followed by 18:0a_18:1-PE.

When analysing the amount of aminoPLs externalized, no significant differences were observed. In fact, healthy volunteers' activated platelets showed slightly but not significant higher levels of externalised aminoPLs than platelets from RA patients (Figure 7.2.B). Nevertheless, these results suggest that the total amount of aminoPLs is somewhat reduced in activated platelets from RA patients compared to healthy controls. Again, 18:0p_20:4-PE was the most abundant aminoPL in the outer membrane. However, 18:0a_18:1-PE was the aminoPL with the highest percentage of externalization.

Overall, these data displayed a big variation, especially in RA patients, probably as a result of intra-individual differences.

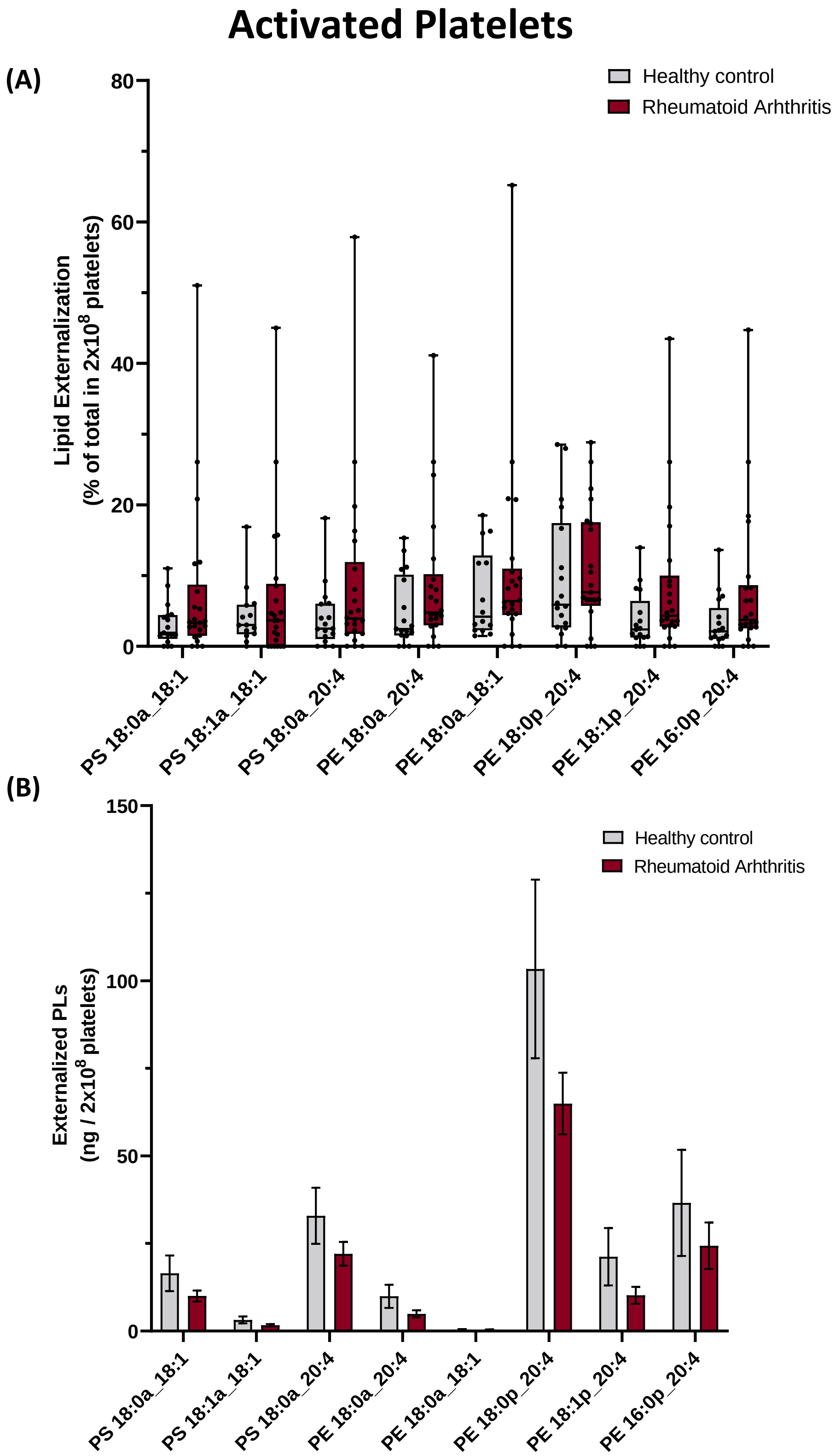

Figure 7.2: Percentage of externalised aminoPL in activated platelets from RA patients are increased compared to healthy controls, despite no difference in amount externalized
Lipids were extracted from platelets isolated from healthy volunteers (n = 25) and RA patients (n = 26) and following activation with thrombin (0.2 U/mL), as described in Methods, and analysed by LC/MS/MS. The percentage of externalised PSs and PEs were calculated for each sample (ng externalised ÷ ng total) (Panel A), as well as amount externalized (ng/2x10^8 platelets) (Panel B). Data are represented as box and whiskers plot and analysed through multiple Mann-Whitney tests.

7.2.3 AminoPL externalisation in resting WBCs was unchanged between RA patients and healthy controls.

Next, WBCs from healthy volunteers and RA patients were analysed for aminoPL externalization. Here, WBCs were isolated and the externalisation of aminoPLs, as well as amounts, was calculated in unstimulated WBCs, as described in Methods. The percentage of aminoPLs externalised, calculated as ng externalised (outer leaflet) ÷ ng total (both outer and inner membrane), and the amount (ng/$4x10^6$ WBCs) was determined.

Resting WBCs did not exhibit a significant difference in % aminoPL externalisation between RA patients and healthy volunteers (Figure 7.3.A). However, healthy control WBCs showed a trend towards an increase, especially for PE, with a total average percentage of 2.26%, compared to 1.6% in RA WBCs. On the contrary, RA WBCs appear to display a slightly higher % externalization in PS species. The main aminoPL externalized was PE 18:0a_20:4 in healthy volunteers, while in RA WBCs, 18:0a_20:4-PS displayed a higher % externalization.

When analysing the ng amount of externalized aminoPL in resting WBCs, once again, no significant difference is observed between RA patients and healthy controls (Figure 7.3.B). Nevertheless, like the % data, a higher level is observed in healthy WBCs for external-facing PE species compared to RA WBCs. However, externalised PS was higher in RA WBCs. In fact, 18:0a_20:4-PS was the main externalized aminoPL present in WBCs from RA patients, while 18:0p_20:4-PE was the highest in healthy controls. These results show that, contrary to platelets, WBCs from RA patients have higher externalised amounts of PS than healthy controls, while in contrast, healthy controls have increased amounts of PE compared to RA patients.

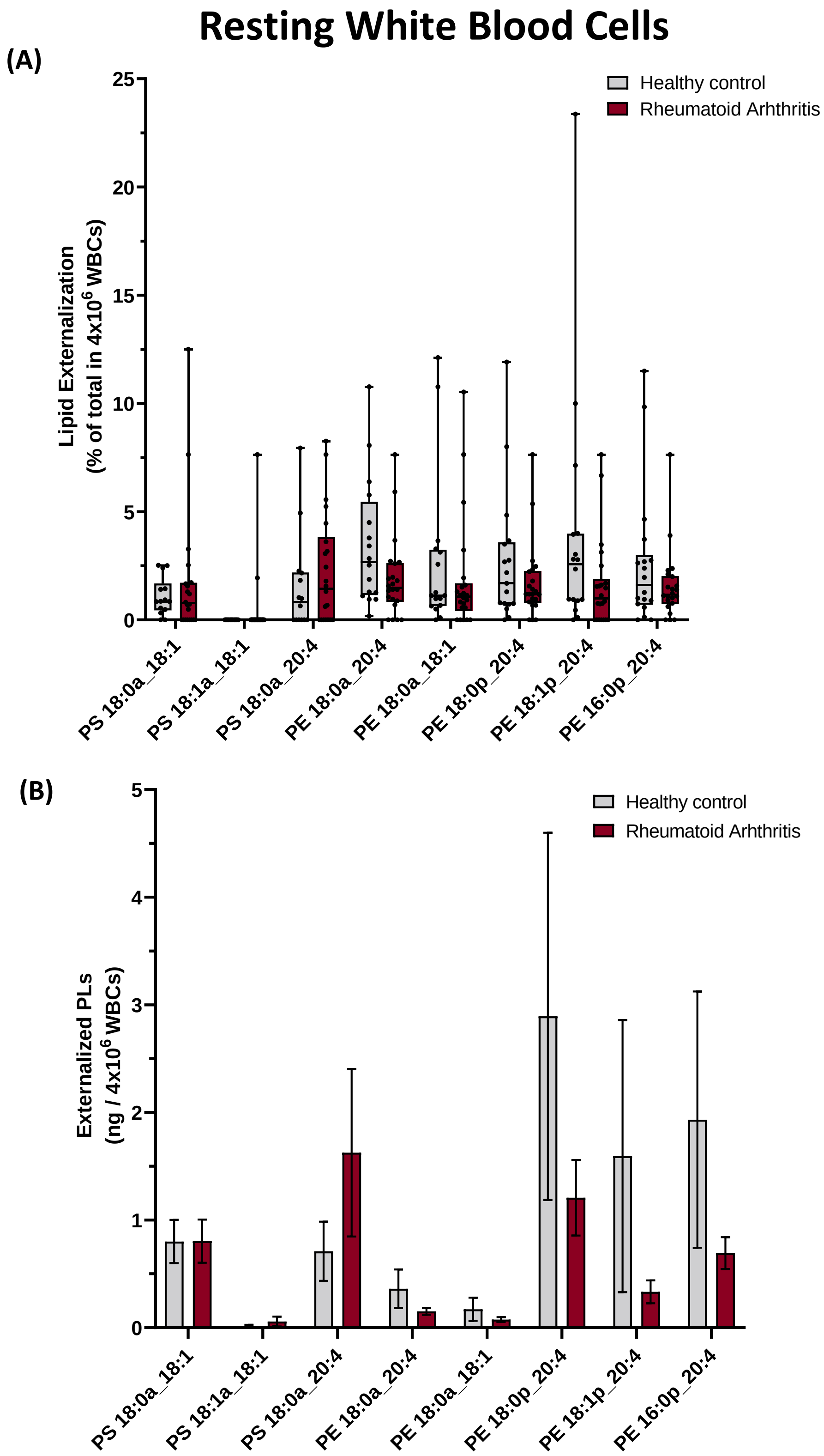

Figure 7.3: Percentage and amounts of externalised aminoPL in resting WBC are similar between RA patients and healthy controls

Lipids were extracted from resting WBCs isolated from healthy volunteers (n = 25) and RA patients (n = 26), as described in Methods, and analysed by LC/MS/MS. The percentage of externalised PSs and PEs were calculated for each sample (ng externalised ÷ ng total) (Panel A), as well as amount externalized (ng/4x10^6 WBCs) (Panel B). Data are represented as box and whiskers plot and analysed through multiple Mann-Whitney tests.

7.2.4 RA and healthy WBC exhibit similar aminoPL externalization following ionophore activation.

WBCs isolated from RA patients and healthy controls were stimulated with 10 µM calcium Ionophore A23187 and 1 mM $CaCl_2$, as described in Methods. Then, the percentage of aminoPL externalised was calculated as described earlier, as well as the amount externalized (ng/4x10^6 WBCs).

Similar to platelets, activated WBCs showed an increase in aminoPL externalisation, from approximately 2 % when resting to 13 % upon activation (Figure 7.4.A). However, upon activation, no difference was observed between RA and healthy controls WBCs for % external aminoPL. The aminoPL with the highest % externalisation was 18:0a_18:1-PS in activated WBCs from both RA and healthy controls.

The ng amount of externalised aminoPLs in activated WBCs was not significantly different between RA and healthy samples (Figure 7.4.B). However, an overall increasing trend was observed for externalised aminoPL amount in WBCs of RA patients compared to healthy controls.

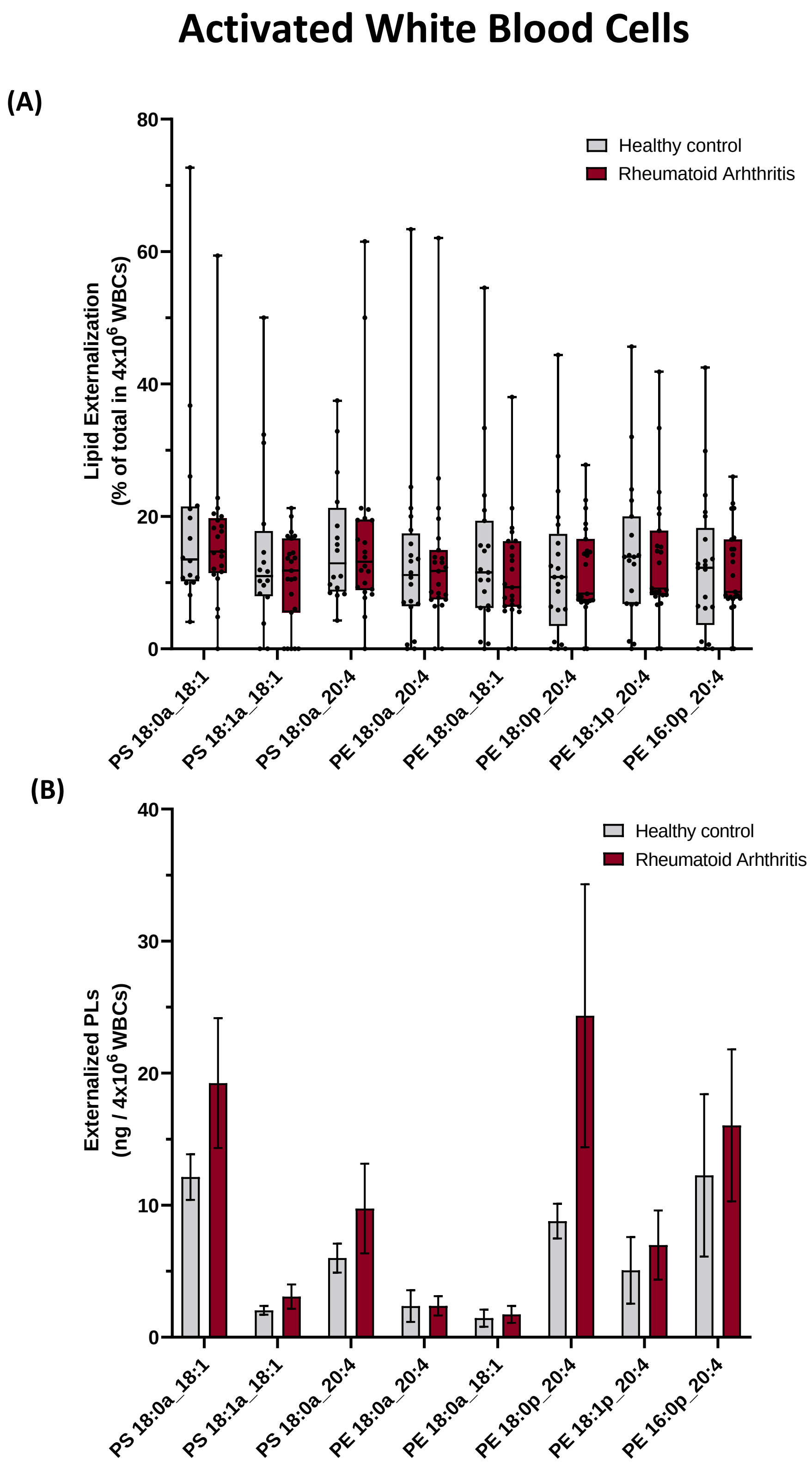

Figure 7.4: Percentage of externalisation and amounts of aminoPL in activated WBCs are similar between RA patients and healthy controls

Lipids were extracted from WBCs isolated from healthy volunteers (n = 25) and RA patients (n = 26), and following activation with Ca^{2+} ionophore (10 µM), as described in Methods, followed by analysis by LC/MS/MS. The percentage of externalised PSs and PEs were calculated for each sample (ng externalised ÷ ng total) (Panel A), as well as amount externalized (ng/4x10^6 WBCs) (Panel B). Data are represented as box and whiskers plot and analysed through multiple Mann-Whitney tests.

7.2.5 EVs from healthy controls have more external facing PEs, while PS is more abundant on the outside of RA patients' EVs.

EVs were obtained from RA patients and healthy control plasma, as described in section 2.2.23 from Methods. Notably, pelleted EVs were all resuspended into the same volume of buffer, with the EV count not determined. This means that differences in EV numbers were not taken into account. Here, the percentage of aminoPL externalised was calculated as described above, as well as the amount externalized (ng/ml of plasma).

A larger variation is observed in externalized % of PE in healthy controls compared to RA patients. As previously described, RA is a highly heterogeneous disease, therefore this variation can be a possible reflection of different EVs subpopulation as a consequence of distinct RA pathotypes[331]. Furthermore, as a human study, composed of genetically unrelated people, variation of data was expected. No lipidomic studies have focus on aminoPLs externalization in EVs, making it impossible to compare these values with other studies, and to understand this variation.

The % external PS in EVs isolated from both RA and healthy plasma was lower than for PE. Overall, approximately 0.1 % of the PS was detected on the outer leaflet, contrasting with 20 % to 40 % of the PE (Figure 7.5.A). Notably, the % external PE was higher for EVs than for activated platelets or WBCs, as previously shown (Figure 7.2.A and Figure 7.4.A).

EVs from RA plasma showed a non-significant higher % of PS on the outside, compared to healthy controls, with 18:0a_20:4-PS showing the highest % (Figure 7.5.A) For PE externalization, a significantly higher % externalisation was seen for healthy controls than for RA for 18:0p_20:4-PE, 18:1p_20:4-PE and 16:0p_20:4-PE (Figure 7.5.B). The PE with the highest external % in healthy control EVs was 18:1p_20:4-PE, with 48 % externalised, while in RA patients, 18:0a_18:1-PE was the highest, with 31 % present in the outer leaflet.

The ng amount of PS on the outside of EVs from RA patients is higher than for healthy controls. A significant increase was observed for 18:0a_18:1-PS in EVs from RA patients compared to healthy controls. 18:0a_20:4-PS was the most abundant PS in RA EVs, but its % on the outside was not significantly elevated in disease. In addition, EVs from RA patients showed trends towards higher amounts of externalised PE than healthy controls. This suggests that the total amount of PE is increased in EVs from RA patients, with more PE remaining in the inner leaflet of EVs in RA when compared to healthy controls.

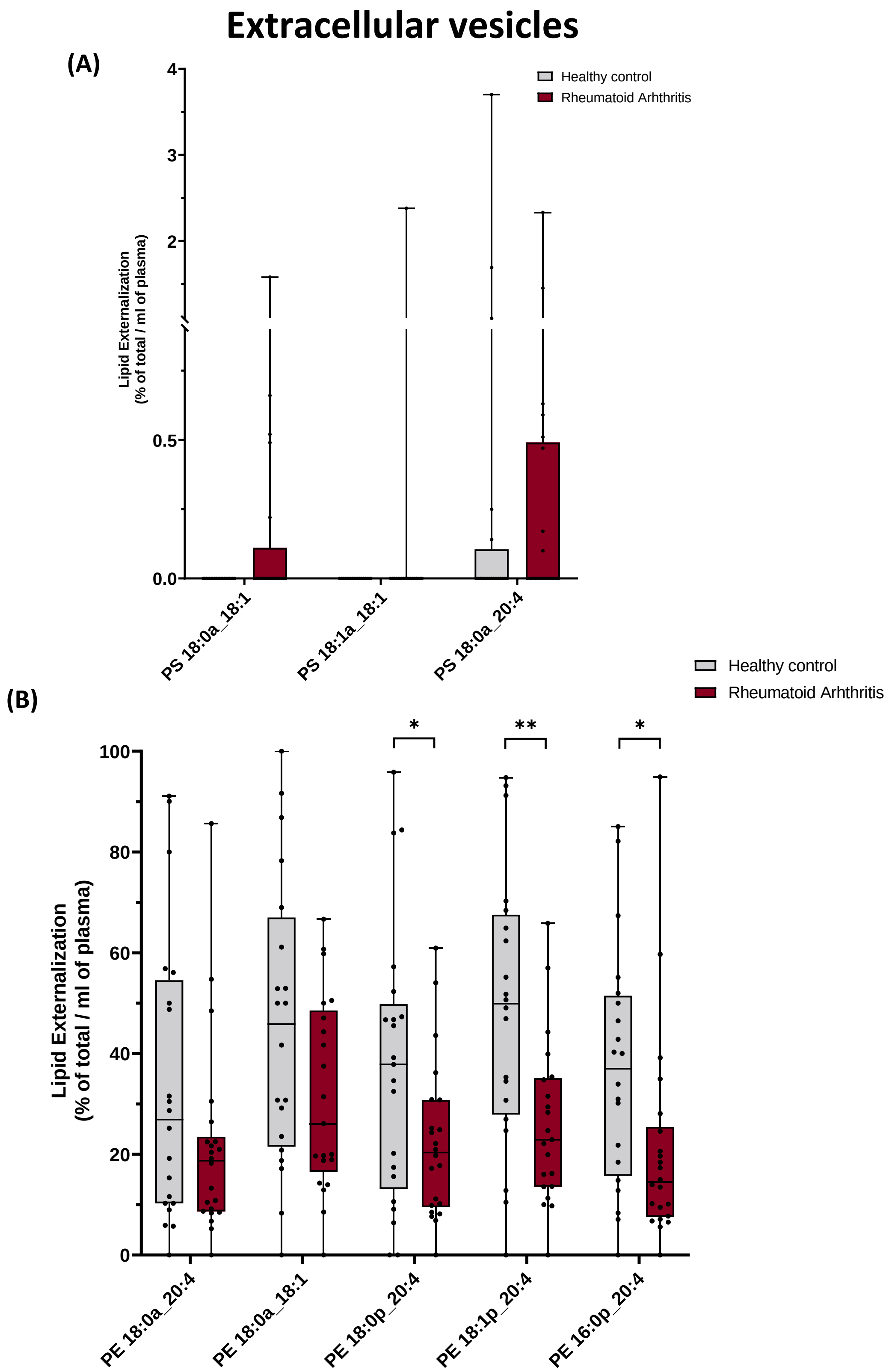

Figure 7.5: Percentage of PE externalised in EVs is higher in healthy volunteers than RA patients

The percentage of externalised PSs (Panel A) and PEs (Panel B) were calculated for each sample (ng externalised ÷ ng total). Lipids were extracted from plasma enriched EVs isolated from healthy volunteers (n = 25) and RA patients (n = 26), as described in Methods, and analysed by LC/MS/MS, followed by calculation of externalised fractions. Data was analysed through multiple Mann-Whitney test (*p<0.05, **p<0.01).

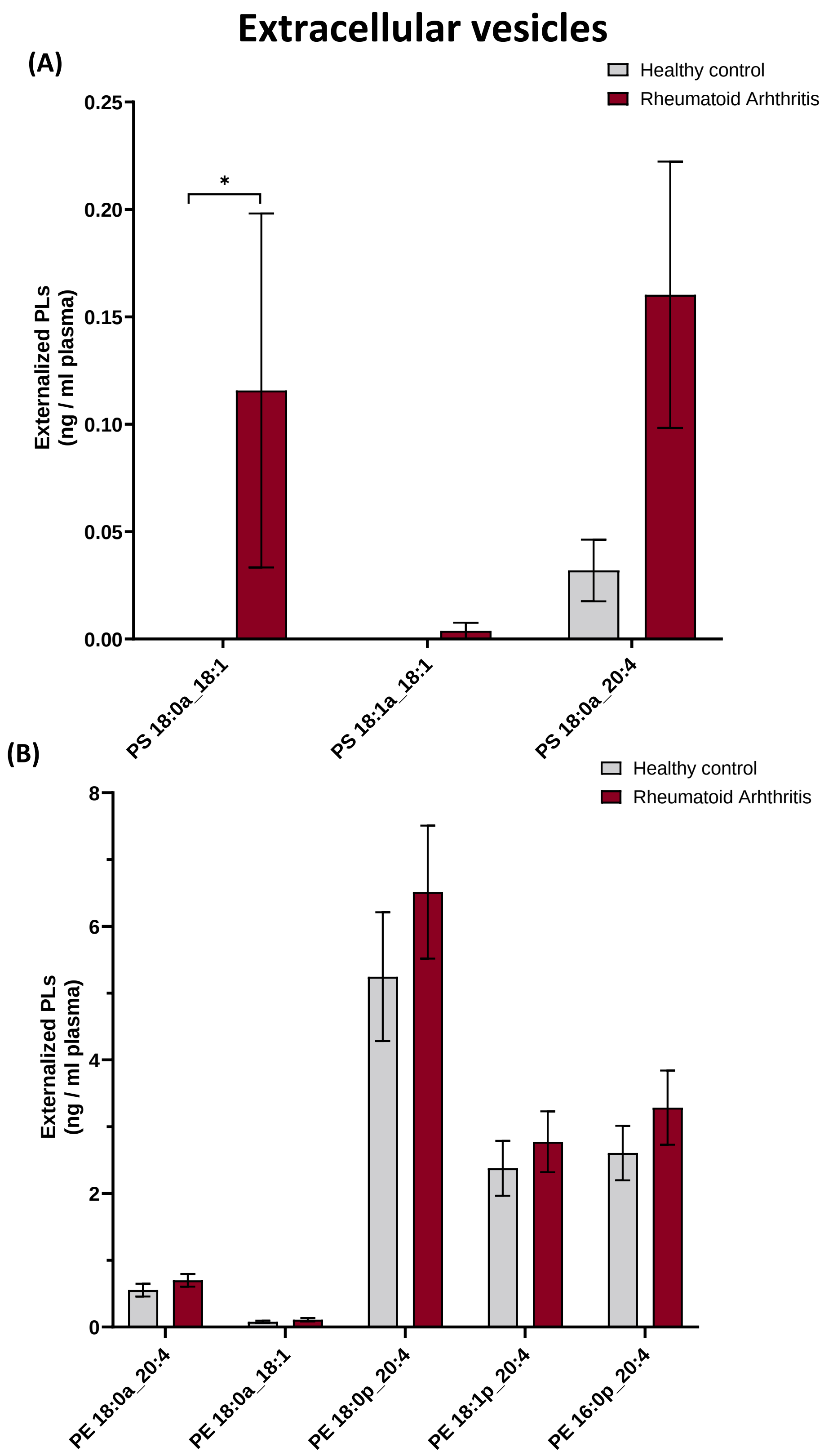

Figure 7.6: EVs from RA patients present higher amounts of externalised PS 18:0a_18:1 compared to healthy controls, while the remaining aminoPLs present similar amounts
Plasma enriched EVs, isolated as described in Methods, from RA patients (n = 26) and healthy volunteers (n = 25) were analysed by LC/MS/MS, and externalised aminoPLs, namely PSs (Panel A) and PEs (Panel B), were quantified (ng/ml plasma). Data are represented as bar chart, with the mean and SEM represented. Data was analysed through multiple Mann-Whitney test (*p<0.05).

Since aminoPLs are considered drivers of thrombin generation on the membrane surface, next, I used correlation analysis to test for relationships between thrombin generation (data from Chapter 6), and the proportion of PE or PS on the outside of EVs, since these were the only sample type to show a significant increase in thrombin generation between RA and healthy controls.

A negative association between thrombin generation and % PE externalisation was observed (Figure 7.7). Due to the majority of PS externalisation falling below the limits of detection, this analysis was only possible for PE.

Statistically significant negative correlations were seen for PE 16:0p_20:4, PE 18:1p_20:4, PE 18:0p_20:4 and PE 18:0a_20:4. The total PE externalized percentage also demonstrated a negative correlation with thrombin generation. Despite this association being relatively weak, it indicates that a higher % of externalised PE on the EV surface results in a lower thrombin generation in the EV pool. Nevertheless, these data do not consider the EV count, therefore, the high EV count described in RA might simply be responsible for the increase in thrombin generation.

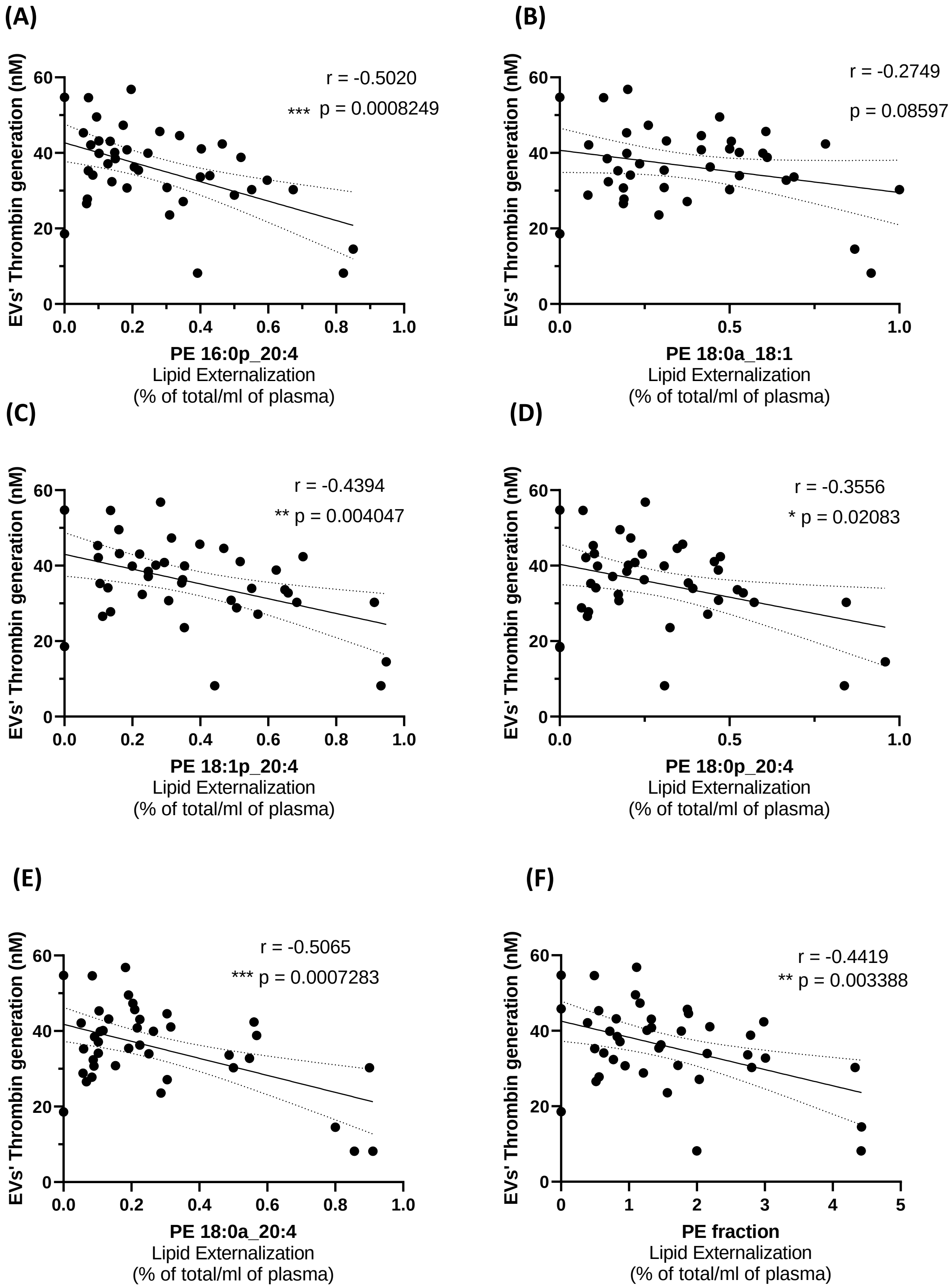

Figure 7.7: Thrombin generation from EVs negatively associates with percentage of PEs externalised

Thrombin generation of plasma enriched EVs, from both healthy volunteers and RA patients, association with lipid externalisation fractions of PE 16:0p_20:4 (Panel A), PE 18:0a_18:1 (Panel B), PE 18:1p_20:4 (Panel C), PE 18:0p_20:4 (Panel D), PE 18:0a_20:4 (Panel E) and total externalised PE percentage (Panel F) was analysed through simple linear regression (n = 44). A weak, but significant negatively association was assessed.

7.3 Discussion

AminoPL exposure provides binding sites for coagulation factors, enabling their activation.[336] In RA, where increased coagulation is described[91], I tested whether these lipids might contribute to the cardiovascular risk by analysing the aminoPL profile of platelets, WBCs and plasma-derived EVs from RA patients and healthy volunteers, both resting and after *in vitro* activation.

Overall, no significant differences for either percentage or ng amount of aminoPLs externalised were observed in resting platelets or WBCs between RA and healthy controls. Importantly, as shown in Chapter 7, these RA patients have elevated counts of platelets, also known as thrombocytosis, which will ultimately increase the total externalized aminoPLs in circulation.

A diminished ng amount of externalized aminoPLs was observed in activated platelets of RA patients compared to healthy control platelets. An increase in externalized PS might have been expected, considering that methotrexate was described as a pro-apoptotic agent that increases PS externalisation, as revealed by annexin V staining[337]. However, *Paul et al.* study was an *in vitro* analysis of washed platelets from healthy volunteers. However, the amount of externalized aminoPLs did not differ in a statistically significant manner between health and disease. Furthermore, the resting state of platelets is more relevant for this study, considering the chronic nature of RA, platelets in circulation will be mainly in a non-activated state. Nevertheless, this suggests that the total amount of aminoPLs is reduced in RA patients' platelets, proposing a disparity between the PL composition of RA platelets compared to healthy controls. This difference might be a result of the increased generation of microparticles by platelets, which was been described in the literature[152,306]. Upon activation, platelets discharge platelet-derived microparticles from the parent cell’s membrane. This increased generation of microparticles by RA platelets might be responsible for the decrease in the total amount of aminoPLs. However, more studies are necessary to understand the role of platelet-derived microparticle generation and function in RA.

Similar to the result of resting WBCs, no difference in either fraction or amount of externalised aminoPLs was observed upon ionophore activation between RA patients and healthy controls. This suggests that, when activated, the WBCs PL membrane of RA is similar to healthy controls. Considering these findings, along with results from Chapters 6, WBCs aminoPL appears to not be important players in the increase of coagulation in RA patients.

In the case of EVs, the increase in externalized PS amount observed might be due to an increase in EV count in RA patients' plasma samples[296]. Thus, increased coagulation observed in RA patients might be a result of the elevated number of EV circulating in these patients' blood. In fact, increased PS in EVs isolated from RA patients' plasma has been described in the literature, using annexin V staining, as well as a positive correlation between PS expression and coagulation in these patients [292].

On the contrary, the % of PE on the EVs' outer leaflet is increased in healthy controls compared to RA patients. However, the amount externalized is not significantly different between them. This indicates that the total amount of PE is higher in EVs from RA patients than in healthy controls, supporting the hypothesis of aminoPL loss as a result of a higher generation of microparticles.

Interestingly, PS externalization has also been associated with increased mineralization in previous studies. Matrix vesicles shed from chondrocytes and osteoclasts, are rich in PS, which enables the assembly of complexes with calcium and phosphate, forming nucleates of hydroxyapatite, which ultimately lead to bone and artery mineralization[338]. Dilution of PS due to increasing PE exposure has been shown to be detrimental to the mineralization process[339]. Since that the analysed EVs were isolated from plasma, and not from synovial fluid, the observed decrease in externalized PE percentage in RA patients might be responsible for the increase of artery calcification observed in these patients[340]. Therefore, the phospholipid composition of circulating EV from RA patients might be responsible for the arterial calcification found in these patients. However, studies on EVs lipid composition and its role in calcification are extremely limited, and a better understanding of the impact of membrane composition in the process of calcification is needed.

Furthermore, thrombin generation and aminoPL externalisation were compared in EVs, where a weak negative correlation was observed. These results indicate that an increase in PE externalisation results in lower thrombin generation by EVs, however, EV count should be performed in order to fully understand these results.

Here, I observed in EVs, high levels of externalisation compared to platelets and WBCs, especially in healthy controls (>50 %). This might lead to extremely high membrane curvature in EVs. The ratio of outer/inner PE modulates membrane curvature. With a smaller polar headgroup than PS, PE displays a conical shape. Therefore, a membrane with an increased PE ratio results in a negative curvature as a result of forcing headgroups together[341]. A negative curvature has been described to enhance enzyme activity, namely diacylglycerol kinase, a lipid kinase involved in the phosphatidylinositol cycle, due to allosteric regulation[342]. Therefore, the high membrane curvature might lead to an inhibition of prothrombinase activity by reducing accessibility to coagulation factors.

Despite oxPL being procoagulant, an extremely high increase in HETE-PE amounts was previously associated with reduced thrombin formation *in vitro* liposomes, potentially due to the loss of colocalization of oxPLs in smaller areas[68]. Therefore, the same logic can be applied to aminoPL in EVs, where high levels of externalization of PE might result in a non-optimal local concentration of oxPLs, leading to the decrease in thrombin generation observed. However, more studies are necessary to confirm these hypothesises, for example, protein-lipid overlay assay, which can provide information on the affinity between different phospholipid compositions and coagulation factors[343].

Overall, I propose that the elevated number of circulating platelets in RA could impact coagulation due to the increased total amounts of external aminoPL available for coagulation factor binding in the outer leaflet. Furthermore, the aminoPL profile in EVs of these patients seems to also contribute to an increase in thrombotic risk through the increased amount of externalised aminoPLs.

General Discussion

Chapter 8

8.1 General Discussion

The main aim of my thesis was to characterise pro-inflammatory and pro-coagulant lipids generated by circulating blood cells from patients with arthritis. The hypothesis was that an altered procoagulant surface in circulating cells may be a contributing factor for the increased coagulation observed, and hence elevated cardiovascular risk in RA. Overall, my data strongly supports this idea, with elevated platelet and EV numbers in RA potentially driving thrombosis risk through the action of aminoPLs and eoxPLs.

RA patients display a high prevalence of *comorbidities,* such as cardiovascular disease, which are often associated with thromboembolic events[91,344]. The incidence of thrombosis, both arterial and venous doubles in RA patients when compared to the healthy population[91,135]. Several thrombotic indices have been found to be elevated in these patients [91], however, this is the first time that the procoagulant surface in circulating blood cells has been characterised in both human and murine arthritis.

Despite coagulation being heavily described as altered in human RA, with increased levels of TAT complexes[142,146], only one study had previously described plasma TAT complexes as being significantly increased in mice, specifically in CIA[227]. However, that study was underpowered, with only four samples analysed per condition. In my thesis, along with WT mice, several other strains, which develop specific synovial pathotypes of RA, were analysed. These included WT [200,201], *IL27ra*$^{-/-}$ [345], *IL6ra*$^{-/-}$ [202] and *IL6*$^{-/-}$ [200] mice, which develop similar features to specific human RA molecular and cellular phenotypes [133,134], more specifically myeloid- or macrophage-rich, lymphoid-rich and fibroblastic-rich pauci-immune pathotype, respectively.

In Chapter 3, I showed an increase in eoxPLs in blood cells from WT and *IL27ra*$^{-/-}$ mice during AIA, the same mice that also exhibited increased TAT complexes and exhibited the highest levels of SAA. These mice were described to represent myeloid-rich and lymphoid-rich arthritis phenotypes, which can be found in human arthritis[206]. On the other hand, the genetic deletion of either IL-6 or its receptor prevented the increase of coagulation and inflammation, as well as eoxPL generation during AIA development. Consistent with these results, the use of Tocilizumab, an IL-6 inhibitor, lowers levels of fibrinogen compared to other biological DMARDs[180]. This suggests that IL-6 is an important mediator in driving both eoxPL generation and coagulation in arthritis.

Considering the increase in eoxPLs seen, *Alox15*$^{-/-}$ mice were analysed to determine the origin of the lipids. Despite *Alox15*$^{-/-}$ mice displaying a bleeding phenotype[212] and being protected against many vascular inflammatory conditions like atherosclerosis[346], hypertension[347] and thrombosis[212], no significant difference was observed in plasma TAT complexes or oxPLs in blood cells during AIA development. This indicates that *Alox15* has no impact on the increased coagulation during AIA, and suggests that *Alox12* is the most likely source of blood cells' eoxPLs during the development of AIA. This indicates that *Alox12* deletion might result in decreased levels of eoxPLs, and lead to reduced coagulation. During my PhD, the AIA model was generated in *Alox12*$^{-/-}$ mice. However, due to time restrictions, samples were collected but not analysed. Similar to the study performed in this thesis on *Alox15*$^{-/-}$ mice, described in Chapter 4 and Chapter 5, *Alox12*$^{-/-}$ mice need to be analysed for coagulation markers, inflammatory markers, and lipidomic studies performed in whole blood pellets.

In addition to coagulation, the joint was also studied during the development of AIA. *Alox15* deletion resulted in a worsened joint phenotype, with a slower resolution of knee swelling, and an increase in synovial infiltration. In addition, I found that on day 10 of AIA, oxPL levels were elevated in the joint tissue of WT but not in *Alox15*$^{-/-}$ mice. This suggests 12/15-LOX might play a protective role in arthritis, especially since oxPLs have been shown to induce an anti-oxidative response[276], and several *Alox15*-derived oxylipins, namely 13-HODE, 15-HETE and 12-HETE, are known PPARγ ligands, therefore suppressors of inflammatory responses. This is consistent with what is described in the literature, where the deletion of *Alox15* was described as detrimental in two distinct arthritis murine models[189]. Nevertheless, the role of *Alox15*-derived lipids in AIA should be further confirmed by providing lipid products, such as 15-HETE, 13-HODE and 12-HETE, which were significantly reduced upon *Alox15* deletion, into the joint of these knockout mice and analysing if this results in an amelioration of disease. In addition, *Alox12*$^{-/-}$ mice need to also be evaluated for arthritis score, and lipidomic studies performed in the joint tissue of these mice during AIA development, to understand whether 12-LOX also provides a protective response in arthritis.

Despite AIA being widely considered a local inflammatory arthritis model, increased systemic inflammation and coagulation was found in the circulation. This indicates that inflammation in joints could be responsible for inducing systemic effects. This suggests a bridge between joint and systemic disease, which might lead to an elevated incidence of thrombosis[91,344], resulting in the increase of cardiovascular risk, an important *comorbidity* in RA. Therefore, it is essential to further study the impact of systemic inflammation in RA, which might ultimately result in cardiovascular disease in these patients.

To complement the findings in the murine arthritis model, RA patients were studied, where an increase in thrombin generation was observed in EVs. In addition, an increase in the amount of aminoPL present in EVs of these patients may also contribute to an increase in thrombin generation since EVs have been described as increased in RA patients' plasma [152,296,306] derived mainly from platelet [296]. Therefore, the observed increase in thrombin generation by EVs from RA patients might be the result of increased EV numbers. To fully understand the impact of EVs in RA, plasma from both healthy controls and RA patients should be further analysed, by quantifying EVs, as well as determining surface area and cell of origin.

Along with this, an increased number of platelets were also found in RA patients. This is consistent with what is described clinically in other studies [150–152]. However, no significant differences were found in individual membrane phospholipid composition of both platelets and WBCs, relating to either oxPLs or aminoPLs exposure. Nevertheless, this elevated platelet number would lead to increased levels of these lipids in circulation. In support of this idea, an immunogenic response against oxPLs was observed in RA plasma, suggesting chronic increased oxPLs exposure in the circulation of these patients. To confirm this hypothesis, prothrombinase assays and oxPL analysis should be repeated without using a standardized number of platelets, and instead using the platelet count of each volunteer.

Despite, the increased incidence of thrombosis in RA, guidelines do not currently recommend long-term prophylactic anticoagulation therapy, with patients following the same rules as the general population[167,168]. Nevertheless, a cohort study has shown diminished coagulation biomarkers in early RA following antirheumatic treatment, especially after therapy with biological DMARDs, such as Tocilizumab and Certolizumab, IL-6 and TNF-α inhibitors respectively, in comparison with conventional DMARDs[180]. Overall, these results support the idea that by suppressing inflammation, thrombosis is also reduced.

To my knowledge, these findings are novel, providing new evidence to suggest that oxPLs derived from platelets, as well as EVs, may be important players in the increased thrombosis of RA patients, representing possible new therapeutic targets for this disease.

8.2 Limitations

The work presented in this thesis presents some limitations. First, all mice used in this thesis were male. This is unfortunately common in animal studies to prevent large data dispersion due to inter-individual variations, as well as the impact of hormone alterations. However, human RA affects more females than males[129], indicating fundament sex differences that need to be studied. Therefore, female mice should also be analysed in the future, as to confirm these results.

Power calculations for the mouse work were performed using an online sample size calculator [218], with data from a previous study on TAT complex values after the development of murine abdominal aorta aneurysm [212]. Despite being determined that each study group should be composed of at least 8 mice, this number was reduced to 4 in the case of both *IL6ra*$^{-/-}$ and *IL6*$^{-/-}$ mice, due to low mice availability. Nevertheless, no difference in TAT complex values was observed in these mice when compared to the naïve group. Power calculation using the TAT values from *IL6ra*$^{-/-}$ and *IL6*$^{-/-}$ mice during AIA development indicated that in order to see significant differences, an impossible number of experiments (≥100) needed to be conducted, which led to the experiment being stopped at the n of 4. In addition, a high data variation was found in PT values for both *IL6ra*$^{-/-}$ and *IL6*$^{-/-}$ mice (Figure 3.5). Despite the no significant difference found compared to the control naive, a higher number of mice could have provided a statistically significant result. Furthermore, for the chiral analysis, performed in Chapter 3, Section 3.2.7, due to the destructive effect of this analysis, only an n of 3 was analysed. In the case of *IL6*$^{-/-}$ mice, an n of 3 was run, however, one data point fell below the limits of detection of the LC/MS/MS, resulting in an n of 2 (Figure 3.10). More experiments are necessary to draw conclusions from the chiral analysis regarding the *IL6*$^{-/-}$ mice. In addition, more experiments are also necessary for the WBC counts within the different strains analysed (Figure 3.12). In Chapter 3, Section 3.2.9, a large variation of WBC was found between all the studied genotypes. However, only 3 or 4 n's were analysed, therefore more experiments might show if any differences in WBC counts are present between these mice.

When considering the human studies, a significant age difference was obtained between RA patients from the *Cardiff Regional Experimental Arthritis Treatment and Evaluation Centre* cohort and their healthy controls (Table 6.1). Furthermore, the sample collection from this cohort extended for a period of 26 months, which might cause some changes in oxPLs levels during storage. The impact of storage in oxidation was already been studied in lipids, where ex vivo synthesis of oxylipins was observed even when the storage was done at -80 °C after 26 weeks [348]. Unfortunately, my work was performed during a global pandemic that limited accessibility to RA patients and healthy volunteers. Indeed, despite meeting the initial objective of the power calculation to obtain statistical significance the sample size of this study is considered small and replication in a larger cohort would be important.

8.3 Future Directions

8.3.1 Studying the role of *Alox12* on AIA

During my PhD, AIA was generated in *Alox12*$^{-/-}$ mice. Unfortunately, due to time restrictions, samples were collected but not analysed. Similar to the study performed in this thesis on *Alox15*$^{-/-}$ mice, described in Chapter 4 and Chapter 5, *Alox12*$^{-/-}$ mice will be analysed for coagulation markers, inflammatory markers, and lipidomic studies will be performed in both whole blood pellets and joints, and histology will be performed, and arthritis score evaluated. This will provide further evidence of the cellular origin of the increased 12-HETE-PEs, and whether elevated TAT complexes observed in WT mice are related to this enzyme.

8.3.2 EVs count and analysis in RA patients

A total of 6 ml of plasma from each volunteer was used to isolate EVs and analysed in a non-standardized manner. Therefore, the observed increase in thrombin generation by EVs from RA patients might be the result of increased EV numbers. In fact, the elevated number of EVs has been heavily described in the literature.[152,296,306] In order to fully understand the impact of EVs in RA, plasma from both healthy controls and RA patients should be further analysed, by quantifying EVs, as well as determining surface area and cell of origin.

8.3.3 Confirming the increase oxPLs in circulation due to thrombocytosis in RA patients

Platelets were analysed during the thesis, using a specific platelet number, namely 2 x 10^8 platelets/ml, where no difference in thrombin generation or oxPLs composition was found. However, thrombocytosis is a common symptom found in RA[150–152], and also found in the *Cardiff Regional Experimental Arthritis Treatment and Evaluation Centre* patient cohort analysed in this thesis. The elevated platelet number in these patients might result in an overall increase in thrombin generation, in oxPLs in circulation and aminoPL exposure. However, in order to confirm this hypothesis, these assays should be repeated without using this standardized number of platelets, and instead using the platelet count of each volunteer.

8.3.4 Platelets as therapeutic targets for auto-immune coagulopathies

The role of platelets in arthritis has been previously described as attractive targets[349]. The work in my thesis goes further into suggesting, for the first time, the role of the pro-coagulant membrane of platelets in arthritis as a therapeutic target. The modulation of *Alox12*, namely the reduced activity of 12-LOX might result in decreased coagulation. Therefore, 12-LOX inhibitors should be investigated and studied in the context of thrombosis in arthritis.

8.4 Conclusion

In conclusion, this thesis set out to characterise procoagulant lipids in RA, through both murine models and human samples. To this end, LC/MS/MS was used to detect eoxPLs, along with oxylipin precursors. In addition, TF-independent coagulation assays were used in human cohort samples, while TAT complexes, D-dimers, CRP and SAA were quantified in arthritis murine mice. it was apparent that procoagulant lipids play a significant role in the increased thrombosis observed in arthritis, being elevated in mice during AIA development when TAT levels were increased. Furthermore, oxPLs in circulation, along with aminoPLs exposure, might increase as a result of thrombocytosis in RA patients. In addition, EVs from these patients displayed increased levels of thrombin generation. Overall, platelets (or platelet-derived EVs) emerged as important players in the elevated systemic coagulation in RA, due to their procoagulant lipid, setting oxPLs as possible therapeutic targets for the treatment of auto-immune associated coagulopathies.

References

Chapter 9

9 References

1. Hu, T. & Zhang, J.-L. L. Mass-spectrometry-based lipidomics. *J. Sep. Sci.* **41**, 351–372 (2018).

2. Triebl, A., Hartler, J., Trötzmüller, M. & C Köfeler, H. Lipidomics: Prospects from a technological perspective. *Biochim. Biophys. acta. Mol. cell Biol. lipids* **1862**, 740–746 (2017).

3. Dennis, E. A. & Norris, P. C. Eicosanoid storm in infection and inflammation. *Nat. Rev. Immunol.* **15**, 511–23 (2015).

4. Blanco, A. & Blanco, G. Lipids. in *Medical Biochemistry* 99–119 (Elsevier, 2017). doi:10.1016/B978-0-12-803550-4.00005-7.

5. O'Donnell, V. B., Aldrovandi, M., Murphy, R. C. & Krönke, G. Enzymatically oxidized phospholipids assume center stage as essential regulators of innate immunity and cell death. *Sci. Signal.* **12**, 1–13 (2019).

6. Smith, S. A. & Morrissey, J. H. Interactions Between Platelets and the Coagulation System. in *Platelets* 393–400 (Elsevier, 2019). doi:10.1016/B978-0-12-813456-6.00021-7.

7. Shindou, H. & Shimizu, T. Acyl-CoA:lysophospholipid acyltransferases. *J. Biol. Chem.* **284**, 1–5 (2009).

8. Tyurina, Y. Y. *et al.* Redox (phospho)lipidomics of signaling in inflammation and programmed cell death. *J. Leukoc. Biol.* **106**, 57–81 (2019).

9. Thomas, C. P. & O'Donnell, V. B. Oxidized phospholipid signaling in immune cells. *Curr. Opin. Pharmacol.* **12**, 471–7 (2012).

10. Braverman, N. E. & Moser, A. B. Functions of plasmalogen lipids in health and disease. *Biochim. Biophys. Acta* **1822**, 1442–52 (2012).

11. Calder, P. C. Dietary arachidonic acid: harmful, harmless or helpful? *Br. J. Nutr.* **98**, 451–3 (2007).

12. Sonnweber, T., Pizzini, A., Nairz, M., Weiss, G. & Tancevski, I. Arachidonic Acid Metabolites in Cardiovascular and Metabolic Diseases. *Int. J. Mol. Sci.* **19**, 3285 (2018).

13. Mouchlis, V. D. & Dennis, E. A. Phospholipase A2 catalysis and lipid mediator lipidomics. *Biochim. Biophys. acta. Mol. cell Biol. lipids* **1864**, 766–771 (2019).

14. Gibellini, F. & Smith, T. K. The Kennedy pathway--De novo synthesis of phosphatidylethanolamine and phosphatidylcholine. *IUBMB Life* **62**, 414–28 (2010).

15. Hishikawa, D., Hashidate, T., Shimizu, T. & Shindou, H. Diversity and function of membrane glycerophospholipids generated by the remodeling pathway in mammalian cells. *J. Lipid Res.* **55**, 799–807 (2014).

16. Wang, B. & Tontonoz, P. Phospholipid Remodeling in Physiology and Disease. *Annu. Rev. Physiol.* **81**, 165–188 (2019).

17. Moreno, J. J. New aspects of the role of hydroxyeicosatetraenoic acids in cell growth and cancer development. *Biochem. Pharmacol.* **77**, 1–10 (2009).

18. Folco, G. & Murphy, R. C. Eicosanoid transcellular biosynthesis: from cell-cell interactions to in

vivo tissue responses. *Pharmacol. Rev.* **58**, 375–88 (2006).

19. Dennis, E. A., Rhee, S. G., Billah, M. M. & Hannun, Y. A. Role of phospholipase in generating lipid second messengers in signal transduction. *FASEB J.* **5**, 2068–77 (1991).

20. Rieger, G. M., Hein, R., Adelmann-Grill, B. C., Ruzicka, T. & Krieg, T. Influence of eicosanoids on fibroblast chemotaxis and protein synthesis in vitro. *J. Dermatol. Sci.* **1**, 347–54 (1990).

21. Miller, A. W. *et al.* Arachidonic acid-induced vasodilation of rat small mesenteric arteries is lipoxygenase-dependent. *J. Pharmacol. Exp. Ther.* **304**, 139–44 (2003).

22. Nie, D., Tang, K., Diglio, C. & Honn, K. V. Eicosanoid regulation of angiogenesis: role of endothelial arachidonate 12-lipoxygenase. *Blood* **95**, 2304–11 (2000).

23. Ricciotti, E. & FitzGerald, G. A. Prostaglandins and inflammation. *Arterioscler. Thromb. Vasc. Biol.* **31**, 986–1000 (2011).

24. Wu, C.-C., Gupta, T., Garcia, V., Ding, Y. & Schwartzman, M. L. 20-HETE and blood pressure regulation: clinical implications. *Cardiol. Rev.* **22**, 1–12 (2014).

25. Nayeem, M. A. Role of oxylipins in cardiovascular diseases. *Acta Pharmacol. Sin.* **39**, 1142–1154 (2018).

26. Yousefi, B., Jadidi-Niaragh, F., Azizi, G., Hajighasemi, F. & Mirshafiey, A. The role of leukotrienes in immunopathogenesis of rheumatoid arthritis. *Mod. Rheumatol.* **24**, 225–35 (2014).

27. Serhan, C. N. Resolution phase of inflammation: novel endogenous anti-inflammatory and proresolving lipid mediators and pathways. *Annu. Rev. Immunol.* **25**, 101–37 (2007).

28. Buckley, C. D., Gilroy, D. W. & Serhan, C. N. Proresolving lipid mediators and mechanisms in the resolution of acute inflammation. *Immunity* **40**, 315–27 (2014).

29. Schebb, N. H. *et al.* Formation, Signaling and Occurrence of Specialized Pro-Resolving Lipid Mediators-What is the Evidence so far? *Front. Pharmacol.* **13**, 838782 (2022).

30. Diskin, C. *et al.* 4-Octyl-Itaconate and Dimethyl Fumarate Inhibit COX2 Expression and Prostaglandin Production in Macrophages. *J. Immunol.* **207**, 2561–2569 (2021).

31. Willenberg, I., Ostermann, A. I. & Schebb, N. H. Targeted metabolomics of the arachidonic acid cascade: current state and challenges of LC-MS analysis of oxylipins. *Anal. Bioanal. Chem.* **407**, 2675–2683 (2015).

32. Serhan, C. N. *et al.* Resolution of inflammation: state of the art, definitions and terms. *FASEB J.* **21**, 325–32 (2007).

33. Fullerton, J. N. & Gilroy, D. W. Resolution of inflammation: a new therapeutic frontier. *Nat. Rev. Drug Discov.* **15**, 551–67 (2016).

34. Mashima, R. & Okuyama, T. The role of lipoxygenases in pathophysiology; new insights and future perspectives. *Redox Biol.* **6**, 297–310 (2015).

35. Kobe, M. J. & Newcomer, M. E. Lipoxygenase Pathway of the Arachidonate Cascade. in *eLS* (Wiley, 2013). doi:10.1002/9780470015902.a0023400.

36. Brash, A. R. Lipoxygenases: occurrence, functions, catalysis, and acquisition of substrate. *J. Biol. Chem.* **274**, 23679–82 (1999).

37. Newcomer, M. E. & Brash, A. R. The structural basis for specificity in lipoxygenase catalysis. *Protein Sci.* **24**, 298–309 (2015).

38. Gaffney, B. J. Connecting Lipoxygenase Function to Structure by Electron Paramagnetic Resonance. *Acc. Chem. Res.* **47**, 3588–3595 (2014).

39. Liavonchanka, A. & Feussner, I. Lipoxygenases: Occurrence, functions and catalysis. *J. Plant Physiol.* **163**, 348–357 (2006).

40. Schneider, C., Pratt, D. A., Porter, N. A. & Brash, A. R. Control of oxygenation in lipoxygenase and cyclooxygenase catalysis. *Chem. Biol.* **14**, 473–88 (2007).

41. Samuelsson, B., Dahlén, S. E., Lindgren, J. A., Rouzer, C. A. & Serhan, C. N. Leukotrienes and lipoxins: structures, biosynthesis, and biological effects. *Science* **237**, 1171–6 (1987).

42. Hajeyah, A. A., Griffiths, W. J., Wang, Y., Finch, A. J. & O'Donnell, V. B. The Biosynthesis of Enzymatically Oxidized Lipids. *Front. Endocrinol. (Lausanne).* **11**, 591819 (2020).

43. Kuklev, D. V. *et al.* Synthesis of keto- and hydroxydienoic compounds from linoleic acid. *Chem. Phys. Lipids* **85**, 125–134 (1997).

44. Vangaveti, V., Baune, B. T. & Kennedy, R. L. Hydroxyoctadecadienoic acids: novel regulators of macrophage differentiation and atherogenesis. *Ther. Adv. Endocrinol. Metab.* **1**, 51–60 (2010).

45. Håkansson, I. *et al.* Oxylipins in cerebrospinal fluid in clinically isolated syndrome and relapsing remitting multiple sclerosis. (2018) doi:10.1016/j.prostaglandins.2018.08.003.

46. Feldstein, A. E. *et al.* Mass spectrometric profiling of oxidized lipid products in human nonalcoholic fatty liver disease and nonalcoholic steatohepatitis. *J. Lipid Res.* **51**, 3046–3054 (2010).

47. Jostarndt, K. *et al.* Dissociation of apoptosis induction and CD36 upregulation by enzymatically modified low-density lipoprotein in monocytic cells. *Biochem. Biophys. Res. Commun.* **290**, 988–993 (2002).

48. Hampel, J. K. A. *et al.* Differential modulation of cell cycle, apoptosis and PPARγ2 gene expression by PPARγ agonists ciglitazone and 9-hydroxyoctadecadienoic acid in monocytic cells. *Prostaglandins Leukot. Essent. Fat. Acids* **74**, 283–293 (2006).

49. Wuest, S. J. A., Crucet, M., Gemperle, C., Loretz, C. & Hersberger, M. Expression and regulation of 12/15-lipoxygenases in human primary macrophages. *Atherosclerosis* **225**, 121–7 (2012).

50. Brash, A. R., Boeglin, W. E. & Chang, M. S. Discovery of a second 15S-lipoxygenase in humans. *Proc. Natl. Acad. Sci. U. S. A.* **94**, 6148–52 (1997).

51. Krieg, P. *et al.* Epidermis-type lipoxygenases. *Adv. Exp. Med. Biol.* **507**, 165–170 (2002).

52. Snodgrass, R. G. & Brüne, B. Regulation and Functions of 15-Lipoxygenases in Human Macrophages. *Front. Pharmacol.* **10**, (2019).

53. Ivanov, I., Kuhn, H. & Heydeck, D. Structural and functional biology of arachidonic acid 15-lipoxygenase-1 (ALOX15). *Gene* **573**, 1–32 (2015).

54. Bryant, R. W., Bailey, J. M., Schewe, T. & Rapoport, S. M. Positional specificity of a reticulocyte lipoxygenase. Conversion of arachidonic acid to 15-S-hydroperoxy-eicosatetraenoic acid. *J. Biol. Chem.* **257**, 6050–5 (1982).

55. Kuhn, H. *et al.* The evolutionary hypothesis of reaction specificity of mammalian ALOX15 orthologs. *Prog. Lipid Res.* **72**, 55–74 (2018).

56. Ornelas, A. *et al.* Beyond COX-1: the effects of aspirin on platelet biology and potential mechanisms of chemoprevention. (2017) doi:10.1007/s10555-017-9675-z.

57. Williams, C. S., Mann, M. & DuBois, R. N. The role of cyclooxygenases in inflammation, cancer, and development. *Oncogene* **18**, 7908–16 (1999).

58. Tejera, N., Boeglin, W. E., Suzuki, T. & Schneider, C. COX-2-dependent and -independent biosynthesis of dihydroxy-arachidonic acids in activated human leukocytes. *J. Lipid Res.* **53**, 87–94 (2012).

59. Rowlinson, S. W. *et al.* Spatial requirements for 15-(R)-hydroxy-5Z,8Z,11Z, 13E-eicosatetraenoic acid synthesis within the cyclooxygenase active site of murine COX-2. Why acetylated COX-1 does not synthesize 15-(R)-hete. *J. Biol. Chem.* **275**, 6586–91 (2000).

60. Mulugeta, S. *et al.* Identification and absolute configuration of dihydroxy-arachidonic acids formed by oxygenation of 5S-HETE by native and aspirin-acetylated COX-2. *J. Lipid Res.* **51**, 575–85 (2010).

61. Capdevila, J. H., Wang, W. & Falck, J. R. Arachidonic acid monooxygenase: Genetic and biochemical approaches to physiological/pathophysiological relevance. *Prostaglandins Other Lipid Mediat.* **120**, 40–49 (2015).

62. Gross, G. J. *et al.* Cytochrome P450 and arachidonic acid metabolites: Role in myocardial ischemia/reperfusion injury revisited. *Cardiovascular Research* vol. 68 18–25 (2005).

63. Morgan, A. H. *et al.* Phosphatidylethanolamine-esterified eicosanoids in the mouse. Tissue localization and inflammation-dependent formation in Th-2 disease. *J. Biol. Chem.* **284**, 21185–21191 (2009).

64. O'Donnell, V. B. & Murphy, R. C. Directing eicosanoid esterification into phospholipids. *J. Lipid Res.* **58**, 837–839 (2017).

65. Clark, S. R. *et al.* Esterified eicosanoids are acutely generated by 5-lipoxygenase in primary human neutrophils and in human and murine infection. *Blood* **117**, 2033–2043 (2011).

66. Gijón, M. A., Riekhof, W. R., Zarini, S., Murphy, R. C. & Voelker, D. R. Lysophospholipid acyltransferases and arachidonate recycling in human neutrophils. *J. Biol. Chem.* **283**, 30235–45 (2008).

67. Guimarães, R. C., Gonçalves, T. T. & Leiria, L. O. Exploiting oxidized lipids and the lipid-binding GPCRs against cardiometabolic diseases. *Br. J. Pharmacol.* **178**, 531–549 (2021).

68. Slatter, D. A. *et al.* Enzymatically oxidized phospholipids restore thrombin generation in coagulation factor deficiencies. *JCI insight* **3**, 12–14 (2018).

69. Hammond, V. J. *et al.* Novel keto-phospholipids are generated by monocytes and macrophages, detected in cystic fibrosis, and activate peroxisome proliferator-activated receptor-γ. *J. Biol. Chem.* **287**, 41651–41666 (2012).

70. Greig, F. H., Kennedy, S. & Spickett, C. M. Physiological effects of oxidized phospholipids and their cellular signaling mechanisms in inflammation. *Free Radic. Biol. Med.* **52**, 266–80 (2012).

71. Bochkov, V. N. & Leitinger, N. Anti-inflammatory properties of lipid oxidation products. *J. Mol.*

Med. **81**, 613–626 (2003).

72. Hu, C. & Ma, S. Recent development of lipoxygenase inhibitors as anti-inflammatory agents. *Medchemcomm* **9**, 212–225 (2018).

73. Elliott, M. R., Koster, K. M. & Murphy, P. S. Efferocytosis signaling in the regulation of macrophage inflammatory responses. doi:10.4049/jimmunol.1601520.

74. Kolb, J. P., Oguin Iii, T. H., Oberst, A. & Martinez, J. Programmed Cell Death and Inflammation: Winter is Coming. doi:10.1016/j.it.2017.06.009.

75. Uderhardt, S. *et al.* 12/15-lipoxygenase orchestrates the clearance of apoptotic cells and maintains immunologic tolerance. *Immunity* **36**, 834–46 (2012).

76. Krönke, G. *et al.* 12/15-Lipoxygenase Counteracts Inflammation and Tissue Damage in Arthritis. *J. Immunol.* **183**, 3383–3389 (2009).

77. Kagan, V. E. *et al.* Appetizing rancidity of apoptotic cells for macrophages: oxidation, externalization, and recognition of phosphatidylserine. *Am. J. Physiol. Lung Cell. Mol. Physiol.* **285**, L1-17 (2003).

78. Wahli, W. & Michalik, L. PPARs at the crossroads of lipid signaling and inflammation. *Trends Endocrinol. Metab.* **23**, 351–63 (2012).

79. Umeno, A. *et al.* Comprehensive analysis of PPARγ agonist activities of stereo-, regio-, and enantio-isomers of hydroxyoctadecadienoic acids. *Biosci. Rep.* **40**, (2020).

80. Itoh, T. *et al.* Structural basis for the activation of PPARgamma by oxidized fatty acids. *Nat. Struct. Mol. Biol.* **15**, 924–31 (2008).

81. Nagy, L., Tontonoz, P., Alvarez, J. G. A., Chen, H. & Evans, R. M. Oxidized LDL regulates macrophage gene expression through ligand activation of PPARgamma. *Cell* **93**, 229–40 (1998).

82. Ricote, M., Li, A. C., Willson, T. M., Kelly, C. J. & Glass, C. K. The peroxisome proliferator-activated receptor-gamma is a negative regulator of macrophage activation. *Nature* **391**, 79–82 (1998).

83. Krönke, G. *et al.* Expression of heme oxygenase-1 in human vascular cells is regulated by peroxisome proliferator-activated receptors. *Arterioscler. Thromb. Vasc. Biol.* **27**, 1276–82 (2007).

84. Villanueva, C. J. & Tontonoz, P. Licensing PPARγ to Work in Macrophages. *Immunity* **33**, 647–649 (2010).

85. Huang, J. T. *et al.* Interleukin-4-dependent production of PPAR-γ ligands in macrophages by 12/15-lipoxygenase. *Nature* **400**, 378–382 (1999).

86. Marder, W. *et al.* The peroxisome proliferator activated receptor-γ pioglitazone improves vascular function and decreases disease activity in patients with rheumatoid arthritis. *J. Am. Heart Assoc.* **2**, e000441 (2013).

87. Ma, J.-D. *et al.* Activation of the Peroxisome Proliferator-Activated Receptor γ Coactivator 1β/NFATc1 Pathway in Circulating Osteoclast Precursors Associated With Bone Destruction in Rheumatoid Arthritis. *Arthritis Rheumatol. (Hoboken, N.J.)* **71**, 1252–1264 (2019).

88. Palma, A. *et al.* Peroxisome proliferator-activated receptor-gamma expression in monocytes/macrophages from rheumatoid arthritis patients: relation to disease activity and

therapy efficacy--a pilot study. *Rheumatology (Oxford).* **51**, 1942–52 (2012).

89. Wu, M.-Y. *et al.* Involvement of 15-lipoxygenase in the inflammatory arthritis. *J. Cell. Biochem.* **113**, 2279–89 (2012).

90. Navickas, R., Petric, V.-K., Feigl, A. B. & Seychell, M. Multimorbidity: What Do We Know? What Should We Do? *J. Comorbidity* **6**, 4–11 (2016).

91. Mameli, A., Barcellona, D. & Marongiu, F. Rheumatoid arthritis and thrombosis. *Clin. Exp. Rheumatol.* **27**, 846–55 (2009).

92. Opal, S. M. Phylogenetic and functional relationships between coagulation and the innate immune response. *Crit. Care Med.* **28**, S77–S80 (2000).

93. Aird, W. C. Coagulation. *Crit. Care Med.* **33**, S485-7 (2005).

94. Chang, J. C. Hemostasis based on a novel 'two-path unifying theory' and classification of hemostatic disorders. *Blood Coagul. Fibrinolysis* **29**, 1 (2018).

95. Palta, S., Saroa, R. & Palta, A. Overview of the coagulation system. *Indian J. Anaesth.* **58**, 515 (2014).

96. Chaudhry, R. & Babiker, H. M. *Physiology, Coagulation Pathways*. *StatPearls* (StatPearls Publishing, 2020).

97. Ratnoff, O. D. & Colopy, J. E. A familial hemorrhagic trait associated with a deficiency of a clot-promoting fraction of plasma. *J. Clin. Invest.* **34**, 602–13 (1955).

98. Monroe, D. M. & Hoffman, M. What does it take to make the perfect clot? *Arterioscler. Thromb. Vasc. Biol.* **26**, 41–48 (2006).

99. Müller, F. *et al.* Platelet Polyphosphates Are Proinflammatory and Procoagulant Mediators In Vivo. *Cell* **139**, 1143–1156 (2009).

100. Arnout, J., Hoylaerts, M. F. & Lijnen, H. R. Haemostasis. in *The Vascular Endothelium II* 1–41 (Springer Berlin Heidelberg, 2006). doi:10.1007/3-540-36028-X_1.

101. Gale, A. J. Current Understanding of Hemostasis. *Toxicol. Pathol.* **39**, 273–280 (2011).

102. Pérez-Gómez, F. & Bover, R. La nueva cascada de la coagulación y su posible influencia en el difícil equilibrio entre trombosis y hemorragia. *Revista Espanola de Cardiologia* vol. 60 1217–1219 (2007).

103. Petelska, A. D., Kazimierska-Drobny, K., Janicka, K., Majewski, T. & Urbaniak, W. Understanding the unique role of phospholipids in the lubrication of natural joints: An interfacial tension study. *Coatings* **9**, 264 (2019).

104. De Caterina, R. *et al.* General mechanisms of coagulation and targets of anticoagulants (Section I). *Thromb. Haemost.* **109**, 569–579 (2013).

105. Belyaev, A. V, Panteleev, M. A. & Ataullakhanov, F. I. Threshold of microvascular occlusion: injury size defines the thrombosis scenario. *Biophys. J.* **109**, 450–6 (2015).

106. Rau, J. C., Beaulieu, L. M., Huntington, J. A. & Church, F. C. Serpins in thrombosis, hemostasis and fibrinolysis. *J. Thromb. Haemost.* **5 Suppl 1**, 102–15 (2007).

107. Walenga, J. M. Normal hemostasis. in *Rodak's Hematology* (ed. Elaine M. Keohane, Catherine

N. Otto, J. M. W.) 626–649 (Elsevier, 2020). doi:10.1016/B978-0-323-53045-3.00044-1.

108. Becker, R. C. Seminars in thrombosis, thrombolysis, and vascular biology. 6. Procoagulant states. *Cardiology* **80**, 51–64 (1992).

109. Raskob, G. E. *et al.* Thrombosis: A major contributor to global disease burden. *Thromb. Res.* **134**, 931–938 (2014).

110. Clemetson, K. J. Platelets and primary haemostasis. *Thromb. Res.* **129**, 220–224 (2012).

111. Furie, B. & Furie, B. C. Mechanisms of thrombus formation. *N. Engl. J. Med.* **359**, 938–49 (2008).

112. Engelmann, B. & Massberg, S. Thrombosis as an intravascular effector of innate immunity. *Nature Reviews Immunology* vol. 13 34–45 (2013).

113. Wakefield, T. W. *et al.* Venous thrombosis-associated inflammation and attenuation with neutralizing antibodies to cytokines and adhesion molecules. *Arterioscler. Thromb. Vasc. Biol.* **15**, 258–268 (1995).

114. Swystun, L. L. & Liaw, P. C. The role of leukocytes in thrombosis. *Blood* **128**, 753–762 (2016).

115. Gaertner, F. & Massberg, S. Blood coagulation in immunothrombosis-At the frontline of intravascular immunity. *Semin. Immunol.* **28**, 561–569 (2016).

116. Schulz, C., Engelmann, B. & Massberg, S. Crossroads of coagulation and innate immunity: The case of deep vein thrombosis. *J. Thromb. Haemost.* **11**, 233–241 (2013).

117. von Brühl, M.-L. *et al.* Monocytes, neutrophils, and platelets cooperate to initiate and propagate venous thrombosis in mice in vivo. *J. Exp. Med.* **209**, 819–35 (2012).

118. Massberg, S. *et al.* Reciprocal coupling of coagulation and innate immunity via neutrophil serine proteases. *Nat. Med.* **16**, 887–896 (2010).

119. Chou, J. *et al.* Hematopoietic cell-derived microparticle tissue factor contributes to fibrin formation during thrombus propagation. *Blood* **104**, 3190–3197 (2004).

120. Palankar, R. & Greinacher, A. Challenging the concept of immunothrombosis. *Blood* **133**, 508–509 (2019).

121. Bevers, E. M., Comfurius, P., Dekkers, D. W. C. & Zwaal, R. F. A. Lipid translocation across the plasma membrane of mammalian cells. *Biochim. Biophys. Acta - Mol. Cell Biol. Lipids* **1439**, 317–330 (1999).

122. Devaux, P. F., Herrmann, A., Ohlwein, N. & Kozlov, M. M. How lipid flippases can modulate membrane structure. *Biochim. Biophys. Acta* **1778**, 1591–600 (2008).

123. Tavoosi, N. *et al.* Molecular determinants of phospholipid synergy in blood clotting. *J. Biol. Chem.* **286**, 23247–23253 (2011).

124. Zwaal, R. F. A., Comfurius, P. & Bevers, E. M. Lipid-protein interactions in blood coagulation. *Biochimica et Biophysica Acta - Reviews on Biomembranes* vol. 1376 433–453 (1998).

125. Lauder, S. N. *et al.* Networks of enzymatically oxidized membrane lipids support calcium-dependent coagulation factor binding to maintain hemostasis. *Sci Signal* **10**, (2017).

126. Bochkov, V. N. *et al.* Oxidized phospholipids stimulate tissue factor expression in human endothelial cells via activation of ERK/EGR-1 and Ca(++)/NFAT. *Blood* **99**, 199–206 (2002).

127. Scott, D. L., Wolfe, F. & Huizinga, T. W. Rheumatoid arthritis. *Lancet* **376**, 1094–1108 (2010).

128. Smolen, J. S., Aletaha, D. & McInnes, I. B. Rheumatoid arthritis. *Lancet (London, England)* **388**, 2023–2038 (2016).

129. Finckh, A. *et al.* Global epidemiology of rheumatoid arthritis. *Nat. Rev. Rheumatol.* (2022) doi:10.1038/s41584-022-00827-y.

130. Balogh, E. *et al.* Oxidative stress impairs energy metabolism in primary cells and synovial tissue of patients with rheumatoid arthritis. doi:10.1186/s13075-018-1592-1.

131. Yap, H. Y. *et al.* Pathogenic Role of Immune Cells in Rheumatoid Arthritis: Implications in Clinical Treatment and Biomarker Development. *Cells* **7**, (2018).

132. Smolen, J. S., Aletaha, D. & McInnes, I. B. Rheumatoid arthritis. *Lancet* **388**, 2023–2038 (2016).

133. Dennis, G. *et al.* Synovial phenotypes in rheumatoid arthritis correlate with response to biologic therapeutics. *Arthritis Res. Ther.* **16**, R90 (2014).

134. Lewis, M. J. *et al.* Molecular Portraits of Early Rheumatoid Arthritis Identify Clinical and Treatment Response Phenotypes. *Cell Rep.* **28**, 2455-2470.e5 (2019).

135. Watson, D. J., Rhodes, T. & Guess, H. A. All-cause mortality and vascular events among patients with rheumatoid arthritis, osteoarthritis, or no arthritis in the UK General Practice Research Database. **30**, 1196–202 (2003).

136. Martel-Pelletier, J. *et al.* Osteoarthritis. *Nat. Rev. Dis. Prim.* **2**, 16072 (2016).

137. Robinson, W. H. *et al.* Low-grade inflammation as a key mediator of the pathogenesis of osteoarthritis. *Nat. Rev. Rheumatol.* **12**, 580 (2016).

138. Ropes, M. W., Rossmeisl, E. C. & Bauer, W. THE ORIGIN AND NATURE OF NORMAL HUMAN SYNOVIAL FLUID 12. *J. Clin. Invest.* **19**, 795–799 (1940).

139. Jónasdóttir, H. S. *et al.* Targeted lipidomics reveals activation of resolution pathways in knee osteoarthritis in humans. *Osteoarthr. Cartil.* **25**, 1150–1160 (2017).

140. Mustonen, A. M. *et al.* Distinct fatty acid signatures in infrapatellar fat pad and synovial fluid of patients with osteoarthritis versus rheumatoid arthritis. *Arthritis Res. Ther.* **21**, (2019).

141. Gálvez, J. *et al.* Microscopic rice bodies in rheumatoid synovial fluid sediments. *J. Rheumatol.* **19**, 1851–8 (1992).

142. So, A. K. *et al.* Arthritis is linked to local and systemic activation of coagulation and fibrinolysis pathways. *J. Thromb. Haemost.* **1**, 2510–2515 (2003).

143. Busso, N., Morard, C., Salvi, R., Péclat, V. & So, A. Role of the tissue factor pathway in synovial inflammation. *Arthritis Rheum.* **48**, 651–659 (2003).

144. Weinberg, J. B., Pippen, A. M. M. & Greenberg, C. S. Extravascular fibrin formation and dissolution in synovial tissue of patients with osteoarthritis and rheumatoid arthritis. *Arthritis Rheum.* **34**, 996–1005 (1991).

145. Beinsberger, J., Heemskerk, J. W. M. & Cosemans, J. M. E. M. Chronic arthritis and cardiovascular disease: altered blood parameters give rise to a prothrombotic propensity. *Semin. Arthritis Rheum.* **44**, 345–52 (2014).

146. Gabazza, E. C. *et al.* Correlation between clotting and collagen metabolism markers in rheumatoid arthritis. *Thromb. Haemost.* **71**, 199–202 (1994).

147. Carmassi, F. *et al.* Assessment of coagulation and fibrinolysis in synovial fluid of rheumatoid arthritis patients. *Fibrinolysis* **8**, 162–171 (1994).

148. Conn, D. L., McDuffie, F. C., Kazmier, F. J., Schroeter, A. L. & Sun, N. C. J. Coagulation abnormalities in rheumatoid disease. *Arthritis Rheum. Off. J. Am. Coll. Rheumatol.* **19**, 1237–1243 (1976).

149. Jurado, M., Páramo, J. A., Gutierrez-Pimentel, M. & Rocha, E. Fibrinolytic potential and antiphospholipid antibodies in systemic lupus erythematosus and other connective tissue disorders. *Thromb. Haemost.* **68**, 516–20 (1992).

150. Farr, M. *et al.* Thrombocytosis of active rheumatoid disease. *Ann. Rheum. Dis.* **42**, 545–549 (1983).

151. Milovanovic, M., Nilsson, E. & Järemo, P. Relationships between platelets and inflammatory markers in rheumatoid arthritis. *Clin. Chim. Acta* **343**, 237–240 (2004).

152. Knijff-Dutmer, E. A. J. J., Koerts, J., Nieuwland, R., Kalsbeek-Batenburg, E. M. & Van De Laar, M. A. F. J. F. J. Elevated levels of platelet microparticles are associated with disease activity in rheumatoid arthritis. *Arthritis Rheum.* **46**, 1498–1503 (2002).

153. Roshal, M. Prothrombin Time. in *Transfusion Medicine and Hemostasis* 799–803 (Elsevier, 2013). doi:10.1016/B978-0-12-397164-7.00124-5.

154. Ignjatovic, V. Thrombin Clotting Time. in 131–138 (Humana Press, Totowa, NJ, 2013). doi:10.1007/978-1-62703-339-8_10.

155. Reitsma, P. H., Versteeg, H. H. & Middeldorp, S. Mechanistic View of Risk Factors for Venous Thromboembolism. *Arterioscler. Thromb. Vasc. Biol.* **32**, 563–568 (2012).

156. van Hinsbergh, V. W. M. Endothelium--role in regulation of coagulation and inflammation. *Semin. Immunopathol.* **34**, 93–106 (2012).

157. Hoppe, B. & Dörner, T. Coagulation and the fibrin network in rheumatic disease: A role beyond haemostasis. *Nat. Rev. Rheumatol.* **8**, 738–746 (2012).

158. Schouten, M., Wiersinga, W. J., Levi, M. & van der Poll, T. Inflammation, endothelium, and coagulation in sepsis. *J. Leukoc. Biol.* **83**, 536–545 (2008).

159. Guillevin, L. & Dörner, T. Vasculitis: mechanisms involved and clinical manifestations. *Arthritis Res. Ther.* **9**, S9 (2007).

160. Mackman, N. Triggers, targets and treatments for thrombosis. *Nat. 2008 4517181* **451**, 914–918 (2008).

161. Roman, M. J. *et al.* Preclinical carotid atherosclerosis in patients with rheumatoid arthritis. *Ann. Intern. Med.* **144**, 249–56 (2006).

162. Liao, K. P. *et al.* The association between reduction in inflammation and changes in lipoprotein levels and HDL cholesterol efflux capacity in rheumatoid arthritis. *J Am Hear. Assoc* **4**, (2015).

163. McGrath, C. M. & Young, S. P. Lipid and Metabolic Changes in Rheumatoid Arthritis. *Curr Rheumatol Rep* **17**, 57 (2015).

164. Han, C. *et al.* Cardiovascular disease and risk factors in patients with rheumatoid arthritis, psoriatic arthritis, and ankylosing spondylitis. *J. Rheumatol.* **33**, (2006).

165. Aubry, M.-C. *et al.* Differences in atherosclerotic coronary heart disease between subjects with and without rheumatoid arthritis. *J. Rheumatol.* **34**, 937–42 (2007).

166. Skeoch, | July ; & Bruce, S. N. Atherosclerosis in rheumatoid arthritis: is it all about inflammation? *Nat. Rev. Rheumatol* **11**, 390–400 (2015).

167. Matta, F., Singala, R., Yaekoub, A. Y., Najjar, R. & Stein, P. D. Risk of venous thromboembolism with rheumatoid arthritis. *Thromb. Haemost.* **101**, 134–8 (2009).

168. Ketfi, C. *et al.* Risk of venous thromboembolism in rheumatoid arthritis. *Jt. bone spine* **88**, 105122 (2021).

169. Lee, J. J. & Pope, J. E. A meta-analysis of the risk of venous thromboembolism in inflammatory rheumatic diseases. *Arthritis Res Ther* **16**, 435 (2014).

170. Smith, B. D. & La Celle, P. L. Blood viscosity and thrombosis: clinical considerations. *Prog. Hemost. Thromb.* **6**, 179–201 (1982).

171. Ertenli, I. *et al.* Pathologic thrombopoiesis of rheumatoid arthritis. *Rheumatol. Int.* **23**, 49–60 (2003).

172. Schafer, A. I. Effects of nonsteroidal antiinflammatory drugs on platelet function and systemic hemostasis. *J. Clin. Pharmacol.* **35**, 209–19 (1995).

173. Lebois, M. & Josefsson, E. C. Regulation of platelet lifespan by apoptosis. *Platelets* **27**, 497–504 (2016).

174. Smolen, J. S., van der Heijde, D., Machold, K. P., Aletaha, D. & Landewé, R. Proposal for a new nomenclature of disease-modifying antirheumatic drugs. *Ann. Rheum. Dis.* **73**, 3–5 (2014).

175. Mian, A., Ibrahim, F. & Scott, D. L. A systematic review of guidelines for managing rheumatoid arthritis. *BMC Rheumatol.* **3**, 42 (2019).

176. European Medicines Agency. *EMA confirms Xeljanz to be used with caution in patients at high risk of blood clots*. www.ema.europa.eu/contact (2019) doi:EMA/608520/2019.

177. Food and Drug Admistration. *FDA approves Boxed Warning about increased risk of blood clots and death with higher dose of arthritis and ulcerative colitis medicine tofacitinib (Xeljanz, Xeljanz XR)*. https://www.fda.gov/drugs/drug-safety-and-availability/fda-approves-boxed-warning-about-increased-risk-blood-clots-and-death-higher-dose-arthritis-and (2019).

178. Kim, S. C. *et al.* Risk of Venous Thromboembolism in Patients with Rheumatoid Arthritis: Initiating Disease-Modifying Antirheumatic Drugs. *Am. J. Med.* **128**, 539.e7-539.e17 (2015).

179. Davies, R. *et al.* Venous thrombotic events are not increased in patients with rheumatoid arthritis treated with anti-TNF therapy: results from the British Society for Rheumatology Biologics Register. *Ann. Rheum. Dis.* **70**, 1831–1834 (2011).

180. Dijkshoorn, B. *et al.* OP0059 PROFOUND ANTICOAGULANT EFFECTS OF INITIAL ANTIRHEUMATIC TREATMENTS IN EARLY RHEUMATOID ARTHRITIS PATIENTS: A NORD-STAR SPIN-OFF STUDY. *Ann. Rheum. Dis.* **81**, 40–41 (2022).

181. Prete, P. E. E., Gurakar-Osborne, A. & Kashyap, M. L. L. Synovial fluid lipids and apolipoproteins: a contemporary perspective. *Biorheology* **32**, 1–16 (1995).

182. Crofford, L. J. *et al.* Cyclooxygenase-1 and -2 expression in rheumatoid synovial tissues. Effects of interleukin-1 beta, phorbol ester, and corticosteroids. *J. Clin. Invest.* **93**, 1095–1101 (1994).

183. Gheorghe, K. R. *et al.* Expression of 5-lipoxygenase and 15-lipoxygenase in rheumatoid arthritis synovium and effects of intraarticular glucocorticoids. *Arthritis Res. Ther.* **11**, R83 (2009).

184. Davidson, E. M., Rae, S. A. & Smith, M. J. H. H. *Leukotriene B4, a mediator of inflammation present in synovial fluid in rheumatoid arthritis*. *Annals of the Rheumatic Diseases* vol. 42 677–679 (Ann Rheum Dis, 1983).

185. Lin, H.-C. C. *et al.* 5-lipoxygenase inhibitors attenuate TNF-α-Induced inflammation in human synovial fibroblasts. *PLoS One* **9**, (2014).

186. Giera, M. *et al.* Lipid and lipid mediator profiling of human synovial fluid in rheumatoid arthritis patients by means of LC-MS/MS. *Biochim Biophys Acta* **1821**, 1415–1424 (2012).

187. Griffiths, R. J. *et al.* Leukotriene B4 plays a critical role in the progression of collagen-induced arthritis. *Proc. Natl. Acad. Sci.* **92**, 517–521 (1995).

188. Chabane, N. *et al.* Human articular chondrocytes express 15-lipoxygenase-1 and -2: potential role in osteoarthritis. *Arthritis Res. Ther.* **11**, R44 (2009).

189. Krönke, G. *et al.* 12/15-lipoxygenase counteracts inflammation and tissue damage in arthritis. *J. Immunol.* **183**, 3383–9 (2009).

190. Chen, K. *et al.* Increased 15-lipoxygenase-1 expression in chondrocytes contributes to the pathogenesis of osteoarthritis. *Cell Death Dis.* **8**, e3109–e3109 (2017).

191. Miossec, P. *et al.* K/BxN Serum-Transfer Arthritis as a Model for Human inflammatory Arthritis. **7**, 213 (2016).

192. Wooley, P. H. The usefulness and the limitations of animal models in identifying targets for therapy in arthritis. *Best Pract. Res. Clin. Rheumatol.* **18**, 47–58 (2004).

193. Jones, G. W., Hill, D. G., Sime, K. & Williams, A. S. In Vivo Models for Inflammatory Arthritis. *Methods Mol Biol* **1725**, 101–118 (2018).

194. Frey, O. *et al.* The role of regulatory T cells in antigen-induced arthritis: aggravation of arthritis after depletion and amelioration after transfer of CD4+CD25+ T cells. *Arthritis Res. Ther.* **7**, R291 (2005).

195. Santos, L. L., Morand, E. F., Hutchinson, P., Boyce, N. W. & Holdsworth, S. R. *Anti-neutrophil monoclonal antibody therapy inhibits the development of adjuvant arthritis*.

196. Choudhary, N., Bhatt, L. K. & Prabhavalkar, K. S. Experimental animal models for rheumatoid arthritis. **40**, 193–200 (2018).

197. Bush, K. A., Walker, J. S., Lee, C. S. & Kirkham, B. W. Cytokine expression and synovial pathology in the initiation and spontaneous resolution phases of adjuvant arthritis: Interleukin-17 expression is upregulated in early disease. *Clin. Exp. Immunol.* **123**, 487–495 (2001).

198. Hersmann, G. H. W., Kriegsmann, J., Simon, J., Hüttich, C. & Bräuer, R. Expression of Cell Adhesion Molecules and Cytokines in Murine Antigen-Induced Arthritis. *Cell Adhes. Commun.* **6**, 69–82 (1998).

199. van den Berg, W. B., Joosten, L. A. B. & van Lent, P. L. E. M. Murine antigen-induced arthritis. *Methods Mol. Med.* **136**, 243–53 (2007).

200. Ohshima, S. *et al.* Interleukin 6 plays a key role in the development of antigen-induced arthritis. *Proc. Natl. Acad. Sci.* **95**, 8222–8226 (1998).

201. Wong, P. K. K. *et al.* Interleukin-6 modulates production of T lymphocyte-derived cytokines in antigen-induced arthritis and drives inflammation-induced osteoclastogenesis. *Arthritis Rheum.* **54**, 158–68 (2006).

202. Hill, D. G. Investigating mechanisms that regulate ectopic lymphoid-like structures in inflammation. (Cardiff University, 2019).

203. Carroll, M. B. Tocilizumab in the treatment of myocardial infarction. *Modern Rheumatology* vol. 28 733–735 (2018).

204. Jones, G. W., Hill, D. G., Cardus, A. & Jones, S. A. IL-27: a double agent in the IL-6 family. *Clin. Exp. Immunol.* **193**, 37–46 (2018).

205. Jones, S. A. & Jenkins, B. J. Recent insights into targeting the IL-6 cytokine family in inflammatory diseases and cancer. *Nat. Rev. Immunol.* **18**, 773–789 (2018).

206. Jones, G. W. *et al.* Interleukin-27 inhibits ectopic lymphoid-like structure development in early inflammatory arthritis. *J Exp Med* **212**, 1793–1802 (2015).

207. Pitzalis, C., Kelly, S. & Humby, F. New learnings on the pathophysiology of RA from synovial biopsies. *Curr. Opin. Rheumatol.* **25**, 334–344 (2013).

208. Manzo, A., Bombardieri, M., Humby, F. & Pitzalis, C. Secondary and ectopic lymphoid tissue responses in rheumatoid arthritis: from inflammation to autoimmunity and tissue damage/remodeling. *Immunol. Rev.* **233**, 267–285 (2010).

209. Gao, C. *et al.* Procoagulant activity of erythrocytes and platelets through phosphatidylserine exposure and microparticles release in patients with nephrotic syndrome. *Thromb. Haemost.* **107**, 681–689 (2012).

210. Tan, X. *et al.* Role of erythrocytes and platelets in the hypercoagulable status in polycythemia vera through phosphatidylserine exposure and microparticle generation. *Thromb. Haemost.* **109**, 1025–1032 (2013).

211. Yang, C. *et al.* Contributions of phosphatidylserine-positive platelets and leukocytes and microparticles to hypercoagulable state in gastric cancer patients. *Tumour Biol.* **37**, 7881–91 (2016).

212. Allen-Redpath, K. *et al.* Phospholipid membranes drive abdominal aortic aneurysm development through stimulating coagulation factor activity. *Proc Natl Acad Sci U S A* **116**, 8038–8047 (2019).

213. Morgan, A. H. *et al.* Quantitative assays for esterified oxylipins generated by immune cells. *Nat. Protoc.* **5**, 1919–1931 (2010).

214. Yoshida, H. *et al.* WSX-1 Is Required for the Initiation of Th1 Responses and Resistance to L. major Infection. *Immunity* **15**, 569–578 (2001).

215. Jones, G. W. *et al.* Loss of CD4 + T Cell IL-6R Expression during Inflammation Underlines a Role for IL-6 Trans Signaling in the Local Maintenance of Th17 Cells. *J. Immunol.* **184**, 2130–2139 (2010).

216. Kopf, M. *et al.* Impaired immune and acute-phase responses in interleukin-6-deficient mice.

Nature **368**, 339–342 (1994).

217. Sun, D. & Funk, C. D. Disruption of 12/15-lipoxygenase expression in peritoneal macrophages. Enhanced utilization of the 5-lipoxygenase pathway and diminished oxidation of low density lipoprotein. *J. Biol. Chem.* **271**, 24055–62 (1996).

218. Kane, S. Sample Size Calculator. ClinCalc: https://clincalc.com/stats/samplesize.aspx. clincalc: https://clincalc.com/stats/samplesize.aspx.

219. Wolfensohn, S. & Lloyd, M. *Handbook of Laboratory Animal Management and Welfare*. (Blackwell Publishing Ltd, 2003). doi:10.1002/9780470751077.

220. Hyc, A., Osiecka-Iwan, A., Dziunycz, P. & Moskalewski, S. Preparation of rat synovial membrane for studies of cytokine secretion. *Folia Histochem. Cytobiol.* **45**, 57–60 (2007).

221. Nowell, M. A. *et al.* Therapeutic targeting of IL-6 trans signaling counteracts STAT3 control of experimental inflammatory arthritis. *J. Immunol.* **182**, 613–22 (2009).

222. Rosen, A. D. Notes on Technic: End-Point Determination in Edta Decalcification Using Ammonium Oxalate. *Stain Technol.* **56**, 48–49 (1981).

223. Majd Protty. Characterising the role of inflammatory procoagulant phospholipids in arterial thrombosis. (Cardiff University, 2021).

224. Thomas, C. P. *et al.* Identification and quantification of aminophospholipid molecular species on the surface of apoptotic and activated cells. *Nat. Protoc.* **9**, 51–63 (2014).

225. Bligh, E. G. & Dyer, W. J. A rapid method of total lipid extraction and purification. *Can. J. Biochem. Physiol.* **37**, 911–7 (1959).

226. Raivo Kolde. Pheatmap: Pretty Heatmaps 1.0.12. *https://CRAN.R-project.org/package=pheatmap* https://cran.r-project.org/package=pheatmap (2019).

227. Salvi, R., Péclat, V., So, A. & Busso, N. Enhanced expression of genes involved in coagulation and fibrinolysis in murine arthritis. *Arthritis Res. Ther.* **2**, 504 (2000).

228. Thomas, C. P. *et al.* Phospholipid-esterified eicosanoids are generated in agonist-activated human platelets and enhance tissue factor-dependent thrombin generation. *J. Biol. Chem.* **285**, 6891–903 (2010).

229. Thuresson, E. D., Lakkides, K. M. & Smith, W. L. Different Catalytically Competent Arrangements of Arachidonic Acid within the Cyclooxygenase Active Site of Prostaglandin Endoperoxide H Synthase-1 Lead to the Formation of Different Oxygenated Products. *J. Biol. Chem.* **275**, 8501–8507 (2000).

230. Morgan, A. H. *et al.* Phosphatidylethanolamine-esterified Eicosanoids in the Mouse. *J. Biol. Chem.* **284**, 21185–21191 (2009).

231. Pruzanski, W. *et al.* Serum phospholipase A2 correlates with disease activity in rheumatoid arthritis. *J. Rheumatol.* **15**, 1351–5 (1988).

232. Bomalaski, J. S. & Clark, M. A. Phospholipase A2 and arthritis. *Arthritis Rheum.* **36**, 190–198 (1993).

233. Torres, W. *et al.* Potential Role of Bioactive Lipids in Rheumatoid Arthritis. *Curr. Pharm. Des.* **27**, 4434–4451 (2021).

234. Honda, T., Segi-Nishida, E., Miyachi, Y. & Narumiya, S. Prostacyclin-IP signaling and prostaglandin E2-EP2/EP4 signaling both mediate joint inflammation in mouse collagen-induced arthritis. *J. Exp. Med.* **203**, 325 (2006).

235. Brackertz, D., Mitchell, G. F. & Mackay, I. R. Antigen-induced arthritis in mice. *Arthritis Rheum.* **20**, 841–850 (1977).

236. Qiang, F. Y., Xu, H. & Sheng, J. Relationship between plasma fibrinogen degradation products(FDP) and D -dimer levels and disease activity in rheumatoid arthritis: A STROBE compliant article. *Med. (United States)* **101**, E30455 (2022).

237. Gabay, C. Interleukin-6 and chronic inflammation. *Arthritis Res. Ther.* **8 Suppl 2**, S3 (2006).

238. Schober, P. & Schwarte, L. A. Correlation coefficients: Appropriate use and interpretation. *Anesth. Analg.* **126**, 1763–1768 (2018).

239. Mitchell, J. A., Akarasereenont, P., Thiemermann, C., Flower, R. J. & Vane, J. R. Selectivity of nonsteroidal antiinflammatory drugs as inhibitors of constitutive and inducible cyclooxygenase. *Proc. Natl. Acad. Sci. U. S. A.* **90**, 11693–11697 (1993).

240. Schmitt, A., Guichard, J., Massé, J. M., Debili, N. & Cramer, E. M. Of mice and men: Comparison of the ultrastructure of megakaryocytes and platelets. *Exp. Hematol.* **29**, 1295–1302 (2001).

241. Hutchinson, R. M., Davis, P. & Jayson, M. I. Thrombocytosis in rheumatoid arthritis. *Ann. Rheum. Dis.* **35**, 138–142 (1976).

242. Niessen, R. W. *et al.* Antithrombin acts as a negative acute phase protein as established with studies on HepG2 cells and in baboons. *Thromb. Haemost.* **78**, 1088–92 (1997).

243. Stouthard, J. M. *et al.* Interleukin-6 stimulates coagulation, not fibrinolysis, in humans. *Thromb. Haemost.* **76**, 738–42 (1996).

244. Deguchi, H., Elias, D. J., Navarro, S., Espana, F. & Griffin, J. H. Plasma Serum Amyloid A Levels Are Increased In Venous Thrombosis Patients and Are Correlated with Blood Coagulability. *Blood* **116**, 155–155 (2010).

245. Dong, Z. *et al.* Serum amyloid A directly accelerates the progression of atherosclerosis in apolipoprotein E-deficient mice. *Mol. Med.* **17**, 1357–64 (2011).

246. Geczy, C. L. *et al.* Factor Serum Amyloid A Induces Monocyte Tissue. *J Immunol Ref.* **178**, 1852–1860 (2007).

247. Cui, X. *et al.* Elevated Levels of IL-27 Are Associated with Disease Activity in Patients with Crohn's Disease. *Mediators Inflamm.* **2021**, (2021).

248. Abo El Magd, N. M., Abdel Salam, S. A., Aly, Y. A. & Fahim, N. A. The Role of Serum Interleukin-27 As A Diagnostic Biomarker For Diagnosis of Neonatal Sepsis. *Egypt. J. Immunol.* **25**, 87–95 (2018).

249. Ku, N.-O. & Mortensen, R. F. The mouse C-reactive protein (CRP) gene is expressed in response to IL-1 but not IL-6☆. *Cytokine* **5**, 319–326 (1993).

250. Bataille, Rég. & Klein, B. C-reactive protein levels as a direct indicator of interleukin-6 levels in humans in vivo. *Arthritis Rheum.* **35**, 982–983 (1992).

251. Paul-Pletzer, K. Tocilizumab: Blockade of interleukin-6 signaling pathway as a therapeutic strategy for inflammatory disorders. *Drugs of Today* vol. 42 559–576 (2006).

252. Heinrich, P. C., Castell, J. V & Andus, T. Interleukin-6 and the acute phase response. *Biochem. J.* **265**, 621–636 (1990).

253. Weinhold, B. & Rüther, U. Interleukin-6-dependent and -independent regulation of the human C-reactive protein gene. *Biochem. J.* **327 (Pt 2**, 425–9 (1997).

254. Weinhold, B., Bader, A., Poli, V. & Rüther, U. Interleukin-6 is necessary, but not sufficient, for induction of the humanC-reactive protein gene in vivo. *Biochem. J.* **325 (Pt 3**, 617–21 (1997).

255. Xue, L. *et al.* Plasma fibrinogen, d-dimer, and fibrin degradation product as biomarkers of rheumatoid arthritis. *Sci. Rep.* **11**, 16903 (2021).

256. van der Poll, T. *et al.* Elimination of interleukin 6 attenuates coagulation activation in experimental endotoxemia in chimpanzees. *J. Exp. Med.* **179**, 1253–9 (1994).

257. O'Donnell, V. B. & Murphy, R. C. New families of bioactive oxidized phospholipids generated by immune cells: identification and signaling actions. *Blood* **120**, 1985–1992 (2012).

258. Cyrus, T. *et al.* Disruption of the 12/15-lipoxygenase gene diminishes atherosclerosis in apo E–deficient mice. *J. Clin. Invest.* **103**, 1597–1604 (1999).

259. Uderhardt, S. *et al.* Enzymatic lipid oxidation by eosinophils propagates coagulation, hemostasis, and thrombotic disease. *J Exp Med* **214**, 2121–2138 (2017).

260. Tyrrell, D. J. & Goldstein, D. R. Ageing and atherosclerosis: vascular intrinsic and extrinsic factors and potential role of IL-6. *Nat. Rev. Cardiol.* **18**, 58–68 (2021).

261. Oleksowicz, L. *et al.* Platelet activation induced by interleukin-6: evidence for a mechanism involving arachidonic acid metabolism. *Thromb. Haemost.* **72**, 302–8 (1994).

262. Davies, R. *et al.* The role of interleukin-6 trans-signalling on cardiovascular dysfunction in inflammatory arthritis. *Rheumatology* **60**, 2852–2861 (2021).

263. Charles-Schoeman, C., Meriwether, D., Lee, Y. Y., Shahbazian, A. & Reddy, S. T. High levels of oxidized fatty acids in HDL are associated with impaired HDL function in patients with active rheumatoid arthritis. *Clin. Rheumatol.* **37**, 615–622 (2018).

264. Marcus, A. J. *et al.* Studies on the mechanism of omega-hydroxylation of platelet 12-hydroxyeicosatetraenoic acid (12-HETE) by unstimulated neutrophils. *J. Clin. Invest.* **79**, 179–187 (1987).

265. Henricks, P. A. J., Engels, F., van der Vliet, H. & Nijkamp, F. P. 9- and 13-hydroxy-linoleic acid possess chemotactic activity for bovine and human polymorphonuclear leukocytes. *Prostaglandins* **41**, 21–27 (1991).

266. Jira, W., Spiteller, G. & Richter, A. Increased levels of lipid oxidation products in low density lipoproteins of patients suffering from rheumatoid arthritis. *Chem. Phys. Lipids* **87**, 81–89 (1997).

267. Wendell, S. G. *et al.* 15-Hydroxyprostaglandin Dehydrogenase Generation of Electrophilic Lipid Signaling Mediators from Hydroxy Ω-3 Fatty Acids. *J. Biol. Chem.* **290**, 5868–5880 (2015).

268. Adili, R. *et al.* First Selective 12-LOX Inhibitor, ML355, Impairs Thrombus Formation and Vessel Occlusion In Vivo With Minimal Effects on Hemostasis. *Arterioscler. Thromb. Vasc. Biol.* **37**, 1828–1839 (2017).

269. Kuhn, H., Banthiya, S. & van Leyen, K. Mammalian lipoxygenases and their biological relevance.

Biochim. Biophys. Acta **1851**, 308–30 (2015).

270. Guichardant, M., Ericel, E. V & Lagarde, M. Biological relevance of double lipoxygenase products of polyunsaturated fatty acids, especially within blood vessels and brain. (2018) doi:10.1016/j.biochi.2018.08.009.

271. Hajeyah, A. A., Griffiths, W. J., Wang, Y., Finch, A. J. & O'Donnell, V. B. The Biosynthesis of Enzymatically Oxidized Lipids. *Front. Endocrinol. (Lausanne).* **11**, (2020).

272. Dioszeghy, V. *et al.* 12/15-Lipoxygenase Regulates the Inflammatory Response to Bacterial Products In Vivo. *J. Immunol.* **181**, 6514–6524 (2008).

273. Iversen, L., Fogh, K. & Kragballe, K. Effect of dihomogammalinolenic acid and its 15-lipoxygenase metabolite on eicosanoid metabolism by human mononuclear leukocytes in vitro: selective inhibition of the 5-lipoxygenase pathway. *Arch. Dermatol. Res.* **284**, 222–226 (1992).

274. Bleich, D. *et al.* Resistance to type 1 diabetes induction in 12-lipoxygenase knockout mice. *J. Clin. Invest.* **103**, 1431–1436 (1999).

275. Weiss, M., Blazek, K., Byrne, A. J., Perocheau, D. P. & Udalova, I. A. IRF5 Is a Specific Marker of Inflammatory Macrophages In Vivo. *Mediators Inflamm.* **2013**, 1–9 (2013).

276. Jyrkkänen, H.-K. *et al.* Nrf2 regulates antioxidant gene expression evoked by oxidized phospholipids in endothelial cells and murine arteries in vivo. *Circ. Res.* **103**, e1-9 (2008).

277. Hayes, J. D. & Dinkova-Kostova, A. T. The Nrf2 regulatory network provides an interface between redox and intermediary metabolism. *Trends Biochem. Sci.* **39**, 199–218 (2014).

278. Wruck, C. J. *et al.* Role of oxidative stress in rheumatoid arthritis: insights from the Nrf2-knockout mice. *Ann. Rheum. Dis.* **70**, 844–50 (2011).

279. Jiang, C., Ting, A. T. & Seed, B. PPAR-γ agonists inhibit production of monocyte inflammatory cytokines. *Nature* **391**, 82–86 (1998).

280. Ahmadian, M. *et al.* PPARγ signaling and metabolism: the good, the bad and the future. *Nat. Med.* **19**, 557–566 (2013).

281. Sun, L. *et al.* 12/15-Lipoxygenase metabolites of arachidonic acid activate PPARγ: a possible neuroprotective effect in ischemic brain. *J. Lipid Res.* **56**, 502–514 (2015).

282. Habouri, L. *et al.* Deletion of 12/15-lipoxygenase accelerates the development of aging-associated and instability-induced osteoarthritis. *Osteoarthr. Cartil.* **25**, 1719–1728 (2017).

283. Abdalla, H. B. *et al.* Activation of PPAR-γ induces macrophage polarization and reduces neutrophil migration mediated by heme oxygenase 1. *Int. Immunopharmacol.* **84**, 106565 (2020).

284. Lee, C. Collaborative Power of Nrf2 and PPARγ Activators against Metabolic and Drug-Induced Oxidative Injury. *Oxid. Med. Cell. Longev.* **2017**, 1378175 (2017).

285. Underwood, K. F. *et al.* A Quantitative Assay to Study Protein:DNA Interactions, Discover Transcriptional Regulators of Gene Expression, and Identify Novel Anti-tumor Agents. *J. Vis. Exp* 50512 (2013) doi:10.3791/50512.

286. Hoffman, M. A cell-based model of coagulation and the role of factor VIIa. *Blood Rev.* **17**, S1–S5 (2003).

287. Van Niel, G., D'Angelo, G. & Raposo, G. Shedding light on the cell biology of extracellular vesicles. *Nat. Rev. Mol. Cell Biol. 2018 194* **19**, 213–228 (2018).

288. Doyle, L. M. & Wang, M. Z. Overview of Extracellular Vesicles, Their Origin, Composition, Purpose, and Methods for Exosome Isolation and Analysis. *Cells* **8**, (2019).

289. Schioppo, T., Ubiali, T., Ingegnoli, F., Bollati, V. & Caporali, R. The role of extracellular vesicles in rheumatoid arthritis: a systematic review. *Clin. Rheumatol.* **40**, 3481–3497 (2021).

290. Withrow, J. *et al.* Extracellular vesicles in the pathogenesis of rheumatoid arthritis and osteoarthritis. *Arthritis Res. Ther.* **18**, 286 (2016).

291. Fu, H., Hu, D., Zhang, L. & Tang, P. Role of extracellular vesicles in rheumatoid arthritis. *Mol. Immunol.* **93**, 125–132 (2018).

292. Stojanovic, A. *et al.* Increased Expression of Extracellular Vesicles Is Associated With the Procoagulant State in Patients With Established Rheumatoid Arthritis. *Front. Immunol.* **12**, (2021).

293. Olech, E. & Merrill, J. T. The prevalence and clinical significance of antiphospholipid antibodies in rheumatoid arthritis. *Curr. Rheumatol. Rep.* **8**, 100–8 (2006).

294. Anderson, J. *et al.* Rheumatoid arthritis disease activity measures: American College of Rheumatology recommendations for use in clinical practice. *Arthritis Care Res. (Hoboken).* **64**, 640–7 (2012).

295. Lardinois, B., Favresse, J., Chatelain, B., Lippi, G. & Mullier, F. Pseudothrombocytopenia-A Review on Causes, Occurrence and Clinical Implications. *J. Clin. Med.* **10**, 1–19 (2021).

296. Sellam, J. *et al.* Increased levels of circulating microparticles in primary Sjögren's syndrome, systemic lupus erythematosus and rheumatoid arthritis and relation with disease activity. **11**, R156 (2009).

297. Offermanns, S. Activation of Platelet Function Through G Protein–Coupled Receptors. *Circ. Res.* **99**, 1293–1304 (2006).

298. Hankey, G. J. & Eikelboom, J. W. Aspirin resistance. *Lancet* **367**, 606–617 (2006).

299. Schafer, A. I. Effects of nonsteroidal anti-inflammatory therapy on platelets. *Am. J. Med.* **106**, 25S-36S (1999).

300. Scully, C. Agents used in the treatment of patients with orofacial disease. in *Oral and Maxillofacial Medicine* 48–79 (Elsevier, 2013). doi:10.1016/B978-0-7020-4948-4.00005-2.

301. McWilliams, D. F. *et al.* Interpretation of DAS28 and its components in the assessment of inflammatory and non-inflammatory aspects of rheumatoid arthritis. *BMC Rheumatol.* **2**, 8 (2018).

302. Benjamin, O., Bansal, P. & Goyal, A. et al. Disease Modifying Anti-Rheumatic Drugs (DMARD). *StatPearls* (2022).

303. Syed, K. M. & Pinals, R. S. Leukocytosis in Rheumatoid Arthritis. *JCR J. Clin. Rheumatol.* **2**, 197–202 (1996).

304. Łukasik, Z. M., Makowski, M. & Makowska, J. S. From blood coagulation to innate and adaptive immunity: the role of platelets in the physiology and pathology of autoimmune disorders. *Rheumatol. Int.* **38**, 959–974 (2018).

305. Beyer, C. & Pisetsky, D. S. The role of microparticles in the pathogenesis of rheumatic diseases. *Nat. Rev. Rheumatol.* **6**, 21 (2010).

306. Michael, B. N. R., Misra, D. P., Chengappa, K. G. & Negi, V. S. Relevance of elevated microparticles in peripheral blood and synovial fluid of patients with rheumatoid arthritis. *Indian J. Rheumatol.* **13**, 222 (2018).

307. Wang, Z. T., Wang, Z. & Hu, Y. W. Possible roles of platelet-derived microparticles in atherosclerosis. *Atherosclerosis* **248**, 10–16 (2016).

308. Pereira, J. *et al.* Circulating platelet-derived microparticles in systemic lupus erythematosus. Association with increased thrombin generation and procoagulant state. *Thromb. Haemost.* **95**, 94–99 (2006).

309. Suades, R., Padró, T., Alonso, R., Mata, P. & Badimon, L. High levels of TSP1+/CD142+ platelet-derived microparticles characterise young patients with high cardiovascular risk and subclinical atherosclerosis. *Thromb. Haemost.* **114**, 1310–1321 (2015).

310. Altman, R., Luciardi, H. L., Muntaner, J. & Herrera, R. N. The antithrombotic profile of aspirin. Aspirin resistance, or simply failure? *Thromb. J.* **2**, 1 (2004).

311. Mello, S. B. V., Barros, D. M., Silva, A. S. F., Laurindo, I. M. M. & Novaes, G. S. Methotrexate as a preferential cyclooxygenase 2 inhibitor in whole blood of patients with rheumatoid arthritis. *Rheumatology (Oxford).* **39**, 533–536 (2000).

312. Ledingham, J. *et al.* BSR and BHPR guideline for the prescription and monitoring of non-biologic disease-modifying anti-rheumatic drugs. *Rheumatology* **56**, 865–868 (2017).

313. Gheorghe, K. R. *et al.* Limited effect of anti-rheumatic treatment on 15-prostaglandin dehydrogenase in rheumatoid arthritis synovial tissue. *Arthritis Res. Ther.* **14**, R121 (2012).

314. Manfredi, A. A. *et al.* Anti-TNFα agents curb platelet activation in patients with rheumatoid arthritis. *Ann. Rheum. Dis.* **75**, 1511–1520 (2016).

315. Leroux, J. L., Damon, M., Chavis, C., Crastes de Paulet, A. & Blotman, F. Effects of a single dose of methotrexate on 5- and 12-lipoxygenase products in patients with rheumatoid arthritis. *J. Rheumatol.* **19**, 863–6 (1992).

316. Hawkes, J. S., Cleland, L. G. & James, M. J. The effect of methotrexate on lipoxygenase metabolism in neutrophils from rats: in vitro and ex vivo studies. *Agents Actions* **40**, 181–185 (1993).

317. Zeng, C. *et al.* Risk of venous thromboembolism in knee, hip and hand osteoarthritis: a general population-based cohort study. *Ann. Rheum. Dis.* **79**, 1616–1624 (2020).

318. Charrière, G. *et al.* Antibodies to types I, II, IX, and XI collagen in the serum of patients with rheumatic diseases. *Arthritis Rheum.* **31**, 325–32 (1988).

319. Sakata, M. *et al.* Autoantibodies to osteopontin in patients with osteoarthritis and rheumatoid arthritis. *J. Rheumatol.* **28**, 1492–5 (2001).

320. Xiang, Y. *et al.* Proteomic surveillance of autoimmunity in osteoarthritis: identification of triosephosphate isomerase as an autoantigen in patients with osteoarthritis. *Arthritis Rheum.* **50**, 1511–21 (2004).

321. Hayem, G. *et al.* Anti-oxidized low-density-lipoprotein (OxLDL) antibodies in systemic lupus

erythematosus with and without antiphospholipid syndrome. *Lupus* **10**, 346–51 (2001).

322. Cvetkovic, J. T., Wållberg-Jonsson, S., Ahmed, E., Rantapää-Dahlqvist, S. & Lefvert, A. K. Increased levels of autoantibodies against copper-oxidized low density lipoprotein, malondialdehyde-modified low density lipoprotein and cardiolipin in patients with rheumatoid arthritis. *Rheumatology (Oxford).* **41**, 988–95 (2002).

323. Hörkkö, S. *et al.* Immunological responses to oxidized LDL. *Free Radic. Biol. Med.* **28**, 1771–9 (2000).

324. Krönke, G. & Leitinger, N. Oxidized phospholipids at the interface of innate and adaptive immunity. *Future Lipidol.* **1**, 623–630 (2006).

325. Cook-Moreau, J. M. *et al.* Expression of 5-lipoxygenase (5-LOX) in T lymphocytes. *Immunology* **122**, 157–66 (2007).

326. Jakobsson, P. -J *et al.* Studies on the regulation and localization of 5-lipoxygenase in human B-lymphocytes. *Eur. J. Biochem.* **232**, 37–46 (1995).

327. Devaux, P. F. & Morris, R. Transmembrane asymmetry and lateral domains in biological membranes. *Traffic* **5**, 241–246 (2004).

328. Bevers, E. M., Comfurius, P., van Rijn, J. L., Hemker, H. C. & Zwaal, R. F. Generation of prothrombin-converting activity and the exposure of phosphatidylserine at the outer surface of platelets. *Eur. J. Biochem.* **122**, 429–36 (1982).

329. Falls, L. A., Furie, B. & Furie, B. C. Role of phosphatidylethanolamine in assembly and function of the factor IXa-factor VIIIa complex on membrane surfaces. *Biochemistry* **39**, 13216–13222 (2000).

330. Daleke, D. L. Regulation of transbilayer plasma membrane phospholipid asymmetry. *J. Lipid Res.* **44**, 233–242 (2003).

331. Sagini, K., Costanzi, E., Emiliani, C., Buratta, S. & Urbanelli, L. Extracellular Vesicles as Conveyors of Membrane-Derived Bioactive Lipids in Immune System. *Int. J. Mol. Sci.* **19**, (2018).

332. Vona, R. *et al.* Potential role of platelets for atherosclerotic events in rheumatoid arthritis. *FEBS Open Bio* **8**, 1888–1896 (2018).

333. Michael, B. N. R., Kommoju, V., Kavadichanda Ganapathy, C. & Negi, V. S. Characterization of cell-derived microparticles in synovial fluid and plasma of patients with rheumatoid arthritis. *Rheumatol. Int.* **39**, 1377–1387 (2019).

334. Zwaal, R. F. A. & Schroit, A. J. Pathophysiologic implications of membrane phospholipid asymmetry in blood cells. *Blood* **89**, 1121–32 (1997).

335. Lhermusier, T., Chap, H. & Payrastre, B. Platelet membrane phospholipid asymmetry: from the characterization of a scramblase activity to the identification of an essential protein mutated in Scott syndrome. *J. Thromb. Haemost.* **9**, 1883–91 (2011).

336. Clark, S. R. *et al.* Characterization of platelet aminophospholipid externalization reveals fatty acids as molecular determinants that regulate coagulation. *Proc. Natl. Acad. Sci. U. S. A.* **110**, 5875–5880 (2013).

337. Paul, M. *et al.* Methotrexate Promotes Platelet Apoptosis via JNK-Mediated Mitochondrial Damage: Alleviation by N-Acetylcysteine and N-Acetylcysteine Amide. *PLoS One* **10**, e0127558

(2015).

338. Bevers, E. M. & Williamson, P. L. Getting to the Outer Leaflet: Physiology of Phosphatidylserine Exposure at the Plasma Membrane. *Physiol. Rev.* **96**, 605–645 (2016).

339. Genge, B. R., Wu, L. N. Y. & Wuthier, R. E. Mineralization of annexin-5-containing lipid-calcium-phosphate complexes: modulation by varying lipid composition and incubation with cartilage collagens. *J. Biol. Chem.* **283**, 9737–48 (2008).

340. Wang, S. *et al.* Prevalence and extent of calcification over aorta, coronary and carotid arteries in patients with rheumatoid arthritis. *J. Intern. Med.* **266**, 445–452 (2009).

341. McMahon, H. T. & Boucrot, E. Membrane curvature at a glance. *J. Cell Sci.* **128**, 1065–1070 (2015).

342. Bozelli, J. C. *et al.* Membrane curvature allosterically regulates the phosphatidylinositol cycle, controlling its rate and acyl-chain composition of its lipid intermediates. *J. Biol. Chem.* **293**, 17780–17791 (2018).

343. Dowler, S., Kular, G. & Alessi, D. R. Protein lipid overlay assay. *Sci. STKE* **2002**, pl6 (2002).

344. Ramos, A. L. *et al.* Comorbidities in patients with rheumatoid arthritis and their association with patient-reported outcomes: Results of claims data linked to questionnaire survey. *J. Rheumatol.* **46**, 564–571 (2019).

345. Jones, G. W. *et al.* Interleukin-27 inhibits ectopic lymphoid-like structure development in early inflammatory arthritis. *J. Exp. Med.* **212**, 1793–802 (2015).

346. Huo, Y. *et al.* Critical Role of Macrophage 12/15-Lipoxygenase for Atherosclerosis in Apolipoprotein E–Deficient Mice. *Circulation* **110**, 2024–2031 (2004).

347. Kriska, T. *et al.* Mice lacking macrophage 12/15-lipoxygenase are resistant to experimental hypertension. *Am. J. Physiol. Heart Circ. Physiol.* **302**, H2428-38 (2012).

348. Jonasdottir, H. S., Brouwers, H., Toes, R. E. M., Ioan-Facsinay, A. & Giera, M. Effects of anticoagulants and storage conditions on clinical oxylipid levels in human plasma. *Biochim. Biophys. acta. Mol. cell Biol. lipids* **1863**, 1511–1522 (2018).

349. Boilard, E., Blanco, P. & Nigrovic, P. A. Platelets: active players in the pathogenesis of arthritis and SLE. *Nat. Rev. Rheumatol.* **8**, 534–42 (2012).

350. PubChem [Internet]. Bethesda (MD): National Library of Medicine (US), National Center for Biotechnology Information; 2004-. PubChem Compound Summary for CID 5289133, PE(18:0/20:4(5Z,8Z,11Z,14Z)); [cited 2021 Feb. 18]. Available from: https://pubchem.ncbi. https://pubchem.ncbi.nlm.nih.gov/compound/5289133.

351. Soria, A. D. Negative regulation of the JAK/STAT signalling pathway in inflammatory arthritis. (Cardiff University, 2020).

Appendix

Chapter 10

10 Appendix

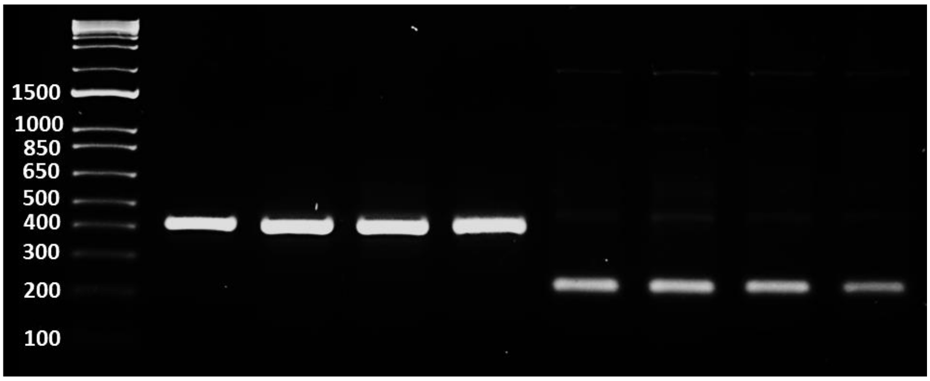

Figure 10.1: Example of genotyping results for *Alox15*$^{-/-}$ mice
Genotyping was confirmed as described in Materials and Methods. As expected, Wild-type (WT) animals display a single band at 417 bp, while Mutants display a band at 200 bp.

Bwrdd Iechyd Prifysgol Caerdydd a'r Fro
Cardiff and Vale University Health Board

University Hospital of Wales
Heath Park
Cardiff
CF14 4XN
Telephone: 029 2074 7747

Healthy Participant Information Sheet

Chief Investigator: Professor Ernest Choy, Professor of Rheumatology and Consultant Rheumatologist

Title of Project:

Cardiff Regional Experimental Arthritis Treatment and Evaluation Centre

Lay Title: Cardiff Regional Experimental Arthritis Treatment and Evaluation Centre

Purpose of the study and why have I been chosen?

You are being invited to take part in a research study. Before you decide, it is important for you to understand why the research is being done and what it will involve. Please take time to read the following information carefully and discuss it with others if you wish. Ask us if there is anything that is not clear or if you would like more information. Take time to decide whether or not you wish to take part.

Purpose of the study

The immune system protects the body from infection e.g. by viruses or bacteria. After an infection has been cleared, the immune response should return to normal. If this does not happen, the body could attack itself, which is what happens in the joints of patients with chronic inflammatory arthritis such as rheumatoid arthritis and psoriatic arthritis. We are interested to know how the immune response is switched on and switched off. This could help us find a cure for chronic inflammatory arthritis and develop laboratory tests that can predict prognosis more precisely. We would like to investigate certain cells and molecules of the immune system that may start and regulate the immune response. These cells and molecules can be found in the blood and the fluid and lining of inflamed joints. We will need to compare the results from patients with chronic inflammatory arthritis with normal health individuals in order to determine whether the finding is related to the disease which if why you have been invited to take part. If you wish to know more, full experimental details are freely available. We request that if we manage to extract more white blood cells than required for a planned experiment, we ask your permission to allow us to store the excess in liquid nitrogen. This means we can access cells without having to come back to you for fresh samples, thus potentially reducing the number of times you are bled. We also ask that we can store these samples for up to 15 years, so we can repeat assays beyond the period of this study as a reference for future projects. If you do not wish your samples to be stored, there is an option in the consent form (statement 4) which you can choose to indicate this. If you choose not to have your sample stored, we will destroy any unused samples.

Do I have to take part?

It is up to you to decide whether or not to take part. If you do decide to take part you will be given this information sheet to keep and be asked to sign a consent form. If you decide to take part you are still free to withdraw at any time and without giving a reason.

What will happen to me if I take part and what do I have to do?

You are being requested to give regular blood samples from which to extract your white blood cells for experiments to be conducted in our laboratory for the duration of the project (5 years). Times for donating a sample will be arranged with you personally and at your convenience. The volume of any single blood sample will be up to a maximum of 50 ml (or a quarter of a small cup). There will be a period of at least 2 weeks between requests for blood samples and a rest period of a month will be applied following any 2 consecutive fortnightly bleeds (ie. frequency of bleeding throughout the year will not average more than once a month). A maximum of 1000 ml may be taken each year. This assumes that you are of average size and that you are not giving blood for any other reason. If you are donating blood to others, the maximum volume of blood that can be taken yearly for this project (1000 ml) will be reduced by the volume you have given elsewhere. If you are under average size, the maximum volume will be reduced to the volume advised by the Blood Transfusion Service for an individual of your size. Please note that we will not risk taking a blood sample if you are anaemic. If there is any reason that you believe you may be anaemic, then please refuse our request. You may refuse to give a blood sample at any time without giving a reason.

What about confidentiality?

All your data will anonymised and be kept confidentially on computer, on files that require passwords. The data will be presented to anyone else in anonymised fashion. No personal or identifiable information will be kept.

Are there any risks?

Blood samples will only be taken by trained phlebotomists, thereby minimising any risks. There may be minor irritation following phlebotomy, but this should pass after a few hours. There may be a long-term risk of anaemia for volunteers donating blood over long periods. However, the amounts of blood taken will be monitored carefully and recorded on a centralised computer server, making the risk of this very low.

What will happen to the results of the research study?

Results of this research will be published as articles in peer-reviewed scientific journals. If you are interested, the lead researchers, Professor Ernest Choy, will provide you with a copy of the manuscript on request. All results will be anonymized in any publication.

How is this study funded and reviewed?

This study is being funded by the Arthritis Research UK. The study has been reviewed by the Research Ethics Committee for Wales (Reference No 12/WA/0045).

What if there is a problem?

In the event of an emergency, dial 999 immediately. If you require emergency care, be sure to tell the emergency care provider about your participation in this study and contact the study doctor as soon as possible. In the event that you become ill or suffer any injury as a direct result of the study procedures, you should inform your study doctor who will arrange for the correct treatment. You must notify the study doctor immediately of any suspected research-related injury. If you have any questions concerning the availability of medical care or if you think you have experienced a research-related illness, injury or emergency, contact:

Professor Ernest Choy
Telephone Number: [redacted]
After Office Hours: [redacted]

Any complaint about the way you have been dealt with during the study or any possible harm you might suffer will be addressed. If taking part in this study harms you, there are no special compensation arrangements. If you are harmed due to someone's negligence then you may have grounds for legal action but you may have to pay for it. If you wish to complain or have any concerns about the way you have been approached or treated during the study, the normal National Health Service complaints mechanisms should be available to you.

Contact Details:

If you would like more information about this study, please contact Prof Ernest Choy on [redacted]

Healthy Volunteer Participant Information Sheet version 3, 21st May 2012

If you decide to take part in the study you will be given this information sheet and a copy of the consent form.

Thank you for taking time to read this information and considering taking part in this study.

Healthy Volunteer Participant Information Sheet version 3, 21st May 2012

Figure 10.2: Patient information leaflet for healthy volunteer, under the study *"Cardiff Regional Experimental Arthritis Treatment and Evaluation Centre"*.

Bwrdd Iechyd Prifysgol Caerdydd a'r Fro
Cardiff and Vale University Health Board

University Hospital of Wales
Heath Park
Cardiff
CF14 4XN
Telephone: 029 2074 7747

CONSENT FORM

Chief Investigator: Professor Ernest Choy, Professor of Rheumatology and Consultant Rheumatologist

Title of Project:

Cardiff Regional Experimental Arthritis Treatment and Evaluation Centre

Lay Title: Cardiff Regional Experimental Arthritis Treatment and Evaluation Centre

Please initial box

1. I confirm that I have read and understand the healthy volunteer information sheet dated 21st May 2012 (version 3) for the above study and have had the opportunity to ask questions. ☐
2. I understand that my participation is voluntary and that I am free to withdraw at any time, without giving any reason. ☐
3. I agree to take part in the above study. ☐
4. I wish/do not wish* to have excess sample stored frozen beyond the period of the project for 15 years beyond the period of the project for research into the cause of and treatment of inflammatory arthritis. ☐

* please delete as appropriate and complete all parts of the form

Name of Participant	Date	Signature
Name of Person taking consent (if different from researcher)	Date	Signature
Researcher	Date	Signature

Healthy Volunteer Consent Form version 3, 21 May 2012

Figure 10.3: Consent form for healthy volunteer, under the study "*Cardiff Regional Experimental Arthritis Treatment and Evaluation Centre*".

PATIENT INFORMATION SHEET

Analysis of autoantibodies against lipids to identify markers of disease and immune responses against lipids.

PARTICIPANT INFORMATION SHEET

You are being invited to take part in a research study. Before you decide whether or not to take part it is important for you to understand why the research is being done and what it will involve. Please take time to read the following information carefully and discuss it with others if you wish. Please ask any questions if you are unsure of anything.

Thank you for reading this.

1. What is the purpose of this research?

Auto-antibody production is associated with autoimmune diseases. We are interested in analyzing rheumatoid arthritis patients serum for the presence of autoantibody against lipids considered relevant in coagulation and compare it to healthy controls.

2. Why have I been invited?

You have been invited because you are a healthy individual aged between 20 and 60.

During the SARS-CoV-2 pandemic, we have included a number of other additional conditions, agreed by Cardiff University, that must be met to ensure the safety of all those involved in the studies. These are that the donor:

1. has not had a fever, cough, shortness of breath, loss of smell/taste or other new symptoms suggestive of COVID-19 within the last 14 days.
2. has not self-isolated within the last 14 days.
3. has not had proven COVID-19, or symptoms and exposure in keeping with a presumptive diagnosis of COVID-19, until 3 months have elapsed after recovery.
4. is not a health care worker or visited health care facilities within the last 14 days.

If you fall under any of the categories, please wait until you drop out of the categories before agreeing to provide a sample.

3. Who should not participate?

For reasons of safety you should not participate if:

- You are unwell at the moment
- You are or might be pregnant
- You have any acute or chronic illness
- You have given blood in the last 1 month either for this study, another research study or for the Welsh Blood Service.

Version 1.0 09/06/2021

CARDIFF UNIVERSITY PRIFYSGOL CAERDYDD

PATIENT INFORMATION SHEET

There will be no direct advantages or benefits to you from taking part, but your contribution will help us understand more about the process of blood coagulation. This study will not produce any clinically relevant findings.

10. What are the possible risks of taking part?

There are some risks associated with giving blood (venepuncture), but these are rare. These are:

- Excessive bleeding from the puncture site.
- Fainting or dizziness.
- Haematoma (a bruise).
- Infection at the puncture site.
- Multiple punctures if a vein is not immediately located.

There is a potential risk of catching SARS-CoV-2 during the COVID-19 pandemic while providing a sample. However, samples will only be taken according to a Standard Operating Procedure (2020-PhlebotomySOPDII_SCV2_v1.3) approved by Cardiff University and Cardiff University School of Medicine that minimises risk of transmission. This will be provided to you to view before any sample is taken.

If you have any questions concerns about any of the above, please ask the researcher. If you decide you do not want to take part, please do not worry, just inform the researcher at this point.

11. Will anyone look at my medical records?

We will not look at your medical records for this study.

12. Will my GP be told I am taking part in the study?

We will not inform your GP that you are taking part in this study.

13. Will my taking part in this study be kept confidential?

All information collected during the study will be kept strictly confidential in accordance with the Data Protection Act 1998. Your name, address or any other identifying information will not be passed onto anyone and your samples will be assigned an anonymous identification code. You will not be identified in any published study results.

a. Only the research team will have access to the information that can identify you and link you to your samples.

14. What happens to my samples at the end of the study?

Your samples will only be stored for the duration of this study and will either be used up during the study or disposed of according to locally approved procedures at the end of the study.

Version 1.0 09/06/2021

PATIENT INFORMATION SHEET

15. What will happen to the results of the study?

The results of this study will be used as part of the research of staff working in the Lipidomics group at Cardiff University. You may obtain a copy of the results at any time (after publication) by asking the researchers. The results may be published in relevant scientific journals. You will not be identified in any version of the published results.

16. What if there is a problem?

If you are harmed by taking part in this research study, there are no special compensation arrangements. If you are harmed due to someone's negligence, then you may have grounds for legal action, but you may have to pay for it.

17. Who is organising and funding this research?

This study is funded by the Medical Research Council and is supervised by Professor Valerie O'Donnell. The project is based at the Cardiff Lipidomics Group of the Institute of Infection and Immunity, School of Medicine, Cardiff University.

18. GDPR (General Data Protection Regulation)

Cardiff University is the sponsor for this study based in the United Kingdom. We will be using information from you in order to undertake this study and will act as the data controller for this study. This means that we are responsible for looking after your information and using it properly. Cardiff University will keep identifiable information about you for no less than 5 years after the study has finished.

Your rights to access, change or move your information are limited, as we need to manage your information in specific ways in order for the research to be reliable and accurate. If you withdraw from the study, we will keep the information about you that we have already obtained. To safeguard your rights, we will use the minimum personally-identifiable information possible.

PATIENT INFORMATION SHEET

Further information about Data Protection, including:

- your rights
- the legal basis under which Cardiff University processes your personal data for research
- Cardiff University's Data Protection Policy
- how to contact the Cardiff University Data Protection Officer
- how to contact the Information Commissioner's Office

may be found at https://www.cardiff.ac.uk/public-information/policies-and-procedures/data-protection

19. Further information and contact details

Should you have any questions relating to this study, or you wish to withdraw your consent, you may contact us during normal working hours:

Daniela Costa, [redacted]

We would like to thank you for considering taking part in this study. If you decide to participate you will be given a copy of the information sheet and a signed consent form to keep.

Participant ID Number	Do not include box for anonymised

CARDIFF UNIVERSITY
PRIFYSGOL CAERDYDD

Consent Form

Title of study: **Analysis of autoantibodies against lipids to identify markers of disease and immune responses against lipids.**

REC/SREC reference and committee: 16/02 - Study: 10
Name of Chief/Principal Investigator: Prof. Valerie O'Donnell
Name and Contact of Researcher: Daniela Costa, [redacted]

	Please initial box
I confirm that I have read and understood the information sheet dated 9th June 2021 version 1.0 for the above study and have had the opportunity to ask questions and these have been answered satisfactorily.	
I understand that my participation is voluntary, and I am free to withdraw at any time without giving a reason and without my medical care or legal right being affected.	
In case I decide to withdraw from the study, I agree that the samples used, or results generated prior to the withdrawal of consent will continue to be part of this study.	
I understand that any information I provide is confidential. My identity will be protected by assigning a participant number which is indicated below in this form. This number will be known only to the researcher and at no time will samples, data or results be labelled with my name.	
I agree to provide a blood sample for the above study (up to 10 ml (2 teaspoons)), I understand my sample will only be used for the purposes of this study and any remaining sample will be disposed of at the end of the study according to locally approved procedures. I understand that any samples will be given as a "gift" and that I will have no right to a share of any profits which might arise from research using them (e.g. as part of a new medical treatment or test).	
I understand that if I have recently given blood elsewhere within the last 4 weeks, as detailed in the information sheet, I will either inform the researcher or refuse to donate.	
I agree to take part in this study	

________________________	________________	________________________
Name of participant (print)	Date	Signature
Name of person taking consent (print)	Date	Signature

THANK YOU FOR PARTICIPATING IN OUR RESEARCH
YOU WILL BE GIVEN A COPY OF THIS CONSENT FORM TO KEEP

Version 1.0 09/06/2021

Figure 10.5: Consent form for healthy volunteers, under the study "*Analysis of autoantibodies against lipids to identify markers of disease and immune responses against lipids*".

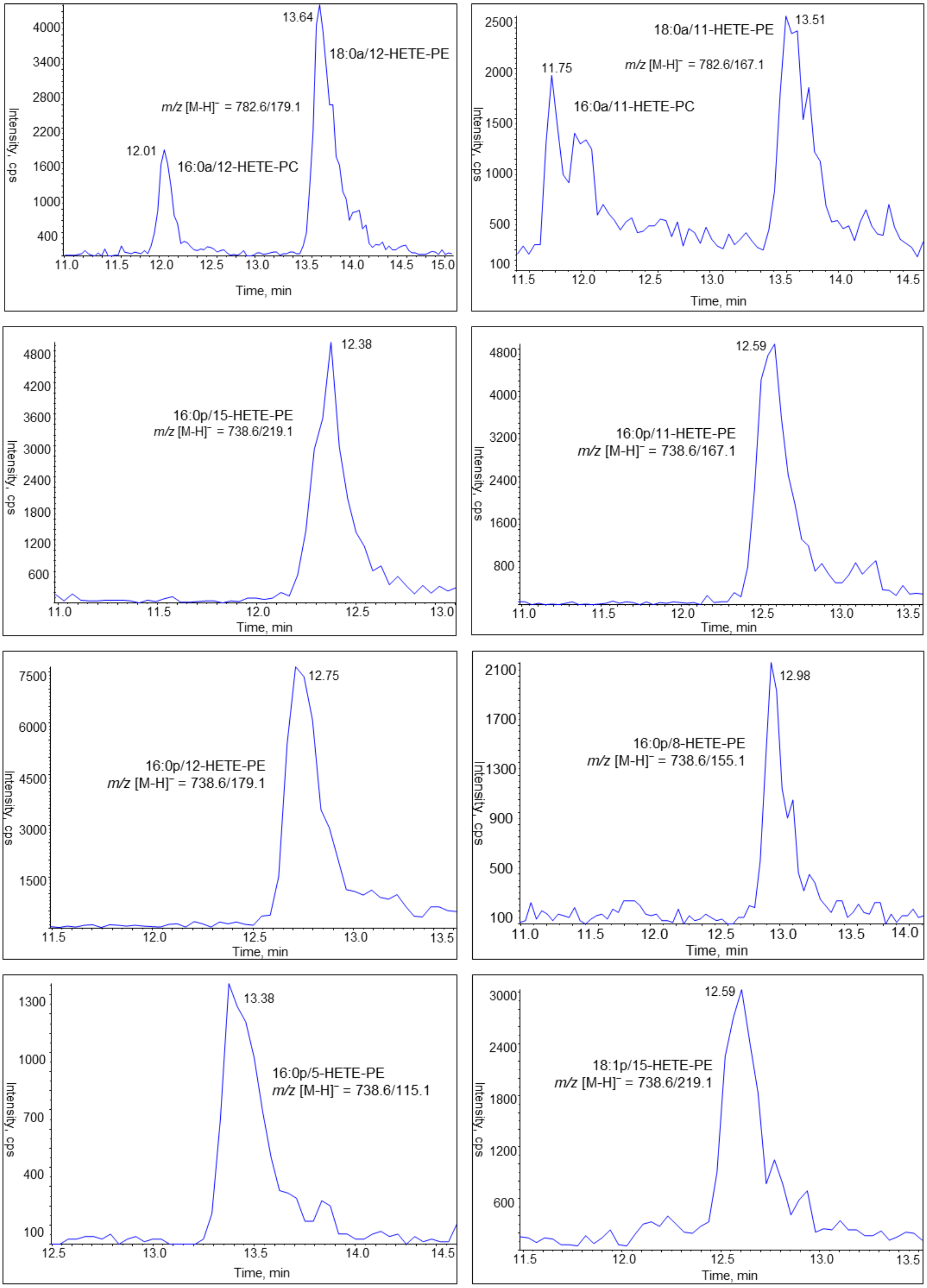
13.64
18:0a/12-HETE-PE
m/z [M-H]⁻ = 782.6/179.1
12.01
16:0a/12-HETE-PC
Intensity, cps
Time, min
13.51
18:0a/11-HETE-PE
m/z [M-H]⁻ = 782.6/167.1
11.75
16:0a/11-HETE-PC
Intensity, cps
Time, min
12.38
16:0p/15-HETE-PE
m/z [M-H]⁻ = 738.6/219.1
Intensity, cps
Time, min
12.59
16:0p/11-HETE-PE
m/z [M-H]⁻ = 738.6/167.1
Intensity, cps
Time, min
12.75
16:0p/12-HETE-PE
m/z [M-H]⁻ = 738.6/179.1
Intensity, cps
Time, min
12.98
16:0p/8-HETE-PE
m/z [M-H]⁻ = 738.6/155.1
Intensity, cps
Time, min
13.38
16:0p/5-HETE-PE
m/z [M-H]⁻ = 738.6/115.1
Intensity, cps
Time, min
12.59
18:1p/15-HETE-PE
m/z [M-H]⁻ = 738.6/219.1
Intensity, cps
Time, min

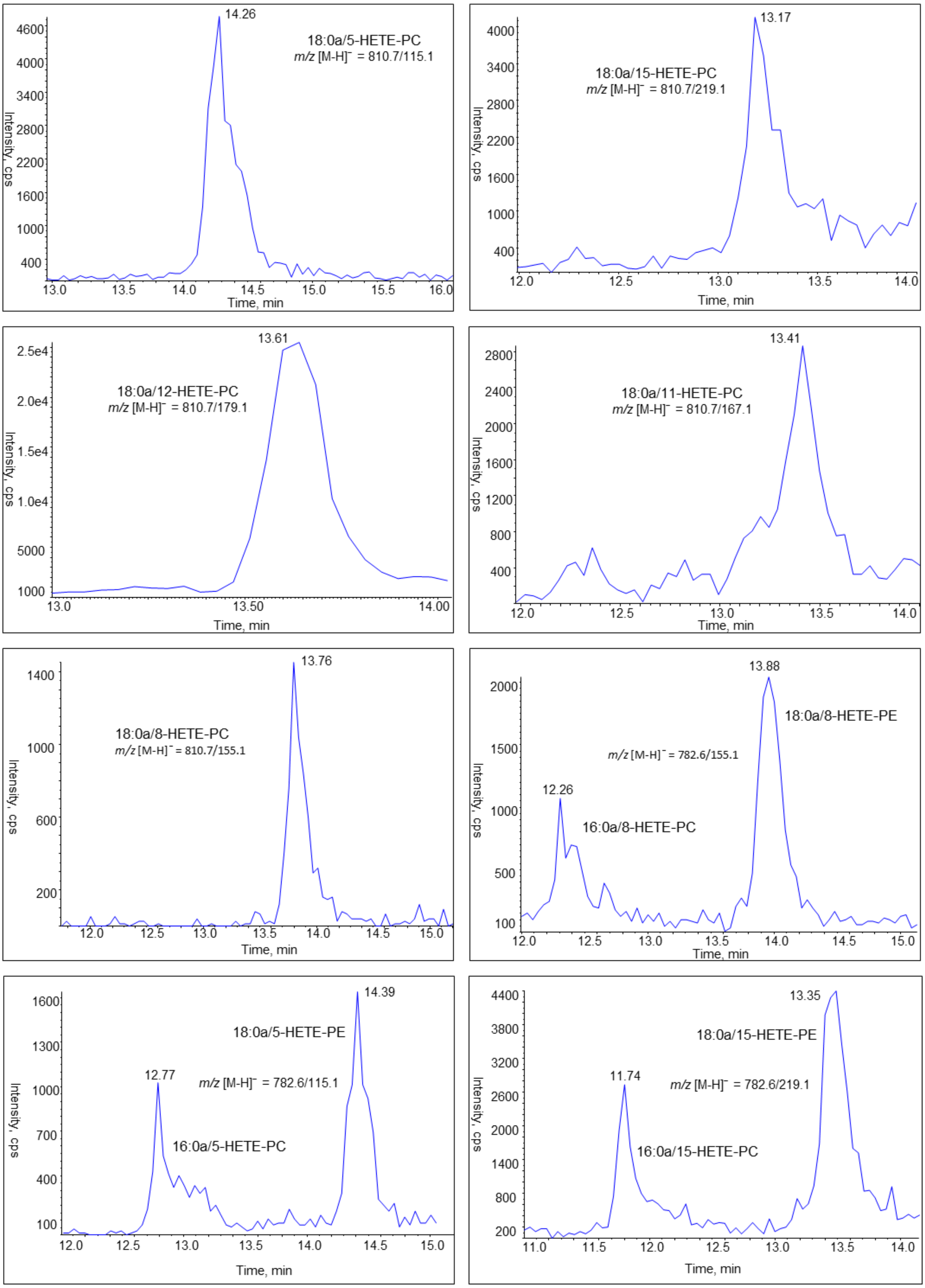
14.26
18:0a/5-HETE-PC
m/z [M-H]- = 810.7/115.1
13.17
18:0a/15-HETE-PC
m/z [M-H]- = 810.7/219.1
13.61
18:0a/12-HETE-PC
m/z [M-H]- = 810.7/179.1
13.41
18:0a/11-HETE-PC
m/z [M-H]- = 810.7/167.1
13.76
18:0a/8-HETE-PC
m/z [M-H]- = 810.7/155.1
13.88
18:0a/8-HETE-PE
m/z [M-H]- = 782.6/155.1
12.26
16:0a/8-HETE-PC
14.39
18:0a/5-HETE-PE
12.77
m/z [M-H]- = 782.6/115.1
16:0a/5-HETE-PC
13.35
18:0a/15-HETE-PE
11.74
m/z [M-H]- = 782.6/219.1
16:0a/15-HETE-PC
Intensity, cps
Time, min

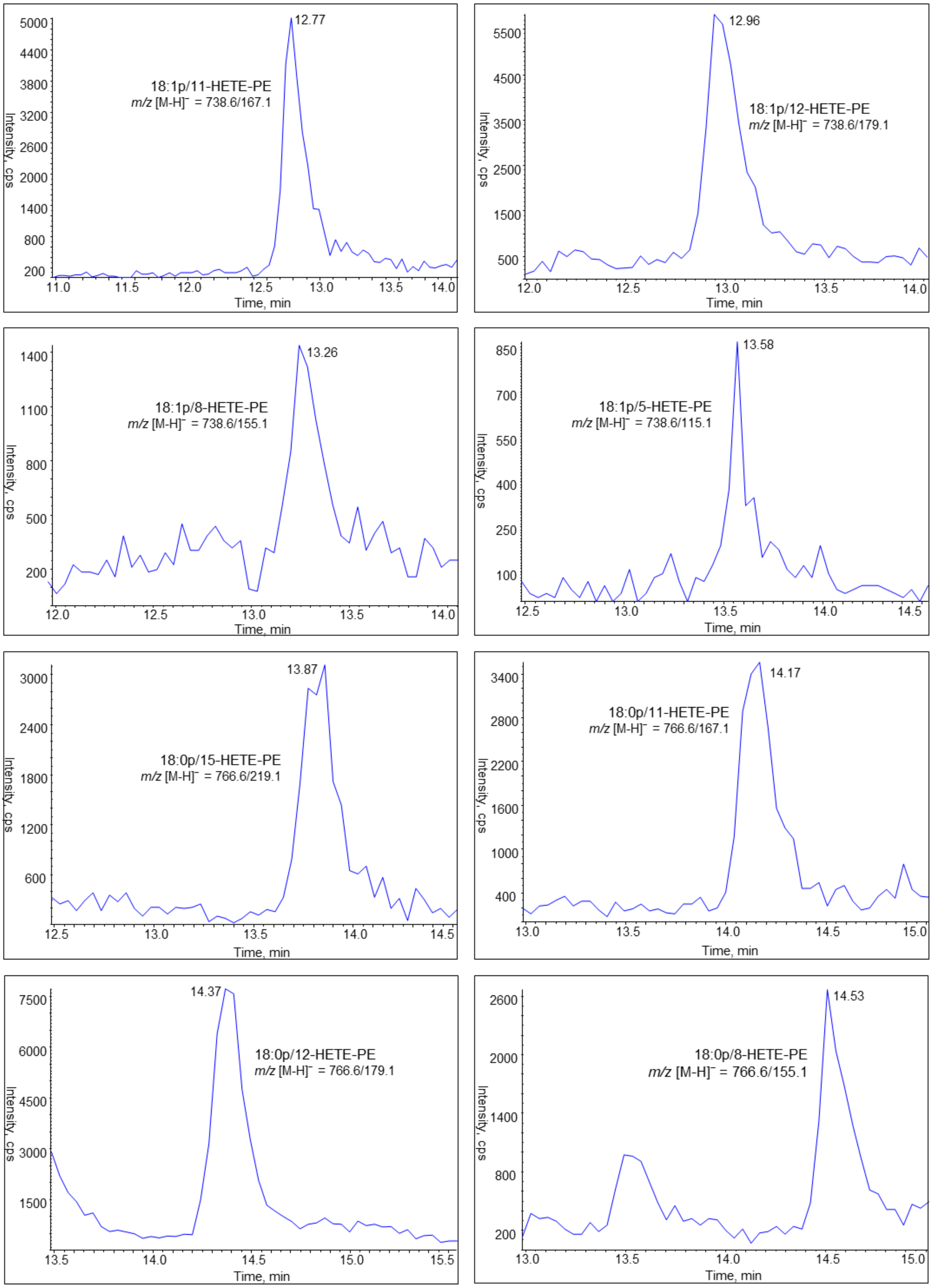
12.77
18:1p/11-HETE-PE
m/z [M-H]⁻ = 738.6/167.1
Intensity, cps
Time, min
12.96
18:1p/12-HETE-PE
m/z [M-H]⁻ = 738.6/179.1
13.26
18:1p/8-HETE-PE
m/z [M-H]⁻ = 738.6/155.1
13.58
18:1p/5-HETE-PE
m/z [M-H]⁻ = 738.6/115.1
13.87
18:0p/15-HETE-PE
m/z [M-H]⁻ = 766.6/219.1
14.17
18:0p/11-HETE-PE
m/z [M-H]⁻ = 766.6/167.1
14.37
18:0p/12-HETE-PE
m/z [M-H]⁻ = 766.6/179.1
14.53
18:0p/8-HETE-PE
m/z [M-H]⁻ = 766.6/155.1

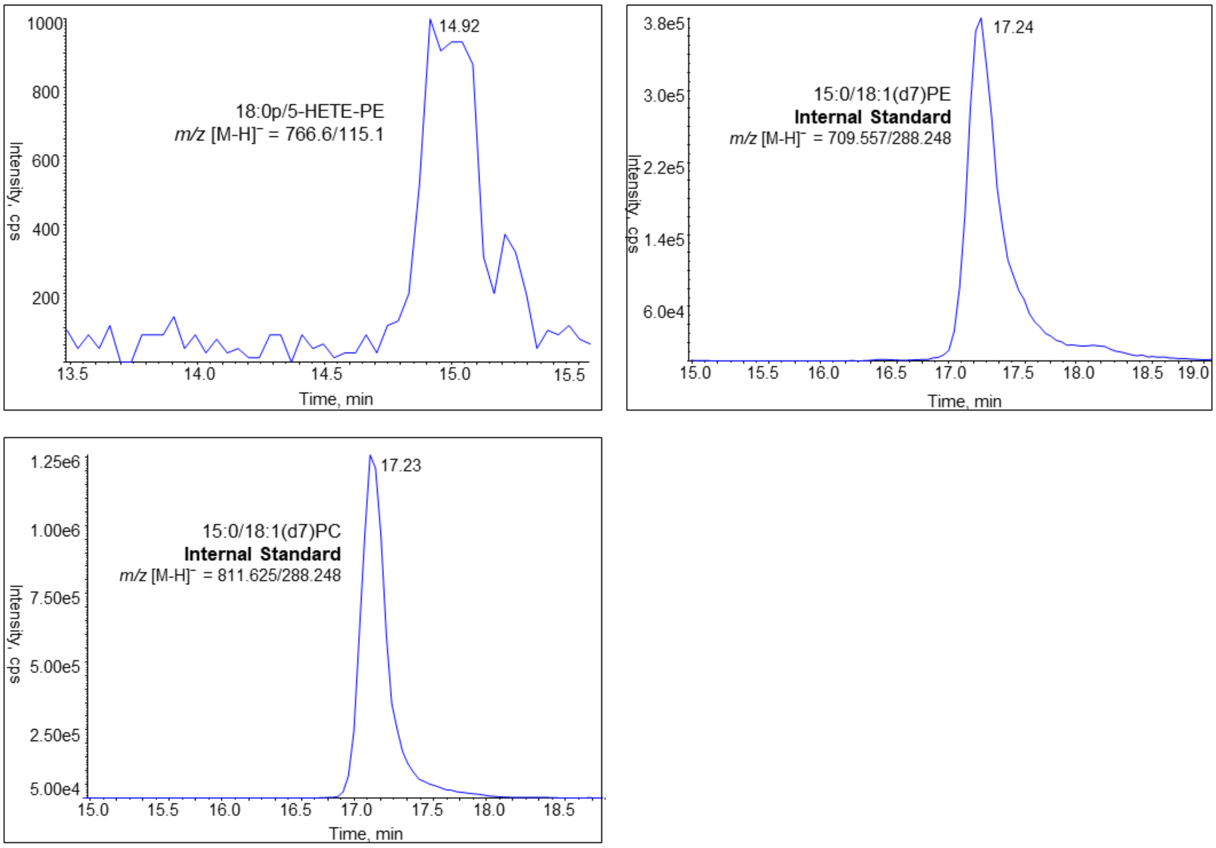

Figure 10.6: Representative chromatograms of the LC-MS/MS analysis of oxidised phospholipids
Lipid extracts were separated using reverse-phase LC/MS/MS, as described in Chapter 2: Materials and Methods. Screenshots were taken from Multiquant software.

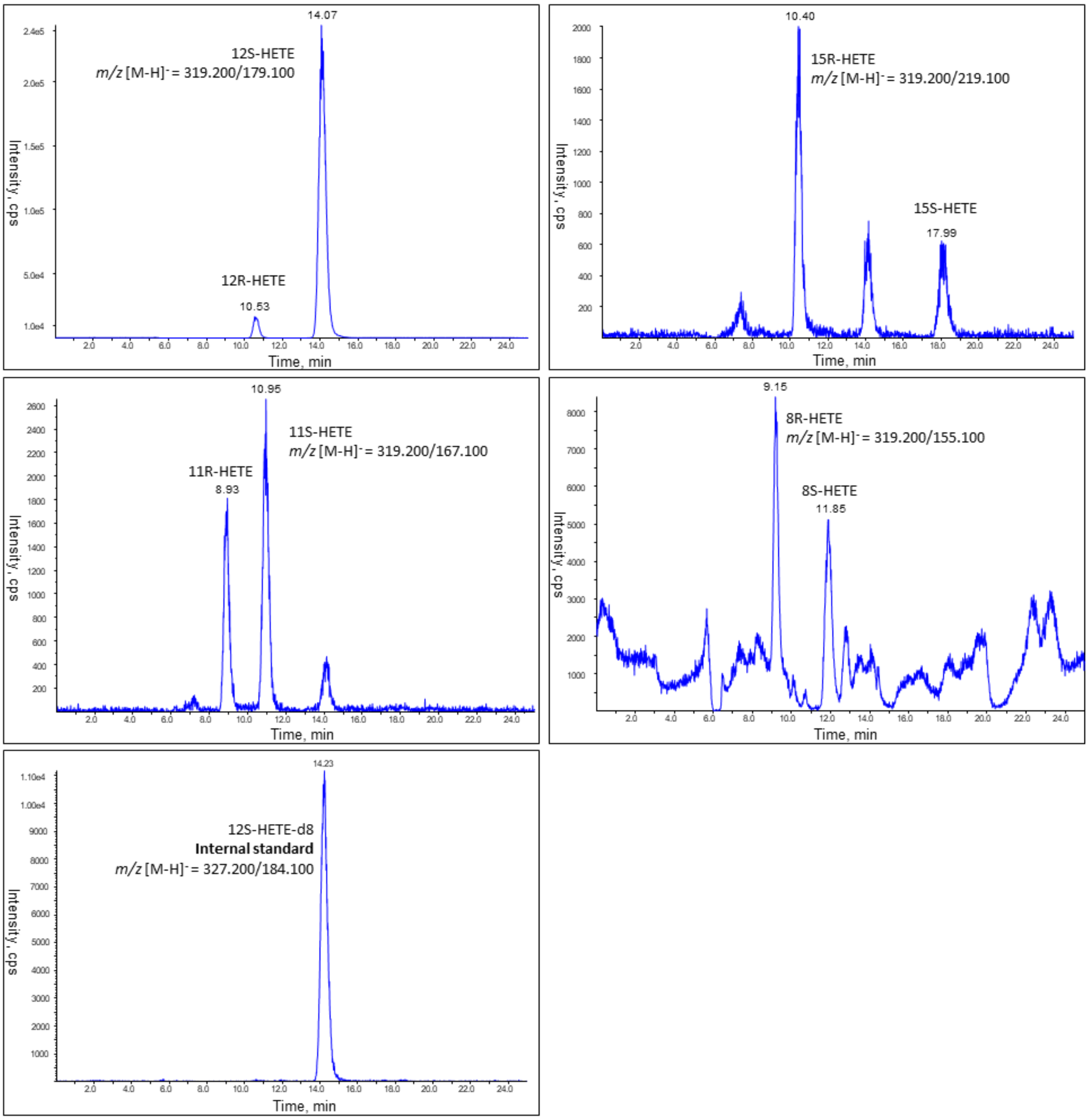

Figure 10.7: Representative chromatograms of the chiral chromatography
Lipid extracts were separated using reverse-phase LC/MS/MS, as described in Chapter 2: Materials and Methods. Screenshots were taken from Multiquant software. Lipids were confirmed by comparing retention time with primary standards run in the same analytical batch.

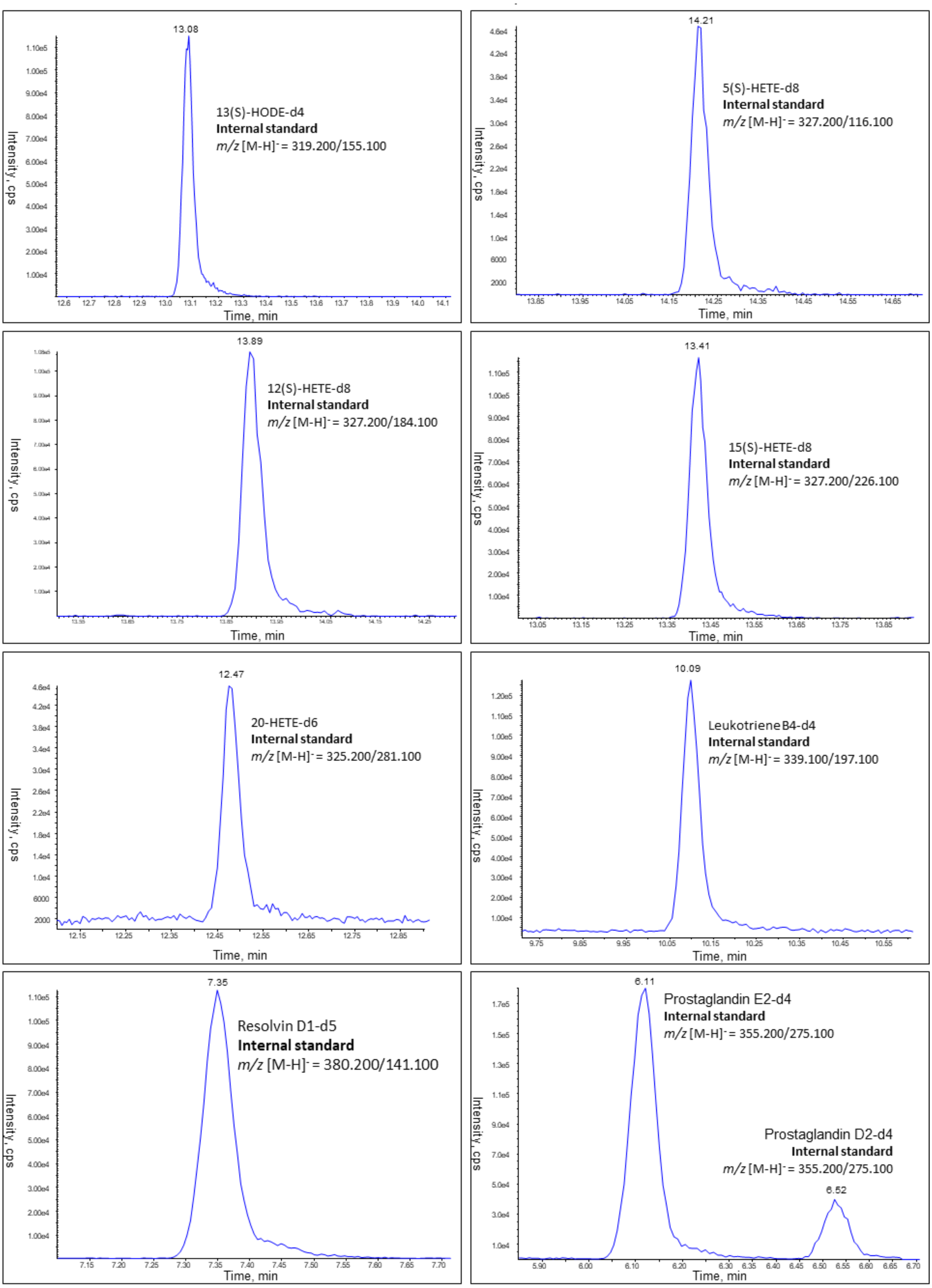
13.08
13(S)-HODE-d4
Internal standard
m/z [M-H]- = 319.200/155.100
Intensity, cps
Time, min
14.21
5(S)-HETE-d8
Internal standard
m/z [M-H]- = 327.200/116.100
Intensity, cps
Time, min
13.89
12(S)-HETE-d8
Internal standard
m/z [M-H]- = 327.200/184.100
Intensity, cps
Time, min
13.41
15(S)-HETE-d8
Internal standard
m/z [M-H]- = 327.200/226.100
Intensity, cps
Time, min
12.47
20-HETE-d6
Internal standard
m/z [M-H]- = 325.200/281.100
Intensity, cps
Time, min
10.09
Leukotriene B4-d4
Internal standard
m/z [M-H]- = 339.100/197.100
Intensity, cps
Time, min
7.35
Resolvin D1-d5
Internal standard
m/z [M-H]- = 380.200/141.100
Intensity, cps
Time, min
6.11
Prostaglandin E2-d4
Internal standard
m/z [M-H]- = 355.200/275.100
Prostaglandin D2-d4
Internal standard
m/z [M-H]- = 355.200/275.100
6.52
Intensity, cps
Time, min

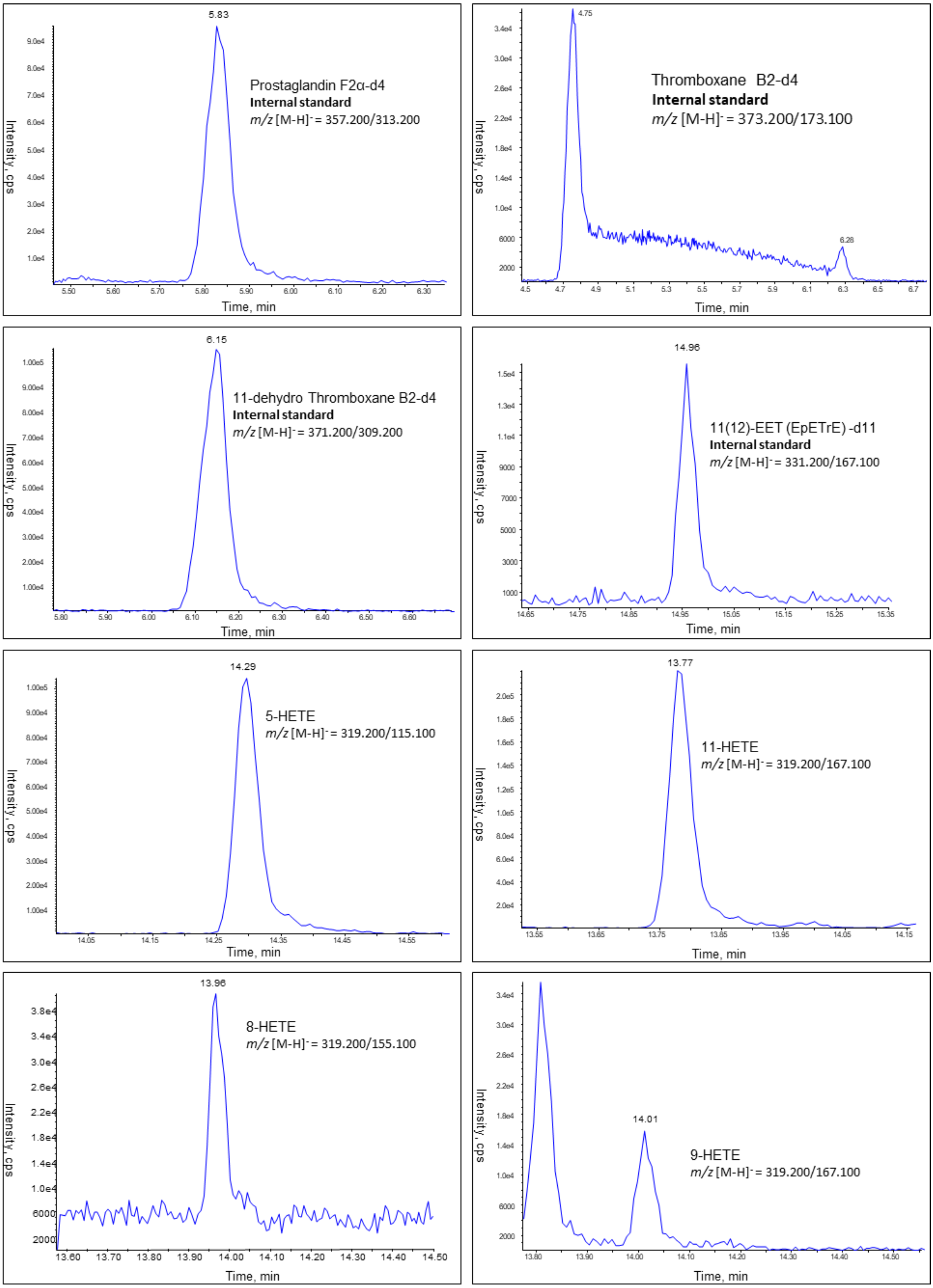
5.83
Prostaglandin F2α-d4
Internal standard
m/z [M-H]- = 357.200/313.200
Intensity, cps
Time, min
4.75
Thromboxane B2-d4
Internal standard
m/z [M-H]- = 373.200/173.100
6.28
Intensity, cps
Time, min
6.15
11-dehydro Thromboxane B2-d4
Internal standard
m/z [M-H]- = 371.200/309.200
Intensity, cps
Time, min
14.96
11(12)-EET (EpETrE) -d11
Internal standard
m/z [M-H]- = 331.200/167.100
Intensity, cps
Time, min
14.29
5-HETE
m/z [M-H]- = 319.200/115.100
Intensity, cps
Time, min
13.77
11-HETE
m/z [M-H]- = 319.200/167.100
Intensity, cps
Time, min
13.96
8-HETE
m/z [M-H]- = 319.200/155.100
Intensity, cps
Time, min
14.01
9-HETE
m/z [M-H]- = 319.200/167.100
Intensity, cps
Time, min

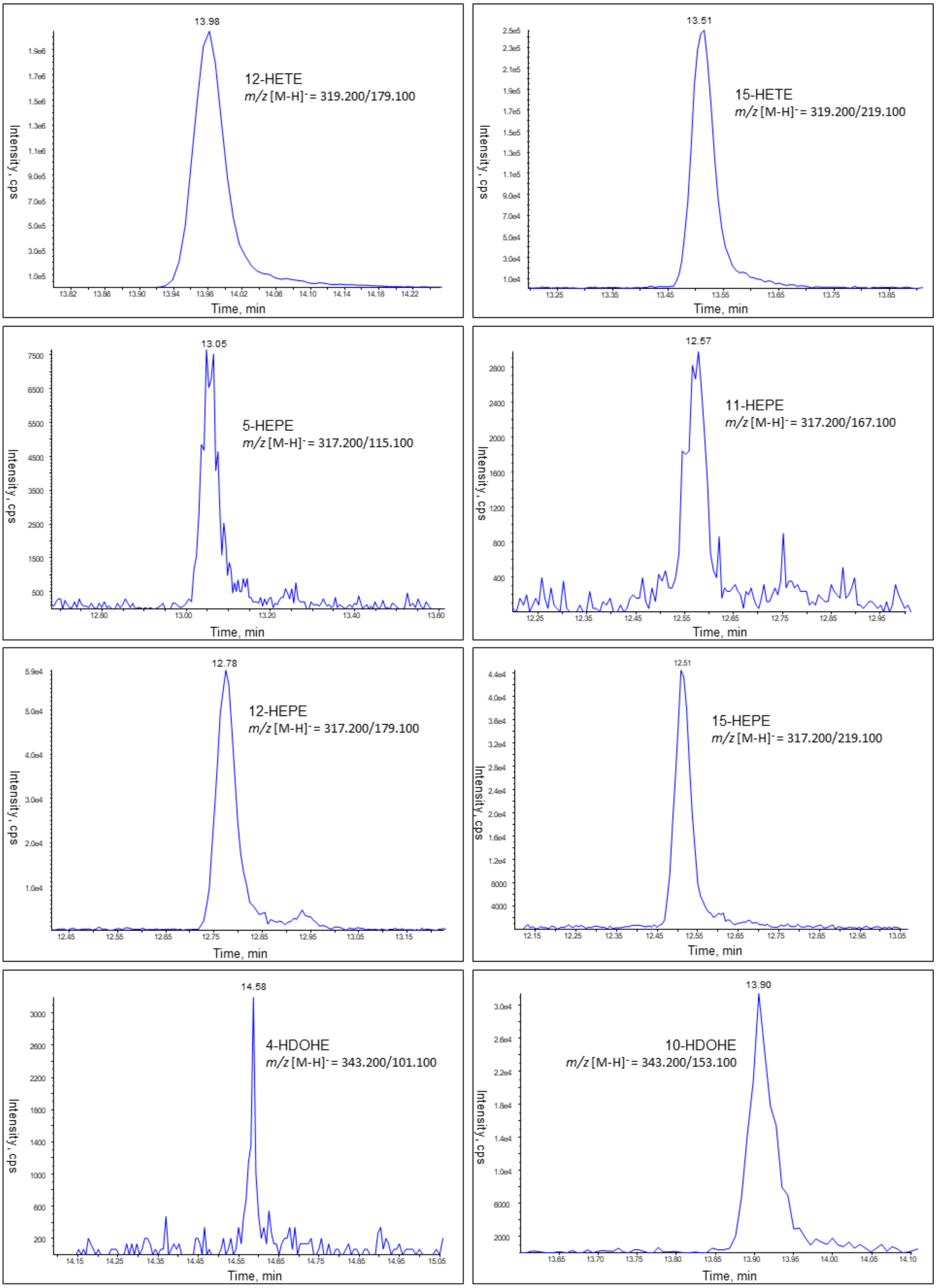
13.98
12-HETE
m/z [M-H]- = 319.200/179.100
Intensity, cps
Time, min
13.51
15-HETE
m/z [M-H]- = 319.200/219.100
Intensity, cps
Time, min
13.05
5-HEPE
m/z [M-H]- = 317.200/115.100
Intensity, cps
Time, min
12.57
11-HEPE
m/z [M-H]- = 317.200/167.100
Intensity, cps
Time, min
12.78
12-HEPE
m/z [M-H]- = 317.200/179.100
Intensity, cps
Time, min
12.51
15-HEPE
m/z [M-H]- = 317.200/219.100
Intensity, cps
Time, min
14.58
4-HDOHE
m/z [M-H]- = 343.200/101.100
Intensity, cps
Time, min
13.90
10-HDOHE
m/z [M-H]- = 343.200/153.100
Intensity, cps
Time, min

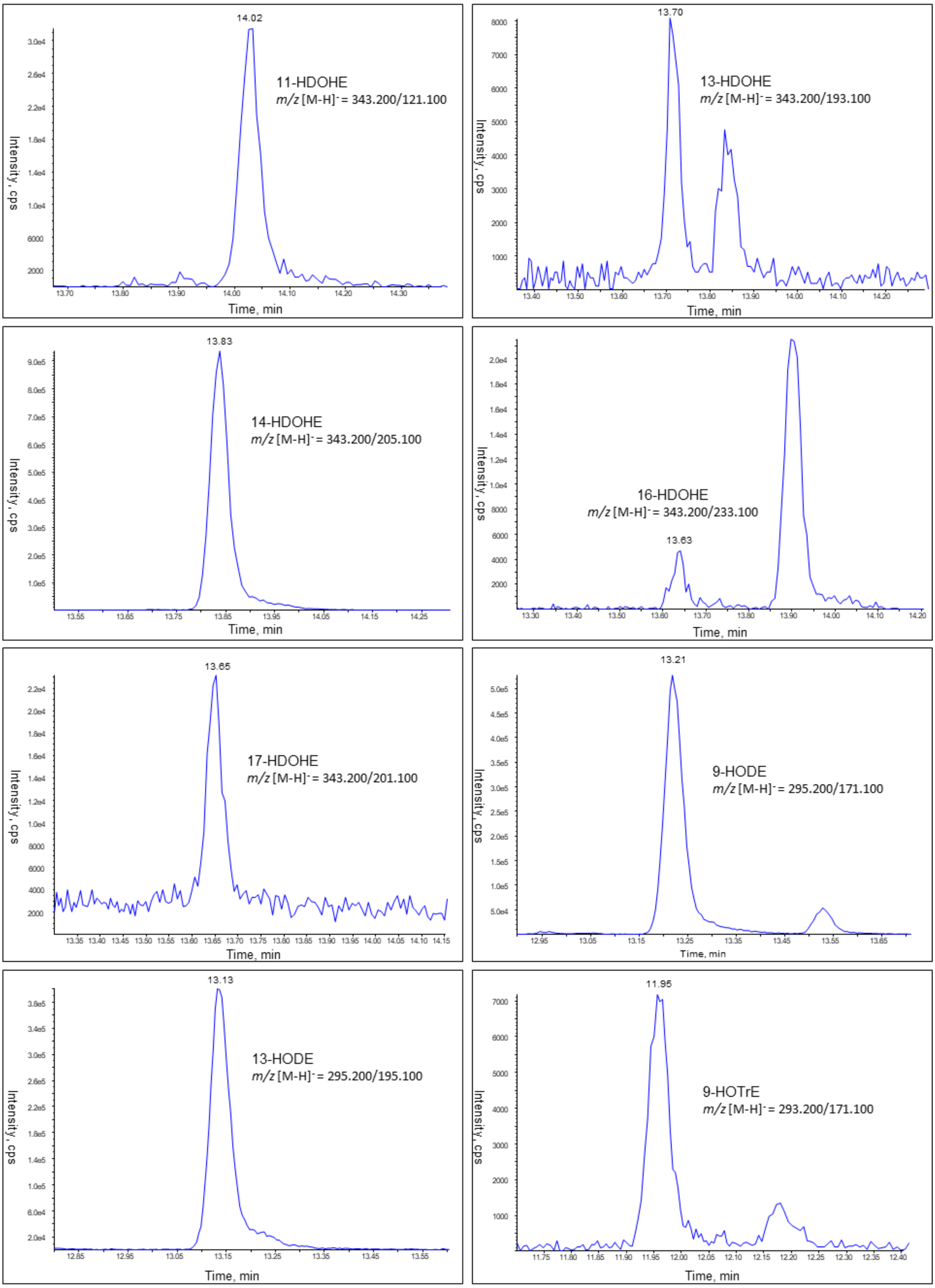
14.02
11-HDOHE
m/z [M-H]⁻ = 343.200/121.100
Intensity, cps
Time, min
13.70
13-HDOHE
m/z [M-H]⁻ = 343.200/193.100
Intensity, cps
Time, min
13.83
14-HDOHE
m/z [M-H]⁻ = 343.200/205.100
Intensity, cps
Time, min
16-HDOHE
m/z [M-H]⁻ = 343.200/233.100
13.63
Intensity, cps
Time, min
13.65
17-HDOHE
m/z [M-H]⁻ = 343.200/201.100
Intensity, cps
Time, min
13.21
9-HODE
m/z [M-H]⁻ = 295.200/171.100
Intensity, cps
Time, min
13.13
13-HODE
m/z [M-H]⁻ = 295.200/195.100
Intensity, cps
Time, min
11.95
9-HOTrE
m/z [M-H]⁻ = 293.200/171.100
Intensity, cps
Time, min

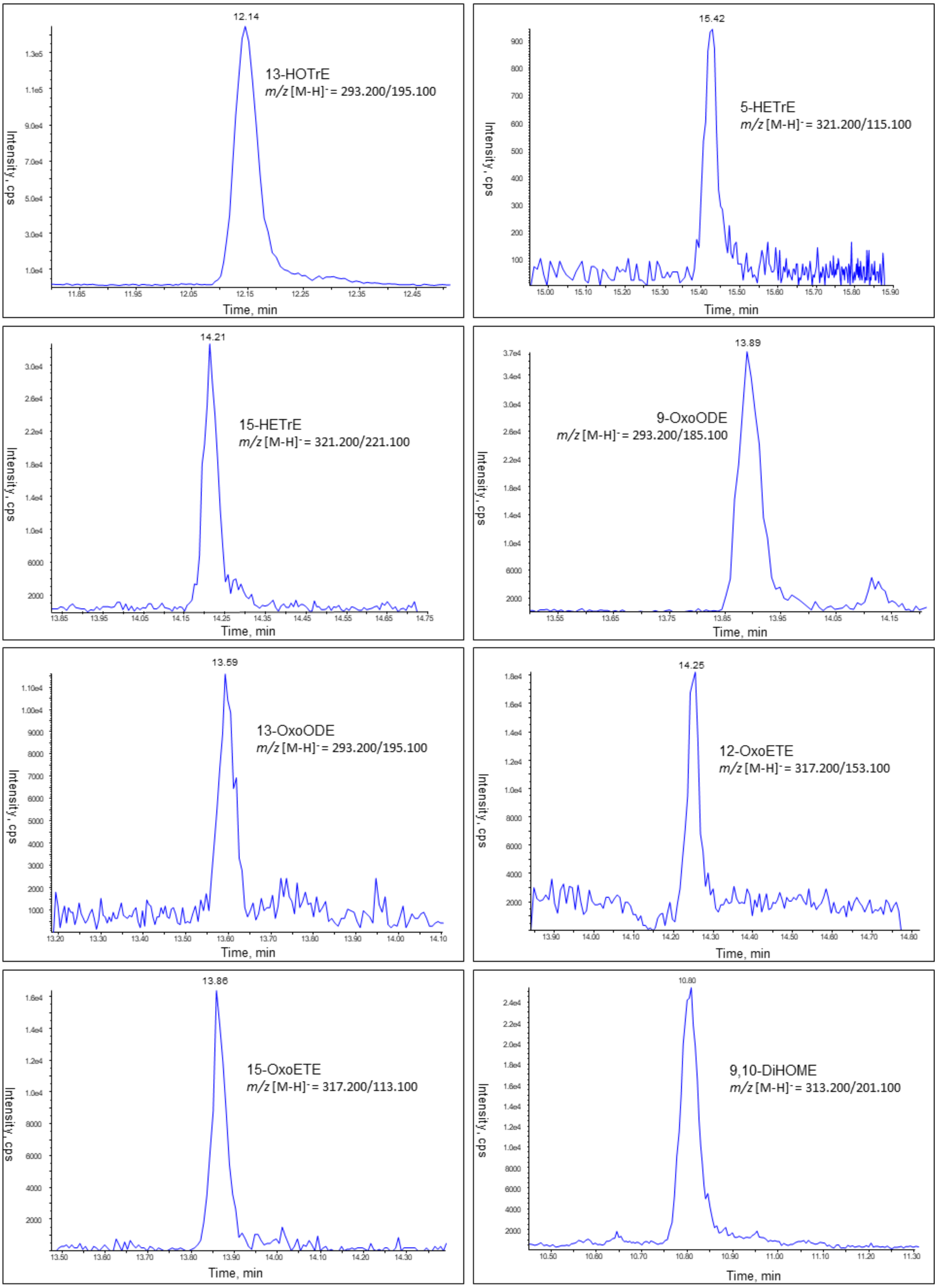
12.14
13-HOTrE
m/z [M-H]$^-$ = 293.200/195.100
Intensity, cps
Time, min
15.42
5-HETrE
m/z [M-H]$^-$ = 321.200/115.100
Intensity, cps
Time, min
14.21
15-HETrE
m/z [M-H]$^-$ = 321.200/221.100
Intensity, cps
Time, min
13.89
9-OxoODE
m/z [M-H]$^-$ = 293.200/185.100
Intensity, cps
Time, min
13.59
13-OxoODE
m/z [M-H]$^-$ = 293.200/195.100
Intensity, cps
Time, min
14.25
12-OxoETE
m/z [M-H]$^-$ = 317.200/153.100
Intensity, cps
Time, min
13.86
15-OxoETE
m/z [M-H]$^-$ = 317.200/113.100
Intensity, cps
Time, min
10.80
9,10-DiHOME
m/z [M-H]$^-$ = 313.200/201.100
Intensity, cps
Time, min

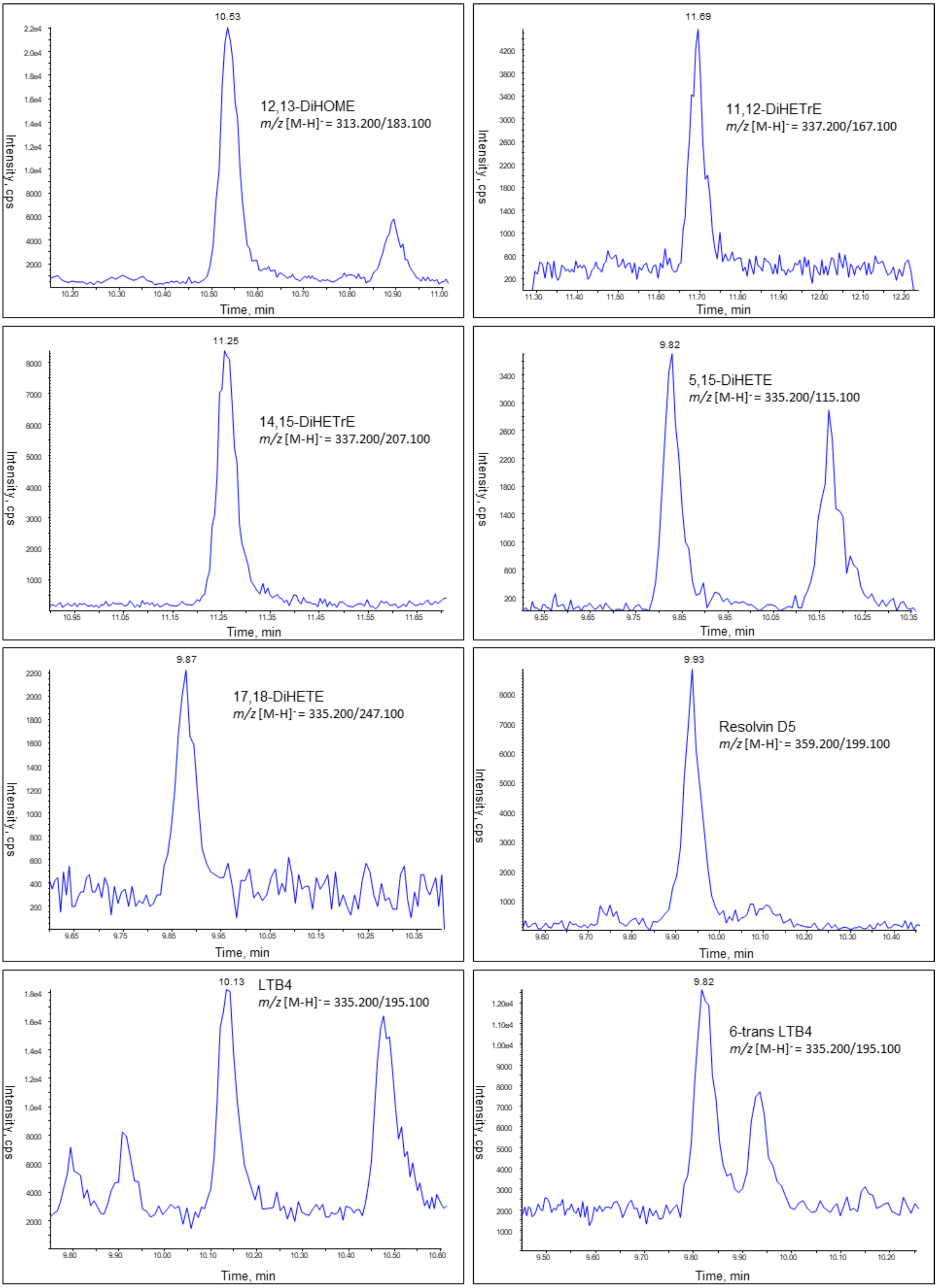
10.53
12,13-DiHOME
m/z [M-H]- = 313.200/183.100
Intensity, cps
Time, min
11.69
11,12-DiHETrE
m/z [M-H]- = 337.200/167.100
Intensity, cps
Time, min
11.25
14,15-DiHETrE
m/z [M-H]- = 337.200/207.100
Intensity, cps
Time, min
9.82
5,15-DiHETE
m/z [M-H]- = 335.200/115.100
Intensity, cps
Time, min
9.87
17,18-DiHETE
m/z [M-H]- = 335.200/247.100
Intensity, cps
Time, min
9.93
Resolvin D5
m/z [M-H]- = 359.200/199.100
Intensity, cps
Time, min
10.13
LTB4
m/z [M-H]- = 335.200/195.100
Intensity, cps
Time, min
9.82
6-trans LTB4
m/z [M-H]- = 335.200/195.100
Intensity, cps
Time, min

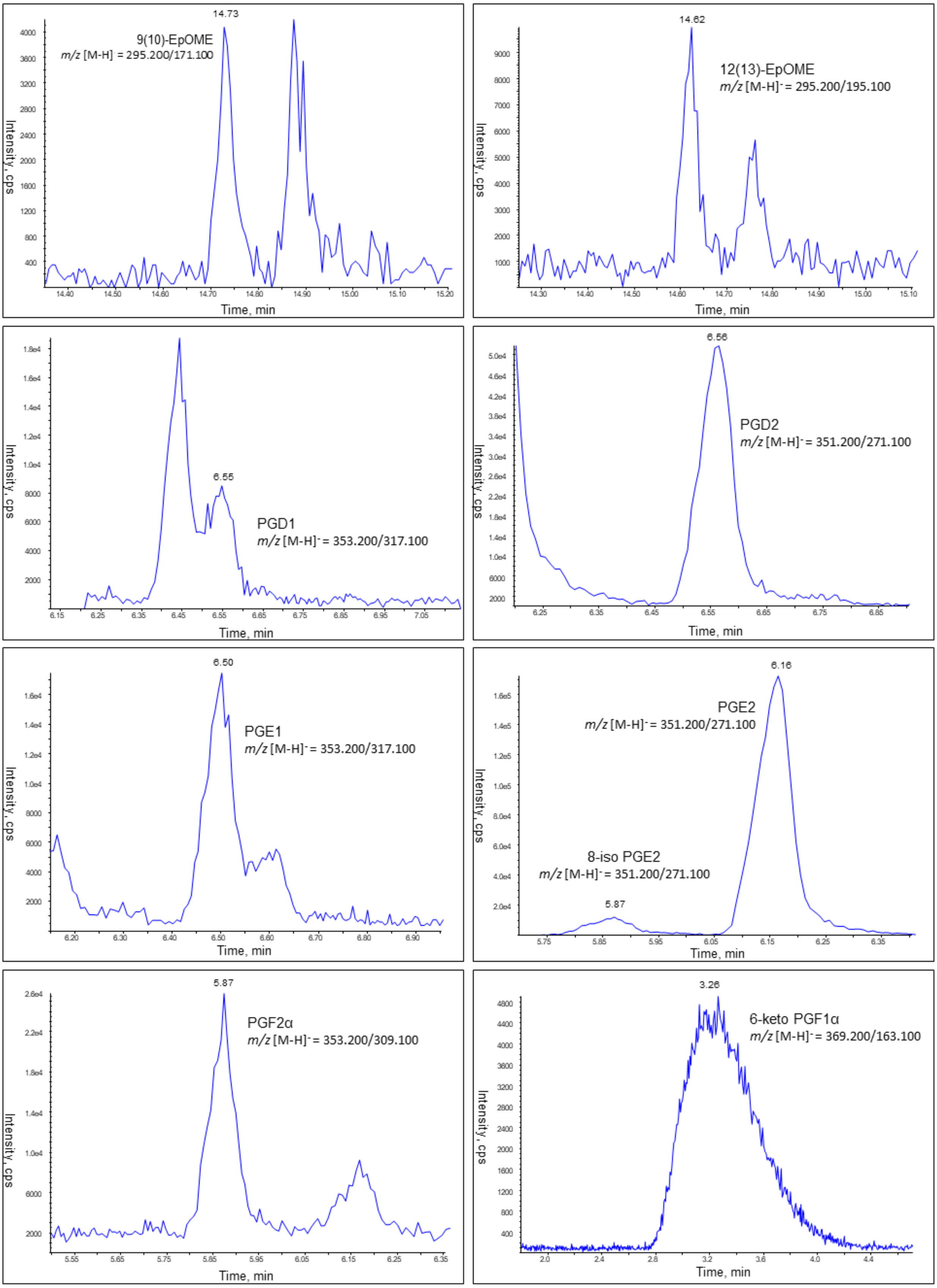
14.73
9(10)-EpOME
m/z [M-H] = 295.200/171.100
Intensity, cps
Time, min
14.62
12(13)-EpOME
m/z [M-H]⁻ = 295.200/195.100
Intensity, cps
Time, min
6.55
PGD1
m/z [M-H]⁻ = 353.200/317.100
Intensity, cps
Time, min
6.56
PGD2
m/z [M-H]⁻ = 351.200/271.100
Intensity, cps
Time, min
6.50
PGE1
m/z [M-H]⁻ = 353.200/317.100
Intensity, cps
Time, min
6.16
PGE2
m/z [M-H]⁻ = 351.200/271.100
8-iso PGE2
m/z [M-H]⁻ = 351.200/271.100
5.87
Intensity, cps
Time, min
5.87
PGF2α
m/z [M-H]⁻ = 353.200/309.100
Intensity, cps
Time, min
3.26
6-keto PGF1α
m/z [M-H]⁻ = 369.200/163.100
Intensity, cps
Time, min

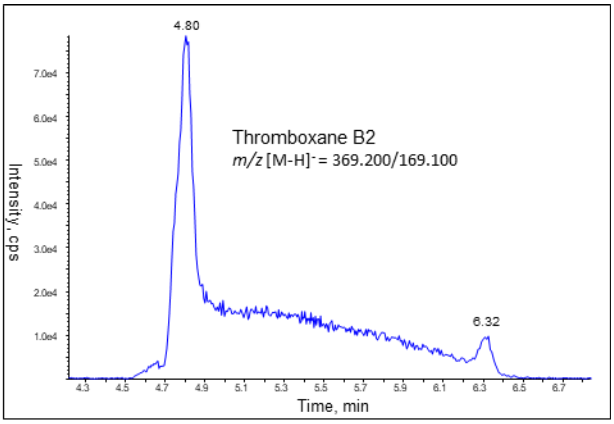

Figure 10.8: Representative chromatograms of oxylipin LC/MS/MS analysis

Lipid extracts were separated using reverse-phase LC/MS/MS, as described in Chapter 2: Materials and Methods. Screenshots were taken from Multiquant software. Lipids were confirmed by comparing retention time with primary standards run in the same analytical batch.

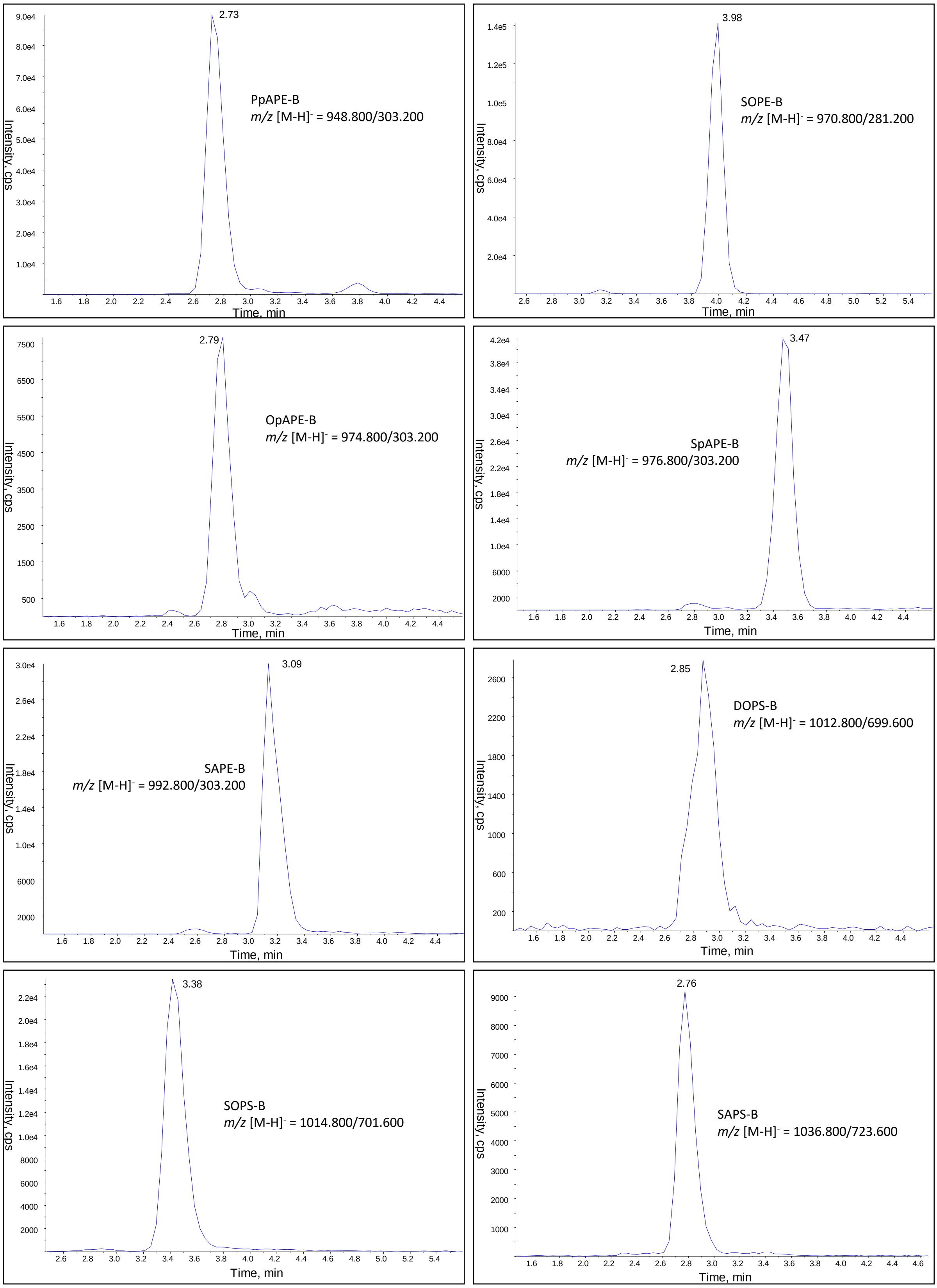
2.73
PpAPE-B
m/z [M-H]- = 948.800/303.200
3.98
SOPE-B
m/z [M-H]- = 970.800/281.200
2.79
OpAPE-B
m/z [M-H]- = 974.800/303.200
3.47
SpAPE-B
m/z [M-H]- = 976.800/303.200
3.09
SAPE-B
m/z [M-H]- = 992.800/303.200
2.85
DOPS-B
m/z [M-H]- = 1012.800/699.600
3.38
SOPS-B
m/z [M-H]- = 1014.800/701.600
2.76
SAPS-B
m/z [M-H]- = 1036.800/723.600
Intensity, cps
Time, min

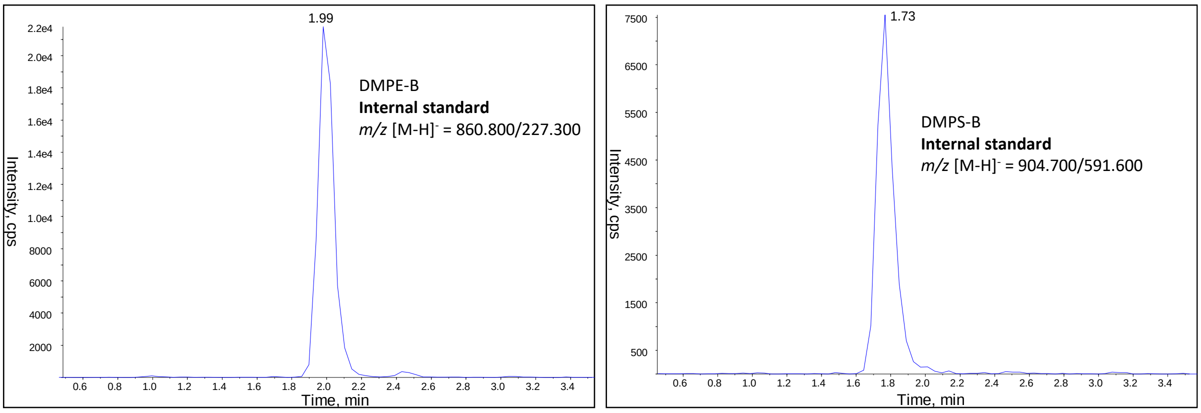

Figure 10.9: Representative chromatograms of aminophospholipids LC/MS/MS analysis
Lipid extracts were separated using reverse-phase LC/MS/MS, as described in Chapter 2: Materials and Methods. Screenshots were taken from Multiquant software. Lipids were confirmed by comparing retention time with primary standards run in the same analytical batch.